DISS. ETH NO. 22027

SUSTAINABILITY ASSESSMENT OF PASSENGER VEHICLES: ANALYSIS OF PAST TRENDS AND FUTURE IMPACTS OF ELECTRIC POWERTRAINS

A dissertation submitted to

ETH ZURICH

for the degree of

Doctor of Sciences (Dr. sc. ETH Zurich)

presented by

JOHANNES HOFER

Dipl.-Phys., LMU Munich
born 27. October 1982
citizen of Austria

accepted on the recommendation of

Prof. Dr. A. Wokaun, examiner
Dr. W. Schenler, co-examiner
Dr. S. Hirschberg, co-examiner
Prof. Dr. T. J. Schmidt, co-examiner

2014

ABSTRACT

Since 1950 the world's passenger car fleet has grown by about 5 % per year, reaching approximately 870 million vehicles in 2011 and consuming more than 20 million barrels of crude oil per day. Rising transportation demand and dependence on petroleum as its primary energy source will continue to be a major cause of greenhouse gas (GHG) and pollutant emissions leading to global warming, and damages to human health and the ecosystem. In addition, oil's security of supply and price stability are uncertain. For these reasons, several advanced vehicle and fuel technologies are currently being developed with the aim of reducing the environmental impacts of road transport and its dependence on fossil oil. However, these technologies enter the market incrementally and must meet performance, utility, and cost requirements to be accepted by consumers.

In Switzerland more than two third of personal mobility is based on gasoline and diesel passenger cars, which contribute a rising share to total Swiss CO_2 emissions. A decomposition analysis has been developed and applied to separate the contributions of changes in new vehicle efficiency, mass, and fuel technology to specific CO_2 emissions from Swiss new vehicles. The analysis showed that in the past, powertrain efficiency improvements have to a large extent been offset by the increased mass and performance of new vehicles. In the period from 2000 to 2012, potential reductions at constant fleet mass would have been ca. 9 % higher than the actual CO_2 emission reduction. The method was furthermore applied to study emissions scenarios showing the conditions under which the regulatory targets for 2015 and beyond can be met.

In this thesis an integrated framework to quantitatively assess technical, economic, and environmental criteria of a wide range of conventional and electric powertrains has been developed. Scenarios from today to 2050 are investigated, and various primary energy sources and vehicle configurations are taken into account. The novel analytic modeling methodology developed allows very short calculation time, making it useful for interactive analysis, scenario modeling and fleet simulations; as well as offering new opportunities for sensitivity analysis and optimization.

The models developed in this thesis can help to create a fundamental understanding of the complex interactions between different powertrain technologies, vehicle configuration parameters, future developments, and the corresponding impacts on cost and environmental indicators. In order to make the results of this thesis accessible to a broader public, several tools for interactive life cycle assessment, scenario analysis, and multi-criteria decision analysis have been developed and implemented online.

Life cycle assessment results show that the environmental impacts of electric vehicles are very dependent on their primary source of energy. If electricity and hydrogen for vehicle propulsion are produced from non-fossil primary energy, life cycle GHG emissions and the related impacts on human and ecosystem health, as well as fossil fuel depletion can be greatly reduced. In general,

the costs and environmental impacts from the vehicle production phase are higher for electric than conventional vehicle technologies. In particular metal use increases in electric vehicles and the further development should aim at reducing metal resource depletion and improving recycling efficiency.

Multi-criteria analysis indicates that there is no single technology which performs best in terms of all relevant criteria at the same time, but that different technologies have tradeoffs relative to each other and can provide advantages depending on the specific usage patterns, e.g. electric relative to conventional vehicles in urban driving conditions, or fuel cell relative to battery electric vehicles in terms range and fueling time. Plug-in hybrid electric vehicles appear to be a robust technology considering a broad set of technical, environmental, and economic criteria.

A model of the Swiss passenger vehicle fleet has been developed to analyze the implications of various future scenarios of electric vehicle sales, primary energy sources, and overall vehicle use patterns on vehicle stock, energy use, and GHG emissions until 2050. The results show that major drivetrain changes are not yet ready for large scale adoption, and will take a long time to penetrate the fleet against the current dominance of gasoline and diesel powertrains. On a long-term perspective (beyond 2030), electric vehicles offer the potential for large reductions of fleet fuel use and GHG emissions, if electricity and hydrogen are produced from non-fossil primary sources.

ZUSAMMENFASSUNG

Seit 1950 wächst die globale Zahl an Personenwagen mit ca. 5 % pro Jahr auf rund 870 Millionen Fahrzeuge im Jahr 2011. Diese verbrauchen pro Tag mehr als 20 Millionen Barrel Rohöl. Eine zunehmende Verkehrsnachfrage und die Abhängigkeit von fossilen Treibstoffen werden auch in Zukunft Hauptgründe für steigende Treibhausgas- und Schadstoffemissionen sein, welche zum Klimawandel beitragen und negative Auswirkungen auf die menschliche Gesundheit und das Ökosystem haben. Unsicher sind zudem die Versorgungssicherheit mit Öl und dessen Preisstabilität. Aus diesem Grund werden derzeit neue Antriebs- und Kraftstofftechnologien entwickelt. Ziel ist es die Umweltauswirkungen des Personenverkehrs sowie die Abhängigkeit von fossilem Öl zu reduzieren. Diese Technologien durchdringen den Markt allerdings nur schrittweise und müssen den Anforderungen der Kunden im Hinblick auf Leistung, Nutzen und Kosten entsprechen.

Mehr als zwei Drittel des Personenverkehrsaufkommens in der Schweiz wird von Benzin- und Dieselfahrzeugen geleistet, welche in steigendem Maße zu den gesamtschweizerischen CO_2-Emissionen beitragen. Im Rahmen dieser Arbeit wurde eine Methodik entwickelt, die es ermöglicht die Entwicklung der spezifischen CO_2-Emissionen von schweizer Neufahrzeugen in die Anteile aus Effizienzsteigerung, Gewichtsänderung und veränderter Kraftstofftechnologie zu trennen. Die Analyse zeigt, dass in der Vergangenheit Effizienzsteigerungen zu einem großen Teil dazu verwendet wurden, Masse und Leistung von Neufahrzeugen zu erhöhen. Im Zeitraum von 2000 bis 2012 war die potenziell mögliche CO_2-Emissionsreduktion bei konstanter Flottenmasse ca. 9 % höher als die eigentlich erreichte. Die Methode wurde zudem dazu verwendet, Emissionsszenarien zu entwickeln welche die Bedingungen aufzeigen, unter denen die Zielvorgaben für das Jahr 2015 und darüber hinaus erfüllt werden können.

In dieser Arbeit wurde ein integriertes Modell für die quantitative Bewertung der technischen, ökonomischen und ökologischen Faktoren einer breiten Auswahl konventioneller und neuer elektrischer Antriebstechnologien entwickelt. Szenarien von heute bis 2050 wurden untersucht und verschiedene Primärenergieträger und Fahrzeugkonfigurationen berücksichtigt. Die neuartige Modellierungsmethodik, welche im Rahmen dieser Arbeit entwickelt wurde, ermöglicht sehr kurze Berechnungszeiten, wodurch interaktive Analysen, Szenariomodellierungen und Flottensimulationen deutlich verbessert werden. Die Methodik eröffnet zudem neue Möglichkeiten im Bereich der Sensitivitätsanalyse und und bei Optimierungsproblemen.

Die Modelle welche im Rahmen dieser Arbeit entwickelt wurden können helfen, das grundlegende Verständnis für die komplexen Zusammenhänge zwischen verschiedenen Antriebstechnologien, Konfigurationsparametern, zukünftigen Entwicklungen, und den entsprechenden Einflüssen auf Kosten und Umweltauswirkungen zu verbessern. Um die Ergebnisse einer breiteren Öffentlichkeit zugänglich zu machen, wurden mehrere Tools für interaktive Ökobilanzierun-

gen, Szenarienanalysen, und multikriterielle Entscheidungsanalysen entwickelt, welche online genutzt werden können.

Die Ergebnisse der Ökobilanzierung zeigen, dass die Umweltauswirkungen von Elektrofahrzeugen sehr stark vom verwendeten Primärenergieträger abhängen. Sofern die Elektrizität und der Wasserstoff für den Antrieb des Fahrzeugs aus nicht-fossiler Primärenergie erzeugt werden, können sowohl die Treibhausgasemissionen über den gesamten Lebenszyklus und die daraus folgenden Auswirkungen auf die Gesundheit des Menschen und des Ökosystems, als auch der Verbrauch fossiler Energieträger deutlich reduziert werden. Die Kosten und Umweltauswirkungen der Produktionsphase sind bei elektrischen Fahrzeugtechnologien generell höher als bei konventionellen Fahrzeugtechnologien. Besonders die Verwendung metallischer Ressourcen steigt bei elektrischen Antrieben. In der Zukunft sollte darauf geachtet werden, die Verwendung dieser Materialien zu reduzieren und die Recyclingeffizienz zu erhöhen.

Die Multi-Kriterien-Analyse zeigt, dass es bisher keine ideale Technologie gibt die alle relevanten Kriterien erfüllt. Stattdessen bieten verschiedene Antriebsarten je nach Verwendungszweck relative Vorteile. So bietet beispielsweise ein elektrischer relativ zu einem konventionellen Antrieb Vorteile in städtischem Verkehr, während Brennstoffzellenfahrzeuge relativ zu batteriebetriebenen Fahrzeugen in Bezug auf Reichweite sowie Tank- bzw. Ladezeit vorteilhaft sind. Plug-in Hybridfahrzeuge scheinen unter Berücksichtigung einer großen Bandbreite technischer, ökologischer und ökonomischer Indikatoren eine verlässliche Fahrzeugtechnologie zu sein.

Ein Modell der schweizer Personenwagenflotte wurde entwickelt, um die Auswirkungen verschiedener Szenarien zukünftiger Verkäufe elektrischer Fahrzeuge, Primärenergieträger, und Verkehrsleistungen auf die Flottenzusammensetzung, den Gesamtenergieverbrauch, und die Treibhausgasemissionen bis 2050 zu untersuchen. Die Ergebnisse zeigen, dass grundlegend neue Antriebstechnologien noch nicht für eine massenhafte Einführung bereit sind und eine lange Zeit benötigen um die Dominanz konventioneller Technologien zu durchbrechen. Langfristig (ab 2030) werden elektrische Antriebstechnologien das Potential für grosse Reduktionen des Flottenkraftstoffverbrauchs und Treibhausgasemissionen bieten, falls Elektrizität und Wasserstoff aus nicht-fossilen Quellen erzeugt werden.

ACKNOWLEDGEMENTS

At this point I would like to thank all people that supported and encouraged me during the thesis.

First I want to thank my supervisor Prof. Alexander Wokaun for providing a very enriching research environment at PSI and for his valuable insights and comments in the development of the thesis. I would also like to thank my direct supervisor Dr. Warren Schenler for his continuous support, for giving me a lot of freedom and new impulses when necessary. He encouraged me a lot with many stimulating suggestions and always had time for discussions. In particular I would like to thank Dr. Stefan Hirschberg and Dr. Peter Burgherr for providing me the opportunity to work on such an interesting research topic and for encouraging me in my work during the last years.

From the electrochemistry group at PSI I would like to thank Prof. Thomas Schmidt for co-refereeing my thesis and Marcel Hofer for the interesting and helpful insights into fuel cell vehicle development.

Furthermore, I want to thank Andrew Simons and Christian Bauer for their help with the development of life cycle assessment tools, for their motivation to collaborate on new ideas, and for sharing their broad knowledge. Many thanks to my former PSI colleagues Erik Wilhelm and Petrissa Eckle for their help in getting started and the great time together. I would also like to thank Matteo Spada, Karin Treyer, Kathrin Volkart, Rebecca Lordan, Rajesh Pattupara, Vinh Dang, Martin Densing, Hal Turton and the entire LEA lab for their constant support, the good atmosphere, nice hiking and skiing trips, and the great time at PSI. It was very interesting supervising the Master thesis of Marco Miotti, Tobias Siegerist, and Dimitri Ottaviano, whose findings contributed to this work in important ways.

For their support throughout this thesis I would like to thank Gil Georges and the other THELMA collaboration partners, in particular Fabrizio Noembrini, Marina Gonzalez Vaya, and Dominik Saner. In addition, I would like to thank Auto-Schweiz for the provision of data which forms the basis for important parts of the thesis as well as Swisselectric Research, the Swiss Erdöl Vereinigung, and the Swiss Competence Center for Energy and Mobility for the financial support of this work.

Finally, I would like to thank my family for their unconditional support throughout the course of my studies. And of course Johanna who reminded me that there is a life besides research and helped me to complete the thesis in many ways.

Contents

List of Tables **xiii**

List of Figures **xviii**

List of Abbreviations **xix**

List of Symbols **xxii**

1 Introduction **1**

1.1 Background and problem 1

1.2 Thesis scope and objective 6

1.3 Outline 9

2 Vehicle mechanical energy demand **10**

2.1 Mechanical energy demand in driving cycles 11

2.1.1 Basic forces and operating modes of a vehicle 11

2.1.2 Driving cycles 12

2.1.3 Contributions to mechanical energy demand 18

2.1.4 Comparison of energy demand for different driving cycles 21

2.1.5 Regeneration potential 23

2.2 Parameterization of the contributions to mechanical energy demand 24

2.2.1 Approach and resulting coefficients for different driving cycles 25

2.2.2 Variability of parameterization coefficients 26

2.3 Sensitivity of energy demand to changes in vehicle characteristics 32

3 Vehicle energy use and configuration **38**

3.1 Calculation of vehicle energy use 38

3.1.1 Overview of existing methods 38

3.1.2 Simulation of different powertrain types 39

3.1.3 Parametric calculation of energy use 46

3.1.4 Parameterization of vehicle efficiencies . . . 49
3.2 Vehicle configuration . . . 52
3.2.1 Car classes . . . 52
3.2.2 Performance requirements . . . 54

4 Mass, cost, and life cycle assessment 58
4.1 Calculation of vehicle mass . . . 58
4.2 Cost assessment . . . 61
4.2.1 Manufacturing cost . . . 61
4.2.2 Total cost . . . 63
4.3 Life cycle assessment . . . 64

5 Analytic evaluation of vehicle mass, energy use, and cost 68
5.1 Basic concept and equations . . . 68
5.1.1 Dynamic coupling of vehicle characteristics and energy use . . . 68
5.1.2 Analytic scaling of vehicle mass and energy use . . . 71
5.2 Scenario analysis of vehicle criteria . . . 75
5.2.1 Baseline scenario . . . 76
5.2.2 Influence of vehicle range and glider mass on vehicle criteria . . . 77
5.2.3 Influence of vehicle range and glider mass (including size effect) . . . 79
5.2.4 Total cost differential . . . 81
5.3 Sensitivity analysis . . . 83
5.3.1 Parameter variations . . . 83
5.3.2 Analytic calculation . . . 85
5.3.3 Probabilistic assessment . . . 87

6 Multi-criteria analysis 89
6.1 Multi-indicator assessment . . . 90
6.1.1 Analysis framework . . . 90
6.1.2 Scenario assumptions . . . 92
6.1.3 Direct vehicle indicators . . . 94
6.1.4 Energy source dependent indicators . . . 99
6.2 Multi-criteria decision analysis . . . 108
6.2.1 MCDA method . . . 108
6.2.2 MCDA results . . . 110
6.3 Interactive analysis tools . . . 115
6.3.1 Matlab GUI implementation . . . 115

6.3.2 Webtool implementation . . . 115

7 Optimal use of advanced technologies 118
7.1 Lightweighting technology and optimization . . . 119
7.2 Effects of weight reduction on vehicle mass and energy use . . . 120
7.3 Lightweighting costs . . . 122
7.4 Cost optimization . . . 125
7.4.1 Cost effects for ICEV . . . 125
7.4.2 Cost effects for BEV . . . 127
7.5 Discussion . . . 129

8 Swiss passenger car fleet analysis 131
8.1 New passenger cars in Switzerland and Europe . . . 131
8.2 Specific CO_2 emissions from Swiss new passenger cars . . . 135
8.2.1 Analytic methodology . . . 137
8.2.2 Decomposition of emissions reduction from 2000 to 2012 . . . 142
8.2.3 Scenario analysis . . . 146
8.3 Swiss passenger car fleet impacts . . . 149
8.3.1 Methodology and scenario assumptions . . . 149
8.3.2 Scenario results . . . 155

9 Conclusions and Outlook 159
9.1 Summary and conclusions . . . 159
9.2 Limitations and outlook . . . 163

A Vehicle efficiencies 167

B Vehicle class characteristics 177

C Life cycle impact assessment data 179

D Swiss new vehicle sales and CO_2 emission by mass category 186

Bibliography 198

List of Tables

2.1 NEDC characteristics . . . 15
2.2 CADC characteristics . . . 16
2.3 WLTP characteristics . . . 17
2.4 Reference car characteristics. . . . 19
2.5 Parameterization coefficients to calculate the contributions to mechanical energy demand in kJ per 100 km for different driving cycles. . . . 27

3.1 Density and lower heating value of fuels [Edwards et al., 2011]. . . . 41
3.2 Assumptions for the development of peak efficiency of the main powertrain components from 2012 to 2050. . . . 51
3.3 Three top sales models by class for the German passenger car market in 2011. . . . 53

4.1 Configuration factors by powertrain technology. . . . 60
4.2 Fixed and variable masses of vehicle components. . . . 61
4.3 Fixed and variable costs of vehicle components. . . . 62
4.4 Electricity and fuel prices ($/GJ) to the end consumer without tax. . . . 64
4.5 ReCiPe mid-point impact categories and indicators. . . . 66
4.6 ReCiPe end-point impact categories and indicators. . . . 67
4.7 RecCiPe mid-point to end-point characterization factors. . . . 67

5.1 Mass independent energy use and its sensitivity to mass by powertrain technology and time. . . . 76
5.2 Aggregated specific mass and cost of powertrain and energy storage. . . . 77

6.1 Vehicle class characteristics for the year 2012 used in this chapter. . . . 93
6.2 Assumed electric and fuel based ranges by drivetrain and year. . . . 94
6.3 MCDA indicators and technology performance scaling. . . . 109

7.1 Reference vehicle configuration. . . . 121

8.1 Summary of scenario parameter settings. . . . 147

8.2 WtW GHG emission for fuel, electricity, and hydrogen supply and combustion (kg CO_2 eq/GJ). 154

A.1 Traction and regeneration efficiencies for average, urban, and highway driving by powertrain, power-to-mass ratio, PHEV operating mode, and year of assessment. . 167

A.2 Parameterization coefficients to calculate traction and regeneration efficiencies by powertrain, driving region, power-to-mass ratio, and year of assessment. 174

B.1 Sales average characteristics by class for the German passenger car market in 2011. Values for frontal area, aerodynamic drag coefficient, and glider mass are estimated. 178

C.1 LCIA data of vehicle components. 180

C.2 LCIA data of road, vehicle maintenance, and exhaust emissions. 181

C.3 LCIA data of exhaust emissions, non-exhaust emissions, and fuel supply. 182

C.4 LCIA data of electricity supply. 183

C.5 LCIA data of electricity and hydrogen supply. 184

C.6 LCIA data of hydrogen supply. 185

D.1 Distribution of average CO_2 emission (g/km) by mass category. 187

D.2 Distribution of sales by mass category. 188

List of Figures

1.1 Global 2010 transport energy use by source (left) and mode (right) [WEC, 2011]. . . 2
1.2 Global transport energy use by mode from 1971 to 2006 [IEA, 2009]. 2
1.3 Passenger car ownership as a function of the average income per capita in several countries from 1970 to 2005 [IEA, 2009]. 3
1.4 Passenger car fleet scenario from 2000 to 2035 in selected regions according to [IEA, 2012b]. 3
1.5 Historic and projected Swiss passenger travel distance by mode from 1960 to 2050. 5
1.6 THELMA project framework with work package tasks and partners. 8

2.1 NEDC velocity and acceleration versus time. 15
2.2 CADC velocity and acceleration versus time. 16
2.3 WLTP velocity and acceleration versus time. 17
2.4 Contributions to the power at the wheel for the NEDC and WLTP driving cycles. . 19
2.5 Mechanical energy demand of a midsize passenger car for different driving cycles. For each cycle the contributions to tractive (left) and regenerable (right bar) energy are shown. 21
2.6 Mechanical energy demand of a midsize passenger car. For each cycle regenerable energy and the contributions to dissipative energy are shown. 22
2.7 Contributions of dissipative and regenerable energy for different driving cycles sorted by regenerable energy (left). Regenerable vs. dissipative energy for different driving cycles (right). The color scale is according to the amount of regenerable energy. 23
2.8 Contributions of dissipative and regenerable energy to tractive energy demand (top left) and regeneration potential for different driving cycles as a function of vehicle mass. 24
2.9 Contributions to the power at the wheel of a passenger car in two different configurations for the higher speed segments of the WLTP cycle (1000-1820 s are shown). 27
2.10 Variability of cycle traction and regeneration periods and of the parameterization coefficients for different driving cycles. 29
2.11 Error of E_{trac}, E_{regen}, and E_{diss} using unadjusted parameterization coefficients. The error is plotted against the cycle average velocity squared times the relative time of regeneration to traction period (left) and sorted by the same value (right). 30

2.12 Traction and regeneration period for the WLTP driving cycle by vehicle mass and frontal area, c_d and c_r constant. 30

2.13 Parameterization coefficients for the WLTP driving cycle by vehicle mass and frontal area. 31

2.14 Error of calculating E_{trac} and E_{regen} with constant parameterization coefficients for the WLTP driving cycle by vehicle mass and frontal area. White points indicate the curb weight and frontal area of new passenger cars sold in Switzerland in 2010. . . 32

2.15 Sensitivities of E_{trac}, E_{diss}, and E_{regen} with respect to changes of vehicle mass, rolling resistance, and aerodynamic drag coefficient. 34

2.16 Absolute (top) and relative (bottom) changes of E_{trac}, E_{diss}, and E_{regen} with respect to an increase of vehicle mass. 35

2.17 Absolute (top) and relative (bottom) changes of E_{trac}, E_{diss}, and E_{regen} with respect to an increase of tire rolling resistance. 36

2.18 Absolute (top) and relative (bottom) changes of E_{trac}, E_{diss}, and E_{regen} with respect to an increase of the aerodynamic drag coefficient. 37

3.1 Overview of drivetrain configurations and power flows between the main components. Abbreviations: Electric motor (EM), electric generator (EG), fuel cell system (FCS), planetary gear set (PGS). 40

3.2 Simulation of the main power flows (left) and gasoline engine efficiency map (right) for a midsize ICEV passenger car driving the NEDC. On the right the engine operating points are indicated with red crosses between the engine efficiency isolines. . 41

3.3 Simulation of the main vehicle power flows (left), and a permanent magnet electric motor efficiency map with maximum torque curve and operating points (right) for a midsize BEV passenger car driving the NEDC. 42

3.4 Battery roundtrip efficiency as a function of average charging power and driving speed. 44

3.5 Fuel cell vehicle hydrogen use (left) and amount of energy stored in the battery (right) as a function of the degree of hybridization. 45

3.6 Traction efficiency of gasoline vehicles for the NEDC driving cycle sold in Switzerland in 2010 versus power-to-mass ratio. 50

3.7 Gasoline ICEV traction efficiency versus power-to-mass ratio and year. Discrete simulation results (red markers) are interpolated with surfaces for which the levels correspond to different driving regions: Highway (top), average (middle), urban (bottom). 52

3.8 Distribution of vehicle power, mass, direct CO_2 emission, and retail price for Germen new passenger car sales in 2011 by vehicle class. 54

3.9 Relation of vehicle mass versus CO_2 emission and power versus retail price separately for gasoline and diesel vehicles. 55

3.10 a) Model for the calculation of acceleration as a function of vehicle speed. b) Calculated and measured acceleration time versus power-to-mass ratio. 56

4.1 Illustration of the LCIA steps related to climate change. 66

5.1 Vehicle criteria for the baseline scenario by year and powertrain technology. 78
5.2 Variation of vehicle mass, energy use, and cost as a function of range by drivetrain and year. 79
5.3 Variation of vehicle mass and energy use as a function of glider mass by drivetrain and year. 80
5.4 Variation of vehicle mass and energy use as a function of range and glider mass by drivetrain in 2012. The red surface corresponds to the BEV, blue to the FCV, and gray to the ICEV. 80
5.5 Comparison of the scaling of vehicle mass and energy use with range and glider mass for models A and B. 82
5.6 Total cost difference between, ICEV, BEV, and FCV as a function of important parameters. The red line indicates equal total costs. 84
5.7 Sensitivity of vehicle mass, energy use, and total cost relative to variations of important parameters. 86
5.8 Comparison of the sensitivity of total cost to changes of important parameters by powertrain and year. 87
5.9 Probability density function of input parameters and resulting BEV criteria in 2030. 88

6.1 Analysis framework: Technical, cost, and environmental indicators for current and future passenger cars are calculated from a given set of exogenous options. 91
6.2 Breakdown of vehicle mass, purchase cost, and energy use by drivetrain for a midsize car in 2012. 96
6.3 Breakdown of vehicle mass, purchase cost, and energy use by drivetrain and class for 2012. 97
6.4 Breakdown of vehicle mass, purchase cost, and energy use by drivetrain for a midsize car from 2012 to 2050. 98
6.5 Energy use by drivetrain and driving cycle in 2012 for the average WLTP driving cycle and its low-speed urban part. 99
6.6 Mid-point indicators by drivetrain and energy source for a midsize car in 2012. . . 101
6.7 Mid-point indicators by drivetrain, energy source, and year for a midsize car. . . . 102
6.8 End-point indicators by drivetrain and energy source for a midsize car in 2012. . . 104
6.9 End-point indicators by drivetrain, energy source, and year for a midsize car. . . . 105
6.10 Development of total costs vs. life cycle GHG emissions and metal vs. fossil depletion for a midsize passenger car in three time steps from 2012 to 2050 (different points in time are connected by a line). 107
6.11 MCDA weighting profiles analyzed. 110
6.12 MCDA result for weighting profiles A to C. 113
6.13 MCDA result for weighting profiles D to F. 114
6.14 Matlab user interface for vehicle indicator analysis. 116
6.15 Screenshots of the multi-indicator analysis (a) and MCDA (b) webtools. 117

7.1 Vehicle mass (a,b) and energy consumption (c) for the ICEV and BEV-200 as a function of variable glider mass reduction. . . . 122
7.2 Total-to-primary BEV weight reduction as a function of vehicle electric range and battery specific energy. . . . 123
7.3 Lightweighting manufacturing cost increase relative to steel. Shown are literature data (circles) and a low, average, and high lightweighting cost function. . . . 124
7.4 Effect of lightweighting on ICEV total cost for a) 150,000 and b) 300,000 vkm. Black points indicate optimal levels of lightweighting minimizing manufacturing and total costs. . . . 126
7.5 Optimal weight reduction minimizing ICEV total cost as a function of lifetime driving distance for different lightweight cost functions. b) Corresponding total cost reduction. . . . 126
7.6 a) Optimal weight reduction (indicated in % in the legend) to minimize total cost of an ICEV as a function of fuel price and driving distance. b) Corresponding total cost reduction (in $). . . . 127
7.7 BEV total cost as a function of variable glider mass reduction for a) 200 km and b) 400 km range. Black points indicate optimal levels of lightweighting minimizing manufacturing and total costs. . . . 128
7.8 a) Optimal weight reduction minimizing BEV total cost as a function of vehicle range. b) Corresponding total cost reduction. . . . 128
7.9 a) Optimal weight reduction (in %) minimizing BEV total cost as a function of specific battery cost and vehicle range. b) Corresponding total cost reduction (in $). . . . 129

8.1 Comparison of the development of average new passenger car characteristics in Switzerland and Europe from 2001 to 2010. . . . 132
8.2 Development of new passenger vehicle sales in Switzerland by class for gasoline and diesel cars. . . . 133
8.3 Specific CO_2 emissions from new Swiss passenger cars as a function of vehicle mass. The sales weighted fits for 1998 and 2012 are compared to the LVC for 2015 and 2020. . . . 134
8.4 Development of the slope of a sales weighted fit for the Swiss and EU passenger car market relative to slope of the LVC. . . . 136
8.5 Gasoline, diesel, and new fleet average characteristics in Switzerland from 2000 to 2012. . . . 137
8.6 Sales share by fuel technology in Switzerland from 2000 to 2012. . . . 138
8.7 Distribution of sales and average specific emission by mass category for all new vehicles sold in 2000 and 2012. . . . 140
8.8 Effect of a change of efficiency and mass to total CO_2 emission reduction for (a) gasoline and (b) diesel vehicles. Abbreviations: Lasp=Laspeyres decomposition, Agg=Aggregated data model. . . . 143
8.9 Decomposition of CO_2 emission from gasoline and diesel vehicles by the contributions from a change of efficiency, mass, and fuel. . . . 144

8.10 a) Decomposition of the shift from gasoline to diesel into the effects of efficiency improvement and mass. b) Potential fleet emission reduction at constant mass. . . 145
8.11 Future sales share by powertrain for (a) Diesel and (b) Diesel + EV scenario. 147
8.12 Specific CO_2 emissions from Swiss new vehicles for different scenarios from 2012 to 2020. Red markers indicate the definitive target for 2015 and as it is proposed for 2020. 148
8.13 Swiss vehicle stock from 1990 to 2013 by fuel type (left) and year of first registration (right). 150
8.14 Overview of passenger car fleet model. 150
8.15 Swiss vehicle stock over time (left) and inferred survival probability (right). 151
8.16 Future sales shares by powertrain for the different scenarios analyzed. 153
8.17 Average specific CO_2 emission by class for Swiss new gasoline vehicles from 2001 to 2011. 154
8.18 Passenger car stock by drivetrain in the four sales scenarios considered. 155
8.19 Distribution of total travel performance by drivetrain in the four sales scenarios considered. 156
8.20 Fleet energy use by drivetrain in the case of constant vehicle resistance characteristics (scenario A). 157
8.21 Fleet energy use by energy carrier in 2012, 2030, and 2050. 158
8.22 Fleet WtW GHG emissions by energy carrier in 2012 and 2050 158

List of Abbreviations

Advisor	Advanced vehicle simulator
ARE	Swiss Federal Office for Spatial Development
ASTRA	Swiss Federal Roads Office
BAFU	Swiss Federal Office for the Environment
BEV	Battery electric vehicle
BFE	Swiss Federal Office of Energy
BFS	Swiss Federal Office of Statistics
CADC	Common Artemis driving cycle
CD	Charge depleting
CHF	Swiss Franc
CG	Coal gasification
CI	Compression ignition
CNG	Compressed natural gas
CO	Carbon monoxide
CO_2	Carbon dioxide
COP	Coefficient of performance
CCS	Carbon Capture and Storage
CS	Charge sustaining
d	day
DALY	disability-adjusted life years
EC	European Commission
EOL	End of life
EU	European Union
EV	Electric vehicle
FCV	Fuel cell vehicle
FCEV	Fuel cell electric vehicle
FCHEV	Fuel cell hybrid electric vehicle
GDP	Gross domestic product
GHG	Greenhouse gas
GUI	Graphical user interface
GWP	Global warming potential

H_2	Hydrogen
HEV	Hybrid electric vehicle
HEV-c	CNG fueled hybrid electric vehicle
HEV-d	Diesel fueled hybrid electric vehicle
HEV-g	Gasoline fueled hybrid electric vehicle
HSS	High-strength steel
ICE	Internal combustion engine
ICEV	Internal combustion engine vehicle
ICEV-c	CNG fueled internal combustion engine vehicle
ICEV-d	Diesel fueled internal combustion engine vehicle
ICEV-g	Gasoline fueled internal combustion engine vehicle
IEA	International Energy Agency
IPCC	Intergovernmental Panel on Climate Change
LCA	Life cycle assessment
LCIA	Life cycle impact assessment
Li-ion	Lithium ion
LVC	Limit value curve
MCDA	Multi-criteria decision analysis
MIT	motorized individual transport
MPV	Multi-purpose vehicle
Mtoe	Million-ton of oil equivalent
NEDC	New European Driving Cycle
NG	Natural gas
NGCC	Natural Gas Combined Cycle
NREL	National Renewable Energy Laboratory
NO_x	Nitrogen oxides
OECD	Organization for Economic Co-operation and Development
OEM	Original equipment manufacturer
PHEV	Plug-in hybrid electric vehicle
PHEV-c	CNG fueled plug-in hybrid electric vehicle
PHEV-d	Diesel fueled plug-in hybrid electric vehicle
PHEV-g	Gasoline fueled plug-in hybrid electric vehicle
PHEV-h	Hydrogen fueled plug-in hybrid electric vehicle
PID	Proportional-integral-derivative control
PM	Particulate matter
PT	Public transport
PV	Photovoltaic
QSS	Quasi-steady state
SI	Spark ignition
SMR	Steam methane reforming

SO_2	Sulfur dioxide
SOC	State-of-charge
SUV	Sport utility vehicle
TtW	Tank-to-Wheel
UCTE	Union for the Co-ordination of Transmission of Electricity
US	United States
US$	United States dollar
VAT	Value-added tax
vkm	Vehicle kilometer
WBCSD	World Business Council for Sustainable Development
WEC	World Energy Council
WEF	World Economic Forum
WLPT	Worldwide harmonized light vehicles test procedure
WtW	Well-to-Wheel
y	year

List of Symbols

A, B, C	Driving cycle parameterization coefficients (traction phase)
A', B', C'	Driving cycle parameterization coefficients (regeneration phase)
AD	Annual driving distance
A_f	Vehicle frontal area
a	Vehicle acceleration
CC_{es}	Constant cost of energy storage and powertrain
CC_{es}	Constant cost of energy storage
CC_{pt}	Constant cost of powertrain
CF_{es}	Configuration matrix for energy storage
CF_p	Configuration matrix for power devices (continuous power scaling)
CF_{pm}	Configuration matrix for power devices (acceleration scaling)
CM	Constant mass of energy storage and powertrain
CM_{es}	Constant mass of energy storage
CM_{pt}	Constant mass of powertrain
c_1, c_2, c_3, c_4	Powertrain efficiency regression coefficients
c_d	Aerodynamic drag coefficient
c_r	Rolling resistance coefficient
DR	Discount rate
E	Vehicle mechanical energy demand per distance
E_{diss}	Dissipative energy demand
E_{nr}	Energy demand without recuperation
E_{pr}	Energy demand with perfect recuperation
E_{regen}	Regenerative energy demand
E_{trac}	Tractive energy demand
EC	Vehicle energy consumption per distance
EC_0	Energy consumption independent of vehicle parameters
$\frac{\partial EC}{\partial A_f}$	Sensitivity of energy consumption to a change of frontal area
$\frac{\partial EC}{\partial m}$	Sensitivity of energy consumption to a change of mass
EP	Energy price
F_a	Aerodynamic drag force
F_g	Gravitational force

F_k	Inertial force
F_r	Rolling resistance force
F_w	Force at the wheel
g	Gravity of earth
LT	Vehicle lifetime
M_{avg}	Fleet average mass
MC	Manufacturing cost
MC_{es}	Manufacturing cost of energy storage
MC_{gl}	Manufacturing cost of glider
MC_{pt}	Manufacturing cost of powertrain
m	Vehicle static mass
m_e	Vehicle equivalent mass
m_{es}	Energy storage mass
m_{gl}	Glider mass
$m_{gl,var}$	Variable glider mass
$m_{gl,fix}$	Fixed glider mass
m_{pt}	Powertrain mass
P_a	Aerodynamic drag power
P_{bat}	Battery power
P_{cont}	Maximum continuous power demand
P_k	Kinetic (ac-/deceleration) power
P/m	Power-to-mass ratio
P_{max}	Maximum power
P_r	Rolling friction power
PP	Purchase price
p	Tire pressure
R	Vehicle range
RP	Regeneration potential
S	MCDA score
SC_{es}	Specific cost of energy storage
SC_{pt}	Specific cost of powertrain
SE	Specific CO_2 emissions
SE_{avg}	Fleet average specific CO_2 emissions
SE_{LVC}	Permitted specific CO_2 emissions according to the limit value curve
ΔSE_{eff}	Change of specific emission due to change of efficiency
ΔSE_{fuel}	Change of specific emission due to change of fuel type
ΔSE_{mass}	Change of specific emission due to change of mass
SM_{es}	Specific mass of energy storage
$SM_{pt,p}$	Specific mass of powertrain (continuous power scaling)
$SM_{pt,pm}$	Specific mass of powertrain (acceleration scaling)

SP	Survival probability
s	Slope of the limit value curve
T	Total duration of the driving cycle
TC	Total cost
TP	Technology performance
t_0	Acceleration time
V	Indicator value
v	Vehicle velocity
v_{max}	Top speed
w	MCDA weight
x_{tot}	Total length of the driving cycle
α	Road inclination angle
γ	Glider structural support factor
δ	Amount of variable glider mass reduction
η	Average operating point efficiency
η_{bat}	Battery efficiency
η_{dc}	DC/DC converter efficiency
η_{eng}	Engine efficiency
η_{fcs}	Fuel cell system efficiency
η_{gen}	Generator efficiency
η_{mot}	Electric motor efficiency
η_{regen}	Regeneration efficiency
$\eta_{regress}$	Powertrain efficiency calculated based on regression
η_{trac}	Traction efficiency
η_{trans}	Transmission efficiency
κ	Regeneration fraction
ρ	Density of air

Chapter 1

Introduction

1.1 Background and problem

In 2010, the global transport sector consumed approximately 2200 million tonnes of oil equivalent (Mtoe), accounting for about 19 % of world's primary energy demand [WEC, 2011; WEF, 2011; IEA, 2012a]. Transport is highly dependent on fossil fuels, in fact 96 % of transport energy demand is supplied by oil (see Fig. 1.1, left), which corresponds to more than 50 % of global oil consumption. Within the transport sector, road transport accounts for about 73 % of energy use and consumed approximately 35 million barrels (mb) of oil per day in 2011 [WEF, 2011; IEA, 2012b]. As shown in Fig. 1.1 on the right, light duty vehicles (including cars, minibuses, and light trucks) represent 52 % of transport energy use, freight trucks 17 %, and buses 4 %.
Since the rise of motor vehicle fleets in Western countries in the 1950's, global oil consumption has continuously increased, except for interruptions such as the oil crisis in 1979. From 1971 to 2006, world transport energy use more than doubled, with the strongest absolute growth from road transport (see Fig. 1.2).
The two main drivers for this increasing energy demand were economic and population growth [WEC, 2011; IEA, 2009]. As shown in Fig. 1.3, vehicle ownership and average income are closely related. Above a GDP per capita of about 5000 $, vehicle ownership rises continuously and flattens at higher income levels. In 2005, there were 424 passenger cars per 1000 inhabitants in Europe, 710 in the United States, and 111 for the world on average [IEA, 2009].
Considering future expected economic and population growth, the International Energy Agency (IEA) assumes that the global passenger car fleet will grow from about 870 million cars in 2011 to 1.7 billion cars in 2035 [IEA, 2012b]. As shown in Fig. 1.4, most of the growth of motorized individual traffic is expected in China and India, while the increase in OECD countries will be only moderate. Despite the strong increase of passenger cars in non-OECD countries, the vehicle ownership rate in China and India is expected to remain significantly below the level in the

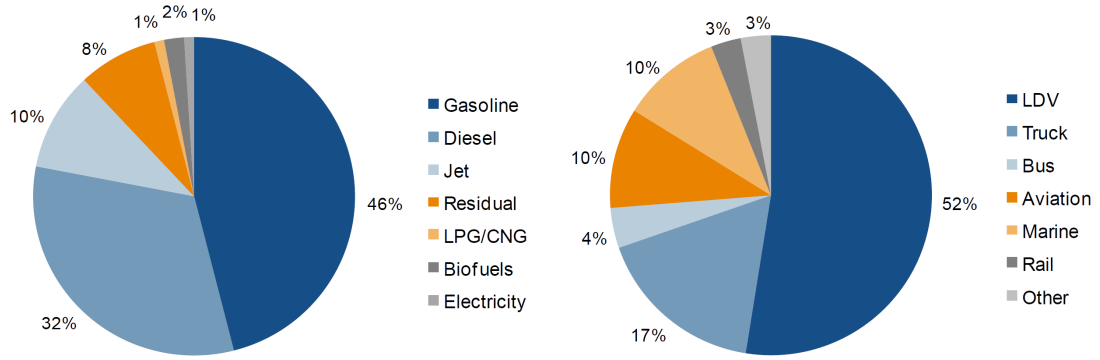

Figure 1.1: Global 2010 transport energy use by source (left) and mode (right) [WEC, 2011].

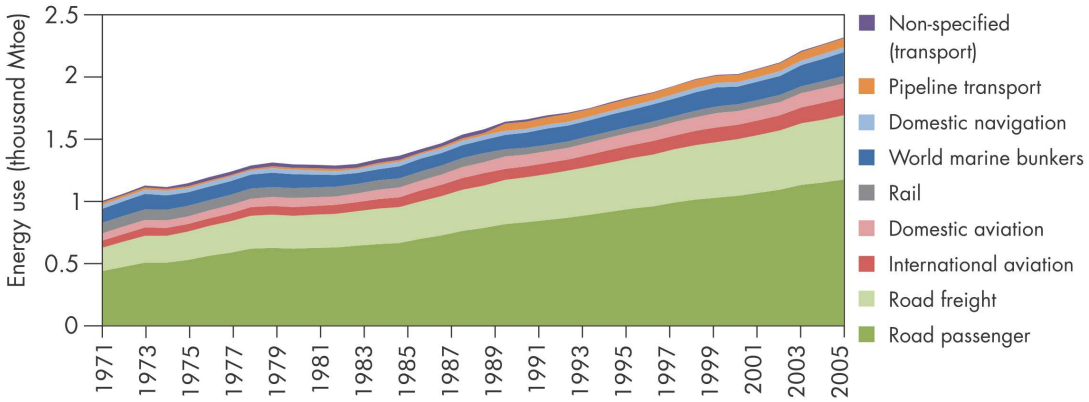

Figure 1.2: Global transport energy use by mode from 1971 to 2006 [IEA, 2009].

United States or Europe, in part due to lack of road infrastructure and environmental problems [IEA, 2012b]. Many other studies also expect a significant growth of transport demand in the coming years, in particular in non-OECD countries [WEC, 2011; WEF, 2011; WBCSD, 2004].

C:/Users/Administrator/Desktop/Hofer/ETHZ/PhD/thesis/

The increase of transportation demand and the high dependence on fossil oil as the primary transport energy source create serious environmental, economic, and social problems challenging future sustainable development.

Due to the uneven distribution of oil resources and demand, most countries rely on imported crude oil and refined oil products. Today, conventional crude oil is mainly extracted in the Middle East (Saudi Arabia, Iran, Iraq, Kuwait, and Qatar account together for 27 % of world's oil produc-

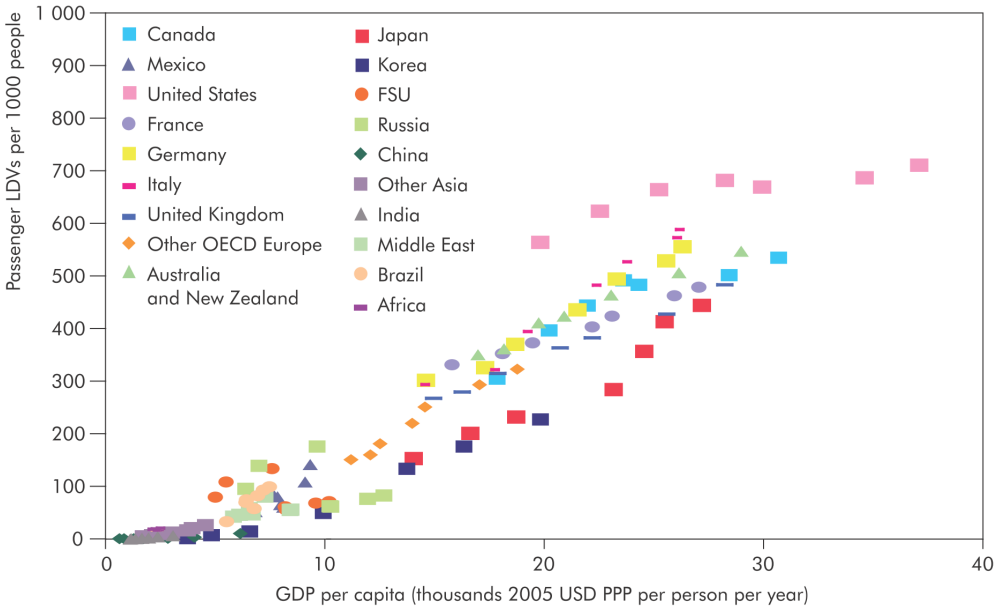

Figure 1.3: Passenger car ownership as a function of the average income per capita in several countries from 1970 to 2005 [IEA, 2009].

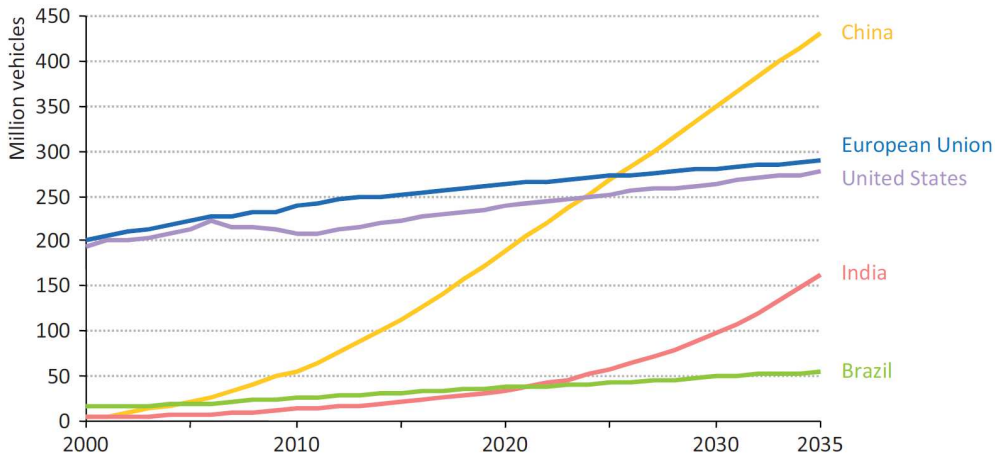

Figure 1.4: Passenger car fleet scenario from 2000 to 2035 in selected regions according to [IEA, 2012b].

tion in 2012 [BP, 2013]), North America (United States, Canada, and Mexico for 17.5 %), Russia 12.8 %, Africa (Nigeria, Lybia, Angola, Algeria for 8.4 %), South America (Venezuela, Brazil, and Colombia for 7.3 %), Europe and Eurasia (Norway, Kazakhstan, and Azerbaijan for 5.2 %), and China for 5%. On the other hand, the United States, China, Japan, and India consumed 19.8 %, 11.7 %, 5.3 %, and 4.2 %, respectively. Although some countries aim to reduce their shares of imported oil, dependence on oil imports is expected to become more severe in the future in average. According to IEA estimates, inter-regional oil trade could increase by about 20 % from 2011 to 2035. Over this time period, oil net-imports will grow particularly in China and India from 4.9 mb/d to 12.3 mb/d and from 2.5 mb/d to 6.9 mb/d, respectively. By contrast, imports in the United States are expected to decrease from 9.5 mb/d to 3.4 mb/d, due to increasing domestic production and improved transport efficiency [IEA, 2012b].
Proven oil reserves, i.e. reserves having a high probability (usually 90 %) to be recovered with existing technology, under current economic and political conditions, are estimated to be on the order of 1600 billion barrels at the end of 2011 [BP, 2013; IEA, 2012b]. Assuming constant future production at today's level (86 mb/d in 2012 [BP, 2013]), the reserves-to-production ratio is on the order of 50 years. Ultimately recoverable resources are much higher, but generally these sources also involve higher production costs and are not yet economically viable. The IEA estimates recoverable resources to be on the order of 5900 billion barrels, with the majority being unconventional oil, including 32 % oil sands and extra-heavy oil, and 18 % kerogen oil (or oil shale). 45 % of conventional resources are in offshore fields, of which about one quarter is expected to be in deep water (in excess of 400 meters depth) [IEA, 2012b]. Due to the increasing oil demand and the declining production from present reserves, the oil production from unconventional sources and in deep water is expected to increase. For example, IEA projects that oil extraction from Canadian oil sands will more than double from 1.6 mb/d in 2011 to 4.3 mb/d in 2035, and that deep water production will augment from 4.8 mb/d in 2011 to 8.7 mb/d in 2035 [IEA, 2012b]. The rising share of unconventional and deep water oil is expected to increase the costs, risks, and environmental impacts of future oil production. Higher volatility of oil prices in recent years [Murray & King, 2012] has exacerbated these concerns.

Due to its reliance on fossil fuels, the transport sector is also a major source of carbon dioxide (CO_2) emissions, the largest driver of global climate change [IPCC, 2013]. In 2011, transport emitted 7 Gt of CO_2 or 22 % of global CO_2 emissions from fossil fuel combustion, compared with electricity and heat production (42 %) and industry (21 %) [IEA, 2013a; Tran et al., 2012]. In addition, emission of air pollutants from road transport such as sulphur dioxide (SO_2), nitrogen oxides (NOx), carbon monoxide (CO), and particulate matter (PM) is an urgent problem in many countries, particularly in urban areas [Takeshita, 2011]. For example, air pollution in Beijing and Paris increasingly reaches levels that may have harmful impacts on the general public, resulting in restricted motor vehicle usage.

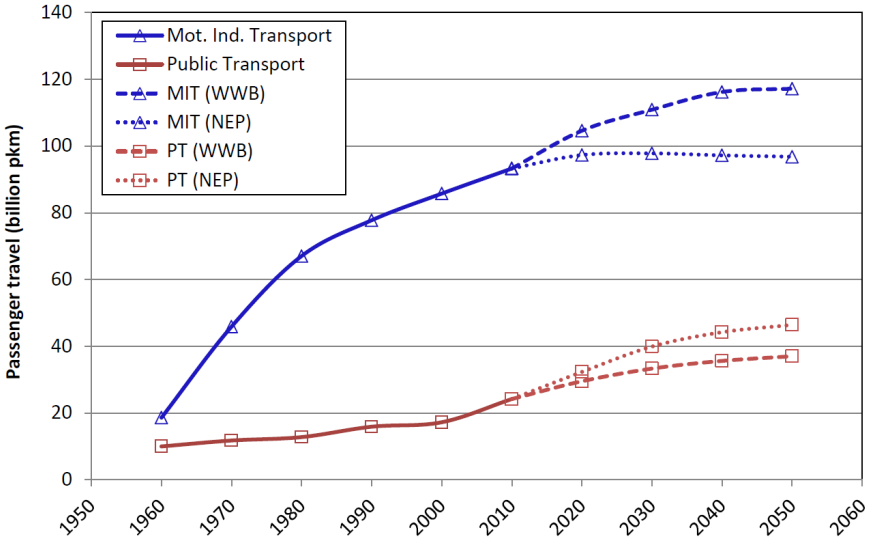

Figure 1.5: Historic and projected Swiss passenger travel distance by mode from 1960 to 2050.

Due to the high influence of road transport on climate change and local air quality several countries have implemented standards limiting vehicle emissions of CO_2 and air pollutants. This includes for example the EU regulations setting CO_2 and pollutant emission limits for new passenger cars.

In Switzerland, about two third of personal mobility in terms of passenger kilometers (pkm) traveled is currently based on gasoline and diesel passenger cars. In 2010, 66.4 % of the average daily travel distance per person is provided by motorized individual transport (MIT), 23.4 % by public transport (PT), and 10.2 % by other modes [BFS, 2012].[1] From 1994 to 2010, the average daily travel distance per person has continuously risen from 31.3 km to 36.7 km. In the same period, the share of PT increased from 17.8 % to 23.4 % and the share of MIT decreased from 69.7 % to 66.4 %. There has also been a decline in the possession of driver's licenses among young people (18-24 years) from 70.7 to 58.7 [BFS, 2014].

Fig. 1.5 shows the development of the Swiss passenger travel distance by PT and MIT from 1960 until today [BFS, 2014]. Two additional scenarios to 2050 are shown according to [Prognos, 2012; ARE, 2006]. The WWB (Weiter wie bisher - Business as usual) and the NEP (Neue Energiepolitik - New energy policy) scenario project an increase of the absolute travel distance by about 31 % and 22 %, respectively. In both scenarios the modal split shifts from individual road to public rail transport, but more strongly in the NEP scenario. Despite this shift, passenger cars are expected to remain the dominant mode of passenger transport in the future.

[1] MIT can be split further down into 65 % traveled with passenger cars and 1.4 % with motorcycles, PT into 19.3 % railway and 4.1 % by bus/tram, and other into 5.5 % pedestrian, 2.1 % bicycle, and 2.6 % other.

From 1990 to 2012, the share of CO_2 emissions from transport continuously increased from 38 % to 45 % of total Swiss CO_2 emissions [BAFU, 2014]. While pollutant emissions from the Swiss passenger car fleet are expected to strongly decrease until 2035 due to an increasing share of vehicles in the fleet that fulfill new emission standards, further reductions of fuel use and CO_2 emissions are limited without significant changes in past trends [BAFU, 2010; Infras, 2007]. Efforts to develop clean vehicle technologies are embedded in the EU framework to limit emissions of new vehicles to 130 grams CO_2 per kilometer by 2015, which has been ratified in the same form by the Swiss parliament.
Electric vehicle (EV) development in Switzerland is currently driven by local utilities, companies producing EVs or EV equipment (e.g. Brusa, Protoscar), and stakeholders starting new business models for marketing EVs (e.g. Migros). The basis for EVs in Switzerland is good: distances are short and people have a high willingness and ability to pay for mobility needs. Also the carbon footprint of Swiss electricity is relatively low, due to the high share of hydro and nuclear power. In Switzerland there are currently no direct financial incentives supporting electric mobility [IEA, 2013b].

1.2 Thesis scope and objective

The exact response of the global climate system to anthropogenic CO_2 as a forcing factor, and the timing of resource depletion and price increases may be in question. But the direction of these trends is clear - conventional solutions may yet serve a while, but there is a great need for sustainable alternatives for the long run.
Moving towards sustainability in the transportation sector is a challenging problem and requires dramatic changes in terms of vehicle petroleum use and greenhouse gas (GHG) emissions. Several options exist to reduce fuel consumption and CO_2 emissions, including reduction of vehicle travel distance (e.g. by shifting to other modes of transport, increasing the average number of vehicle occupants, or by reducing passenger travel distances in general) and technical options to reduce vehicle energy efficiency. The analysis in this thesis will focus on the latter, which includes among other options the reduction of vehicle resistance losses (due to mass, aerodynamic drag, and rolling friction), improvements of conventional vehicle efficiency, switching to alternative fuels, and electrification via hybrid or all-electric powertrains. However, these technologies enter the market incrementally and must meet performance, utility, and cost requirements to be accepted by consumers.

The objective of this thesis is to develop an integrated framework for the analysis and comparison of advanced vehicle technologies in terms technical, economic, and environmental criteria. The method to assess those criteria should be capable of covering

- a broad range of conventional and advanced electric powertrains
- different vehicle configurations in terms of size, performance, and range
- different primary energy sources
- interdependencies among vehicle configuration and technical characteristics
- future scenarios considering changes of component performance and cost, energy prices, reduction of vehicle resistances, and other scenario parameters

In addition, the method needs to be transparent and fast, allowing stakeholders to modify input assumptions, enabling interactive analysis, and the evaluation of aggregate fleet impacts.

The goal of this thesis is to create a fundamental understanding of the complex interactions between different powertrain technologies, configuration parameters, future developments, and the corresponding impacts on cost and environmental indicators. In particular, the thesis focuses on the following research questions:

- How do conventional and electric powertrains compare to each other in terms of energy use, costs, and environmental impacts?
- What are the fundamental drivers of vehicle mechanical energy demand?
- What are the influences of performance, range, and driving region on vehicle energy use and mass?
- How do changes of vehicle resistance parameters affect vehicle energy use and induce secondary effects?
- How can advanced technologies best be implemented to minimize vehicle costs and environmental impacts?
- How have past trends for size and performance influenced fuel use? And how can future emission targets be met?
- What are the expected fleet impacts from a high EV penetration scenario relative to a scenario based on conventional technology?

Compared to previous work, this thesis contains several novelties that are described throughout the text. To increase the accessibility of the method and results, several interactive analysis tools have been developed and implemented online. These tools are powerful instruments for communicating the diversity of results and involving stakeholders in e.g. multi criteria analysis.

This thesis was carried out within the project THELMA (TecHnology-centered ELectric Mobility Assessment), which has been performed by several research groups within the domain of the Swiss Federal Institutes of Technology and was funded by Swiss Electric Research, the Competence Center for Energy and Mobility, and the Swiss Erdöl Vereinigung. The goal of the THELMA project was to assess the technical, environmental and economic tradeoffs of electric vehicles compared to other drivetrain technologies. For this purpose, vehicle technology modeling (work package two - WP2) was coupled to life-cycle assessment (WP1) to assess and analyze the multi-criteria aspects of a broad range of current and future drivetrain and primary energy source options. This was extended with agent based transport system modeling (WP4) and electric vehicle penetration scenarios to determine the incremental loads on the electric grid (WP3). Fig. 1.6 shows the THELMA project framework. Further information on THELMA is available at: http://www.thelma-emobility.net/

The methods developed in this thesis primarily contributed to THELMA WP2 and WP5. The vehicle simulation results generated in WP2 were furthermore combined with life cycle analysis in WP1, which served as input to multi-criteria analysis and fleet impact assessment in WP5 and WP3.

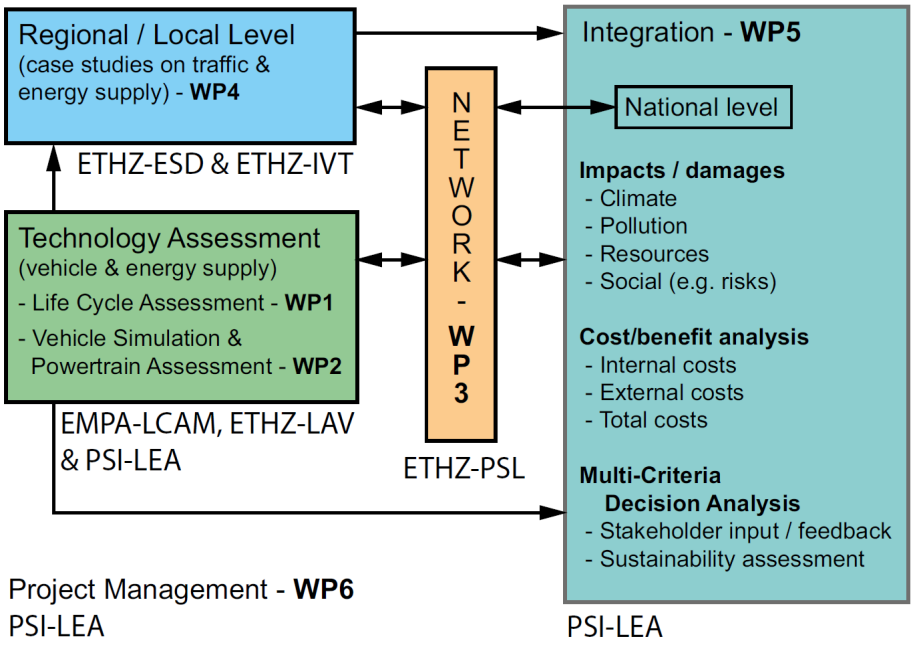

Figure 1.6: THELMA project framework with work package tasks and partners.

1.3 Outline

Chapter 2 introduces the method used for the calculation of vehicle mechanical energy demand and applies it to study the sensitivity of energy demand to changes of vehicle characteristics. In chapter 3, this approach is developed further to calculate energy consumption for various conventional and electric drivetrains. Chapter 4 describes the method and data used for the calculation of vehicle mass, cost, and life cycle indicators. In chapter 5, an analytic scaling method for vehicle energy use and mass as a function of configuration and technical parameters is presented and applied. Chapter 6 presents integrated results of vehicle criteria for a broad range of current and future passenger vehicles, combining different drivetrain technologies, primary energy sources, vehicle size and utility classes. It also shows results for multi-criteria decision analysis and the implementation of tools for interactive analysis. Chapter 7 applies the developed method to investigate the optimal degree of weight reduction (using lightweight technology) to minimize the total costs of conventional and electric vehicles. Chapter 8 closes with an analysis of past trends and potential future impacts of electric powertrains on the Swiss passenger car fleet in terms of energy use and GHG emissions. Chapter 9 concludes.

Chapter 2

Vehicle mechanical energy demand

Independent of the type of powertrain, every vehicle has to overcome certain forces acting on it, depending on its exterior characteristics (mass, frontal area, aerodynamic drag, rolling resistance coefficient) and the driving conditions. These forces consist of dissipative and conservative parts and can be integrated over a driving cycle to calculate mechanical energy demand.
The aim of this chapter is to first introduce in section 2.1 the main forces acting on a vehicle and to analyze mechanical energy demand as a function of different vehicle characteristics and driving cycles. Mechanical energy demand is split into dissipative and regenerative contributions which is among other things useful to assess the regeneration potential in different driving conditions. In section 2.2 the contributions to mechanical energy demand are parameterized as a function of vehicle characteristics and driving cycle coefficients. This approach will be used in chapter 3 to calculate vehicle energy use which takes additionally into account powertrain efficiency. In section 2.3 the sensitivity of mechanical energy demand to changes in vehicle characteristics is analyzed for different driving cycles.
Several previous studies have approached the calculation of mechanical energy demand in a similar way [Guzzella & Sciarretta, 2013; Sovran & Blaser, 2003; Sovran, 2013; Ott et al., 2013; Simpson, 2005; Gantt, 2011], and the work presented here has been influenced in particular by [Guzzella & Sciarretta, 2013]. Progress of the work presented here includes the full parameterization of the individual contributions to mechanical energy demand, including the separation into dissipative and regenerative energy demand, for many different driving cycles. In addition, the validity of the parameterization, in particular with regard to the decoupling of driving cycle coefficients and vehicle characteristics is studied for the first time.

2.1 Mechanical energy demand in driving cycles

2.1.1 Basic forces and operating modes of a vehicle

Any vehicle driving along the ground is subject to several conservative and non-conservative (or dissipative) forces. While dissipative forces are always greater than zero, conservative forces can be positive or negative. The main forces relevant for passenger vehicles are the following.

Conservative forces:

- *Inertial/kinetic force* F_k for acceleration and deceleration of the vehicle and its rotating parts

$$F_k = m_e \cdot a = m_e \cdot \dot{v} \tag{2.1}$$

  where m_e is the equivalent mass of vehicle static mass m and its rotational inertia, a is vehicle acceleration, and v is vehicle velocity. The equivalent mass is typically on the order of $m_e \approx 1.03 \cdot m$ [Sovran, 2013].

- *Gravitational force* F_g to reach higher or lower altitudes

$$F_g = m \cdot g \cdot \sin\alpha \tag{2.2}$$

  where g is the gravity of earth, and α the road inclination angle.

Dissipative forces:

- *Aerodynamic drag* F_a

$$F_a = \frac{1}{2} \cdot \rho \cdot A_f \cdot c_d \cdot v^2 \tag{2.3}$$

  where ρ is the density of air, A_f is the projected frontal vehicle area, and c_d is the aerodynamic drag coefficient. Generally Eq. 2.1.1 is an approximation, as c_d is dependent on vehicle velocity and the direction of wind flow. But in the speed range of standard driving cycles it can be assumed to be constant [Sovran, 2013]. Consideration of other effects such as crosswind sensitivity is only possible with specific measurements in a wind tunnel [Guzzella & Sciarretta, 2013] and beyond the scope of this analysis.

- *Rolling resistance* F_r

$$F_r = c_r \cdot m \cdot g \cdot \cos\alpha \tag{2.4}$$

  where c_r is the tire rolling resistance coefficient. Among other things c_r depends on the vehicle speed, tire pressure p, and road surface conditions. It increases approximately pro-

portional to $\frac{1}{\sqrt{p}}$ with tire pressure, decreases on wet and rough surfaces relative to dry and smooth surfaces, and increases slowly at lower and substantially at higher driving speed [Heisler, 2002; Guzzella & Sciarretta, 2013].

The sum of the forces in Eq. 2.1 to 2.4 is often called traction force, although it not only propels the car in traction phases but also delivers energy to the brakes or a recuperative device if negative. For this reason it is in the following work called the force at the wheel F_w

$$F_w = F_a + F_r + F_k + F_g \tag{2.5}$$

Power at the wheel P_w is in the following defined as

$$P_w = F_w \cdot v \tag{2.6}$$

P_w acts on the wheel axle and needs to be provided (if positive) by the mechanical drivetrain or is transferred (if negative) to a recuperative device or dissipated in the brakes. Depending on the value of P_w three operating modes can be distinguished:

- $P_w > 0$, *Traction:* The engine and/or electric motor generate a positive torque to propel the vehicle.
- $P_w = 0$, *Idling/Coasting:* The power at the wheel is zero if the vehicle stops or if conservative and dissipative forces balance each other. No positive or negative torque needs to be provided.
- $P_w < 0$, *Braking/Regeneration:* The power at the wheel is negative if the sum of kinetic and gravitational force is more negative than the sum of dissipative power terms is positive. The brakes and/or a recuperative device absorb the negative torque.

The conditions on F_w to distinguish traction, coasting, and regeneration mode are the same as for P_w, except that $F_w = 0$ is valid for coasting but not at rest (which is attributed to $F_w > 0$). For this reason the distinction of operating modes based on P_w is preferred and used in the following.

2.1.2 Driving cycles

Driving cycles are created by different countries and organizations to measure vehicle fuel economy and pollutant emissions under standardized conditions for vehicle homologation (type approval) or other test purposes. A driving cycle prescribes a speed versus time profile, most often on a flat road (without gradient). It is usually performed on a chassis dynamometer, a roller test bench which is equipped with an electric motor to imitate aerodynamic drag and vehicle inertia,

in the absence of wind disturbances, at pre-specified gear shifting and temperature conditions.
Generally there are two types of driving cycles: a) Steady state (or modal) driving cycles which involve several discrete speed and acceleration values with abrupt changes, and b) transient cycles which involve many continuous changes of velocity and correspond to more realistic driving patterns. Examples of modal cycles are the New European Driving Cycle (NEDC), used for emission certification in the European Union, and the Japanese 10-15 Mode cycle. Transient cycles include the FTP-75 (Federal Test Procedure) used in the United States and the Common Artemis Driving Cycle (CADC) which is based on a statistical analysis of European driving patterns [André, 2004]. Throughout the world vehicle test procedures vary significantly which makes vehicle certification expensive for manufacturers and difficult to compare. In addition, test procedures such as the NEDC, do not correspond to real world driving conditions and are considered to underestimate fuel use [Mock et al., 2012; BAFU, 2012]. Therefore many countries are collaborating within the United Nations Working Party on Pollution and Energy to develop a new worldwide harmonized light vehicles test procedure (WLTP). The WLTP is a transient driving cycle and based on statistical analysis of driving conditions from EU, India, Japan, Korea, Switzerland, and USA [ICCT, 2013b]. When finished it is expected to replace the NEDC for emission certification in Europe [BAFU, 2012]. In the following the main characteristics of the NEDC, CADC, and WLTP will be discussed further and used for simulations of vehicle energy use. The methods introduced are however also applicable to most other driving cycles.
As shown in Fig. 2.1 the entire NEDC consists of four repeated urban segments (ECE) and one extra-urban or highway segment (EUDC). Fig. 2.1 also clearly shows the discrete character of the speed and acceleration profile for the NEDC which is typical for a modal cycle. The transient CADC (Fig. 2.2) and WLTP (Fig. 2.3) cycles on the other hand show more continuous speed and acceleration profiles. Table 2.1, 2.2, and 2.3 present a summary of selected parameters for the NEDC, CADC, and WLTP, respectively. Also shown are the characteristics for urban, rural, and highway segments.
For the NEDC the top speed is 50 km/h in the urban part and 120 km/h in the highway part. The speed distribution for the NEDC given in Table 2.1 shows that a significant amount of time the vehicle is stopped, especially in urban driving. This leads to high auxiliary and idling losses especially for conventional vehicles not equipped with a start-stop system which turns the engine off while idling. Idling time is much shorter for the CADC and WLTP, but follows the same trend of longer idling periods in urban than in highway driving. Compared to the NEDC, the CADC and WLTP are characterized by higher speeds, especially for highway driving.
Even though average acceleration is similar for the NEDC and CADC (and slightly smaller for the WLTP), CADC and WLTP are characterized by more peak acceleration events, especially the urban part of the CADC. For all cycles, acceleration is higher in the urban than the highway segments. Deceleration follows a similar pattern to acceleration (only opposite in sign) for the

CADC and WLTP. By contrast, for the NEDC deceleration is on average higher than acceleration and lower in urban than highway driving due to strong deceleration at the end of the highway cycle.
The distribution of idling, traction, and braking/regeneration phases shows that urban driving is characterized by a higher share of braking/regeneration versus traction compared to highway driving. This trend is similar for all cycles, only the NEDC has a higher share of idling time.

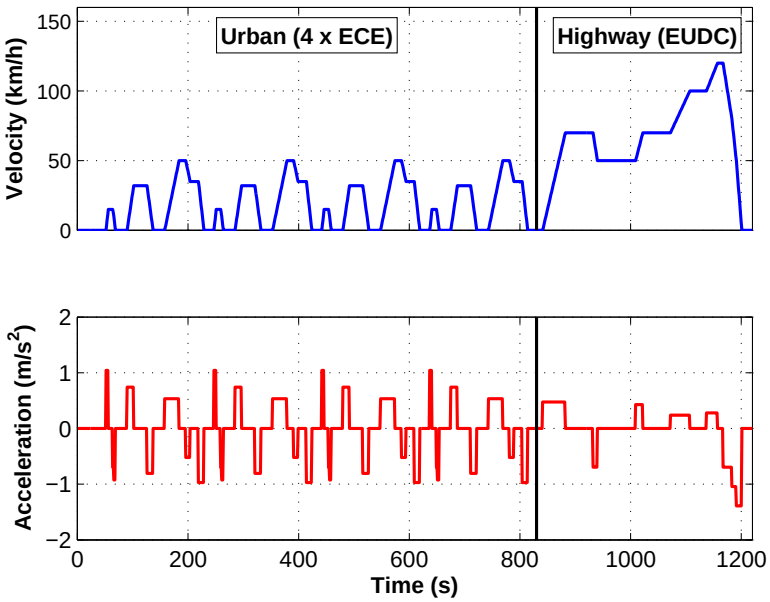

Figure 2.1: NEDC velocity and acceleration versus time.

Table 2.1: NEDC characteristics

	Unit	All	Urban	Highway
Distance	km	10.9	1.0	6.9
Total time	s	1220	205	400
Average driving speed	km/h	44.4	27.4	69.4
Maximum speed	km/h	120	50	120
Average acceleration	m/s^2	0.53	0.65	0.36
Average deceleration	m/s^2	-0.82	-0.79	-0.92
Speed distribution	%			
Stop (v = 0km/h)		27	36	10
Low speed ($0 < v \leq 50$)		52	64	27
Medium speed ($50 < v \leq 90$)		14	0	42
High speed ($v > 90$)		7	0	21
Acceleration distribution	%			
Low ($0 < a \leq 0.75$ m/s^2)		94	90	100
Medium ($0.75 < a \leq 1.5$)		6	10	0
High ($a > 1.5$)		0	0	0
Deceleration distribution	%			
Low ($0 > a \geq -0.75$ m/s^2)		36	29	57
Medium ($-0.75 > a \geq -1.5$)		64	71	43
High ($a < -1.5$)		0	0	0
Phase distribution (reference car)	%			
Stop/Coasting ($P_w = 0$)		27	36	10
Traction ($P_w > 0$)		58	48	79
Braking/Regeneration ($P_w < 0$)		15	17	11

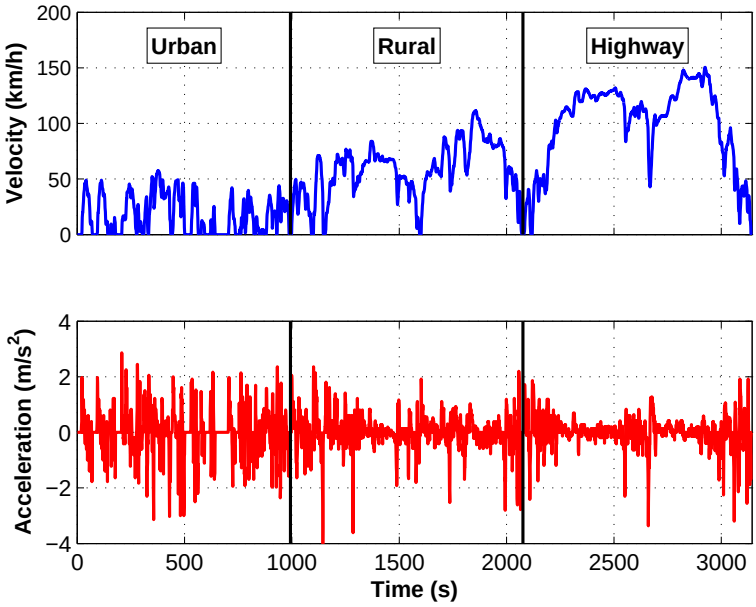

Figure 2.2: CADC velocity and acceleration versus time.

Table 2.2: CADC characteristics

	Unit	All	Urban	Rural	Highway
Distance	km	51.7	4.9	17.3	29.6
Total time	s	3143	993	1082	1068
Average driving speed	km/h	66.2	24.7	59.3	101.2
Maximum speed	km/h	150	58	112	150
Average acceleration	m/s^2	0.54	0.74	0.5	0.43
Average deceleration	m/s^2	-0.59	-0.78	-0.51	-0.5
Speed distribution	%				
Stop (v = 0km/h)		11	28	3	1
Low speed ($0 < v \leq 50$)		38	69	31	15
Medium speed ($50 < v \leq 90$)		25	2	59	13
High speed ($v > 90$)		26	0	7	70
Acceleration distribution	%				
Low ($0 < a \leq 0.75$ m/s^2)		75	60	78	84
Medium ($0.75 < a \leq 1.5$)		21	30	19	15
High ($a > 1.5$)		5	10	3	2
Deceleration distribution	%				
Low ($0 > a \geq -0.75$ m/s^2)		75	61	81	81
Medium ($-0.75 > a \geq -1.5$)		16	25	12	12
High ($a < -1.5$)		9	14	6	7
Phase distribution (reference car)	%				
Stop/Coasting ($P_w = 0$)		11	28	3	1
Traction ($P_w > 0$)		63	40	68	81
Braking/Regeneration ($P_w < 0$)		26	32	29	18

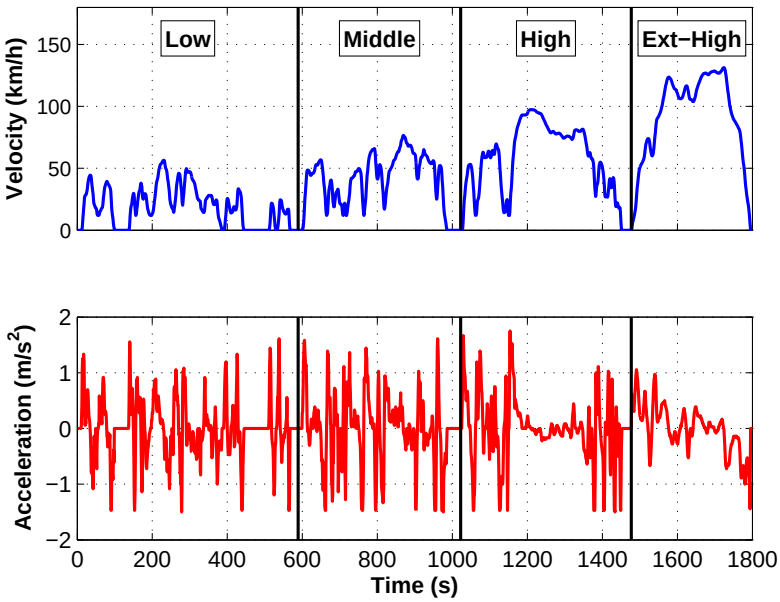

Figure 2.3: WLTP velocity and acceleration versus time.

Table 2.3: WLTP characteristics

	Unit	All	Low	Mid	High	Ext-high
Distance	km	23.3	3.1	4.8	7.2	8.3
Total time	s	1800	589	433	455	323
Average driving speed	km/h	53.5	25.4	44.5	60.7	94.1
Maximum speed	km/h	131	57	77	97	131
Average acceleration	m/s^2	0.43	0.49	0.45	0.44	0.31
Average deceleration	m/s^2	-0.44	-0.44	-0.55	-0.41	-0.34
Speed distribution	%					
Stop (v = 0km/h)		13	25	11	7	2
Low speed ($0 < v \leq 50$)		46	72	52	30	12
Medium speed ($50 < v \leq 90$)		27	3	37	50	23
High speed ($v > 90$)		15	0	0	14	63
Acceleration distribution	%					
Low ($0 < a \leq 0.75$ m/s^2)		81	76	79	78	92
Medium ($0.75 < a \leq 1.5$)		18	23	20	21	8
High ($a > 1.5$)		1	1	1	2	0
Deceleration distribution	%					
Low ($0 > a \geq -0.75$ m/s^2)		81	82	72	80	90
Medium ($-0.75 > a \geq -1.5$)		19	18	28	20	10
High ($a < -1.5$)		0	0	0	0	0
Phase distribution (reference car)	%					
Stop/Coasting ($P_w = 0$)		13	25	11	7	2
Traction ($P_w > 0$)		61	43	61	71	79
Braking/Regeneration ($P_w < 0$)		26	32	28	22	19

2.1.3 Contributions to mechanical energy demand

For a level road the power at the wheel is the sum of aerodynamic drag, rolling friction, and ac-/deceleration power

$$P_w = P_a + P_r + P_k \tag{2.7}$$

Mechanical energy demand per distance E can be calculated for a given driving cycle by integrating the power at the wheel over the entire cycle

$$E = \frac{1}{x_{tot}} \int_{t=0}^{T} P_w \, dt \tag{2.8}$$

where x_{tot} is the length and T the duration of the cycle. Note that in Eq. 2.8 it is assumed that perfect regeneration is possible. For a more detailed discussion it is useful to separate the contributions to the total energy demand into the tractive energy demand E_{trac} in traction phases

$$E_{trac} = \frac{1}{x_{tot}} \int_{P_w>0} P_w \, dt \tag{2.9}$$

regenerative energy E_{regen} in braking/regeneration phases

$$E_{regen} = \frac{1}{x_{tot}} \int_{P_w<0} P_w \, dt \tag{2.10}$$

and dissipative energy E_{diss} of aerodynamic drag and rolling resistance for the entire cycle

$$E_{diss} = \frac{1}{x_{tot}} \int_{t=0}^{T} (P_a + P_r) \, dt \tag{2.11}$$

This separation can be better understood by looking at Fig. 2.4 which shows the contributions of aerodynamic drag, rolling friction, and ac-/deceleration power to the power at the wheel for the NEDC and WLTP driving cycles for a reference midsize passenger car with the characteristics as listed in Table 2.4. Tractive energy demand represents the sum of all power terms in cases for which the total power at the wheel is positive and regenerable energy the sum of all power terms in cases for which the total power is negative. Dissipative energy is the sum of aerodynamic drag and rolling resistance over the entire cycle. Note that E_{regen} is negative and that it is also called circulating energy [Guzzella & Sciarretta, 2013; Ott et al., 2013] because it is temporarily stored as kinetic energy and available at the wheels during braking/regeneration periods.

Table 2.4: Reference car characteristics.

c_r	0.01
A_f (m^2)	2.1
m (kg)	1500
c_d	0.3

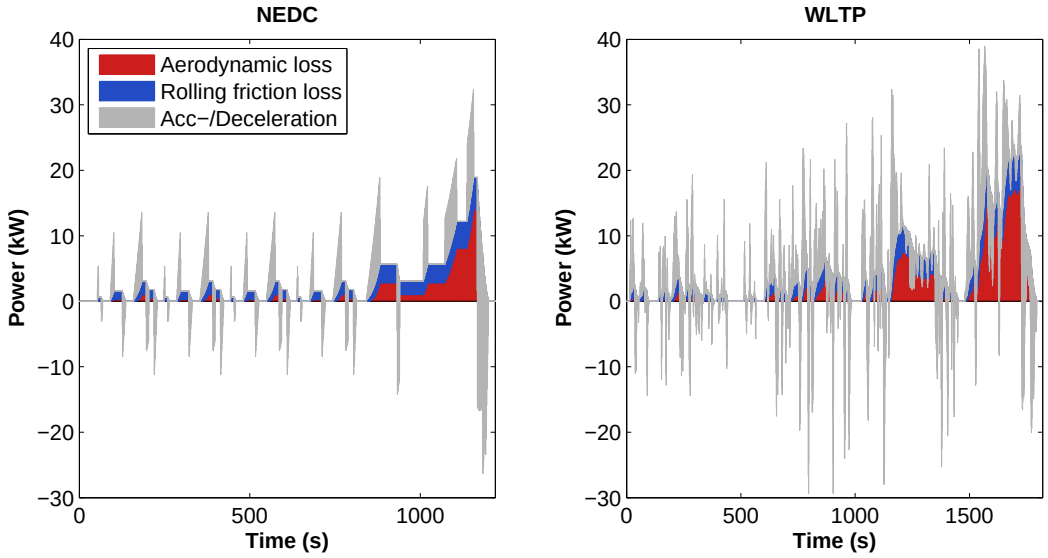

Figure 2.4: Contributions to the power at the wheel for the NEDC and WLTP driving cycles.

If the velocity at the beginning and the end of a driving cycle is zero and no elevation profile is considered, the integral of ac-/deceleration power over an entire cycle is zero

$$\int_{t=0}^{T} P_k \, dt = \int_{P_w>0} P_k \, dt + \int_{P_w<0} P_k \, dt = 0 \tag{2.12}$$

Aerodynamic drag and rolling resistance are always positive, which means that not all the kinetic energy during acceleration $\int_{P_k>0} P_k \, dt$ is available as negative power at the wheel in regeneration phases. Part of the energy from deceleration is spent to overcome aerodynamic drag and rolling friction in regeneration phases.

When analyzing the total mechanical energy demand for a vehicle over a specific driving cycle, it is useful to distinguish the cases in which regeneration is possible and those in which it is not [Guzzella & Sciarretta, 2013]. In the hypothetical case in which all regenerable energy is recuperated (perfect regeneration), mechanical energy demand E_{pr} can be calculated by integrating the

power at the wheel over the entire cycle which yields

$$ED_{pr} = \frac{1}{x_{tot}} \int_{t=0}^{T} P_w \, dt \tag{2.13}$$

$$= \frac{1}{x_{tot}} \int_{t=0}^{T} (P_a + P_r) \, dt + \frac{1}{x_{tot}} \int_{t=0}^{T} P_k \, dt \tag{2.14}$$

$$= E_{diss} \tag{2.15}$$

Since $\int_{t=0}^{T} P_k \, dt$ is zero (Eq. 2.12) it is equal to the dissipative energy. In the case that no regeneration is possible, mechanical energy demand E_{nr} is calculated as the integral of P_w during traction periods

$$ED_{nr} = \frac{1}{x_{tot}} \int_{P_w>0} P_w \, dt \tag{2.16}$$

$$= E_{trac} \tag{2.17}$$

Alternatively E_{nr} can be written as

$$ED_{nr} = \frac{1}{x_{tot}} \int_{P_w>0} P_w \, dt \tag{2.18}$$

$$= \frac{1}{x_{tot}} \left(\int_{P_w>0} (P_a + P_r) \, dt + \int_{P_w<0} (P_a + P_r) \, dt - \int_{P_w<0} (P_a + P_r) \, dt + \int_{P_w>0} P_k \, dt \right) \tag{2.19}$$

$$= E_{diss} - \frac{1}{x_{tot}} \left(\int_{P_w<0} (P_a + P_r) \, dt + \int_{P_w<0} P_k \, dt \right) \tag{2.20}$$

$$= E_{diss} - E_{regen} \tag{2.21}$$

In the last step $\int_{P_w>0} P_k \, dt$ is replaced by $\int_{P_w<0} -P_k \, dt$ according to Eq. 2.12. In summary this means that for perfect regeneration mechanical energy demand is equal to dissipative energy and if no regeneration is possible mechanical energy demand is equal to the difference of dissipative and regenerable energy (which is of course more than for perfect regeneration as E_{regen} is negative).

2.1.4 Comparison of energy demand for different driving cycles

After the basic principles of vehicle mechanical energy demand have been introduced, it is now interesting to compare the contributions to the mechanical energy demand for the different driving cycles discussed in Section 2.1.2.
Fig. 2.5 shows the mechanical energy demand of a midsize passenger car as defined in Table 2.4 for those different driving cycles. For each cycle the contributions of aerodynamic drag, rolling friction, and ac-/deceleration to tractive and regenerable energy are shown. The tractive energy must be provided by any drivetrain technology during traction mode, part of the regenerable energy can be recovered if recuperation is possible. The individual contributions to tractive and regenerable energy are positive, except for the kinetic energy in regeneration mode, which is equal and opposite to the kinetic energy in traction mode. It is clearly visible that only a part of the kinetic energy can be regenerated because some of it is lost due to aerodynamic drag and rolling resistance.

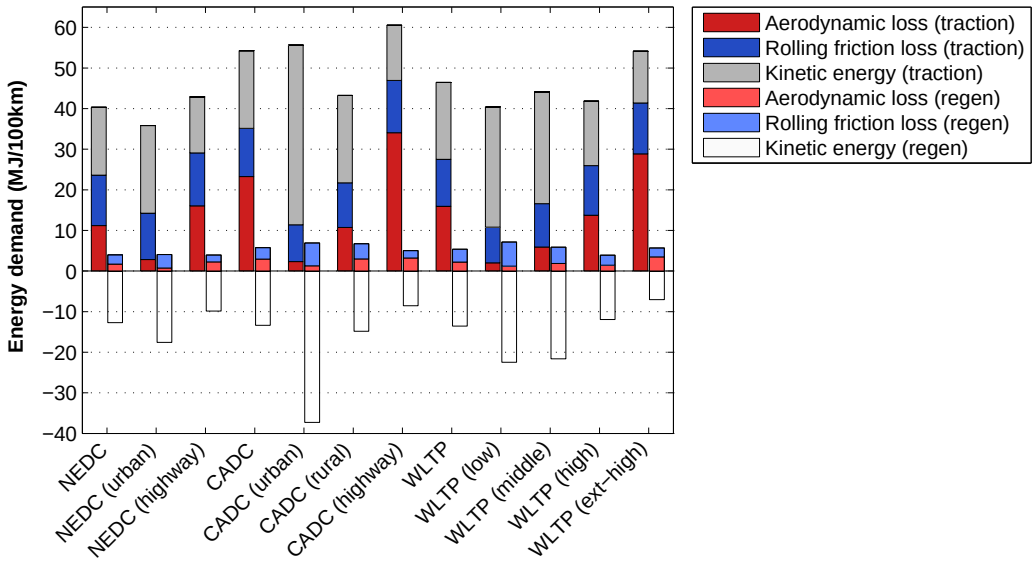

Figure 2.5: Mechanical energy demand of a midsize passenger car for different driving cycles. For each cycle the contributions to tractive (left) and regenerable (right bar) energy are shown.

Fig. 2.6 shows the mechanical energy demand for the same car and driving cycles, but now summing up the dissipative power in the traction and regeneration phases (blue and red colors) and the regenerable kinetic energy (white). The sum of dissipative loss and regenerable energy must be provided by any vehicle during traction phases. In regeneration phases with negative power at the wheel, regenerable energy can be partly recovered by vehicles with a recuperative device.

In the ideal case of perfect recuperation only the dissipative energy needs to be provided. For vehicles without recuperation capability, regenerable energy is dissipated in friction brakes.
Fig. 2.5 and 2.6 show that tractive energy demand is generally highest for highway driving, followed by urban driving, and lowest for rural driving. For urban driving the dominating contribution to energy demand comes from acceleration while for highway driving it comes from aerodynamic loss. Rolling friction loss is relatively cycle-independent. Accordingly dissipative energy loss is highest for highway driving, followed by rural driving, and lowest for urban driving. For regenerable energy it is exactly the opposite.

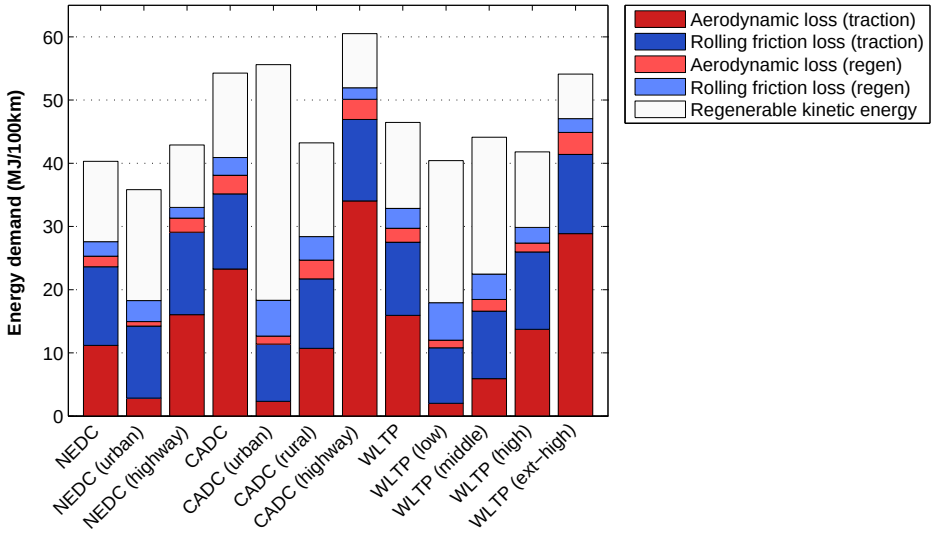

Figure 2.6: Mechanical energy demand of a midsize passenger car. For each cycle regenerable energy and the contributions to dissipative energy are shown.

Fig. 2.7 shows the contributions of dissipative and regenerable energy (sorted by regenerable energy) for the same car and driving cycles as discussed above. It is obvious that highway cycles are dominated by dissipative energy loss due to the high aerodynamic drag and only a small amount of regenerable energy. Urban cycles on the other hand offer a large amount of regenerable energy. Accordingly highway cycles are grouped to the left while urban cycles are to the right of the figure. The trade-off between dissipative energy loss and regenerable energy is also illustrated Fig. 2.7.
The high share of regenerable energy in urban relative to highway cycles can be explained as follows: Urban cycles do have many more and on average higher ac-/deceleration events than highway cycles. Kinetic energy in traction and regeneration periods is therefore higher for all urban cycles as can be seen in Fig. 2.5. In addition, aerodynamic drag is much higher for highway cycles, which means that more deceleration power is used to overcome aerodynamic drag in

periods of negative kinetic energy. Therefore less kinetic energy is available for regeneration in highway cycles. This can be seen for example in Figure 2.4.

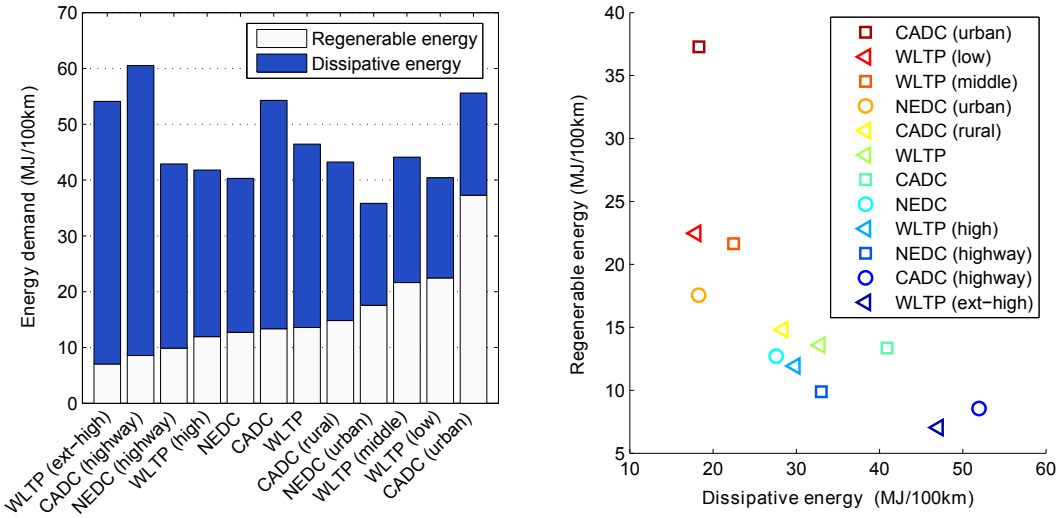

Figure 2.7: Contributions of dissipative and regenerable energy for different driving cycles sorted by regenerable energy (left). Regenerable vs. dissipative energy for different driving cycles (right). The color scale is according to the amount of regenerable energy.

2.1.5 Regeneration potential

The regeneration potential RP is defined as the amount of regenerable to tractive energy demand

$$RP = -\frac{E_{regen}}{E_{trac}} = -\frac{E_{regen}}{E_{diss} - E_{regen}} \tag{2.22}$$

It states how much of the energy demand in traction phases can be regenerated and ranges from 0 to 1. The higher RP is, the more important it is to use vehicles with a recuperative device such as an electric motor or a hybrid pneumatic engine [Guzzella & Sciarretta, 2013].
As already shown in Fig. 2.7, RP strongly depends on the driving cycle. In addition, it also depends on vehicle characteristics, in particular the ratio of conservative to dissipative forces which is given by the ratio of vehicle inertia relative to the aerodynamic drag and rolling resistance coefficient. Fig. 2.8 shows the dependence of the dissipative and regenerable energy as a function of vehicle mass at constant frontal area, aerodynamic drag and rolling resistance coefficient (A_f and c_r according to Table 2.4). In this case the contribution of aerodynamic drag is constant while rolling resistance and kinetic energy demand increase linearly with mass. Fig. 2.8 also illustrates

the corresponding regeneration potential as defined in Eq. 2.22 for the different driving cycles considered. The analysis shows that the importance of regeneration increases strongly for urban relative to highway driving. It is also more important in vehicles of high kinetic to dissipative energy demand, i.e. heavy vehicles relative to vehicles with high aerodynamic drag and rolling resistance coefficient.

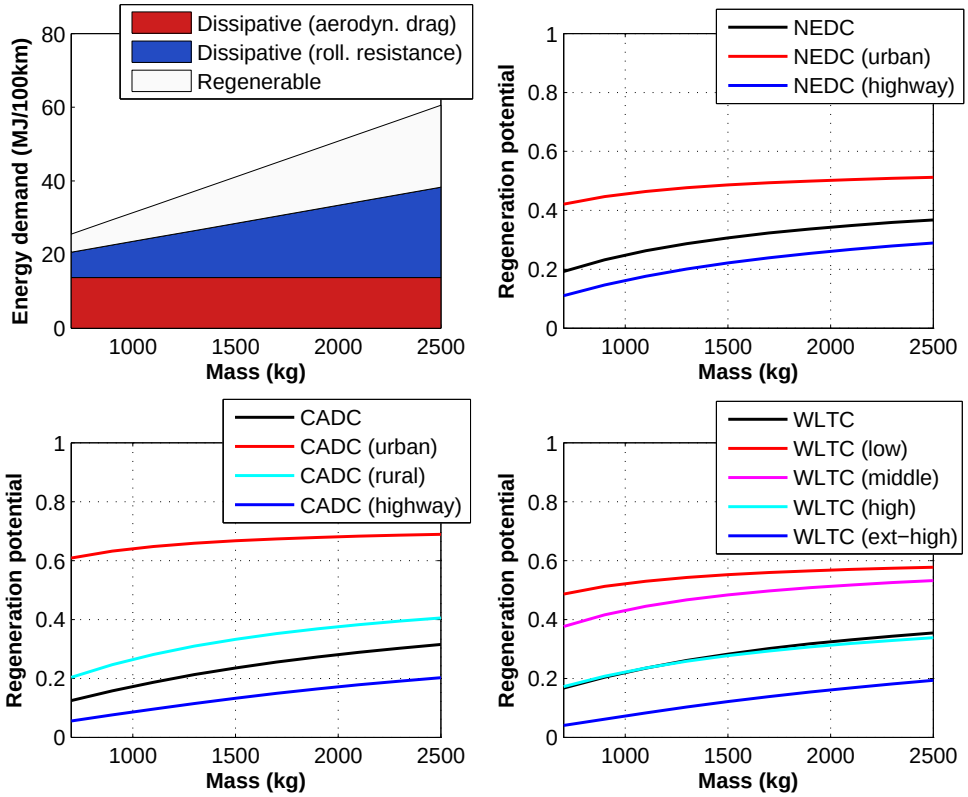

Figure 2.8: Contributions of dissipative and regenerable energy to tractive energy demand (top left) and regeneration potential for different driving cycles as a function of vehicle mass.

2.2 Parameterization of the contributions to mechanical energy demand

In the previous section the contributions to mechanical energy demand were calculated by integrating the aerodynamic drag, rolling resistance, and ac-/deceleration power over a driving cycle of interest. In this section a parameterization of the contributions to mechanical energy demand is performed in order to analytically calculate mechanical energy demand based on vehicle

characteristics and specific driving cycle coefficients. The parameterization is useful as it allows separate analysis of the contributions to energy demand as well as study of the sensitivity of energy demand to variations in vehicle characteristics. It also constitutes the basis for the analytic calculation of vehicle energy use in the next chapter.

The approach described in the following is in principal very similar to the procedure presented in [Guzzella & Sciarretta, 2013], except that the parameterization is not only valid for the two extreme cases of perfect and no regeneration but for any desired amount of regeneration. The coefficients for a range of different driving conditions representing average, urban, and highway driving patterns are given. The decoupling of driving cycle coefficients and vehicle characteristics is not perfect and the variability of the coefficients to changes in vehicle characteristics depends on the driving cycle. This variation of the parameterization coefficients is analyzed in detail. In addition, the sensitivity of energy demand to variations in vehicle characteristics is analyzed.

2.2.1 Approach and resulting coefficients for different driving cycles

The parameterization approach consists in calculating the contributions of aerodynamic drag, rolling resistance, and kinetic energy to energy demand in traction and regeneration phases based on a decoupling of vehicle characteristics m, A_f, c_d, c_r and driving cycle dependent coefficients termed in the following A, B, C for traction and A', B', C' for regeneration mode. For E_{trac} this yields

$$E_{trac} = \frac{1}{x_{tot}} \int_{P_w>0} P_w \, dt = \frac{1}{x_{tot}} \int_{P_w>0} (P_a + P_r + P_k) \, dt \tag{2.23}$$

$$= \frac{1}{x_{tot}} \int_{P_w>0} \left(\frac{1}{2} \cdot \rho \cdot c_d \cdot A_f \cdot v^3 + c_r \cdot m \cdot g \cdot v + m \cdot a \cdot v \right) dt \tag{2.24}$$

$$= A \cdot c_d \cdot A_f + B \cdot c_r \cdot m + C \cdot m \tag{2.25}$$

with the coefficients A, B, and C defined as

$$A = \frac{\rho}{2 \cdot x_{tot}} \int_{P_w>0} v^3 \, dt \tag{2.26}$$

$$B = \frac{g}{x_{tot}} \int_{P_w>0} v \, dt \tag{2.27}$$

$$C = \frac{1}{x_{tot}} \int_{P_w>0} a \cdot v \, dt \tag{2.28}$$

Similarly, E_{regen} is expressed as

$$E_{regen} = A' \cdot c_d \cdot A_f + B' \cdot c_r \cdot m + C' \cdot m \tag{2.29}$$

with the coefficients A', B', and C' calculated the same as in Eq. 2.26, 2.27, 2.28 but for regeneration ($P_w < 0$) instead of traction phases. In addition to E_{trac} and E_{regen}, E_{diss} can be also calculated as

$$E_{diss} = (A + A') \cdot c_d \cdot A_f + (B + B') \cdot c_r \cdot m \tag{2.30}$$

The evaluation of the integrals in Eq. 2.26 to 2.28 is performed by summing v^3, v, and $a \cdot v$ over the discrete instants of the driving cycle (usually the given time step is one second) that belong to traction or regeneration phases. As an example the integral for velocity in traction mode is calculated as

$$\int_{P_w>0} v\,dt = \sum_i v_i \quad where\ i \in\ traction \tag{2.31}$$

The distinction of traction and regeneration phases is based on P_w, i.e. for each instant of the driving cycle P_w is calculated for a given car type and compared to zero. Alternatively this distinction can be based on the coasting velocity, i.e. comparing for each instant of the driving cycle the coasting velocity with the velocity prescribed by the driving cycle [Guzzella & Sciarretta, 2013]. Both approaches lead to the same results.
The share of traction relative to regeneration periods depends on the relation of vehicle characteristics m, A_f, c_d, c_r. Since the parameterization coefficients are calculated based on integration during traction and regeneration periods, the parameterization coefficients also depend on the relation of vehicle characteristics. The amount of variation depends on the driving cycle and will be analyzed in more detail in the next section. For the reference car characteristics as given in Table 2.4 the parameterization coefficients to calculate the contributions to energy demand in $\frac{kj}{100\,km}$ are given in Table 2.5. For this calculation the assumed density of air is 1.2 $\frac{kg}{m^3}$. Note that the coefficients C and C' are equal but opposite as expected according to Eq. 2.12.

2.2.2 Variability of parameterization coefficients

As mentioned in the previous section, the driving cycle specific parameterization coefficients A, B, C, A', B', C' are not completely independent of the vehicle characteristics m, A_f, c_d, c_r. The reason

Table 2.5: Parameterization coefficients to calculate the contributions to mechanical energy demand in kJ per 100 km for different driving cycles.

		NEDC			CADC				WLTP				
	Unit	Avg	Urb	Hwy	Avg	Urb	Rur	Hwy	Avg	Low	Mid	High	Ext-high
A	$\frac{kg}{m\,s^2}$	18969	4800	27202	39535	3957	18181	57882	27072	3410	10079	23314	48992
B	$\frac{m}{s^2}$	829	760	869	795	603	735	861	774	586	716	819	839
C	$\frac{m}{s^2}$	11.1	14.4	9.2	12.7	29.5	14.3	9.0	12.6	19.7	18.3	10.5	8.4
A′	$\frac{kg}{m\,s^2}$	2855	1231	3799	4872	2138	5027	5232	3692	2065	3068	2350	5826
B′	$\frac{m}{s^2}$	152	221	112	186	378	246	120	207	395	265	162	142
C′	$\frac{m}{s^2}$	-11.1	-14.4	-9.2	-12.7	-29.5	-14.3	-9.0	-12.6	-19.7	-18.3	-10.5	-8.4

for this is that the split between traction and regeneration periods, and as such the split between A, B, C and A', B', C', depends on the relation between dissipative and conservative forces which in turn depends on the vehicle characteristics.

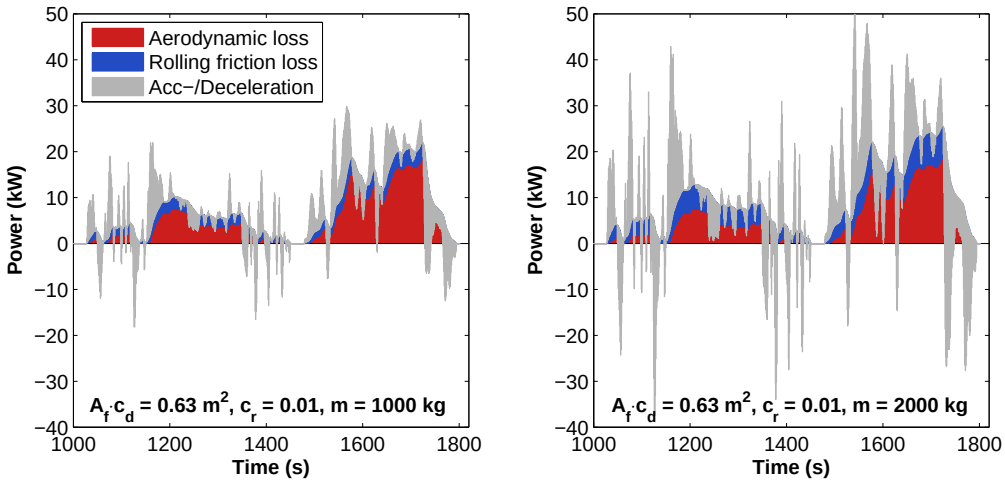

Figure 2.9: Contributions to the power at the wheel of a passenger car in two different configurations for the higher speed segments of the WLTP cycle (1000-1820 s are shown).

This can be better understood by looking at Fig. 2.9 which shows the contributions to the power at the wheel of a car driving part of the WLTP cycle. The figure shows on the left P_w for a car with $A_f \cdot c_d = 0.63$ m^2, $c_r = 0.01$, $m = 1000$ kg and on the right P_w for a car having same aerodynamic drag and rolling resistance coefficient but a mass of 2000 kg. Aerodynamic loss is equal in both cases, while rolling resistance and ac-/deceleration power differ by a factor of two. The increase of the relative share of kinetic to dissipative power (from left to right), leads to an increase of the time period the vehicle spends in regeneration instead of traction mode. This leads to an increase

of the coefficients A', B', C, and an equal decrease of A, B, C'. In the extreme case for which $P_k >> (P_a + P_r)$ dissipative losses are negligible compared to ac-/deceleration power, which means that ac-/deceleration becomes equivalent with the condition of being in traction/regeneration mode. For the other extreme in which $P_k << (P_a + P_r)$, dissipative losses are dominant so that there are only traction and no regeneration periods. Accordingly A', B' as well as $C'$and C approach zero. In this case all deceleration power is used to overcome aerodynamic and/or rolling resistance.

The described effect of the variation of parameterization coefficients obviously depends on the type of driving cycle. High-speed cycles are generally characterized by higher changes of coefficients than low-speed urban cycles, due to a higher share of dissipative to kinetic power and lower average deceleration. For urban cycles deceleration usually clearly offsets dissipative power, while for higher speed cycles the sum of deceleration and dissipative power is often close to zero and therefore the attribution to traction or regeneration phases is more sensitive to changes in characteristics that influence the relation of dissipative to kinetic power. The effect is also more pronounced for transient than steady-state driving cycles, because those involve a smooth transition between acceleration and deceleration which makes the split between traction and regeneration more sensitive.

Fig. 2.10 shows the change of traction and regeneration period for a car with $A_f \cdot c_d = 0.63\ \mathrm{m}^2$, $c_r = 0.01$, and $m = 2000$ kg relative to a car with the same aerodynamic and rolling resistance coefficient but a mass of 1000 kg for different driving cycles. Also shown are the corresponding changes of the parameterization coefficients. As expected, the regeneration period and the coefficients A', B', C increase (for the heavier relative to the lighter vehicle), while traction period and A, B, C' decrease by the same amount.

For the coefficients the following relations hold

$$A + A' = const. \tag{2.32}$$

$$B + B' = const. \tag{2.33}$$

$$C + C' = 0 \tag{2.34}$$

This means that although the coefficients A, B, C, A', B', C' vary with vehicle characteristics, dissipative energy losses are constant and kinetic energy is preserved.
Fig. 2.10 also shows that the changes are very small for the NEDC (steady-state cycle) and the urban segments of the CADC and WLTP. On the other hand variations are higher for the CADC and WLTP (transient cycles), in particular for its high-speed parts.

Fig. 2.11 shows the error that would occur for E_{trac}, E_{regen}, and E_{diss} with coefficients calculated for a car with $A_f \cdot c_d = 0.63\ \mathrm{m}^2$, $c_r = 0.01$, and $m = 1000$ kg and evaluated for a car with the same aerodynamic and rolling resistance coefficient but a mass of 2000 kg. It can be seen that

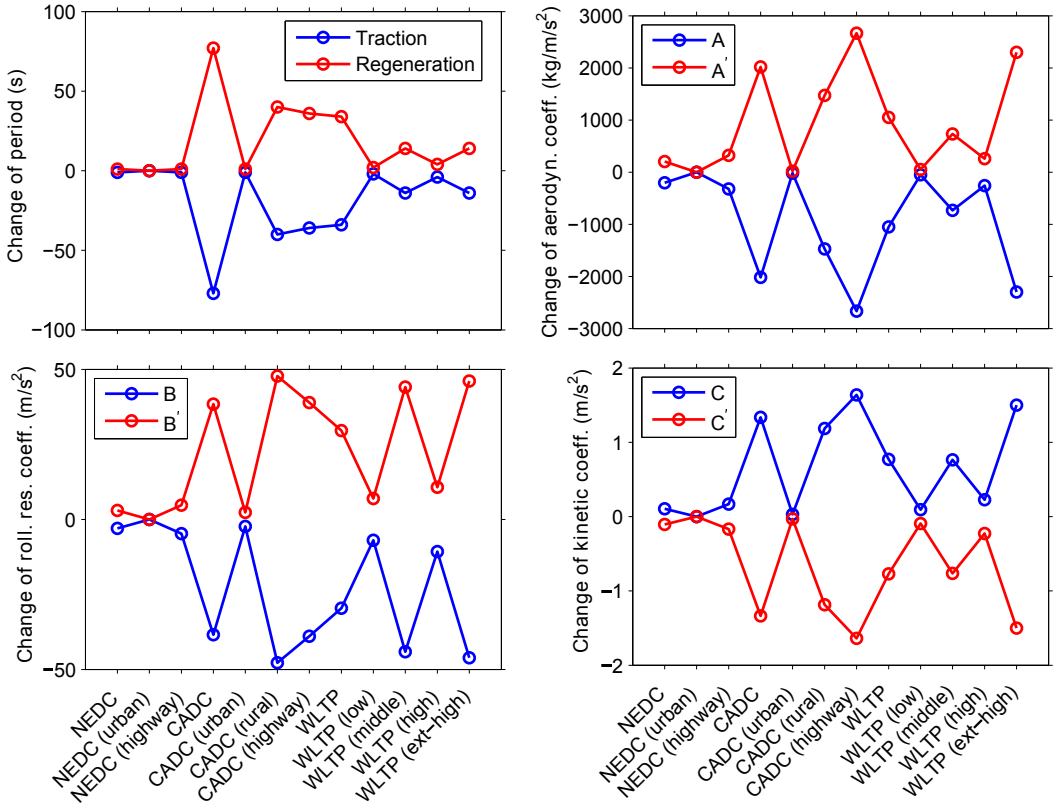

Figure 2.10: Variability of cycle traction and regeneration periods and of the parameterization coefficients for different driving cycles.

the error strongly increases with the average velocity of the driving cycle and the relative time of regeneration to traction periods for the particular cycle. Furthermore the figure shows that the error is higher for E_{regen} than E_{trac}. This can be explained by the simple fact that a similar change for E_{regen} and E_{trac} results in a higher relative change of E_{regen} as $E_{trac} > E_{regen}$. The change of E_{diss} is zero as dissipative energy losses are constant.

To better understand the variability of parameterization coefficients with vehicle characteristics, it is useful to vary several vehicle parameters at the same time. Fig. 2.12 shows the traction and regeneration period for the WLTP driving cycle against vehicle mass and frontal area. The aerodynamic and rolling resistance coefficient are constant at $c_d = 0.3$ and $c_r = 0.01$. As expected, the time in regeneration mode increases with higher mass and lower frontal area, while the time in traction mode is reduced by the same amount. The reason is that conservative to dissipative power increases, as explained above. Note that instead of varying the frontal area, a similar trend

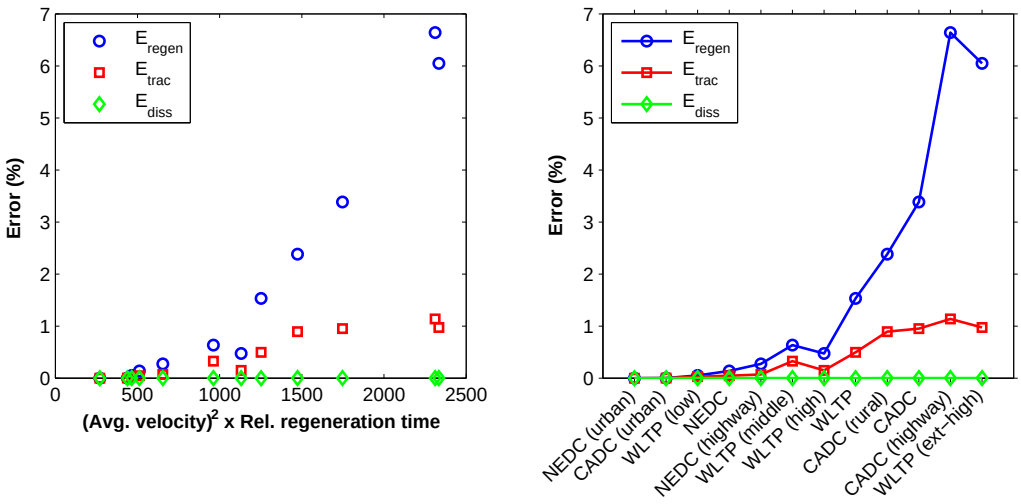

Figure 2.11: Error of E_{trac}, E_{regen}, and E_{diss} using unadjusted parameterization coefficients. The error is plotted against the cycle average velocity squared times the relative time of regeneration to traction period (left) and sorted by the same value (right).

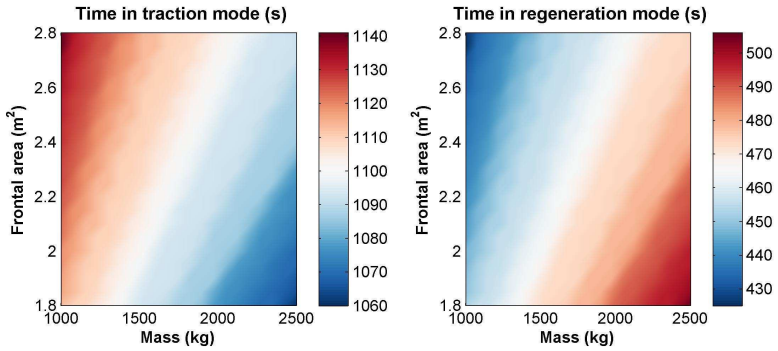

Figure 2.12: Traction and regeneration period for the WLTP driving cycle by vehicle mass and frontal area, c_d and c_r constant.

would be observable by varying c_d and c_r.

Fig. 2.13 depicts the corresponding change of the parameterization coefficients. A, B, and C' change in a very similar way as the traction period in Fig. 2.12, while A', B', and C change very similarly to the regeneration period.

Fig. 2.14 finally shows the corresponding error for E_{trac} and E_{regen} using constant parameterization coefficients calculated for a mass and frontal area in the middle of the varied interval. The

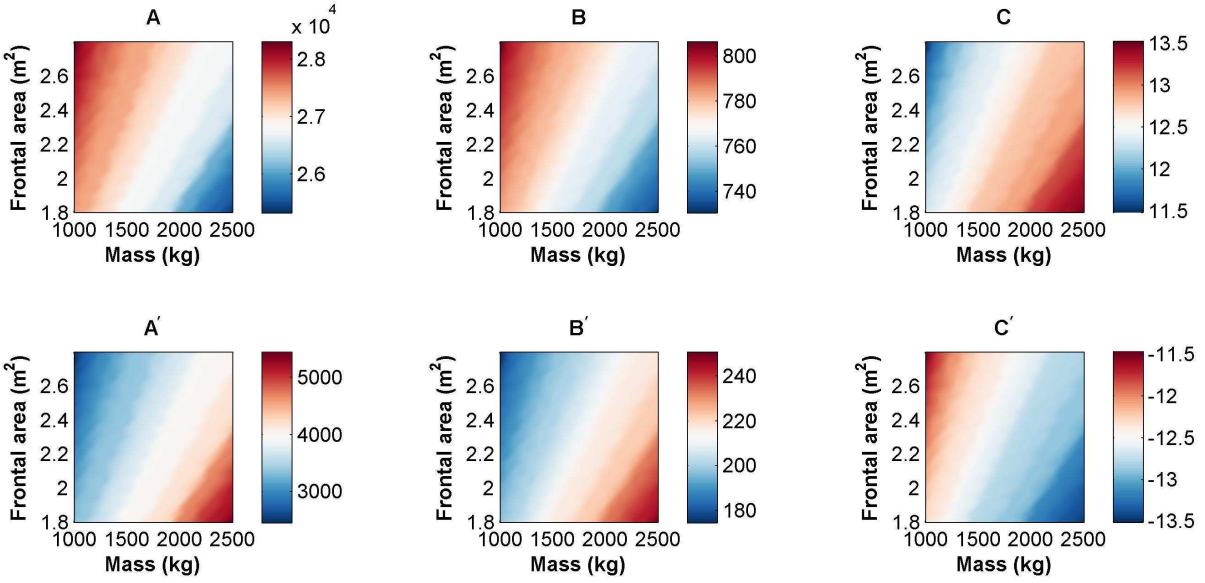

Figure 2.13: Parameterization coefficients for the WLTP driving cycle by vehicle mass and frontal area.

white data points represent the curb weight and frontal area[1] values of new passenger cars sold in Switzerland in 2010 [2] to see where in this plane actual vehicles are located. The data points indicate that the frontal area on average increases with vehicle mass and that most vehicles observed in the fleet follow approximately the same trend as a region of constant traction/regeneration time and parameterization coefficients (compare also to Fig. 2.12 and 2.13). This means that the related error of calculating E_{trac} and E_{regen} for the WLTP driving cycle with unadjusted parameterization coefficients is for most vehicles below 0.2 % and 1 %, respectively.

In conclusion, for passenger vehicles constant parameterization coefficients are valid for the NEDC driving cycle and the low-speed, urban segments of the WLTP and CADC. For the WLTP and CADC (in particular its highway segments), unadjusted parameterization coefficients can lead to a small error for the calculation of traction and regeneration energy if vehicle characteristics are varied in such a way that the ratio of dissipative to kinetic power alters significantly.

Note that besides the variation of vehicle characteristics, a change of the density of air ρ also leads to a change of the parameterization coefficients. As defined in Eq. 2.26 ρ enters linearly into the calculation of A and A'. In this work ρ is assumed to be 1.2 kg/m^3, which is typical for dry air at an altitude of about 300 m at 10 degree Celsius. However, ρ significantly rises at lower temperatures

[1]The reference frontal area was calculated based on the height and width of the vehicle times 0.8 according to [Goodall & Thompson, 1977].

[2]Based on a dataset from Auto Schweiz of approximately 7000 unique vehicle models representing Swiss passenger car sales of the year 2010.

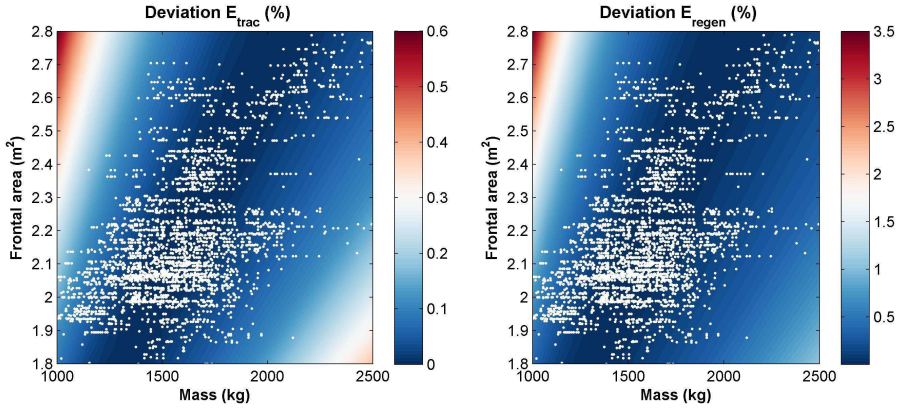

Figure 2.14: Error of calculating E_{trac} and E_{regen} with constant parameterization coefficients for the WLTP driving cycle by vehicle mass and frontal area. White points indicate the curb weight and frontal area of new passenger cars sold in Switzerland in 2010.

and altitudes and decreases at higher altitude and temperature. At sea level and −10 °C, ρ reaches 1.34 kg/m^3, and 0.96 kg/m^3 at 2000 m altitude and +20 °C [Troen & Lundtang, 1989]. This means that $A + A'$ and the aerodynamic drag can also vary by a factor of 40 % for these conditions.

2.3 Sensitivity of energy demand to changes in vehicle characteristics

A very useful property of the analytic parameterization described in the previous section is the possibility to calculate the partial derivatives with respect to vehicle characteristics. The partial derivative indicates the sensitivity of energy demand to changes in the corresponding property. In the following the sensitivity of E_{trac}, E_{diss}, and E_{regen} to changes of m, c_d, and c_r will be analyzed. The sensitivities with regard to changes of vehicle mass are

$$\frac{\partial E_{trac}}{\partial m} = \frac{\partial(A \cdot c_d \cdot A_f + B \cdot c_r \cdot m + C \cdot m)}{\partial m} = B \cdot c_r + C \tag{2.35}$$

$$\frac{\partial E_{diss}}{\partial m} = \frac{\partial\left((A + A') \cdot c_d \cdot A_f + (B + B') \cdot c_r \cdot m\right)}{\partial m} = (B + B') \cdot c_r \tag{2.36}$$

$$\frac{\partial E_{regen}}{\partial m} = \frac{\partial(A' \cdot c_d \cdot A_f + B' \cdot c_r \cdot m + C' \cdot m)}{\partial m} = B' \cdot c_r + C' \tag{2.37}$$

Similarly, the sensitivities with regard to changes of the rolling resistance coefficient are

$$\frac{\partial E_{trac}}{\partial c_r} = B \cdot m \tag{2.38}$$

$$\frac{\partial E_{diss}}{\partial c_r} = (B + B') \cdot m \tag{2.39}$$

$$\frac{\partial E_{regen}}{\partial c_r} = B' \cdot m \tag{2.40}$$

And the sensitivities with regard to changes of the aerodynamic drag coefficient are

$$\frac{\partial E_{trac}}{\partial c_d} = A \cdot A_f \tag{2.41}$$

$$\frac{\partial E_{diss}}{\partial c_d} = (A + A') \cdot A_f \tag{2.42}$$

$$\frac{\partial E_{regen}}{\partial c_d} = A' \cdot A_f \tag{2.43}$$

The sensitivities of E_{trac}, E_{diss}, and E_{regen} with respect to vehicle mass (Eq. 2.36 to 2.37) depend on the rolling resistance coefficient and are depicted in Fig. 2.15a.

It is interesting to note that $\frac{\partial E_{trac}}{\partial m}$ and $\frac{\partial E_{diss}}{\partial m}$ increase with c_r which means that the reduction of vehicle mass influences energy demand most for vehicles with high tire rolling resistance. $\frac{\partial E_{regen}}{\partial m}$ (as well as E_{regen}) is negative which means that regenerative energy increases with vehicle mass. Fig. 2.15b shows the sensitivities of E_{trac}, E_{diss}, and E_{regen} with respect to changes of the tire rolling resistance coefficient (Eq. 2.39 to 2.40). $\frac{\partial E_{trac}}{\partial c_r}$ and $\frac{\partial E_{diss}}{\partial c_r}$ increase with m which means that the reduction of tire rolling resistance is particularly important for heavy vehicles. Fig. 2.15c finally shows the sensitivities of E_{trac}, E_{diss}, and E_{regen} with respect to changes of the aerodynamic drag coefficient. $\frac{\partial E_{trac}}{\partial c_d}$ and $\frac{\partial E_{diss}}{\partial c_d}$ increase with A_f, which means that the reduction of the aerodynamic drag coefficient reduces energy demand most effectively in vehicles with large frontal area. The absolute change of tractive energy demand for the variation of a variable x can be calculated as

$$\Delta E_{trac} = \frac{\partial E_{trac}}{\partial x} \cdot \Delta x \tag{2.44}$$

The relative change with regard to a baseline tractive vehicle energy demand $E_{trac,0}$ can then be calculated as

$$\frac{\Delta E_{trac}}{E_{trac,0}} = \frac{\partial E_{trac}}{\partial x} \cdot \frac{\Delta x}{E_{trac,0}} \tag{2.45}$$

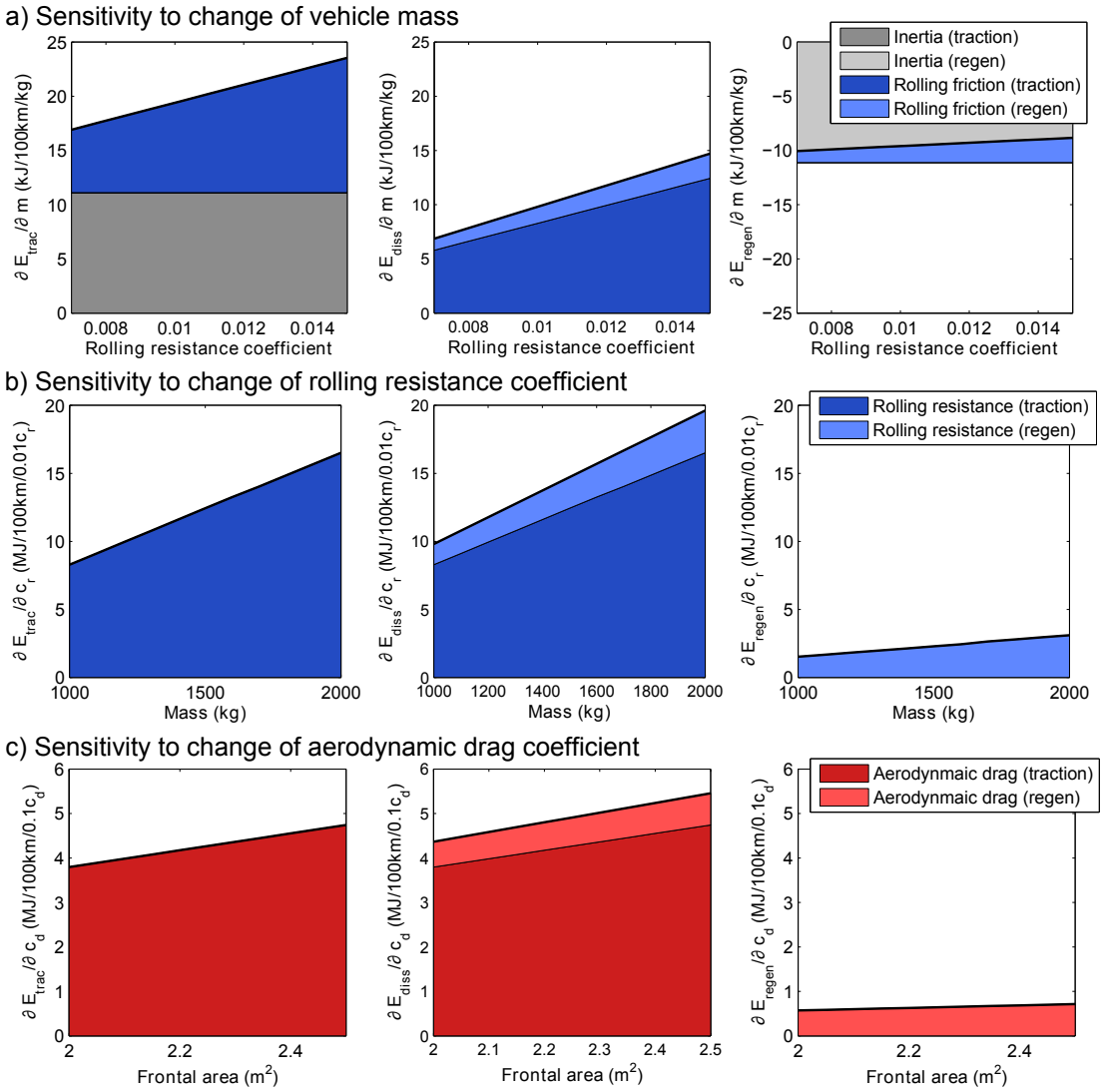

Figure 2.15: Sensitivities of E_{trac}, E_{diss}, and E_{regen} with respect to changes of vehicle mass, rolling resistance, and aerodynamic drag coefficient.

In the same way as Eq. 2.44 and 2.45 for the tractive energy demand, the absolute and relative changes for dissipative and regenerative energy can be calculated.

Fig. 2.16 shows on top the absolute change of E_{trac}, E_{diss}, and E_{regen} for one kg of mass increase for different driving cycles. The bottom row of Fig. 2.16 shows the relative change of E_{trac}, E_{diss}, and E_{regen} in percent for one percent of mass increase. As can be seen from the figure, the sensitivity of tractive and regenerative energy demand with regard to a change of mass is highly dependent on the type of driving pattern. It is lowest for highway and highest for urban driving with a low and high share kinetic energy, respectively.

Fig. 2.17 shows on top the increase of E_{trac}, E_{diss}, and E_{regen} for a change of $\Delta c_r = 0.01$ and below

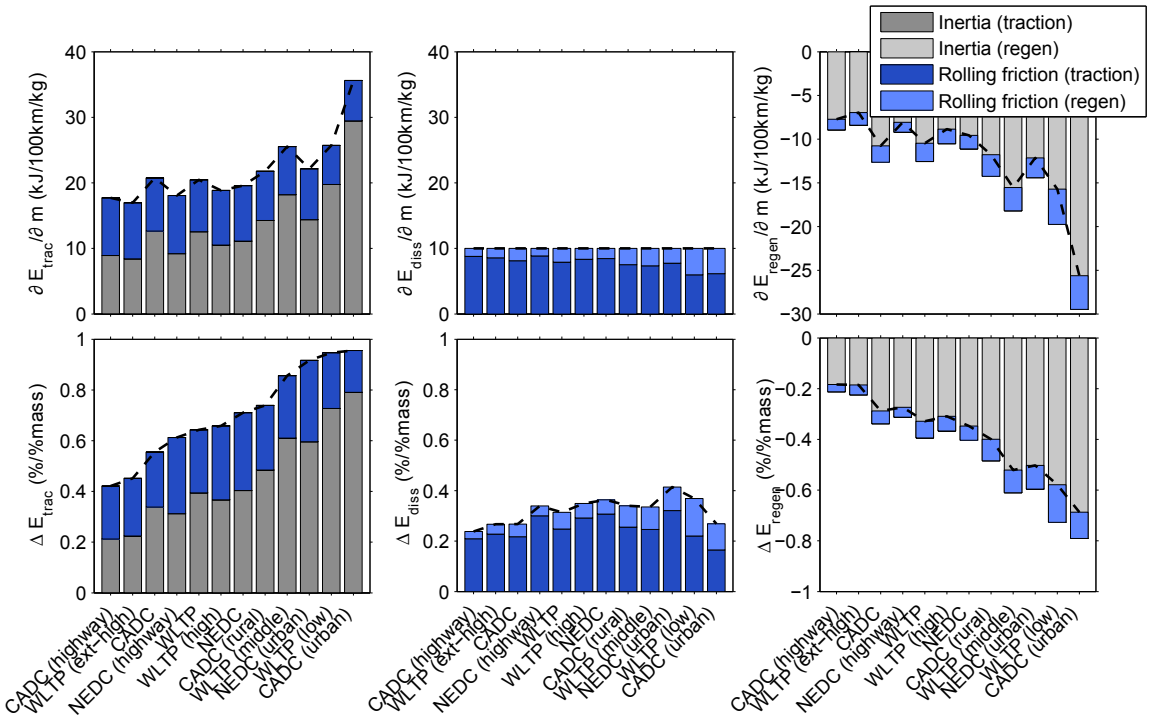

Figure 2.16: Absolute (top) and relative (bottom) changes of E_{trac}, E_{diss}, and E_{regen} with respect to an increase of vehicle mass.

the relative change for a percentage increase of c_r. There is no clear dependence on highway or urban driving. As can be seen in Fig. 2.6 rolling resistance has a relatively low share compared to tractive energy demand for the CADC and a high share for the CADC driving cycle. This leads to the relatively low and high sensitivity of tractive energy demand to a change of c_r for the CADC and NEDC, respectively.

Fig. 2.18 shows on top the increase of E_{trac}, E_{diss}, and E_{regen} for a change of $\Delta c_d = 0.01$ and below the relative change for a percentage increase of c_d. As expected, an increase of the aerodynamic drag influences energy demand much more in highway than in urban driving.

In conclusion, the parametric calculation method offers a very clear and intuitive way to evaluate the sensitivities of energy demand to changes of vehicle characteristics. It is also well suited to compare those sensitivities for different driving cycles and vehicle types.

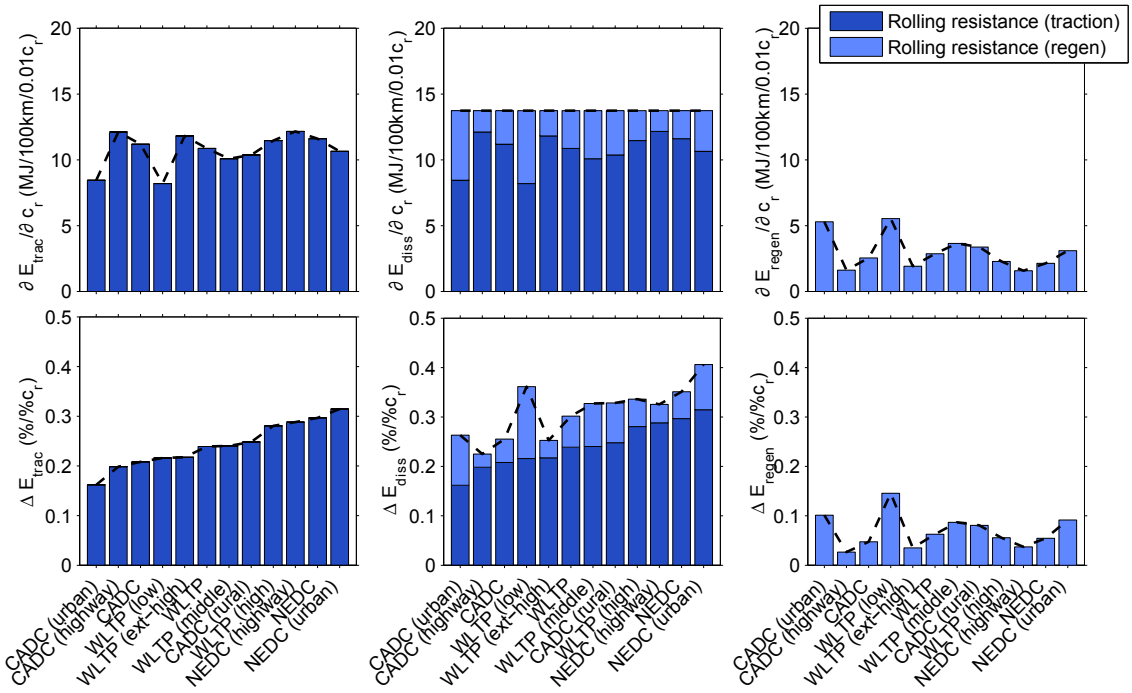

Figure 2.17: Absolute (top) and relative (bottom) changes of E_{trac}, E_{diss}, and E_{regen} with respect to an increase of tire rolling resistance.

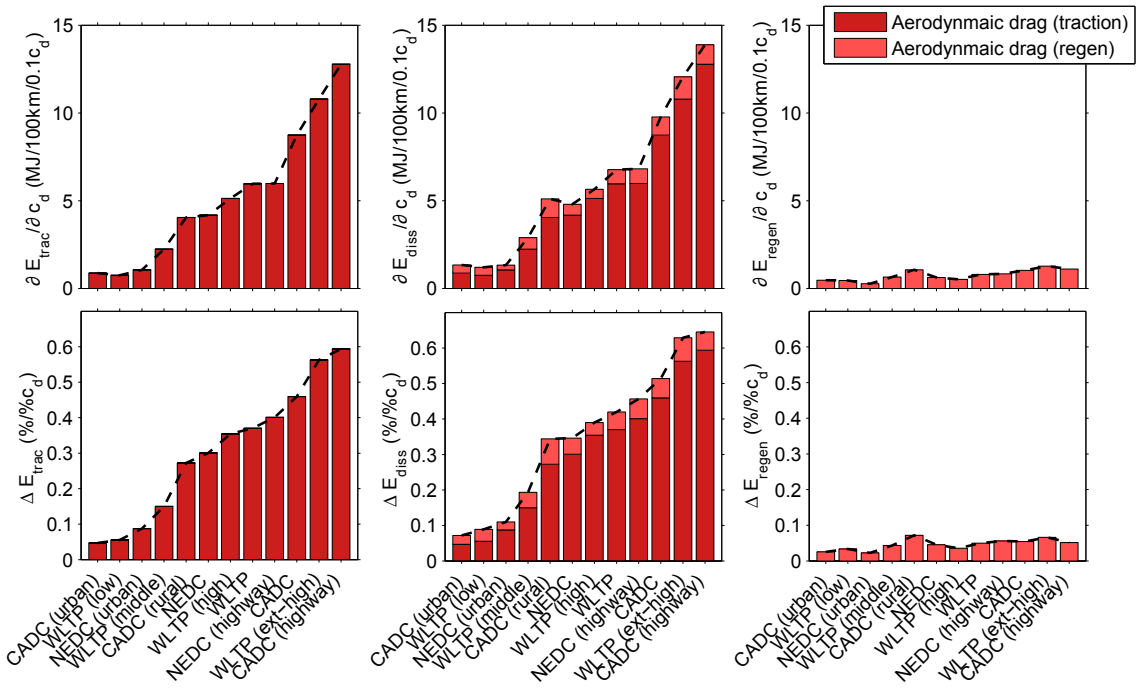

Figure 2.18: Absolute (top) and relative (bottom) changes of E_{trac}, E_{diss}, and E_{regen} with respect to an increase of the aerodynamic drag coefficient.

Chapter 3

Vehicle energy use and configuration

In the previous chapter the parametric calculation of vehicle mechanical energy demand independent of the type of powertrain was introduced. In section 3.1 this approach is developed further to calculate vehicle energy use for conventional and advanced electric powertrains. Section 3.2 presents the car classes analyzed and introduces the performance requirements relevant for the calculation of vehicle configuration.

3.1 Calculation of vehicle energy use

3.1.1 Overview of existing methods

Vehicle modeling and simulation are important for concept evaluation and control optimization of new powertrain configurations. Depending on the level of detail and the type of application, different methods exist varying in complexity and computational effort [Gao et al., 2007].
Due to the broad scope of the analysis presented here a fast and transparent method for the calculation of vehicle energy use and configuration is required. For the calculation of energy use, in [Guzzella & Sciarretta, 2013] three approaches are distinguished: average operating point, quasistatic, and dynamic modeling. The main idea of the average operating point approach is to combine all powertrain operating points into one representative average efficiency. Knowing the mechanical energy demand for a specific driving cycle and the average powertrain efficiency for this cycle, vehicle energy use is then calculated. This approach is simple, transparent and can be very fast once implemented. It is not suited however to optimize complex, hybrid powertrain control strategies. The quasistatic approach uses the speed and acceleration profile from the driving cycle together with the vehicle characteristics as input parameters to calculate for each instant the tractive or regenerative forces acting on the vehicle. Based on efficiency maps of the vehicle components (usually generated in laboratory tests) the powertrain losses for each operating point

are evaluated. The quasistatic approach is well suited for the optimization of hybrid energy management strategies and usually performed in a backward facing simulation, i.e. the calculation starts with the tractive effort at the wheels and works backward (against the physical causality) to the engine or electric motor. The quasistatic approach is often implemented in numeric vehicle simulation tools using Matlab Simulink such as Advisor [Markel et al., 2002] developed by the National Renewable Energy Laboratory or the QSS Toolbox developed at ETH Zurich [Guzzella & Sciarretta, 2013]. Dynamic models usually better represent the real physical system with a set of differential equations and are implemented as a forward facing simulation with a driver model such as a PID controller to match a target speed profile [Gao et al., 2007; Guzzella & Sciarretta, 2013].

The approach used in this work is a combination of the quasistatic and the average operating point approach. First vehicle tractive and regenerative efficiencies for different powertrain types, driving cycles, and performance levels are calculated using quasistatic modeling. Based on the parameterization of mechanical energy demand, the vehicle efficiencies are then used to calculate energy use. Once the average operating point efficiencies are determined, this approach is much faster in terms of simulation time than a pure quasistatic model because it is solely based on evaluating analytic equations instead of numeric simulations.

Several previous studies have used analytic approaches for the calculation of vehicle energy use: In [Guzzella & Sciarretta, 2013] the average operating point method is applied to calculate the energy use of an ICEV for the NEDC driving cycle. In [Simpson, 2005] a framework for the parametric calculation of the energy use of different advanced powertrains is developed. As pointed out by the author, the parameterization approach fails to correctly separate tractive and regenerative energy which leads to errors in the prediction of fuel consumption on the order of 5-20 %. In [Gantt, 2011] vehicle energy use is calculated based on the tractive energy demand and average component efficiencies measured in a test of a real BEV. In [Katrašnik, 2009; 2010; 2011] the calculation of average operating point efficiencies is performed for hybrid electric vehicle configurations.

Novelties of the present work include the combination of the parameteric calculation of energy demand for different driving cycles with the parameterization of vehicle efficiencies for a broad range of advanced powertrain types, driving patterns, and performance levels.

3.1.2 Simulation of different powertrain types

The drivetrain types considered in this work and the possible power flows between the main components are illustrated in Fig. 3.1. The simulation of the different powertrain technologies is mainly performed with a vehicle simulation tool called Advisor. It is open-source, implemented in Matlab Simulink, and includes several pre-defined powertrain configurations, a database of conventional and electric drivetrain component models, and can be adjusted for the purpose of

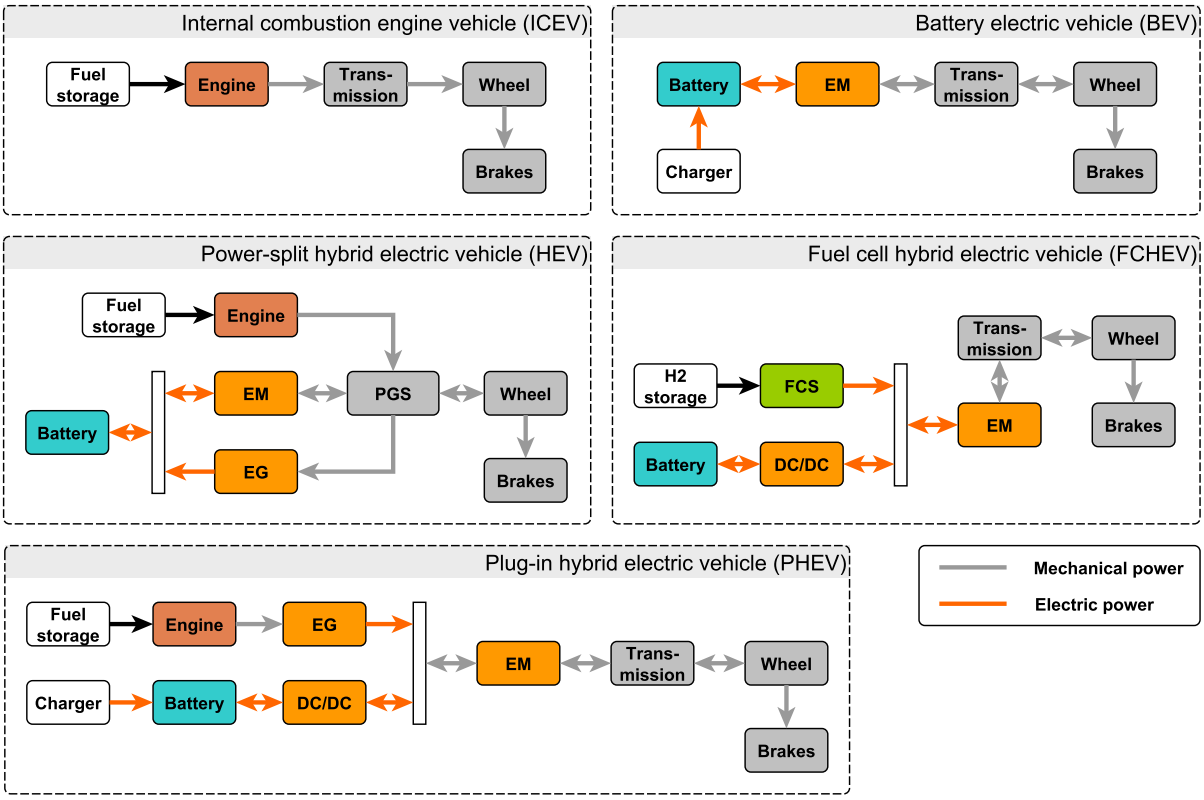

Figure 3.1: Overview of drivetrain configurations and power flows between the main components. Abbreviations: Electric motor (EM), electric generator (EG), fuel cell system (FCS), planetary gear set (PGS).

this analysis. For a detailed description of Advisor please see [Markel et al., 2002]. In the following, an overview of the different drivetrain technologies will be given and the important aspects of the simulation briefly discussed.

Internal combustion engine vehicle (ICEV). An ICEV is powered by an internal combustion engine (ICE) which transfers power via the transmission to the wheels in traction phases. As no recuperative device is present, negative power at the wheels is dissipated in the friction brakes. The simulation starts by calculating the tractive effort at the wheels for a given driving cycle based on the vehicle characteristics m, A_f, c_d, c_r. A manual transmission including a differential, gearbox with five gear ratios, and a clutch transmits the torque and speed from the engine to the wheels. The gearbox reduces the speed and increases the torque from the engine. The requested speed and torque from the transmission determines the engine operating points and fuel use. As such, the selection of gear ratios and the gear shift strategy is critical regarding ICEV energy use. In addition to the transmission and engine, the losses in the wheels, axle bearings, tire slip, and the

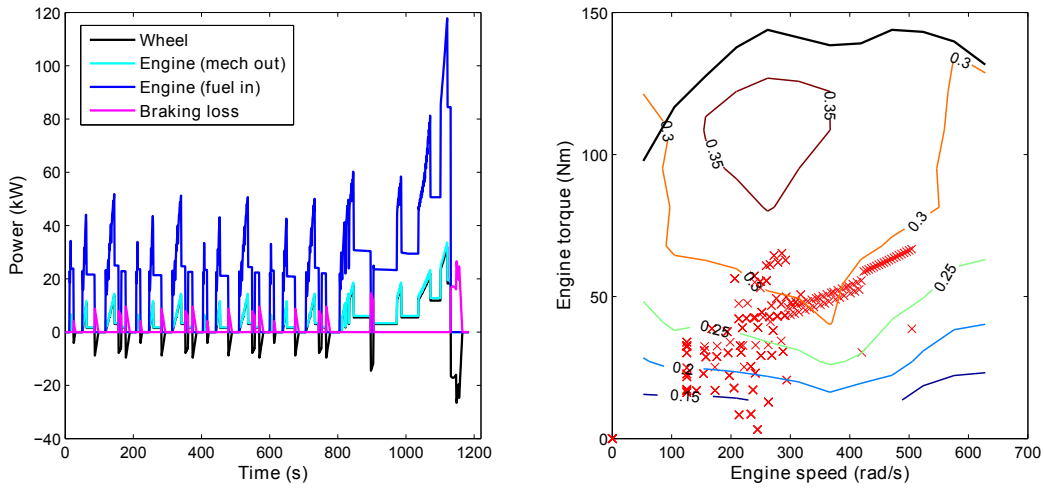

Figure 3.2: Simulation of the main power flows (left) and gasoline engine efficiency map (right) for a midsize ICEV passenger car driving the NEDC. On the right the engine operating points are indicated with red crosses between the engine efficiency isolines.

control strategy of friction brakes are simulated. The vehicle is modeled with a start-stop system, which eliminates idling losses while stopping. This is particularly relevant for urban driving with a comparably high share of stops. The ICEV is modeled as fueled either by gasoline, diesel, or compressed natural gas (CNG), with different engine efficiency maps for each fuel technology. Based on the fuel mass flow rate and the lower heating value (LHV) of the fuel, the power flow in the engine is calculated. Table 3.1 summarizes the assumed density and heating value of the major fuels considered. As an example Fig. 3.2 shows the simulation of a midsize ICEV-gasoline passenger car on the NEDC driving cycle.

Table 3.1: Density and lower heating value of fuels [Edwards et al., 2011].

	Gasoline	**Diesel**	**CNG**	**Hydrogen**
LHV (MJ/kg)	43.2	43.1	45.1	120.1
Density (kg/m^3)	745	832		

Hybrid electric vehicle (HEV). Depending on the connection of the electric motor and engine to the mechanical drivetrain, three main HEV configurations are distinguished: series, parallel, and series-parallel (also called power-split or combined) hybrid. In this work the power-split configuration is modeled as it is used e.g. in the Toyota Prius. The electric motor and the battery are sized to propel the vehicle without the engine up to a certain power requirement (this is called a full hybrid in contrast to a mild hybrid which cannot provide all-electric propulsion). As

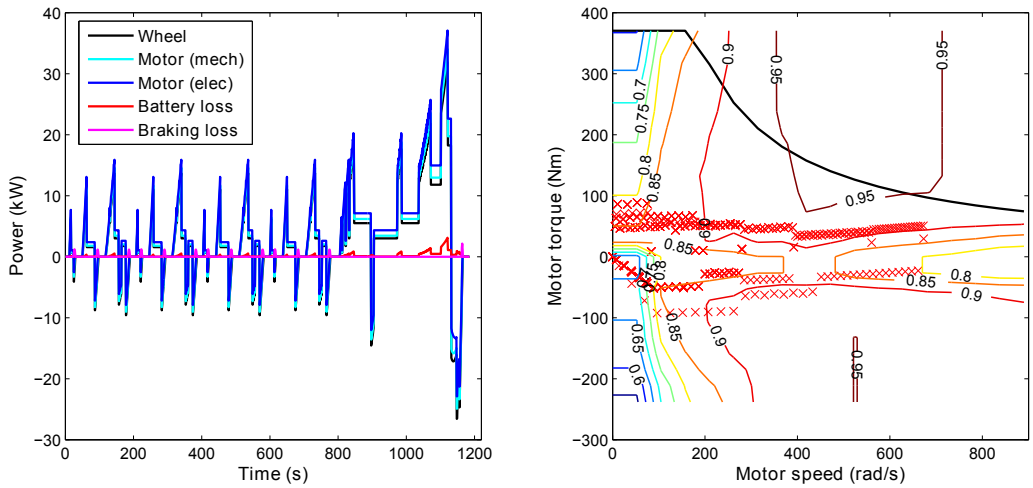

Figure 3.3: Simulation of the main vehicle power flows (left), and a permanent magnet electric motor efficiency map with maximum torque curve and operating points (right) for a midsize BEV passenger car driving the NEDC.

shown in Fig. 3.1 a power-split hybrid is equipped with an electric motor, generator, and engine that are mechanically connected through a planetary gear set to the driveshaft. Compared to the ICEV, a HEV provides several possibilities to reduce energy use: The electric motor assists the engine in periods of high load. Therefore the engine can be downsized and operate at higher average efficiency. In addition, the electric motor can recuperate energy in regeneration periods. In periods of low load the engine can be off or operate at higher power than required and transfer excess power to the electric generator. This increases the average operating efficiency of the ICE. Electric energy gained in recuperation or generated from the engine through the generator is stored in the battery and released at a later time to propel the vehicle via the electric motor. The HEV cannot be charged from an external power source and is modeled with a gasoline, diesel, or CNG engine.

Battery electric vehicle (BEV). A BEV is equipped with an electric motor that propels the vehicle. Electricity from an external power source is stored in a battery that provides enough power to reach the desired top speed and acceleration. A BEV can recuperate in regeneration phases and store the energy in the battery for later use. Due to the large speed and torque range of the electric motor a single-speed transmission is sufficient to reach all performance requirements. Fig. 3.3 shows the simulation of a midsize BEV passenger car with an electric motor and a Li-ion battery for the NEDC driving cycle. Braking losses are strongly reduced and traction efficiency increased.

Battery simulation is performed with an electrical equivalent circuit model which is composed

of an internal resistance and one or two resistance-capacitance elements in series to model the ohmic resistance, charge transfer, and diffusion polarization respectively [Chen & Rincon-Mora, 2006; Guzzella & Sciarretta, 2013]. The resistance and capacitance values are modeled as a function of the battery temperature and state of charge (SOC) of the battery. The actual dependencies of the resistance and capacitance values on temperature and SOC are based on experimental data retrieved from the literature and other publicly available sources. With this model the energy and power capability of various cells as a function of temperature, discharge rate, and SOC have been investigated. It has been shown that the energy capability, i.e. the available discharge energy from the battery, significantly decreases at higher discharge rates and lower temperatures, and that the charge and discharge power capability strongly depend on the SOC and temperature. For more details about the method and results please see [Ottaviano, 2012].
For the assessment of BEV energy use several cells were arranged in series-parallel connection to achieve the desired capacity, voltage, and power capability. Since battery ohmic heat losses are primarily dependent on the charging/discharging power and the battery internal resistance, battery efficiency was analyzed for typical charging/discharging profiles and different Li-ion chemistries. Regarding different Li-ion cathode/anode material pairs currently implemented in electric vehicles, Lithium Nickel Manganese Cobalt Oxide / Graphite (NMC-G) and Lithium Nickel Cobalt Aluminium Oxide / Graphite (NCA-G) are characterized by high voltage and specific energy but also relatively high internal resistance and energy losses. On the other hand Lithium Iron Phosphate / Graphite (LFP-G), Lithium Manganese Oxide / Graphite (LMO-G), and Lithium Manganese Oxide / Lithium Titanate (LMO-LTO) possess lower voltage, specific energy, internal resistance and energy losses [Nelson et al., 2011; Ottaviano, 2012]. Regarding different driving patterns, battery efficiency decreases in highway relative to urban driving because of the higher average tractive power. Fig. 3.4 shows the influence of charging power and average driving speed on the battery round-trip energy efficiency. In this case a 400 V battery was modeled with an internal resistance of about 150 mOhm, which is typical for a 20 kWh Li-ion battery at moderate temperatures [Brusa, 2014]. The round-trip efficiency drops below 90 % at charging powers considered relevant for fast charging of electric vehicles. This is in agreement with observations of relatively strong heat generation during fast charging for some Li-ion battery types. Advances in battery research open possibilities to improve the efficiency of electrochemical processes in the battery and to further increase the charging power and reduce charging time, as shown for example by [Lee et al., 2012]. Note that in addition to losses in the battery, losses in the charger must be considered. Depending on the type of charger and the power level, the average efficiency is on the order of 90-95 % [ABB, 2014].

Fuel cell (hybrid) electric vehicle (FCEV/FCHEV). A FCEV is equipped with a hydrogen tank and a hydrogen fuel cell system that provides the power to propel the vehicle with an electric motor. Note that hydrogen can also be produced with a reformer from another fuel such as methanol

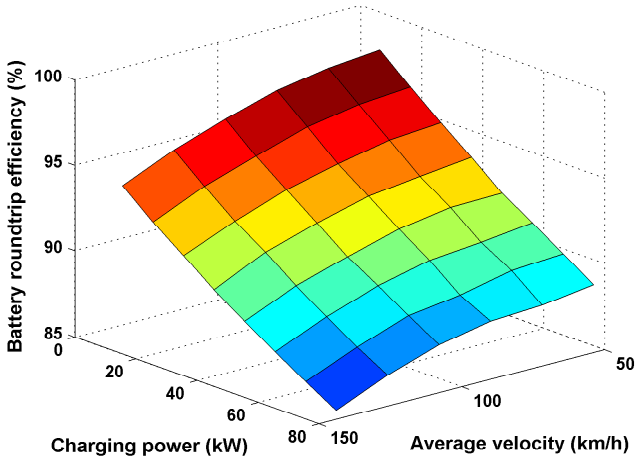

Figure 3.4: Battery roundtrip efficiency as a function of average charging power and driving speed.

or natural gas onboard the vehicle. These concepts are however not analyzed within this work. Similarly to the BEV, the FCEV is modeled with a one-speed gearbox. A FCEV can recuperate part of the regenerative energy and store it in the battery. The battery is used to balance the response time of the fuel cell, especially at start-up periods when the fuel cell is cold. Compared to the FCEV, the FCHEV is equipped with a larger battery which provides full regeneration capability and allows the fuel cell to be further downsized. It also allows operation of the fuel cell at higher average efficiency. In this case the fuel cell power is decoupled from the power requirement of the vehicle and operates at high efficiency. Missing or excess electric power from the fuel cell is balanced by the battery. However over the long term the battery operates in a charge sustaining mode as it is not charged from an external source.

Fig 3.5 shows the simulated energy use of a fuel cell vehicle with midsize passenger car characteristics according to Table 2.4 for the Artemis driving cycle against the degree of hybridization (DoH). DoH is defined here as the ratio of battery power to the total power of the battery and fuel cell. In this example the drivetrain power and vehicle mass are set independently of the DoH to 120 kW and 1500 kg, respectively. Note that in principle vehicle mass changes with DoH as the battery and fuel cell have in general different specific powers. However this example is only to show the theoretical effect of hybridization on vehicle energy use. The power-to-energy ratio of the battery is 15 kW/kWh. The battery operates in a charge sustaining mode, i.e. the battery SOC is equal at the beginning and the end of the cycle. It is obvious that vehicle energy use decreases with increasing DoH, most strongly for the urban driving cycle. This can be explained by two effects. First, the amount of regenerated energy increases with DoH as the charge power capability of the battery increases. Depending on the driving cycle the amount of energy the battery can

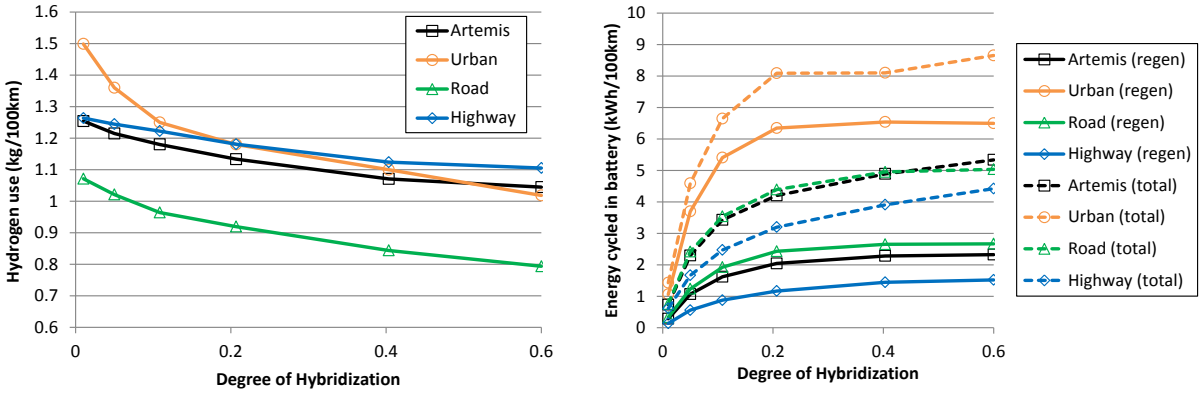

Figure 3.5: Fuel cell vehicle hydrogen use (left) and amount of energy stored in the battery (right) as a function of the degree of hybridization.

store from regeneration saturates at DoH ≈ 0.2 - 0.5, as can be seen in the right pane of Fig. 3.5. Second, with an increasing DoH more energy can intermediately be stored in the battery and the fuel cell operated at higher average efficiency. This control strategy slightly increases average fuel cell efficiency.

Plug-in hybrid electric vehicle (PHEV). A PHEV shares the characteristics of a hybrid and a pure battery electric vehicle. It is equipped with an engine and an electric motor, as well as a battery that can be charged from an external power source. Similar to an HEV, a PHEV can be implemented in a series, parallel, and series-parallel configuration. In the following a series configuration will be assumed, which is illustrated in Fig. 3.1 and can be found for example in the Chevrolet Volt. A PHEV can recuperate negative power at the wheel, similarly to a BEV. Generally, two main PHEV operating modes can be distinguished: charge depleting (CD) and charge sustaining (CS). CD mode means that the engine is off and the vehicle propelled by the electric motor with electricity stored in the battery. This operating mode is very similar to driving a BEV. When the battery reaches its minimum state of charge (or earlier) the engine switches on. It is connected to an electric generator which generates electricity that is used in an electric motor to propel the vehicle and/or stored in the battery. Usually the control strategy aims for a constant battery charge level (CS mode) as the battery should be primarily charged from an external source. Note that in CS mode the engine operating point is independent of the actual power demand of the vehicle. It can therefore operate at a point of high efficiency. The PHEV is simulated with a gasoline, diesel, and CNG engine, or a hydrogen fuel cell instead of an engine.

3.1.3 Parametric calculation of energy use

As described in chapter 2, tractive energy demand E_{trac} and regenerable energy E_{regen} can be parametrically calculated as a function of vehicle characteristics and driving cycle coefficients. The goal of this section is now to parametrically calculate vehicle energy use based on tractive and regenerable energy for the different drivetrain configurations described in the last section. For any drivetrain, energy consumption EC for vehicle propulsion per driving distance can be calculated as

$$EC = \frac{1}{\eta_{trac}} \cdot (E_{trac} + \eta_{regen} \cdot \kappa \cdot E_{regen}) \tag{3.1}$$

where η_{trac} is the average traction and η_{regen} the average regeneration efficiency for a specific vehicle and driving cycle. κ ($\in [0, 1]$) indicates the fraction of regenerative versus friction braking.[1] Eq. 3.1 can be explained in the following way: The energy demand in traction mode E_{trac} is reduced by the amount of regenerated energy that is used again during traction periods, i.e. $\eta_{regen} \cdot \kappa \cdot E_{regen}$ (note that E_{regen} is negative). The remaining energy must be provided by the powertrain with an efficiency η_{trac}. Note that in Eq. 3.1 η_{regen} is defined as the efficiency for a complete cycle backwards (storage) and forwards (use) through the powertrain, i.e. $\eta_{regen} = \eta^{use}_{regen} \cdot \eta^{store}_{regen}$. For vehicles for which the $\eta^{use}_{regen} = \eta_{trac}$, Eq. 3.1 can be written as

$$EC = \frac{1}{\eta_{trac}} \cdot (E_{trac} + \eta_{regen} \cdot \kappa \cdot E_{regen}) = \frac{1}{\eta_{trac}} \cdot E_{trac} + \eta^{store}_{regen} \cdot \kappa \cdot E_{regen} \tag{3.2}$$

Eq. 3.2 is valid e.g. for BEVs and can be interpreted intuitively: the total energy use is the difference of energy use during traction phases $\frac{1}{\eta_{trac}} \cdot E_{trac}$ and the amount of stored regenerable energy $\eta^{store}_{regen} \cdot \kappa \cdot E_{regen}$.

For PHEVs EC depends on the energy use in CS and CD mode. The PHEV utility factor UF defines the share of distance driven in CD mode relative to the total distance. The weighted energy use EC_{phev} is then calculated as

$$EC_{phev} = UF \cdot EC_{CD} + (1 - UF) \cdot EC_{CS} \tag{3.3}$$

[1] The value of κ depends on the limitations of the recuperative system regarding its power and energy storage capabilities. The actual load on the electric motor and the battery in regeneration periods is strongly influenced by the driving pattern, in particular the specific amount and duration of deceleration and the velocity distribution. Generally κ decreases at low speeds because then a certain amount of friction braking is required.

UF can be evaluated as a function of the vehicle electric range R_{el}. The equation $UF = 0.15 \cdot \log(R_{el})$ provides a good estimate compared to data shown in [Bradley & Qinn, 2010].[2]
The calculation of η_{trac} and η_{regen} is based on the product of the cycle-averaged efficiencies of the relevant vehicle components and the power flows between them. Section 3.1.2 describes the simulation of the power flows in and out of the relevant components within a specific drivetrain technology. The average operating point efficiency of a component can now be evaluated by integrating the power in and out of the component

$$\eta_{comp} = \frac{\sum P_{comp,out}}{\sum P_{comp,in}} \tag{3.4}$$

If the power flow of the device is bidirectional as in the case of an electric motor, η^{+}_{comp} refers to the efficiency in traction/forward and η^{-}_{comp} in regeneration/backward mode. For a battery the efficiency in traction and regenration mode is defined as the processed energy divided by the processed energy and the losses generated by the battery in this period

$$\eta_{bat} = \frac{\sum P_{bat}}{\sum P_{bat} + \sum P_{bat,loss}} \tag{3.5}$$

where the losses are calculated based on the battery current I_{bat} and the internal resistance R_{int} as $P_{bat,loss} = I^2_{bat} \cdot R_{int}$. In the following, the calculation of η_{trac} and η_{regen} for the different drivetrain types considered will be explained.

- For an ICEV η_{trac} can be calulated as the product of the average engine efficiency η_{eng} and transmission efficiency η_{trans}. Recuperation is not possible. Accordingly the equations for η_{trac} and η_{regen} are

$$\eta_{trac,icev} = \eta_{eng} \cdot \eta_{trans} \tag{3.6}$$

$$\eta_{regen,icev} = 0 \tag{3.7}$$

  where η_{eng} and η_{trans} are calculated for a specific driving cycle according to Eq. 3.4.

- For a BEV η_{trac} and η_{regen} are calculated as

$$\eta_{trac,bev} = \eta^{+}_{bat} \cdot \eta^{+}_{mot} \cdot \eta^{+}_{trans} \tag{3.8}$$

$$\eta_{regen,bev} = \eta^{+}_{trans} \cdot \eta^{+}_{mot} \cdot \eta^{+}_{bat} \cdot \eta^{-}_{bat} \cdot \eta^{-}_{mot} \cdot \eta^{-}_{trans} \tag{3.9}$$

[2] In addition to range, UF depends among other factors on the battery SOC at the beginning of the trip.

where η_{bat} and η_{mot} are the efficiencies of the battery and motor including the inverter, respectively. The superscripts + and − indicate that the power flow is in or out of the component. For the BEV this is equivalent to positive or negative power at the wheel, i.e. the distinction between traction and regeneration periods, respectively.

- In the case of a power-split HEV the calculation of η_{trac} is more complicated as multiple pathways are possible. The engine can either directly propel the vehicle or generate electric power with the generator which is stored in the battery and used at a later point to propel the vehicle with the electric motor. These efficiencies are calculated as

$$\eta_{trac,\,hev,\,p1} = \eta_{eng} \cdot \eta^{+}_{trans} \tag{3.10}$$

$$\eta_{trac,\,hev,\,p2} = \eta_{eng} \cdot \eta_{gen} \cdot \eta^{-}_{bat} \cdot \eta^{+}_{bat} \cdot \eta^{+}_{mot} \cdot \eta^{+}_{trans} \tag{3.11}$$

  The total traction efficiency can then be calculated as

$$\eta_{trac,\,hev} = \frac{1}{E_{p1}/\eta_{trac,\,hev,\,p1} + E_{p2}/\eta_{trac,\,hev,\,p2}} \tag{3.12}$$

  where E_{p1} and E_{p2} are the fractions of energy processed in path 1 and 2, respectively. Similar to the BEV, the calculation of the regeneration efficiency is

$$\eta_{regen,\,hev} = \eta^{+}_{trans} \cdot \eta^{+}_{mot} \cdot \eta^{+}_{bat} \cdot \eta^{-}_{bat} \cdot \eta^{-}_{mot} \cdot \eta^{-}_{trans} \tag{3.13}$$

- In a FCEV the equations for η_{trac} and η_{regen} are

$$\eta_{trac,\,fcev} = \eta_{fcs} \cdot \eta^{+}_{mot} \cdot \eta^{+}_{trans} \tag{3.14}$$

$$\eta_{regen,\,fcev} = \eta^{+}_{trans} \cdot \eta^{+}_{mot} \cdot \eta^{+}_{bat} \cdot \eta^{-}_{bat} \cdot \eta^{-}_{mot} \cdot \eta^{-}_{trans} \tag{3.15}$$

$$\tag{3.16}$$

  where η_{fcs} is the average operating efficiency of the fuel cell system including the balance of plant.

- A FCHEV possesses a large battery which allows full regeneration and operation of the fuel cell at a higher average efficiency. When the fuel cell power exceeds the required power of the vehicle, additional electricity is stored in the battery. There are accordingly two possible pathways for traction: Either the fuel cell powers the motor directly or stores energy in the battery, which is released later to propel the vehicle. The corresponding calculation of η_{trac}

is similar to Eq. 3.10 to 3.12 for the HEV

$$\eta_{trac,\,fchev,\,p1} = \eta_{fcs} \cdot \eta^{+}_{mot} \cdot \eta^{+}_{trans} \tag{3.17}$$

$$\eta_{trac,\,fchev,\,p2} = \eta_{fcs} \cdot \eta_{dc} \cdot \eta^{-}_{bat} \cdot \eta^{+}_{bat} \cdot \eta_{dc} \cdot \eta^{+}_{mot} \cdot \eta^{+}_{trans} \tag{3.18}$$

$$\eta_{trac,\,fchev} = \frac{1}{E_{p1}/\eta_{trac,\,fchev,\,p1} + E_{p2}/\eta_{trac,\,fchev,\,p2}} \tag{3.19}$$

$$\eta_{regen,\,fchev} = \eta^{+}_{trans} \cdot \eta^{+}_{mot} \cdot \eta^{+}_{bat} \cdot \eta^{-}_{bat} \cdot \eta^{-}_{mot} \cdot \eta^{-}_{trans} \tag{3.20}$$

- For a PHEV the traction efficiency is different in the charge depleting (CD) and charge sustaining (CS) modes. $\eta_{trac,\,phev,\,cs}$ is determined by the engine/generator efficiency, $\eta_{trac,\,phev,\,cd}$ is calculated as the traction efficiency of a BEV

$$\eta_{trac,\,phev,\,cd} = \eta^{+}_{bat} \cdot \eta^{+}_{mot} \cdot \eta^{+}_{trans} \tag{3.21}$$

$$\eta_{trac,\,phev,\,cs} = \eta_{eng} \cdot \eta_{gen} \cdot \eta^{+}_{mot} \cdot \eta^{+}_{trans} \tag{3.22}$$

$$\eta_{regen,\,phev} = \eta^{+}_{trans} \cdot \eta^{+}_{mot} \cdot \eta^{+}_{bat} \cdot \eta^{-}_{bat} \cdot \eta^{-}_{mot} \cdot \eta^{-}_{trans} \tag{3.23}$$

Eq. 3.1 is used for the calculation of energy use for vehicle propulsion. To calculate total vehicle energy use auxiliary loads must also be taken into account. For the calculation of auxiliary loads, electric accessories for safety and entertainment as well as vehicle size dependent heating and cooling requirements are considered. For a midsize car, electric auxiliaries of 300 W_{el}, a heating load of 3 kW_{th} and a cooling load of 1.5 kW_{th} throughout half and one third of the year are assumed, respectively. The heating of most electric vehicles today is based on resistive electric heating, however some manufacturers such as Renault already implement reversible heat pumps for heating and cooling in order to reduce vehicle energy use and increase range. Heat pumps can use outside air and/or waste heat from batteries and electric devices and reach a coefficient of performance (COP) of approximately 3 for heating at 0 °C and 2 at −10 °C in electric vehicle applications [Ahn et al., 2014; De Haan et al., 2013]. In this study it is assumed that ICEVs and HEVs cover the full heating demand using engine waste heat and that all vehicles without ICE (incl. PHEV in CD mode) are equipped with a reversible heat pump with a COP of 2 for 2012, 2.5 for 2030, and 3 for 2050. The total energy use per distance for auxiliaries is calculated based on the total electric auxiliary power demand, the average driving cycle velocity, and the efficiency of electric power provision.

3.1.4 Parameterization of vehicle efficiencies

As explained in the previous section 3.1.3, vehicle energy use can be calculated based on the mechanical energy demand for a certain driving cycle and the average operating point efficiencies for traction and regeneration. Mechanical energy demand is based in turn on driving cycle

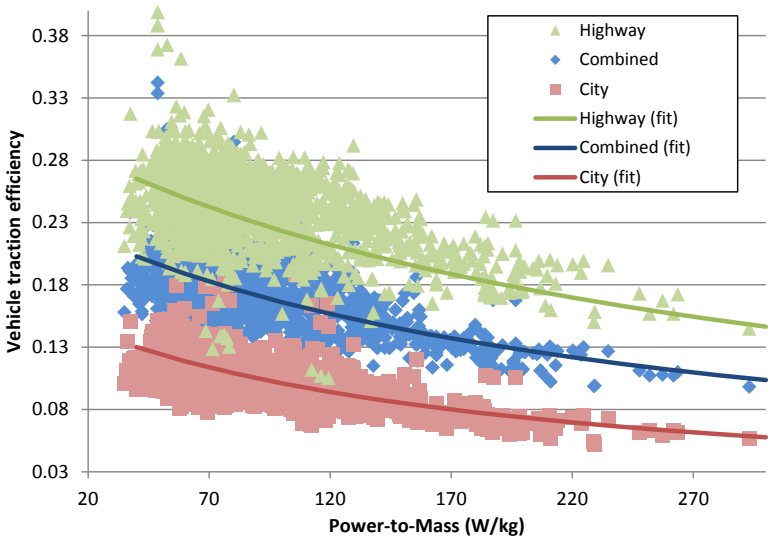

Figure 3.6: Traction efficiency of gasoline vehicles for the NEDC driving cycle sold in Switzerland in 2010 versus power-to-mass ratio.

coefficients and vehicle characteristics as explained in chapter 2. The aim of this section is to parameterize vehicle energy use according to vehicle performance and year of assessment. As mechanical energy demand is independent of those variables, the parameterization will only be applied to traction and regeneration efficiencies.

The main vehicle performance criterion influencing powertrain efficiency is acceleration time, which is approximately inversely proportional to the power-to-mass ratio (power of the prime mover to vehicle mass). With increasing power-to-mass ratio the efficiency generally decreases as the engine or electric motor are operated at lower efficiency operating points (compare Fig. 3.2 and 3.3). Fig. 3.6 shows the traction efficiency of new gasoline ICEVs sold in Switzerland in 2010 against the power-to-mass ratio. The efficiency is calculated based on the estimated vehicle mechanical energy demand[3] and the actual fuel consumption as reported by vehicle manufacturers for the NEDC, ECE, and EUDC driving cycles.[4] The efficiency therefore refers to those driving conditions. The analysis shows that the vehicle traction efficiency is highest for highway driving and lowest for urban driving with high and low average loads, respectively. The traction efficiency decreases with the power-to-mass ratio. Note that both effects are less significant for electric powertrains and that the decrease in traction efficiency with the power-to-mass ratio is smaller for diesel than gasoline engines.

In addition to the performance dependence, several future developments are expected to increase

[3] According to the the appropriate driving cycle coefficients (see Table 2.5) and the vehicle characteristics m, A_f, c_d, c_r. Since only m and A_f were available simplifying assumptions for c_d and c_r had to be made.

[4] Based on a dataset from Auto Schweiz representing Swiss passenger car sales of the year 2010.

powertrain efficiency.[5] Table 3.2 summarizes the assumptions for the development of peak efficiency of the main powertrain components from 2012 to 2050.

Table 3.2: Assumptions for the development of peak efficiency of the main powertrain components from 2012 to 2050.

Technology	**2012**	**2030**	**2050**
SI engine (Gasoline)	37	42	45
SI engine (CNG)	42	46.5	49
CI engine (Diesel)	38	43	46
Electric motor	94	95	96
Fuel cell system	58	60	61.5

In order to parameterize vehicle traction and regeneration efficiency according to the power-to-mass ratio and the year of assessment, all drivetrains were simulated for three discrete power-to-mass ratios (50, 100, 150 W/kg) and years (2012, 2030, 2050). Table A.1 lists the simulated traction and regeneration efficiencies for the average, urban (low speed), and highway (extra-high speed) segment of the WLTP driving cycle by powertrain, power-to-mass ratio, and year of assessment. Based on these results a nonlinear regression was performed to evaluate traction and regeneration efficiencies at any power-to-mass ratio and year within the given range. The following equation provided a good fit to the calculated data points

$$\eta_{regress} = \frac{1}{c_1 + c_2 \cdot \left(\frac{P}{m}\right) + \frac{c_3}{c_4 + y}} \tag{3.24}$$

where $\frac{P}{m}$ is the power-to-mass ratio and y the year of assessment. The coefficients c_1, c_2, c_3, c_4 are assessed using iterative least square fitting. Table A.2 lists the resulting parameterization coefficients c_1, c_2, c_3, c_4 by powertrain and driving region. Note that in this case $y \in [1, 3]$ with $y = 1$ corresponding to the year 2012 and $y = 3$ to the year 2050. Fig. 3.7 depicts simulation results of the gasoline ICEV traction efficiency versus power-to-mass ratio and year. In addition to the discrete simulations (red markers), the interpolated surfaces for different driving patterns are shown. As can be seen in the figure the form of Eq. 3.24 ensures a concave relation with regard to the power-to-mass ratio and a convex relation with regard to the future development.

[5] At this point only improvements of powertrain efficiency and no reduction of vehicle resistance parameters m, A_f, c_d, c_r are considered.

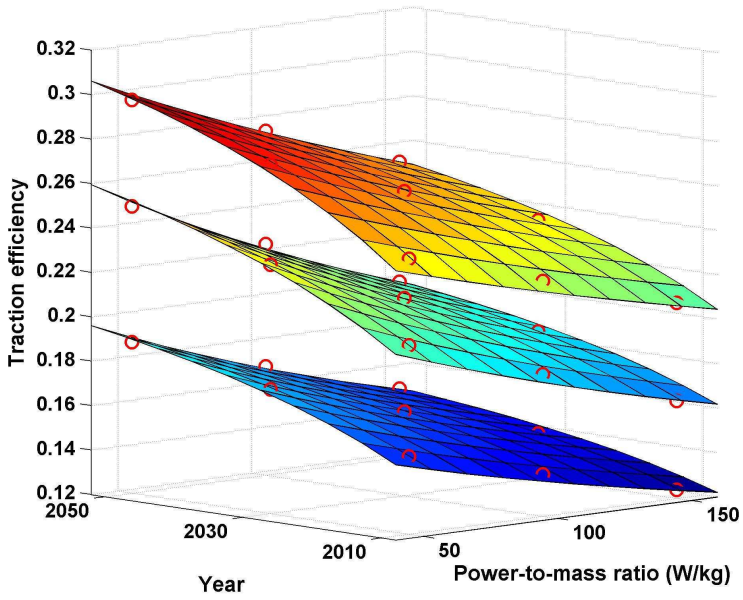

Figure 3.7: Gasoline ICEV traction efficiency versus power-to-mass ratio and year. Discrete simulation results (red markers) are interpolated with surfaces for which the levels correspond to different driving regions: Highway (top), average (middle), urban (bottom).

3.2 Vehicle configuration

In this section the car classes analyzed are presented and important performance requirements introduced.

3.2.1 Car classes

For the calculation of vehicle component sizes and energy use it is important to know several basic vehicle design parameters, e.g. A_f, c_d, c_r, the power-to-mass ratio, and glider mass.[6] In order to base these parameters on real vehicles, an analysis of the current passenger car market has been performed. New passenger cars are offered in a broad range of classes, varying greatly in size and performance characteristics. To capture this spread in the corresponding characteristics relevant for the simulation, sales-average characteristics by vehicle class have been calculated based on German passenger car sales of the year 2011.[7] Table 3.3 indicates the three most often sold car

[6]The glider is defined as the sum of all components that can be assumed equal among different powertrain types, e.g. the body, chassis, interior, etc.

[7]To reveal information on average vehicle characteristics by class, sales data that was originally issued from the German Federal Motor Transport Authority was complemented by IHS Global Insight with vehicle class related infor-

models for every considered class.

Table 3.3: Three top sales models by class for the German passenger car market in 2011.

Class	Manufacturer and model
Mini	Smart Fortwo, Renault Twingo, Fiat 500
Small	VW Polo, Opel Corsa, Ford Fiesta
Low-Midsize	VW Golf, Opel Astra, Ford Focus
Midsize	VW Passat, Mercedes C-Class, BMW Series 3
Up-Midsize	Mercedes E-Class, BMW Series 5, Audi A6
Luxury	BMW Series 7, Mercedes S-Class, Audi A8
Comp-MPV	VW Touran, Opel Meriva, Opel Zafira
MPV	VW Sharan, Ford S-Max, Mercedes Viano
Comp-SUV	VW Tiguan, BMW X1, Nissan Qashqai
SUV	BMW X3, Mercedes GLK-Class,VW Touareg
Comp-Sport	VW Scirocco, Mazda MX-5, Hyundai Veloster
Sport	Mercedes SLK-Class, Porsche 911, Audi TT
Transporter	VW Caddy, VW Transporter, Fiat Ducato

Fig. 3.8 shows the distribution of engine power, vehicle mass, direct CO_2 emission, and retail price (for the base model without additional features) by vehicle class using box plots.[8] The figure shows that the classification scheme used clearly separates the data for those characteristics. This is in particular the case for the high-volume, small and midsize segments, but less the case for the luxury and sport segments.

Table B.1 summarizes the sales-average power, mass, CO_2 emissions, retail price, and power-to-mass ratio by segment. In addition, values for frontal area and the aerodynamic drag coefficient are indicated based on a manual assessment of the top sales models. Glider mass is estimated as the difference of vehicle mass and the masses for engine, transmission, tank, and powertrain support.

To better illustrate the relation among the criteria assessed above, Fig. 3.8 shows vehicle mass versus CO_2 emission and engine power versus retail price for the same dataset. Obviously fuel consumption and hence CO_2 emissions increase with vehicle mass, however there is also a large spread in the data which can be explained in part by the higher efficiency of diesel relative to gasoline engines. In addition, the power-to-mass ratio strongly affects vehicle efficiency as mentioned in section 3.1.4, but is not considered in this representation. Note that the relation deviates from linearity due to a an increase of vehicle performance at higher mass. The relation between power and retail price is more linear and diesel vehicles on average are slightly more expensive at the same engine power.

mation.

[8] On each box the central black mark indicates the median of the data and the edges of the box are the upper and lower quartile. Within the box 50 % of the data values are located. The whiskers (thin line) extend to the lowest and highest values of the dataset that are not considered outliers. Outliers are plotted individually in gray circles [MathWorks, 2014].

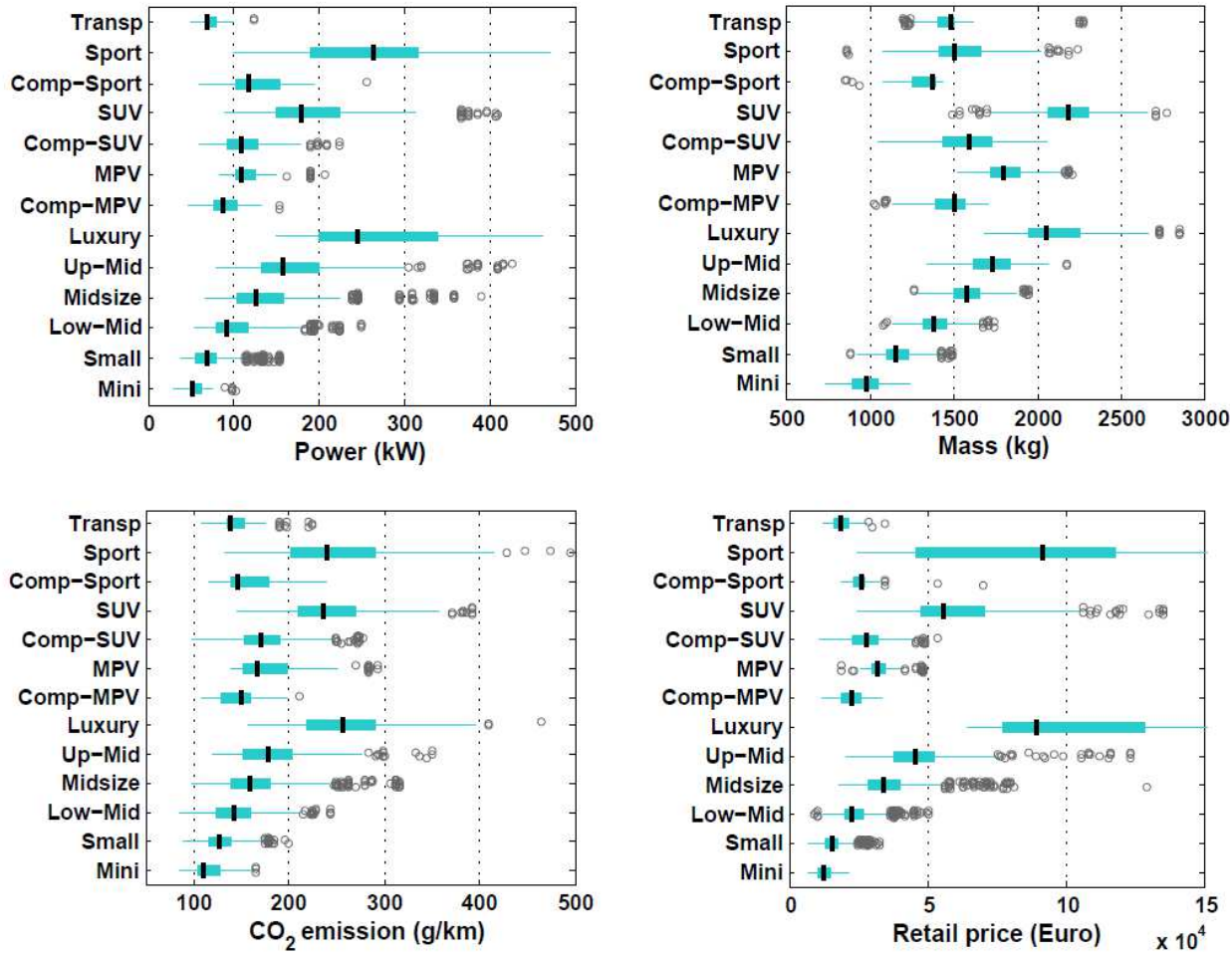

Figure 3.8: Distribution of vehicle power, mass, direct CO_2 emission, and retail price for Germen new passenger car sales in 2011 by vehicle class.

3.2.2 Performance requirements

As discussed in section 3.2.1, class related characteristics are important input parameters to the powertrain simulation. In addition, three main performance indicators are considered in the simulation and discussed in following.

Top speed

At high speed the power demand of the vehicle is largely dominated by aerodynamic drag and therefore vehicle top speed v_{max} is determined by the aerodynamic resistance and the maximum power P_{max} the powertrain can transmit to the wheels [Guzzella & Sciarretta, 2013]. Based on Eq.

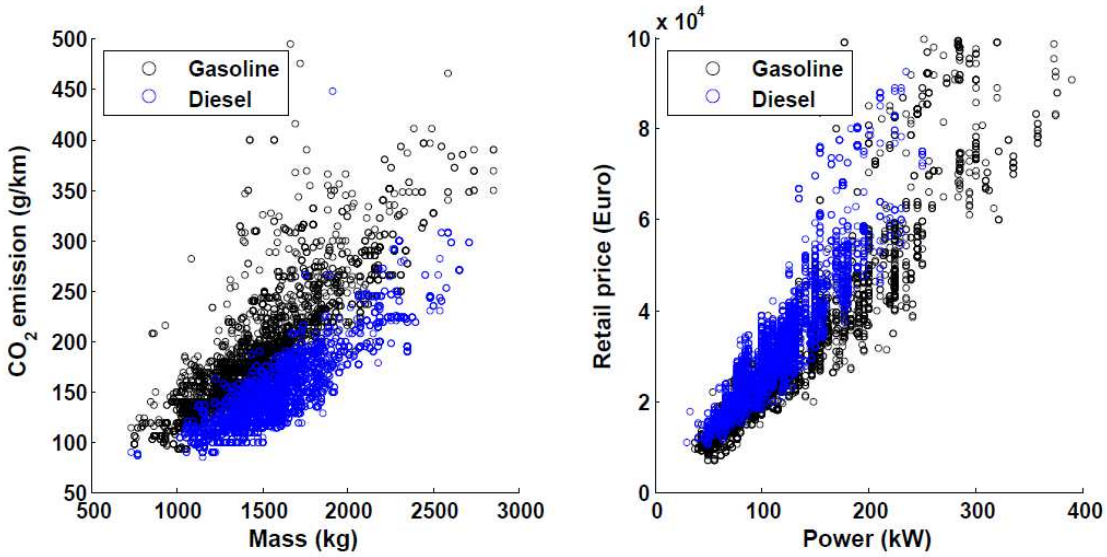

Figure 3.9: Relation of vehicle mass versus CO_2 emission and power versus retail price separately for gasoline and diesel vehicles.

2.1.1 v_{max} can be calculated as

$$v_{max} \approx \left(\frac{2 \cdot P_{max}}{\rho \cdot A_f \cdot c_d}\right)^{1/3} \tag{3.25}$$

For vehicles with a manual transmission the largest gear ratio is generally chosen to satisfy the maximum towing requirement while the smallest gear ratio is chosen to either reach the desired top speed or to maximize fuel economy [Guzzella & Sciarretta, 2013]. Due to the large speed and torque range of the electric motor, electric vehicles can use a single-speed transmission with a gear ratio set to meet both requirements.

Acceleration time

Another important performance attribute is the ability to reach a certain speed within an indicated time, e.g. the necessary time to accelerate the vehicle from 0 to 100 km/h. According to [Guzzella & Sciarretta, 2013] this time can be estimated as follows. Neglecting all vehicle resistances the energy E_0 required to accelerate to the desired speed is equal to the vehicle kinetic energy $\frac{1}{2} \cdot m \cdot v_0^2$. Assuming that half of the maximum engine power P_{max} is used to overcome the energy demand E_0, the acceleration time t_0 can be estimated as

$$t_0 \approx \frac{v_0^2 \cdot m}{P_{max}} \tag{3.26}$$

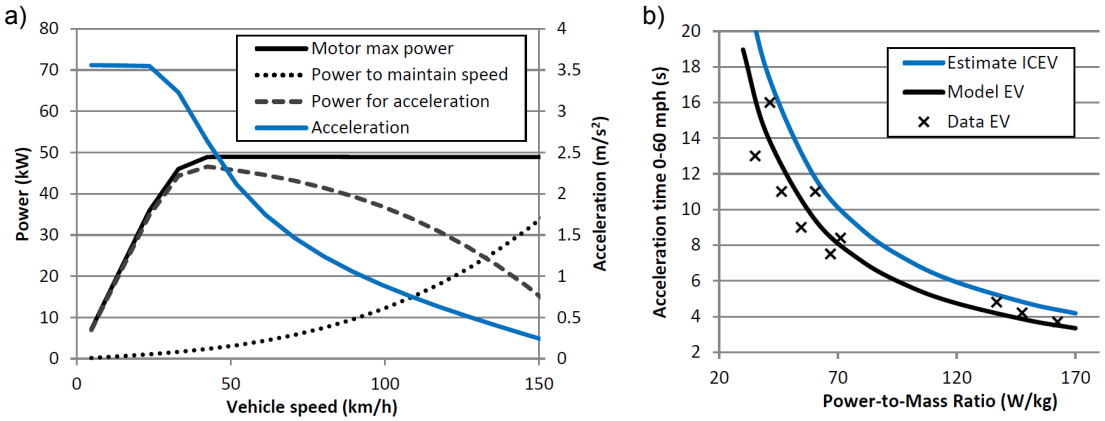

Figure 3.10: a) Model for the calculation of acceleration as a function of vehicle speed. b) Calculated and measured acceleration time versus power-to-mass ratio.

[Guzzella & Sciarretta, 2013] show that this approximation agrees well with the measured acceleration time for gasoline ICEVs.

In addition to this theoretical derivation, the acceleration time can be also estimated based on the torque versus speed characteristic of the motor or engine. For a typical electric motor torque is highest until the maximum power of the motor is reached, afterwards the power stays constant and maximum torque decreases (compare Fig. 3.3). In a vehicle with a single-speed transmission the motor speed can be directly related to vehicle speed based on the gear ratio and the wheel radius. Considering the maximum power the motor can deliver and the aerodynamic and rolling resistance losses, acceleration versus vehicle speed can be derived as shown in Fig. 3.10a. Calculating the time to reach a certain velocity for different power-to-mass (or P/m) ratios, the relation of t_0 to the P/m ratio can be evaluated. Fig. 3.10b compares the results to the approach based on Eq. 3.26 and measured data for several electric vehicles currently sold. The comparison shows that for both approaches t_0 is inversely proportional to the P/m ratio and that electric vehicles perform slightly better at the same value of P/m. The latter can be explained by the favorable torque-speed characteristic of the electric motor compared to an ICE and the missing gear-shift time losses. In the following, Eq. 3.26 will be used for the estimation of the maximum drivetrain power to reach a specified acceleration time. The slightly different relative performance of gasoline, diesel, and CNG engines as well as electric motors is accounted for by using an adjusted P/m ratio by powertrain technology.

Vehicle range

Vehicle range is an important vehicle design parameter, particularly for electric vehicles which have smaller energy storage capacities than conventional ICEVs. It can be calculated based on the energy storage capacity C_{es} and vehicle energy consumption per driving distance

$$R \approx \frac{C_{es}}{EC} \tag{3.27}$$

For BEVs C_{es} should refer to the useable energy considering the maximum operating range of the battery. If the vehicle has two energy storage and operating modes as in the case of a PHEV, two ranges can also be calculated based on the storage size and energy use for each mode.

Chapter 4

Mass, cost, and life cycle assessment

In this chapter the calculation of vehicle mass, cost, and life cycle indicators is introduced for a broad range of powertrain types and energy sources.

4.1 Calculation of vehicle mass

The powertrain and energy storage size of conventional and electric vehicles are linked to the performance and driving range of the car. In order to assess these dependencies, the vehicle is subdivided into three main components, the glider, powertrain, and energy storage. As mentioned earlier the glider refers to the sum of all components that can be assumed equal among different drivetrains and do not scale with the power or energy demand. The powertrain consists of the main power devices that propel the vehicle and scale with the power demand for maximum acceleration and speed. The energy storage size depends on the energy consumption and the desired range of the vehicle. Accordingly, vehicle mass is calculated as the sum of glider mass m_{gl}, powertrain mass m_{pt}, and energy storage system mass m_{es}

$$m = m_{gl} + \gamma \cdot \left(m_{pt} + m_{es}\right) \tag{4.1}$$

The factor γ is introduced to account for additional structural support of the powertrain and energy storage beyond the glider baseline [Bandivadekar et al., 2008] and is assumed to be 1.3. In the following the calculation of m_{pt} and m_{es} in Eq. 4.1 will be defined for different powertrains. The powertrain mass is calculated as

$$m_{pt} = P_{cont} \cdot SM_{pt,p} + \frac{P}{m} \cdot m \cdot SM_{pt,pm} + CM_{pt} \tag{4.2}$$

where P_{cont} is the maximum continuous power demand of the vehicle. P_{cont} is usually given by the top speed requirement according to Eq. 3.25 and the power-to-mass ratio $\frac{P}{m}$ by the acceleration requirement according to Eq. 3.26. $SM_{pt,p}$ and $SM_{pt,pm}$ are the sum of the specific powertrain masses that scale with maximum continuous power and the maximum power based on acceleration time, respectively. CM_{pt} is the fixed mass for all power devices used. $SM_{pt,p}$, $SM_{pt,pm}$, and CM_{pt} are calculated as

$$SM_{pt,p} = \sum_i CF_{p,i} \cdot SM_{pd,i} \tag{4.3}$$

$$SM_{pt,pm} = \sum_i CF_{pm,i} \cdot SM_{pd,i} \tag{4.4}$$

$$CM_{pt} = \sum_j CM_{pd,j} \tag{4.5}$$

where CF_p and CF_{pm} are the configuration factors for power devices according to Table 4.1 and SM_{pd} and CM_{pd} are the variable and fixed mass of power devices according to Table 4.2. The summation over i takes into account all power devices listed in Table 4.1 and 4.2 and the summation over j all power devices used, i.e. those for which either CF_{pm} or CF_p is unequal to zero.

The calculation of the energy storage system mass for different powertrains is

$$m_{es} = \sum_i C_{es,i} \cdot CF_{es,i} \cdot SM_{es,i} + \sum_j CM_{es,j} \tag{4.6}$$

where C_{es} is the energy storage capacity (defined by the range and energy use of the vehicle), CF_{es} the energy storage configuration factor according to Table 4.1, and SM_{es} and CM_{es} the variable and fixed mass of the energy storage components according to Table 4.2. The summation over i takes into account all energy storage devices listed in Table 4.1 and 4.2 and the summation over j all energy storage devices used.

Regarding the configuration factors CF_p, CF_{pm}, and CF_{es} as listed in Table 4.1, it is assumed that the maximum vehicle power results from the acceleration requirement rather than from the top speed requirement. In general, it is easily possible to also define configuration factors for the the opposite case in which the top speed requirement results in higher power. However, to avoid a distinction of cases for the evaluation of SM_p and SM_{pm}, the acceleration time and top speed requirements are tied together into a single performance indicator.[1]

Table 4.2 shows the assumed reference values of the specific masses for the power and energy

[1] Therefore, for every value of the acceleration time the resulting vehicle power and top speed are evaluated based on a midsize passenger car configuration. The relation $v_{max} \approx 430 \cdot t_0^{-0.35}$ is used in the following.

Table 4.1: Configuration factors by powertrain technology.

		ICEV-gasoline	ICEV-diesel	ICEV-cng	HEV-gasoline	HEV-diesel	HEV-cng	BEV	FCEV	FCHEV	PHEV-gasoline	PHEV-diesel	PHEV-cng	PHEV-h2
CF_{pm}	Gasoline engine	1	0	0	0.75	0	0	0	0	0	0	0	0	0
	Diesel engine	0	1	0	0	0.75	0	0	0	0	0	0	0	0
	CNG engine	0	0	1	0	0	0.75	0	0	0	0	0	0	0
	Motor	0	0	0	0.55	0.55	0.55	1	1	1	1	1	1	1
	Power battery	0	0	0	0.55	0.55	0.55	0	0.55	1	0	0	0	0
	Fuel cell	0	0	0	0	0	0	0	1	0	0	0	0	0
	ICEV trans.	1	1	1	0	0	0	0	0	0	0	0	0	0
	HEV trans.	0	0	0	1	1	1	0	0	0	0	0	0	0
	EV trans.	0	0	0	0	0	0	1	1	1	1	1	1	1
CF_{p}	Gasoline engine	0	0	0	0	0	0	0	0	0	1	0	0	0
	Diesel engine	0	0	0	0	0	0	0	0	0	0	1	0	0
	CNG engine	0	0	0	0	0	0	0	0	0	0	0	1	0
	Motor/Generator	0	0	0	0	0	0	0	0	0	1	1	1	0
	Power battery	0	0	0	0	0	0	0	0	0	0	0	0	0
	Fuel cell	0	0	0	0	0	0	0	0	1	0	0	0	1
	ICEV trans.	0	0	0	0	0	0	0	0	0	0	0	0	0
	HEV trans.	0	0	0	0	0	0	0	0	0	0	0	0	0
	EV trans.	0	0	0	0	0	0	0	0	0	0	0	0	0
CF_{es}	Battery	0	0	0	0	0	0	1	0	0	1	1	1	1
	Hydrogen tank	0	0	0	0	0	0	0	1	1	0	0	0	1
	Fuel tank	1	1	0	1	1	0	0	0	0	1	1	0	0
	CNG tank	0	0	1	0	0	1	0	0	0	0	0	1	0

storage devices. It consists of a fixed and variable part in order to realistically evaluate the component mass for different amounts of power and energy.[2] The specific mass of not yet fully developed technologies (such as batteries) is expected to decrease significantly over time. Table 4.2 lists the baseline assumptions for the current status and future development of specific masses of different vehicle components. The sensitivity of the resulting vehicle criteria to changes of important parameters will be analyzed in more detail in section 5.3, in particular regarding the future development of battery specific energy.

[2]Note that specific mass is inverse proportional to the more commonly used quantity of specific power or specific energy. Specific mass is preferably used because of its linear relation to mass which simplifies most equations used.

Table 4.2: Fixed and variable masses of vehicle components.

		Unit	2012	2030	2050	Sources
Power devices	Gasoline Engine	kg	60	54	50	[NRC, 2011; Brooker et al., 2013; Bandivadekar et al., 2008]
		kg/kW	0.70	0.50	0.40	
	Diesel Engine	kg	69	62	58	[Edwards et al., 2011]
		kg/kW	0.81	0.58	0.46	
	CNG Engine	kg	63	57	53	[Edwards et al., 2011]
		kg/kW	0.74	0.53	0.42	
	Motor and controller	kg	22	18	15	[Duleep et al., 2011; Graham, 2001; Simpson, 2006]
		kg/kW	0.85	0.70	0.60	
	Battery	kg	8	7	5	[Kalhammer et al., 2007; Nelson et al., 2011]
		kg/kW	1.00	0.75	0.50	
	Fuel cell system	kg	40	34	30	[Miotti, 2013; IEA, 2007]
		kg/kW	1.1	0.7	0.5	
	ICEV transmission	kg	55	50	50	[NRC, 2011]
		kg/kW	0.55	0.50	0.50	
	EV transmission	kg	35	30	30	[NRC, 2011; Kromer & Heywood, 2007]
		kg/kW	0.35	0.30	0.30	
Energy storages	Battery	kg	30	20	15	[Duleep et al., 2011; Gerssen-G. & Faaij, 2012; Nelson et al., 2011]
		kg/kWh	8.3	4.2	2.7	
	Hydrogen tank	kg	40	35	30	[Hua et al., 2010]
		kg/kWh	0.34	0.30	0.25	
	ICEV tank	kg	10	10	10	[NRC, 2011]
		kg/kWh	0.14	0.14	0.14	
	CNG tank	kg	25	20	20	[Edwards et al., 2011]
		kg/kWh	0.24	0.22	0.20	

4.2 Cost assessment

4.2.1 Manufacturing cost

Vehicle manufacturing costs MC are calculated as the sum of glider, energy storage, and powertrain manufacturing cost

$$MC = MC_{gl} + MC_{es} + MC_{pt} \tag{4.7}$$

The manufacturing costs of the powertrain MC_{pt} and energy storage MC_{es} are calculated as the sum of the costs for individual powertrain and energy storage devices

$$MC_{pt} = \sum_i MC_{pt,i} = \sum_i \left(P_i \cdot SC_{pt,i} + CC_{pt,i}\right) \tag{4.8}$$

$$MC_{es} = \sum_i MC_{es,i} = \sum_i \left(C_{es,i} \cdot SC_{es,i} + CC_{es,i}\right) \tag{4.9}$$

After the calculation of component sizes in Eq. 4.2 to 4.6, MC_{pt} and MC_{es} are evaluated based on the power P_i and the energy storage capacity $C_{es,i}$ per component and their variable and fixed specific costs SC and CC, respectively. The baseline assumptions for the variable and fixed costs of the power and energy storage devices are listed in Table 4.3. The specific costs of not yet fully developed technologies (in particular batteries and fuel cells) is assumed to decrease significantly over time due to efficiency gains, experience effects, and increase of production volume. An exchange rate of 0.8 Euro to 1 US$ has been used to compare reports prepared in different currencies. All prices are inflation adjusted to 2010 US$ according to the US consumer price index.
Manufacturing costs of the glider are either assessed per kg of material if only a single vehicle class is analyzed or per class based on the average retail price by segment (compare Table B.1) minus the estimated markup and the costs of powertrain and energy storage. The baseline glider costs are equal for different powertrain types, however 8 $/kg is accounted for additional support beyond glider baseline (similar to Eq. 4.1 for vehicle mass).[3] Note that the values given in Table 4.3 refer to the cost to the vehicle manufacturer. To convert this to the retail price of the car, a markup factor of 1.4 is assumed [NRC, 2011].

Table 4.3: Fixed and variable costs of vehicle components.

		Unit	2012	2030	2050	Sources
Power devices	Gasoline Engine	$	1000	1300	1500	[NRC, 2011; Edwards et al., 2011]
		$/kW	7.4	9.2	11.0	
	Diesel Engine	$	1150	1495	1725	[Edwards et al., 2011]
		$/kW	8.5	10.6	12.7	
	CNG Engine	$	1050	1365	1575	[Edwards et al., 2011]
		$/kW	7.8	9.7	11.6	
	Motor and controller	$	500	420	370	[Duleep et al., 2011; Graham, 2001; Simpson, 2006]
		$/kW	28	20	17	
	Battery	$	1000	600	400	[Kalhammer et al., 2007; Nelson et al., 2011]
		$/kW	50	32	24	
	Fuel cell system	$	10000	6000	1500	[Miotti, 2013; IEA, 2007]
		$/kW	400	90	40	
	ICEV transmission	$	800	900	1000	[NRC, 2011; Bandivadekar et al., 2008]
		$/kW	6	6	6	
	EV transmission	$	500	400	300	[NRC, 2011; Kromer & Heywood, 2007]
		$/kW	3	3	3	
Energy storages	Battery	$	8000	2500	1500	[Duleep et al., 2011; Gerssen-G. & Faaij, 2012; Nelson et al., 2011]
		$/kWh	440	150	120	
	Hydrogen tank	$	1500	1200	1000	[James, 2012]
		$/kWh	9.2	8.2	7.3	
	ICEV tank	$	300	300	300	[NRC, 2011]
		$/kWh	0.6	0.6	0.6	
	CNG tank	$	800	700	600	[Edwards et al., 2011]
		$/kWh	5.0	4.5	4.0	

[3] 8 $ is the approximate manufacturing cost per kg chassis of a conventional passenger car according to a mass and cost breakdown in [NRC, 2011].

4.2.2 Total cost

Total cost TC per vehicle-kilometer (vkm) is calculated as the sum of the vehicle purchase price PP and discounted energy costs

$$TC = \frac{PP + \sum_{i=1}^{LT} \frac{EC \cdot EP \cdot AD}{(1+DR)^i}}{AD \cdot LT} \tag{4.10}$$

where EP is the electricity or fuel price to the end consumer, AD the annual driving distance, LT the vehicle lifetime in years and DR the discount rate. As noted earlier, the purchase price is calculated based on manufacturing cost multiplied by a retail price equivalent markup factor minus any subsidy that may apply. Vehicle maintenance and repair costs, insurance, and parking costs are not considered. In the reference case a vehicle lifetime of 15 years, a total lifetime mileage of either 150,000 vkm or 250,000 vkm,[4] and a discount rate of either 0 or 5 % are assumed.
The lifetime of current batteries and fuel cells for automotive applications is limited. In the reference case the lifetime of current batteries and fuel cells is assumed to be 150,000 vkm in agreement with typical values indicated by the automotive industry [Hawkins et al., 2012a;b] and measured in fuel cell vehicle demonstration projects [Wipke et al., 2012; Spendelow et al., 2011]. Accordingly the cost of the battery and fuel cell is multiplied by the ratio of the assumed total vehicle mileage divided by the assumed distance after which the battery or fuel cell must be replaced. No discounting of future battery costs is assumed.
A broad range of primary energy sources for the production of fossil fuels, hydrogen, and electricity has been taken into account. The selection is based on [IEA, 2012a; LEA, 2010; Roth et al., 2009; Simons & Bauer, 2011b;a] and the availability of LCA datasets (compare section 4.3). Biofuels, Carbon Capture and Storage (CCS), and geothermal electricity have not been considered. Table 4.4 summarizes the assumed electricity and fuel prices to the end consumer at the charging or fueling station. Note that these prices do not include tax. In the following analysis an energy based tax of 24.1 $/GJ and a VAT of 8 % are added, which correspond to the taxation of gasoline fuel for transportion in Switzerland in 2013. Alternatively a vkm based tax independent of the drivetrain technology is assumed in order to ensure a constant tax revenue.

In the scenario from 2012 to 2050 the crude oil price increases from 95 to 149 $/bbl, the natural gas European import price from 9 to 14 $/mbtu, and the OECD coal import price from 100 to 126 $/tonne. Values for 2050 are according to the IEA Energy Technology Perspectives 6 degree C scenario, which assumes an extension of current trends and results in the highest fossil fuel prices among the different IEA scenarios. Levelized cost of electricity generation from coal in-

[4] A total lifetime mileage of 250,000 vkm is slightly lower than the average for passenger cars in the European Union [Smokers, 2011]

Table 4.4: Electricity and fuel prices ($/GJ) to the end consumer without tax.

		2012	2030	2050
Fuel	Gasoline	27.4	31.5	36.2
	Diesel	26.9	31.0	35.7
	CNG	27.9	30.1	32.6
Charging	CH mix	67.2	67.2	67.2
	NG	68.4	71.2	74.0
	Coal	60.1	62.9	65.6
	Nuclear	60.1	62.9	62.9
	Wind	68.4	65.6	64.3
	PV	124.0	82.3	68.4
	Hydro	68.4	68.4	68.4
Hydrogen	SMR distributed	42.1	37.3	37.2
	CG central	60.1	48.2	44.2
	Elec-CH distr.	106.7	94.8	87.0
	Elec-Nuclear central	81.9	70.8	63.3
	Elec-Wind central	94.3	74.8	65.2
	Elec-PV distr.	155.6	99.7	71.7
	Elec-Hydro central	94.3	78.7	70.9

creases from 0.07 to 0.09 $/kWh, for natural gas combined cycle (NGCC) power generation from 0.1 to 0.12 $/kWh, for nuclear from 0.07 to 0.08 $/kWh, and decreases for wind from 0.1 to 0.085 $/kWh, for photovoltaic (PV) utility-scale generation from 0.3 to 0.1 $/kWh, and remains constant for hydro at 0.1 $/kWh [IEA, 2012a; LEA, 2010]. Furthermore gasoline refining and station costs of 10.4 $/GJ, an electricity network cost of 0.086 $/kWh, and a charging station cost of 0.06 $/kWh are assumed [Elcom, 2014; Chang, 2012]. For comparison the current Swiss electricity mix (CH mix) is also indicated. Hydrogen production costs for coal gasification (CG), steam methane reforming (SMR) of natural gas, biomass gasification (BG), and electrolysis using average Swiss, nuclear, wind, PV, and hydro electricity, as well as hydrogen delivery, compression and station costs are assessed according to [DOE, 2014; Simbeck & Chang, 2002].

4.3 Life cycle assessment

Life Cycle Assessment (LCA) aims to quantify the burdens and expected impacts on the environment and on human health considering all processes contributing to the production, use and disposal of each vehicle. The basic approach used here disaggregates the total LCA result into the contributions from road construction and maintenance, vehicle production and disposal by subcomponent, fuel and/or electricity supply, exhaust emissions, and non-exhaust emissions from tire, brake, road wear, and fuel evaporation. The LCA from subcomponent production is calculated by multiplying the mass of the component by a mass specific LCA impact factor. Similarly,

road infrastructure and non-exhaust emissions are vehicle mass dependent, while fuel and/or electricity supply and exhaust emissions are calculated by taking into account vehicle energy consumption. Road and vehicle maintenance, as well as regulated emissions are calculated per vehicle-km. The connection between vehicle simulation and LCA ensures consistency among the different models and easy calculation of LCA results for different vehicle types and energy sources.

The actual life cycle inventories (LCI) of road infrastructure, vehicle components, fuel and electricity supply are established according to guidelines provided by ISO 14040/14044 [ISO, 2006a;b]. The analysis is performed within the SimaPro software using LCI data from the ecoinvent database [Spielmann et al., 2007; Simons, 2013; Ecoinvent, 2014] and special inventories for electric powertrains developed within the THELMA project [Notter et al., 2010; Althaus & Gauch, 2010; Simons & Bauer, 2010; Habermacher, 2011; Miotti, 2013]. The LCI of hydrogen production chains are documented in [Simons & Bauer, 2011b;a]. LCI of current and future electricity supply chains are based on ecoinvent version 2.2 and [Roth et al., 2009]. The functional unit that is used to compare the different vehicle and fuel options is one vehicle-km, i.e. one km driven with a certain vehicle and fuel type.

In order to interpret the life cycle inventory results of consumed resources and emissions with regard to the potential impact on the environment and on human health, different life cycle impact assessment (LCIA) methods exist. LCIA links the life cycle inventory through environmental mechanisms to the effects on protected areas such as human health. Impact categories are selected according to the most relevant environmental mechanisms and depend on the scope and regional context of the study. ISO 14042 describes the general framework and specifies the key requirements for LCIA. The calculation approach described above can in principal be applied to any life cycle inventory analysis and/or LCIA method.

The LCIA method used in this study is ReCiPe, which determines 18 relatively robust mid-point indicators close to the origin of the environmental mechanism and 3 highly aggregated and uncertain end-point indicators to evaluate the damage on human health, ecosystems, and resource availability [Goedkoop et al., 2009]. An example of LCIA in ReCiPe is the mid-point impact category climate change which is caused by the emission of greenhouse gases into the atmosphere. The mid-point indicator used in this case is the global warming potential (GWP), which is calculated based on the absorption properties of a species and its atmospheric lifetime. It is expressed as the IPCC CO_2 equivalent GWP over a certain timescale, usually 100 years.[5] Going a step further, GHG emission can be linked to an increase in temperature leading to different effects on human health. The corresponding mechanisms to evaluate the human health damage in terms of loss of life years and the damage to ecosystem diversity in terms of loss of species are explained

[5]For the ReCiPe method, the timescale varies depending on the perspective. Three cultural perspectives are distinguished: Individualist (short term, optimistic about future technology), hierarchist (consensus model), and egalitarian (long term, precautionary thinking). In this work the hierarchist perspective is always chosen.

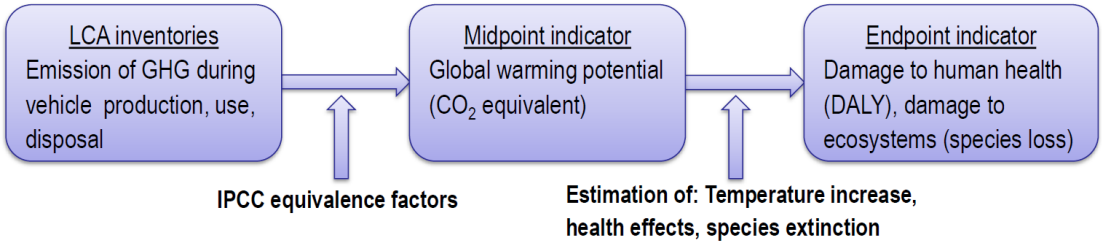

Figure 4.1: Illustration of the LCIA steps related to climate change.

in [Goedkoop et al., 2009]. This example is illustrated in Fig. 4.1.

Table 4.5 and 4.6 list the mid- and end-point impact categories and indicators implemented in ReCiPe and used throughout this work. Table C.1 to C.6 summarize the LCIA data used for the analysis. Table 4.7 lists the employed mid- to end-point characterization factors according to [Goedkoop et al., 2009]. The tables in the Appendix only include the data for mid-point and aggregated end-point indicators. The end-point indicators corresponding to each mid-point indicator individually can be calculated with the characterization factors in Table 4.7.

Table 4.5: ReCiPe mid-point impact categories and indicators.

Impact category	**Abbr.**	**Indicator**	**Unit**
Climate change	CC	Global warming potential	kg CO_2 eq
Ozone depletion	OD	OD potential	kg CFC-11 eq
Terrestrial acidification	TA	TA potential	kg SO_2 eq
Freshwater eutrophication	FE	FE potential	kg P eq
Marine eutrophication	ME	ME potential	kg N eq
Human toxicity	HT	HT potential	kg 1,4-DB eq
Photochemical oxidant formation	POF	POF potential	kg NMVOC
Particulate matter formation	PMF	PMF potential	kg PM10 eq
Terrestrial ecotoxicity	TET	TET potential	kg 1,4-DB eq
Freshwater ecotoxicity	FET	FET potential	kg 1,4-DB eq
Marine ecotoxicity	MET	MET potential	kg 1,4-DB eq
Ionising radiation	IR	IR potential	kg U235 eq
Agricultural land occupation	ALO	ALO potential	m^2a
Urban land occupation	ULO	ULO potential	m^2a
Natural land transformation	NLT	NLT potential	m^2
Water depletion	WD	WD potential	m^3
Metal depletion	MD	MD potential	kg Fe eq
Fossil depletion	FD	FD potential	kg oil eq

[6]* indicates that there is not a single characterization factor but that there are several depending on the type of substance or land use.

[7]NA indicates that even though this is an important link, no quantitative connection is established in ReCiPe so far.

Table 4.6: ReCiPe end-point impact categories and indicators.

Impact category	**Abbr.**	**Indicator**
Damage to human health	HH	Disability-adjusted loss of life years (DALY)
Damage to ecosystem diversity	ED	Loss of species during a year (species.yr)
Damage to resource availability	RA	Increased cost ($)

Table 4.7: RecCiPe mid-point to end-point characterization factors.

Code	**Unit**	**Human health (DALY)**	**Ecosystems (species.yr)**	**Resources ($)**
CC	kg CO2 eq	1.40E-06	7.93E-09	0
OD	kg CFC-11 eq	*[6]	NA[7]	0
TA	kg SO2 eq	0	5.8E-09	0
ME	kg N eq	0	NA	0
FE	kg P eq	0	4.44E-08	0
HT	kg 1,4-DB eq	7.00E-07	0	0
POF	kg NMVOC	3.90E-08	NA	0
PMF	kg PM10 eq	2.60E-04	0	0
TET	kg 1,4-DB eq	0	1.51E-07	0
FET	kg 1,4-DB eq	0	8.61E-10	0
MET	kg 1,4-DB eq	0	1.76E-10	0
IR	kg U235 eq	1.64E-08	NA	0
ALO	m2a	0	*	NA
ULO	m2a	0	*	NA
NLT	m2	0	*	NA
WD	m3	0	0	NA
MD	kg Fe eq	0	0	0.072
FD	kg oil eq	0	0	0.17

Chapter 5

Analytic evaluation of vehicle mass, energy use, and cost

The calculation of vehicle mass as introduced in section 4.1 shows that mass, energy use, and configuration parameters (such as range and acceleration performance) are interlinked, i.e. vehicle mass is dependent on range, energy use, and vice versa. In numeric vehicle simulations such as Advisor this coupling of mass and energy use is usually solved in an iterative calculation approach. The analytic calculation method of vehicle energy demand and energy use developed in chapter 2 and 3 allows to develop analytic expressions for vehicle mass and energy use as a function of configuration and technology parameters. The method described in this chapter enables scaling of component sizes and energy use based on vehicle design and technical parameters. Relative to previous methods the described approach is characterized by fast calculation time and offers new possibilities for sensitivity analysis and optimization. In this chapter the basic equations for the analytic calculation of vehicle criteria are first introduced and then applied to scenario and sensitivity analysis.

5.1 Basic concept and equations

5.1.1 Dynamic coupling of vehicle characteristics and energy use

Combining the analytic calculation of energy consumption in Eq. 3.1 with the analytic expressions of tractive and regenerative energy demand in Eq. 2.25 and 2.29, EC can be written as

$$EC = \frac{1}{\eta_{trac}} \cdot \left(E_{trac} + \eta_{regen} \cdot \kappa \cdot E_{regen}\right) \tag{5.1}$$

$$\begin{aligned} &= \frac{1}{\eta_{trac}} \cdot \Big(\left(A \cdot c_d \cdot A_f + B \cdot c_r \cdot m + C \cdot m\right) \\ &\quad + \eta_{regen} \cdot \kappa \cdot \left(A' \cdot c_d \cdot A_f + B' \cdot c_r \cdot m + C' \cdot m\right) \Big) \end{aligned} \tag{5.2}$$

The basic idea that allows dynamic coupling of vehicle characteristics and energy use is to express Eq. 5.2 as the sum of a vehicle parameter (e.g. m) dependent and independent part. In the following work two cases will be discussed. First, the dynamic coupling of mass and energy use, and second, the coupling of mass, size, and energy use.

Coupling of vehicle mass and energy use

In this approach EC is expressed as the sum of its mass-independent and mass-dependent parts, i.e.

$$EC = EC_0 + \frac{\partial EC}{\partial m} \cdot m \tag{5.3}$$

where EC_0 is defined as the energy use independent of vehicle mass and $\frac{\partial EC}{\partial m}$ the sensitivity of vehicle energy consumption to mass. Eq. 5.2 can be used to define EC_0 and $\frac{\partial EC}{\partial m}$

$$EC_0 = \frac{1}{\eta_{trac}} \cdot \left(A \cdot A_f \cdot c_d + \eta_{regen} \cdot \kappa \cdot A' \cdot A_f \cdot c_d\right) \tag{5.4}$$

$$\frac{\partial EC}{\partial m} = \frac{1}{\eta_{trac}} \cdot \left((B \cdot c_r + C) + \eta_{regen} \cdot \kappa \cdot (B' \cdot c_r + C')\right) \tag{5.5}$$

While the mass-independent part EC_0 depends on the aerodynamic drag in both the traction and regeneration phases, $\frac{\partial EC}{\partial m}$ depends on rolling resistance and kinetic energy. Auxiliary load is assumed to be independent of vehicle mass and added to EC_0 in Eq. 5.4. Eq. 5.4 and 5.5 can be evaluated at specific conditions for which the vehicle efficiencies and A_f, c_d, c_r are known, e.g. for a specific powertrain type and vehicle class.
The method can be also used to estimate an increase in energy use ΔEC corresponding to a certain mass increase Δm according to

$$\Delta EC = \frac{\partial EC}{\partial m} \cdot \Delta m \tag{5.6}$$

Note that in Eq. 5.6 it is assumed that the average operating point efficiencies η_{trac} and η_{regen} are independent of a change of mass, which is approximately valid if the power-to-mass ratio is constant.

Coupling of vehicle mass, size, and energy use

In general an increase of vehicle mass is accompanied by a change of vehicle size. The increase of frontal area is important for the calculation of vehicle energy use. To consider the effect of a change of mass on frontal area and hence on energy use the following method can be applied. If the relation between mass and A_f is known it can be considered by adding the sensitivity of energy consumption to frontal area in Eq. 5.3

$$EC = EC_0 + \frac{\partial EC}{\partial m} \cdot m + \frac{\partial EC}{\partial A_f} \cdot A_f \tag{5.7}$$

In this case $\frac{\partial EC}{\partial A_f}$ is calculated according to

$$\frac{\partial EC}{\partial A_f} = \frac{1}{\eta_{trac}} \cdot \left(A \cdot A_f \cdot c_d + \eta_{regen} \cdot \kappa \cdot A' \cdot A_f \cdot c_d \right) \tag{5.8}$$

EC_0 now only includes auxiliary loads and $\frac{\partial EC}{\partial m}$ is calculated in the same way as in Eq. 5.5. The change in vehicle energy use for a change in mass (that is accompanied by a change of frontal area) can now be calculated as

$$\Delta EC = \frac{\partial EC}{\partial m} \cdot \Delta m + \frac{\partial EC}{\partial A_f} \cdot \Delta A_f(\Delta m) \tag{5.9}$$

The correct relation between mass and frontal area $A_f(m)$ must be defined in the context of the analysis.

The results calculated with Eq. 5.3, 5.6, 5.7, and 5.9 show exact agreement when compared against numeric vehicle simulations.

5.1.2 Analytic scaling of vehicle mass and energy use

As defined in Eq. 4.1 vehicle mass is calculated as the sum of glider, energy storage, powertrain, and structural support mass. Rewriting Eq. 4.1 to 4.6, vehicle mass can be calculated as

$$m = m_{gl} + \gamma \cdot \left(P_{cont} \cdot SM_{pt,p} + \frac{P}{m} \cdot m \cdot SM_{pt,pm} + EC \cdot R \cdot SM_{es} + CM \right) \tag{5.10}$$

Here it is assumed that the energy storage capacity is given by vehicle energy consumption EC times vehicle range R. The fixed masses of powertrain and energy storage are summarized in CM. For the calculation of powertrain mass, power devices that scale with the maximum continuous power versus the acceleration power requirement are distinguished. In the simplest case $SM_{pt,p}$ is zero and the maximum acceleration power requirement is sufficient to define the component configuration, e.g. for the ICEV, HEV, BEV, and FCEV (compare Table 4.1). In this case Eq. 5.10 simplifies to

$$m = m_{gl} + \gamma \cdot \left(\frac{P}{m} \cdot m \cdot SM_{pt,pm} + EC \cdot R \cdot SM_{es} + CM \right) \tag{5.11}$$

As can be seen from Eq. 5.10 and 5.11 vehicle mass depends on the energy consumption of the vehicle which in turn depends on its mass. Using a numeric vehicle simulation the relation between mass and energy consumption is usually evaluated iteratively [Markel et al., 2002; Campanari et al., 2009; Gerssen-G. & Faaij, 2012], i.e. an initial value for the energy consumption is assumed and the powertrain and energy storage system mass stepwise adjusted to reach the desired range and performance. In the following a new analytic approach is introduced based on the sensitivity of vehicle energy consumption to mass and by solving two recursive sequences that describe the relation between vehicle mass, energy consumption, range, and power-to-mass ratio.

Four cases are distinguished:

- **Case A** Calculation of vehicle mass according to Eq. 5.11, without consideration of the coupling of vehicle mass and size.
- **Case B** Calculation of vehicle mass according to Eq. 5.11, including consideration of the coupling of vehicle mass and size.
- **Case C** Calculation of vehicle mass according to Eq. 5.10, without consideration of the coupling of vehicle mass and size.
- **Case D** Calculation of vehicle mass according to Eq. 5.10, including consideration of the

coupling of vehicle mass and size.

Case A

Using Eq. 5.11 vehicle mass is calculated by solving the recursive sequence

$$m[n+1] = m_{gl} + \gamma \cdot \left(\frac{P}{m} \cdot m[n] \cdot SM_{pt,pm} + EC(m) \cdot R \cdot SM_{es} + CM \right) \tag{5.12}$$

which converges to

$$m = \frac{m_{gl} + \gamma \cdot (CM + EC(m) \cdot R \cdot SM_{es})}{1 - \gamma \cdot \frac{P}{m} \cdot SM_{pt,pm}} \tag{5.13}$$

Eq. 5.13 depends on vehicle energy consumption which is a priori not known. Using the relation between mass and energy use according to Eq. 5.3 energy consumption can be calculated by solving the second recursive sequence

$$EC[n+1] = EC_0 + \frac{\partial EC}{\partial m} \cdot m(EC) \tag{5.14}$$

$$= EC_0 + \frac{\partial EC}{\partial m} \cdot \left(\frac{m_{gl} + \gamma (\cdot CM + EC[n] \cdot R \cdot SM_{es})}{1 - \gamma \cdot \frac{P}{m} \cdot SM_{pt,pm}} \right) \tag{5.15}$$

which converges to

$$EC = \frac{EC_0 + \frac{\partial EC}{\partial m} \cdot (m_{gl} + \gamma \cdot CM) - \gamma \cdot EC_0 \cdot \frac{P}{m} \cdot SM_{pt,pm}}{1 - \gamma \cdot \frac{\partial EC}{\partial m} \cdot R \cdot SM_{es} - \gamma \cdot \frac{P}{m} \cdot SM_{pt,pm}} \tag{5.16}$$

Substituting Eq. 5.16 in Eq. 5.13 gives vehicle mass independent of energy consumption

$$m = \frac{m_{gl} + \gamma \cdot (CM + EC_0 \cdot R \cdot SM_{es})}{1 - \gamma \cdot \frac{\partial EC}{\partial m} \cdot R \cdot SM_{es} - \gamma \cdot \frac{P}{m} \cdot SM_{pt,pm}} \tag{5.17}$$

Eq. 5.16 and Eq. 5.17 are the two fundamental equations used for the calculation of vehicle energy consumption and mass as a function of the glider mass, range, and specific masses of energy storage and powertrain.

Case B

In this case the calculation of vehicle mass is equivalent to Eq. 5.12 and Eq. 5.13, however Eq. 5.7 is used instead of Eq. 5.3 for the calculation of energy consumption

$$EC[n+1] = EC_0 + \frac{\partial EC}{\partial m} \cdot m(EC) + \frac{\partial EC}{\partial A_f} \cdot A_f(m(EC)) \tag{5.18}$$

$$\begin{aligned} &= EC_0 + \frac{\partial EC}{\partial m} \cdot \left(\frac{m_{gl} + \gamma \cdot CM + \gamma \cdot EC[n] \cdot R \cdot SM_{es}}{1 - \gamma \cdot \frac{P}{m} \cdot SM_{pt,pm}} \right) \\ &\quad + \frac{\partial EC}{\partial A_f} \cdot \left(A_{f,0} + \frac{\partial A_f}{\partial m} \cdot \left(\frac{m_{gl} + \gamma \cdot CM + \gamma \cdot EC[n] \cdot R \cdot SM_{es}}{1 - \gamma \cdot \frac{P}{m} \cdot SM_{pt,pm}} \right) \right) \end{aligned} \tag{5.19}$$

which converges to

$$EC = \frac{EC_0 + \left(A_{f,0} \cdot \frac{\partial EC}{\partial A_f} + \frac{\partial EC}{\partial m} \right) \cdot \left(m_{gl} + \gamma \cdot CM \right) - \gamma \cdot EC_0 \cdot \frac{P}{m} \cdot SM_{pt,pm} + A_{f,0} \cdot \left(\frac{\partial EC}{\partial A_f} - \gamma \cdot \frac{\partial EC}{\partial A_f} \cdot \frac{P}{m} \cdot SM_{pt,pm} \right)}{1 - \left(\frac{\partial A_f}{\partial m} \cdot \frac{\partial EC}{\partial A_f} + \frac{\partial EC}{\partial m} \right) \cdot \gamma \cdot R \cdot SM_{es} - \gamma \cdot \frac{P}{m} \cdot SM_{pt,pm}} \tag{5.20}$$

Substituting Eq. 5.20 in Eq. 5.13 gives vehicle mass independent of energy consumption

$$m = \frac{m_{gl} + \gamma \cdot \left(CM + \left(A_{f,0} \cdot \frac{\partial EC}{\partial A_f} + EC_0 \right) \cdot R \cdot SM_{es} \right)}{1 - \gamma \cdot \left(\frac{\partial A_f}{\partial m} \cdot \frac{\partial EC}{\partial A_f} + \frac{\partial EC}{\partial m} \right) \cdot R \cdot SM_{es} - \gamma \cdot \frac{P}{m} \cdot SM_{pt,pm}} \tag{5.21}$$

Case C

In this case vehicle mass is calculated according to Eq. 5.10. The recursive sequence

$$m[n+1] = m_{gl} + \gamma \cdot \left(P_{cont} \cdot SM_{pt,p} + \frac{P}{m} \cdot m[n] \cdot SM_{pt,pm} + EC(m) \cdot R \cdot SM_{es} + CM \right) \tag{5.22}$$

converges to

$$m = \frac{m_{gl} + \gamma \cdot \left(CM + P_{cont} \cdot SM_{pt,p} + EC(m) \cdot R \cdot SM_{es} \right)}{1 - \gamma \cdot \frac{P}{m} \cdot SM_{pt,pm}} \tag{5.23}$$

Using the relation between mass and energy use according to Eq. 5.3 energy consumption is calculated by solving

$$EC[n+1] = EC_0 + \frac{\partial EC}{\partial m} \cdot m(EC) \tag{5.24}$$

$$= EC_0 + \frac{\partial EC}{\partial m} \cdot \left(\frac{m_{gl} + \gamma \cdot \left(CM + P_{cont} \cdot SM_{pt,p} + EC[n] \cdot R \cdot SM_{es} \right)}{1 - \gamma \cdot \frac{P}{m} \cdot SM_{pt,pm}} \right) \tag{5.25}$$

which converges to

$$EC = \frac{EC_0 + \frac{\partial EC}{\partial m} \cdot \left(m_{gl} + \gamma \cdot \left(CM + P_{cont} \cdot SM_{pt,p} \right) \right) - \gamma \cdot EC_0 \cdot \frac{P}{m} \cdot SM_{pt,pm}}{1 - \gamma \cdot \frac{\partial EC}{\partial m} \cdot R \cdot SM_{es} - \gamma \cdot \frac{P}{m} \cdot SM_{pt,pm}} \tag{5.26}$$

Substituting Eq. 5.26 in Eq. 5.23 gives vehicle mass independent of energy consumption

$$m = \frac{m_{gl} + \gamma \cdot \left(CM + P_{cont} \cdot SM_{pt,p} + EC_0 \cdot R \cdot SM_{es} \right)}{1 - \gamma \cdot \frac{\partial EC}{\partial m} \cdot R \cdot SM_{es} - \gamma \cdot \frac{P}{m} \cdot SM_{pt,pm}} \tag{5.27}$$

Case D

In this final case the calculation of vehicle mass is equivalent to Eq. 5.22. Eq. 5.7 is used for the calculation of energy consumption

$$EC[n+1] = EC_0 + \frac{\partial EC}{\partial m} \cdot m(EC) + \frac{\partial EC}{\partial A_f} \cdot A_f(m(EC)) \tag{5.28}$$

$$= EC_0 + \frac{\partial EC}{\partial m} \cdot \left(\frac{m_{gl} + \gamma \cdot \left(CM + P_{cont} \cdot SM_{pt,p} + EC[n] \cdot R \cdot SM_{es} \right)}{1 - \gamma \cdot \frac{P}{m} \cdot SM_{pt,pm}} \right) + \frac{\partial EC}{\partial A_f} \cdot \left(A_{f,0} + \frac{\partial A_f}{\partial m} \cdot \left(\frac{m_{gl} + \gamma \cdot \left(CM + P_{cont} \cdot SM_{pt,p} + EC[n] \cdot R \cdot SM_{es} \right)}{1 - \gamma \cdot \frac{P}{m} \cdot SM_{pt,pm}} \right) \right) \tag{5.29}$$

which converges to

$$EC = \frac{EC_0 + \left(A_{f,0} \cdot \frac{\partial EC}{\partial A_f} + \frac{\partial EC}{\partial m}\right) \cdot \left(m_{gl} + \gamma \cdot \left(CM + P_{cont} \cdot SM_{pt,p}\right)\right) - \gamma \cdot EC_0 \cdot \frac{P}{m} \cdot SM_{pt,pm} + A_{f,0} \cdot \left(\frac{\partial EC}{\partial A_f} - \gamma \cdot \frac{\partial EC}{\partial A_f} \cdot \frac{P}{m} \cdot SM_{pt,pm}\right)}{1 - \left(\frac{\partial A_f}{\partial m} \cdot \frac{\partial EC}{\partial A_f} + \frac{\partial EC}{\partial m}\right) \cdot \gamma \cdot R \cdot SM_{es} - \gamma \cdot \frac{P}{m} \cdot SM_{pt,pm}} \tag{5.30}$$

Substituting Eq. 5.30 in Eq. 5.23 gives vehicle mass independent of energy consumption

$$m = \frac{m_{gl} + \gamma \cdot \left(CM + P_{cont} \cdot SM_{pt,p} + \left(A_{f,0} \cdot \frac{\partial EC}{\partial A_f} + EC_0\right) \cdot R \cdot SM_{es}\right)}{1 - \gamma \cdot \left(\frac{\partial A_f}{\partial m} \cdot \frac{\partial EC}{\partial A_f} + \frac{\partial EC}{\partial m}\right) \cdot R \cdot SM_{es} - \gamma \cdot \frac{P}{m} \cdot SM_{pt,pm}} \tag{5.31}$$

The scaling of vehicle mass and energy use resulting from the models developed in this section was compared against numeric vehicle simulations and showed exact agreement. The coverage of cases in this section is not exhaustive, but the employed scaling methods are very flexible and can be adjusted to the type of problem investigated. Based on the knowledge of vehicle mass and energy use, the mass and cost of individual components can be easily calculated considering the component configuration used according to Table 4.1, and the specific masses and costs of components according to Table 4.2 and Table 4.3. Furthermore, vehicle energy use and component sizes can be linked to model vehicle life cycle indicators as explained in section 4.3. For brevity the explicit equations for vehicle costs and life cycle indicators are not given, but can be expressed in a closed form similar to the above equations for vehicle mass and energy use.

5.2 Scenario analysis of vehicle criteria

The method developed in the previous section is now applied to analyze the development of ICEV, BEV, and FCEV mass, energy use, and cost from 2012 to 2050. Vehicle mass, energy use, and cost are calculated for a midsize passenger car platform. The variation of vehicle criteria as a function of range and glider mass is analyzed relative to a baseline scenario. Furthermore the total cost difference between the different drivetrain technologies is investigated as a function of important parameters.

As explained in the previous section, various methods for the scaling of vehicle mass and energy use are possible according to configuration parameters. Eq. 5.11 will be used for the calculation of ICEV, BEV, and FCEV mass in the following. The influence of a change of vehicle mass (e.g. by changing vehicle range) on vehicle size is not considered in detail. Therefore such an effect is neglected in the baseline analysis and the coefficients A_f, c_d, c_r assumed to be constant and independent of mass. Accordingly vehicle mass and energy use are calculated based on the

equations developed in section 5.1.2, Case A. This model is valid for the reference car but slightly underestimates the scaling of vehicle mass and energy use with range and glider mass. The effect of a connection between vehicle mass and frontal area (by the use of the equations developed in section 5.1.2, Case B) on the results will be discussed in section 5.2.3.

5.2.1 Baseline scenario

This section explains the baseline assumptions for the calculation of ICEV, BEV, and FCEV mass, energy use, and cost from 2012 to 2050 according to the model of section 5.1.2d. For the 2012 vehicle this work assumes the frontal area, aerodynamic drag, and rolling resistance coefficients of a midsize passenger car according to Table 2.4 and a baseline glider mass of 950 kg. In the future scenario glider mass, c_d, and c_r are annually reduced by 0.5 %, which equates to a total reduction of ca. 17 % by 2050. A power-to-mass ratio of 70 W/kg for the ICEV and 65 W/kg for the BEV and FCV is assumed for all years assessed corresponding to an acceleration time of approximately 11 s from 0 to 100 km/h. The reference range of the BEV is increased from 150 km in 2012 to 250 km in 2030 and to 350 km in 2050. The range of the FCV and ICEV is assumed constant at 700 km. Vehicle traction and regeneration efficiencies are calculated for a gasoline ICEV, BEV, and FCEV for the NEDC driving cycle as explained in section 3.1.4. Auxiliary loads according to section 3.1.3 are assumed. EC_0 and $\frac{\partial EC}{\partial m}$ are calculated using Eq. 5.4, 5.5 and the coefficients for the NEDC driving cycle in Table 2.5. Table 5.1 lists the values of EC_0 and $\frac{\partial EC}{\partial m}$ calculated this way and used in the following analysis. Note that the use of the NEDC driving cycle ensures constant energy demand coefficients over a broad range of vehicle parameters as analyzed in section 2.2.2.

Table 5.1: Mass independent energy use and its sensitivity to mass by powertrain technology and time.

		ICEV			**BEV**			**FCV**		
	Unit	2012	2030	2050	2012	2030	2050	2012	2030	2050
EC_0	MJ/km	0.89	0.72	0.62	0.31	0.27	0.24	0.5	0.43	0.38
$\frac{\partial EC}{\partial m}$	kJ/(km·kg)	1.15	0.94	0.84	0.2	0.18	0.17	0.43	0.39	0.35

Specific mass and cost of powertrain and energy storage are calculated according to section 4.1 and 4.2, taking into account the specific mass and cost of individual components as listed in Table 4.2 and 4.3. The resulting aggregated values are summarized in Table 5.2.

Total costs are calculated per vkm with a lifetime driving distance of 150,000 km (in the reference case) and without discounting. Energy prices refer to the Swiss electricity mix (in constant 2010 US$ for future scenarios), gasoline fuel, and hydrogen from SMR according to section 4.2.2 and Table 4.4. An energy based tax is assumed for all energy carriers and assessment years.

Table 5.2: Aggregated specific mass and cost of powertrain and energy storage.

			ICEV			BEV			FCV		
		Unit	2012	2030	2050	2012	2030	2050	2012	2030	2050
Mass	$SM_{pt,pm}$	kg/kW	1.3	1.0	0.9	1.2	1.0	0.9	2.9	2.1	1.9
	SM_{es}	kg/MJ	0.039	0.039	0.039	2.31	1.17	0.75	0.09	0.08	0.07
	CM	kg	125	114	110	87	68	60	145	124	110
Cost	$SC_{pt,pm}$	\$/kW	13	15	17	31	23	20	459	131	73
	SC_{es}	\$/MJ	0.17	0.17	0.17	122.2	41.7	33.3	2.6	2.3	2.0
	CC	\$	2100	2500	2800	9000	3320	2170	13500	8620	3570

Fig. 5.1 shows the resulting vehicle mass, energy use, manufacturing and total cost using the baseline assumptions described above. The acceleration performance is equal for the different drivetrain technologies and assessment years. Note that for all criteria secondary effects are also considered, e.g. that a lighter glider requires smaller energy storage for a given range and acceleration performance, which allows further weight reduction, leading to lower energy consumption, etc. Over time the mass of all vehicles is decreasing due to lighter gliders and an increasing specific power and energy of the powertrain and energy storage. The mass of the FCV is highest due to the relatively high range that is assumed and the many components in the powertrain. The mass of the BEV is highly sensitive to range, as shown in the next section. Due to reductions of glider mass, c_d, and c_r, as well as powertrain efficiency improvements, the energy use of all drivetrains is reduced over time. The manufacturing costs of the BEV and FCV are much higher than for the ICEV in 2012 but are expected to significantly decrease in the future, mainly due to reductions in battery and fuel cell costs. In 2012 the total costs of the BEV and FCV are significantly higher than for the ICEV and are dominated by manufacturing costs. For the assumed development of battery, fuel cell, and energy costs, total costs of the ICEV and BEV converge by 2030 and total costs for all drivetrains converge by 2050.

5.2.2 Influence of vehicle range and glider mass on vehicle criteria

This section analyzes the variation of vehicle criteria as a function of range and glider mass using the equations derived in section 5.1, in particular for Case A (Eq. 5.16 and 5.17). This model assumes that the coefficients A_f, c_d, c_r remain constant for a variation of range and glider mass. The possible feedback of a change of mass on A_f is considered in the next section.

Fig. 5.2 shows the variation of vehicle mass, energy use, manufacturing cost, and total cost as a function of range by drivetrain for the year 2012 and 2050. BEV mass in 2012 is highly sensitive to range due to the relatively low energy density of the energy storage. The effect is much smaller

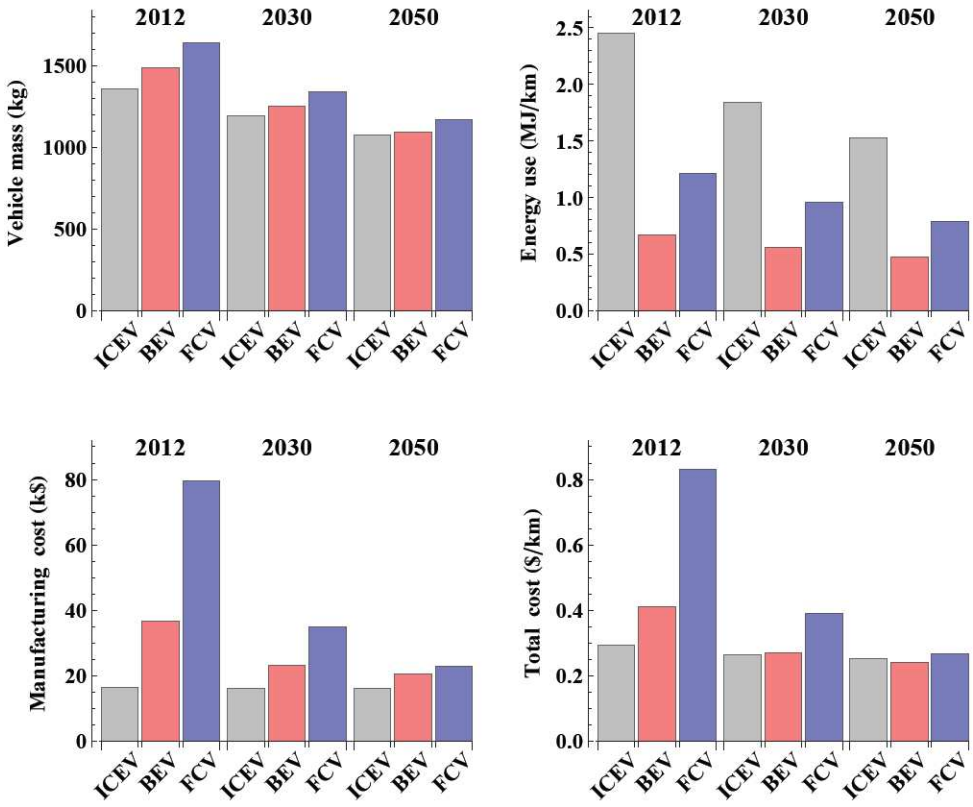

Figure 5.1: Vehicle criteria for the baseline scenario by year and powertrain technology.

for the FCV and ICEV. For comparison, the assumed energy density for storing 10 liter gasoline equivalent with a gasoline tank, hydrogen tank, and a Li-ion battery in 2012 is 14.3, 4.6, and 0.4 MJ/kg, respectively (based on Table 4.2). Even though the efficiency of the BEV is much higher, the net energy density[1] of the ICEV gasoline tank is still much higher than for the BEV battery. By 2050 it is assumed that battery energy density increases to 1.3 MJ/kg, which makes ranges above 600 km possible. Fig. 5.2 also shows the effects of a variation of range on energy use, manufacturing, and total costs. Again the influence is strongest for the BEV due to the high specific mass and cost of the energy storage.

Fig. 5.3 shows the variation of vehicle mass and energy use as a function of glider mass. The influence of glider mass on vehicle mass is very similar for the different drivetrain types and slightly lower in 2050 than in 2012. The dominant contribution to an increase of vehicle mass comes from the glider itself. The mass effects of powertrain and energy storage compounding to meet the same performance and range are similar among the different drivetrains. The influence of an increase of glider mass on energy use is ordered by powertrain efficiency, i.e. highest for the

[1]The net energy density takes into account the average powertrain efficiency, i.e. the provided mechanical energy per weight of energy storage.

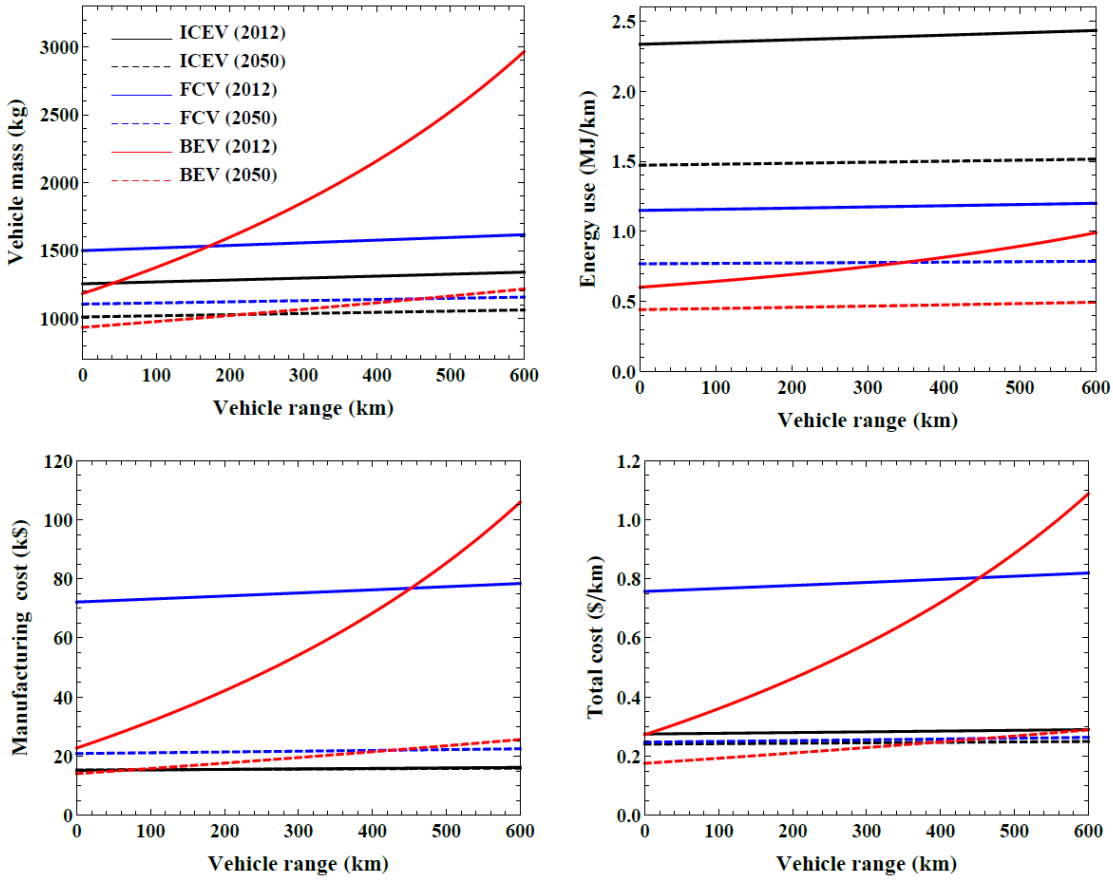

Figure 5.2: Variation of vehicle mass, energy use, and cost as a function of range by drivetrain and year.

ICEV in 2012 and lowest for the BEV in 2050.

Fig. 5.4 shows the combined influence of a variation of range and glider mass on vehicle mass and energy use for the year 2012. Fig. 5.2 and 5.3 can be interpreted as cross sections of Fig. 5.4 at specific range and glider mass values, respectively.

5.2.3 Influence of vehicle range and glider mass (including size effect)

This section includes the possible effect of a change of vehicle mass on frontal area in the scaling of vehicle mass and energy use. The scaling of vehicle mass and energy use is compared with the results from the previous section 5.2.2 where this feedback is not considered. Instead of the equations from section 5.1.2 Case A, now the equations of Case B are used.

In this model it is assumed that a change of vehicle mass has an effect on vehicle size, in particular A_f which is the most relevant parameter for the calculation of energy use. The exact relation between vehicle mass and frontal area should be actually based on more profound analysis of the

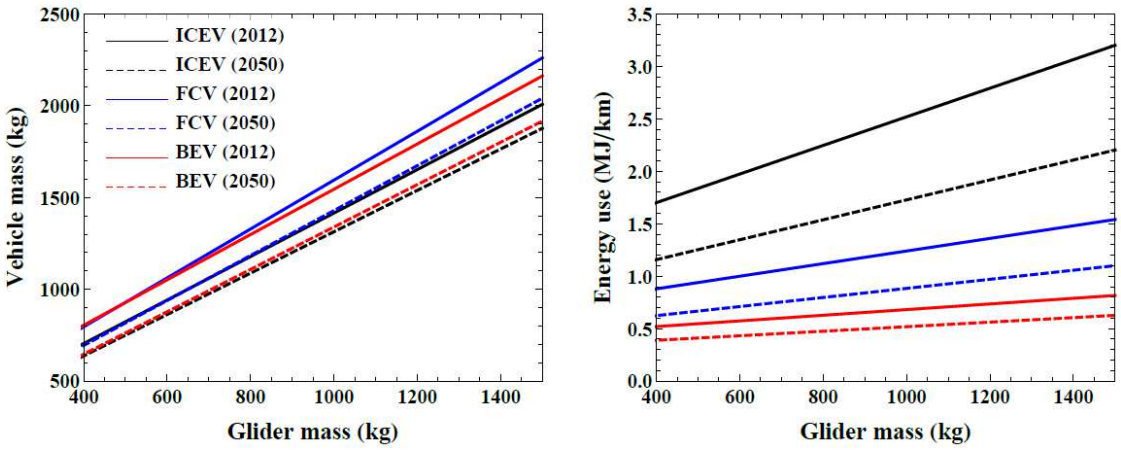

Figure 5.3: Variation of vehicle mass and energy use as a function of glider mass by drivetrain and year.

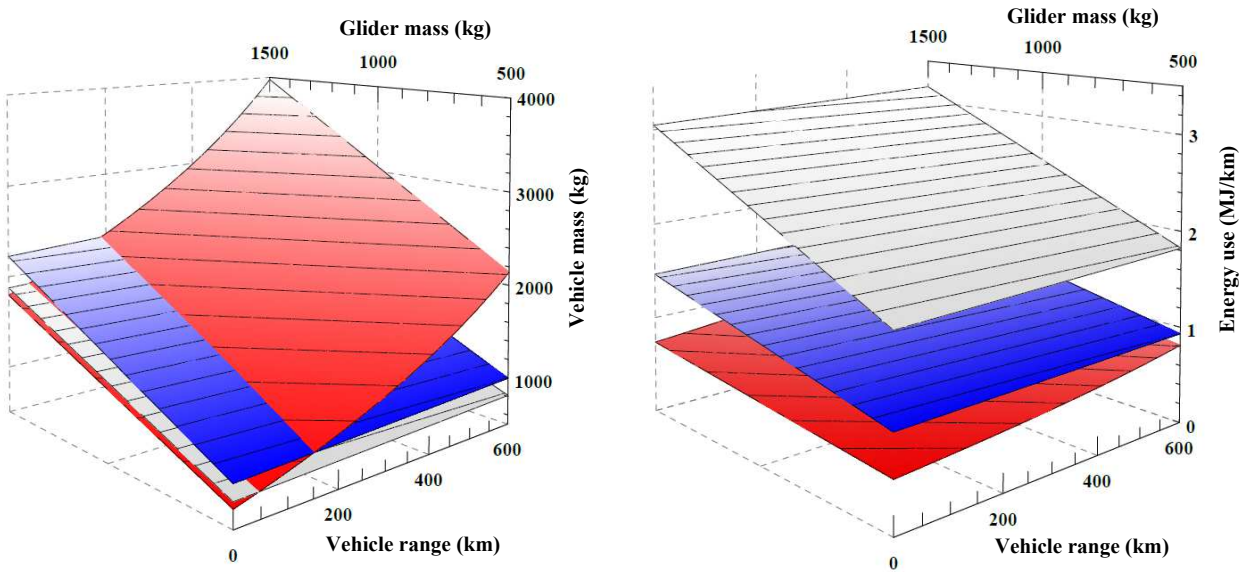

Figure 5.4: Variation of vehicle mass and energy use as a function of range and glider mass by drivetrain in 2012. The red surface corresponds to the BEV, blue to the FCV, and gray to the ICEV.

physical density of the components that cause the increase in mass. Since no such analysis has been performed, the average relation which is observed in the Swiss passenger car fleet is used. If a linear relation is assumed, A_f is calculated as

$$A_f(m) = A_{f,0} + \frac{\partial A_f}{\partial m} \cdot m \tag{5.32}$$

A linear fit for all new passenger cars sold in Switzerland in 2010 reveals $A_{f,0} \approx 1.2$ m^2 and $\frac{\partial A_f}{\partial m} \approx 0.00065\,\mathrm{m}^2/\mathrm{kg}$. These values can be used to calculate vehicle energy use and mass according to Eq. 5.20 and 5.21.

Fig. 5.5 compares the scaling of vehicle mass and energy use with range and glider mass for the models A and B. Obviously model B (which includes the effect of mass on size) results in a larger variation of mass and energy use with range and glider mass. BEV mass and energy use is most sensitive to the variation of vehicle range among the different powertrains. Therefore a variation of range induces the biggest change of frontal area for the BEV, which explains why the difference of the two models is largest for the BEV. There is very little difference in vehicle mass of the two models resulting from variation of glider mass. Therefore the induced change in frontal area is also similar across the different powertrains, which results in the highest change of energy use for the ICEV and the lowest for BEV, inverse to the order of powertrain efficiency. In summary, the comparison shows that the difference of model results is largest for variations that induce a large change of mass (e.g. range for BEV) and decreases with powertrain efficiency.

As mentioned earlier, the exact relation between the mass and frontal area of the vehicle depends on the type of components used. In principal it would be best to account for the size of each component separately and to calculate the corresponding effects on frontal area. However, this hasn't been investigated. Therefore the following chapter only uses model A for the analysis, which gives correct solutions for the reference case and good approximations for variation of parameters beyond the reference values.

5.2.4 Total cost differential

Total cost is an important criterion in assessing the economic viability of technologies [Tseng et al., 2013; Neubauer et al., 2012; Werber et al., 2009]. In this section the total cost (including vehicle purchase and fueling/charging costs) between the BEV, ICEV, and FCV is analyzed as a function of important parameters using the method developed in section 5.1 and the scenario assumptions from section 5.2.1.

As shown in Fig. 5.2, BEV total cost is currently very sensitive to range. On the other hand ICEV total cost is very sensitive to the fuel price. Fig. 5.6 shows on top the total cost difference between

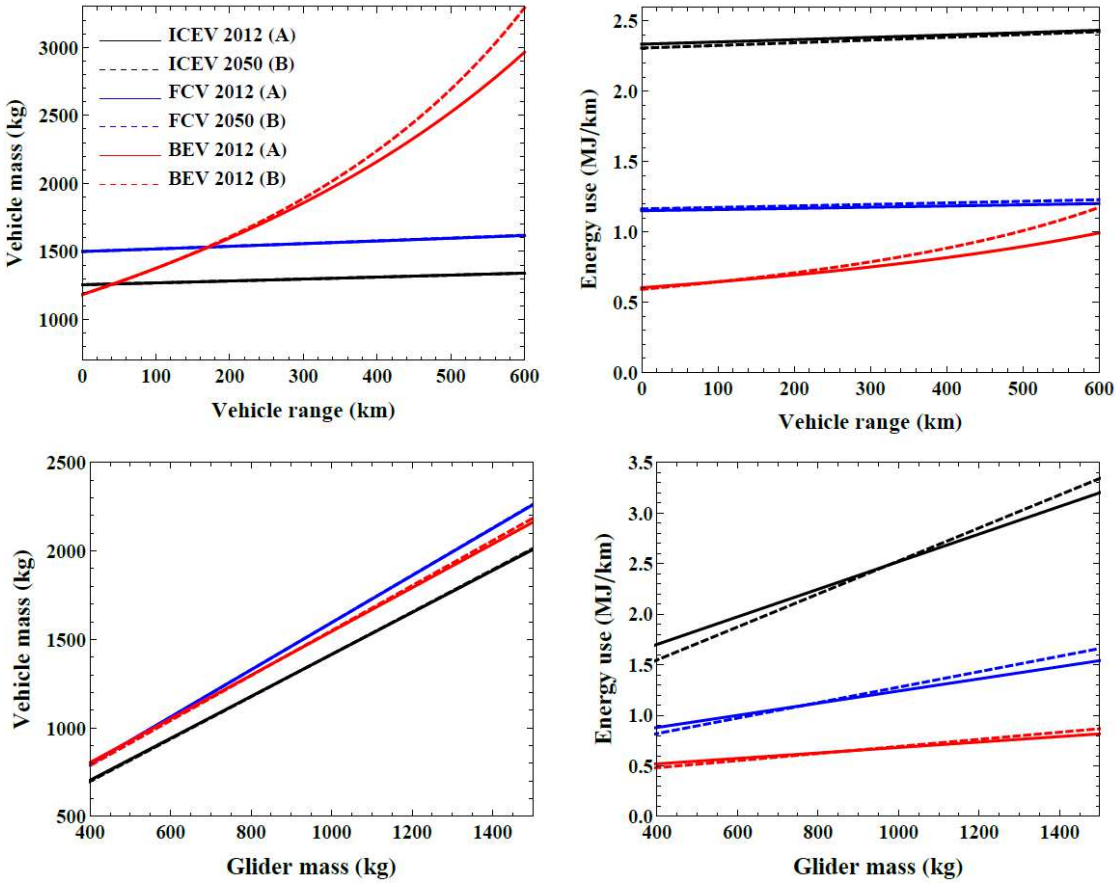

Figure 5.5: Comparison of the scaling of vehicle mass and energy use with range and glider mass for models A and B.

ICEV and BEV as a function of vehicle range and fuel price in 2012 and 2050. In 2012 the total cost difference is more sensitive to range than fuel price within the considered interval. At fuel prices above ca. 1.6 $/L the BEV becomes cost competitive, however only at very short ranges. From 2012 to 2050 the sensitivity of the total cost difference shifts from range to fuel price, and the total cost difference becomes smaller in absolute terms. In 2050 the BEV is cheaper up to a range of ca. 500 km at a fuel price of 2.5 $/L.

The middle of Fig. 5.2 shows the total cost difference between the FCV and BEV in 2012 and 2050 as function of vehicle range and hydrogen price. In 2012 the FCV is cost competitive only at very high ranges that are in practice not observed for a BEV. Similar to the previous case, from 2012 to 2050 the sensitivity of the total cost difference shifts slightly from range towards the hydrogen price, and the total cost difference becomes smaller in absolute terms. In 2050 the FCV has smaller total cost than the BEV at ranges above 300 to 600 km, depending on the price of hydrogen.

The bottom of Fig. 5.2 shows the total cost difference between the FCV and ICEV in 2050 at 150'000 vkm and 250'000 vkm as a function fuel and hydrogen price. Both vehicles offer the same

driving range. Assuming a hydrogen price of 8 $/kg total cost parity is reached at a fuel price of ca. 2.4 $/L (at 150'000 vkm) and 1.9 $/L (at 250'000 vkm).
Note that in addition to the parameters analyzed in this section, many other factors influence total cost, including battery and fuel cell cost reductions, battery lifetime, or vehicle driving region (for example the reduction of energy use of the BEV and FCV relative to the ICEV is particularly high in urban traffic).

5.3 Sensitivity analysis

The scenario analysis presented in the last section involves many highly uncertain assumptions about future developments. Sensitivity analysis helps in understanding which way changes of input parameters influence the results and in assessing the range of possible outcomes. The analytic calculation approach developed in section 5.1 is particularly suited for sensitivity analysis and various methods are used. The following work analyzes the sensitivities of the results generated in section 5.2.1 with regard to the relevant input parameters using parameter variations relative to the reference value, analytic sensitivity analysis, and probabilistic sampling to study the effect of well-defined probabilistic uncertainty assumptions for one or several input parameters on the resulting criteria.

5.3.1 Parameter variations

This method consists of varying the variable of interest relative to its baseline value while keeping all other variables fixed. The corresponding change of vehicle mass, energy use, and cost is analyzed graphically.
The top of Fig. 5.7 shows the variation of ICEV, BEV, and FCV mass relative to a change of glider mass from -75 % to +75 % for 2012, 2030, and 2050. The variation of BEV mass relative to a change of range is also shown. The sensitivity of vehicle mass to a change of glider mass is similar across the different powertrains and years in relative terms. The sensitivity of BEV mass to a change of range decreases from 2012 to 2050 due to the strong increase of battery specific energy, even though the absolute range increases.
The middle of Fig. 5.7 shows the sensitivity of energy use with regard to the same variables. The sensitivity of energy use to a change of glider mass is highest for the ICEV and lowest for the BEV due to the different powertrain efficiency. For a specific powertrain type it decreases over time in absolute terms but remains approximately constant in relative terms. The sensitivity of BEV energy use to a change of range is much smaller than to a change of glider mass and decreases even further by 2050.
The bottom of Fig. 5.7 shows the sensitivity of total costs to a change of several variables as indi-

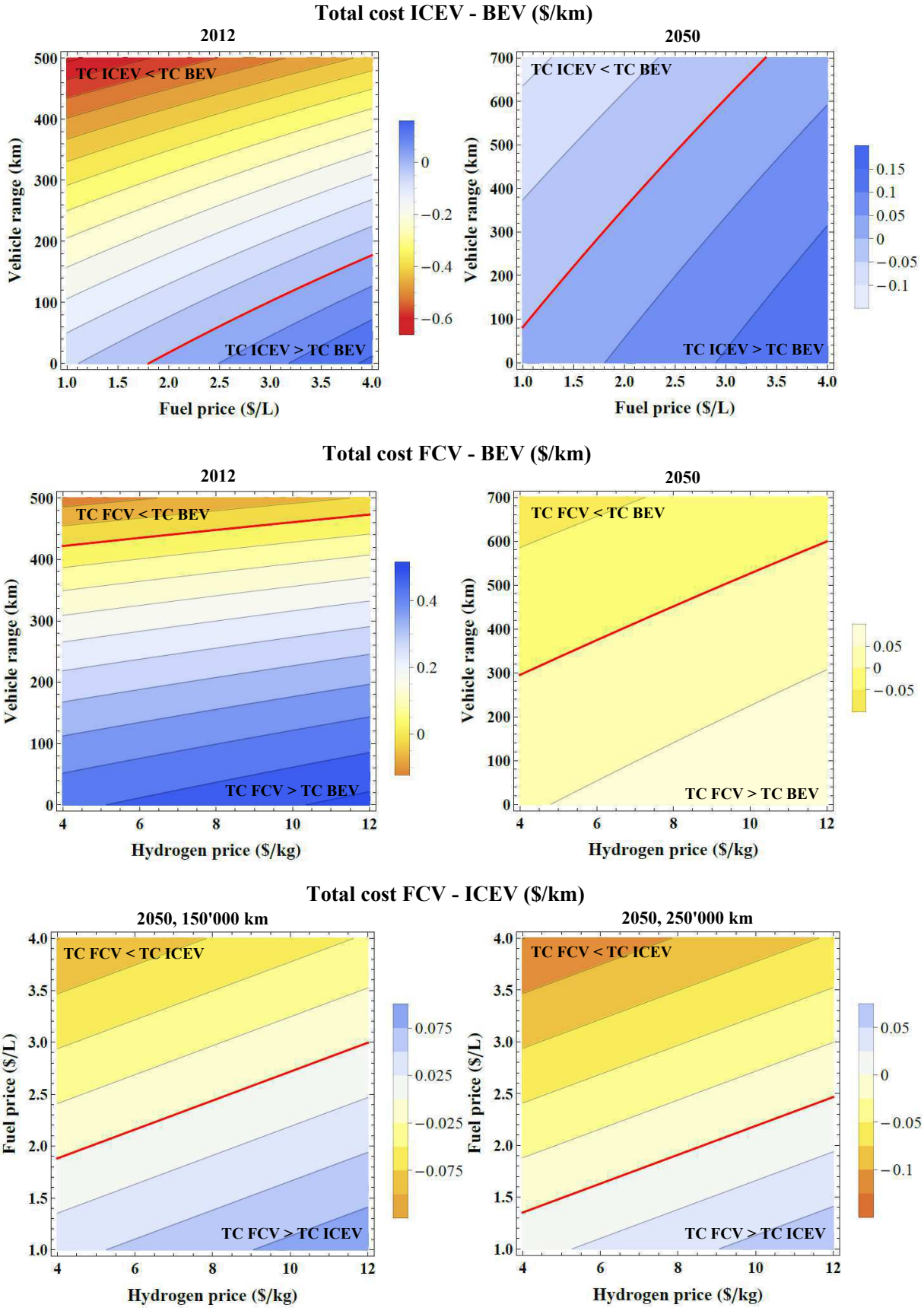

Figure 5.6: Total cost difference between, ICEV, BEV, and FCV as a function of important parameters. The red line indicates equal total costs.

cated in the figure. For the BEV the sensitivity is highest for a change of range, for the FCV for a change of powertrain cost, and for the ICEV for a change of fuel cost. The total cost of the BEV and ICEV converge by 2030 and the total cost difference is very sensitive to the range and fuel price as already pointed out in the previous section 5.2.4. By 2050 the total cost of the FCV and ICEV converge and the total cost difference is sensitive to the fuel and hydrogen cost.

5.3.2 Analytic calculation

The sensitivity analysis presented in the last section is good for graphical analysis of the relative effect of changes of parameters on vehicle criteria. In order to retrieve the actual values in a non-graphical way and to study the sensitivity using a more systematic approach, the analytic method is used to calculate the partial derivatives with respect to a parameter of interest, similar to the sensitivity analysis of energy demand in section 2.3. If the partial derivative of a criterion Y (e.g. total cost) relative to a parameter x (e.g. fuel price) $\frac{\partial Y}{\partial x}$ is evaluated at the reference points for all remaining parameters, the resulting value corresponds to the slope of the curves in Fig. 5.7. One way to calculate the sensitivity is to evaluate the change of criteria ΔY for a change of a parameter Δx relative to the reference value Y_0 as[2]

$$\frac{\Delta Y}{Y_0} = \frac{\partial Y}{\partial x} \cdot \frac{\Delta x}{Y_0} \tag{5.33}$$

It is convenient to evaluate Eq. 5.33 e.g. for $\Delta x = 0.01 \cdot x_0$ corresponding to the relative change of Y per percent parameter change. Fig. 5.8 shows the sensitivity calculated in this way for total costs relative to changes of vehicle range, specific cost of the energy storage, charging or fueling cost, specific mass of the energy storage, and specific cost of the powertrain. It is always expressed as the change of total cost per percent parameter change relative to the reference total cost. Comparing the sensitivity to these parameter changes for each powertrain separately, it can be seen that BEV total cost is most sensitive to range and the specific cost of the battery, and that the sensitivity to specific battery and energy costs reaches equal levels by 2050. Among the analyzed parameters, ICEV total cost is clearly most sensitive to fuel price and FCV total cost in 2012 to specific powertrain cost. Over time the sensitivity of FCV total cost to specific powertrain cost decreases and to hydrogen cost increases, reaching approximately equal sensitivity by 2050. Comparing the sensitivity to parameter changes among the different powertrains, it is obvious that the BEV is most sensitive to range, the ICEV least sensitive to range and most sensitive to energy costs, the BEV and FCV are approximately equally sensitive to energy costs, and the FCV is most sensitive to powertrain costs.

[2]This approach is similar to the calculation of elasticity in economics.

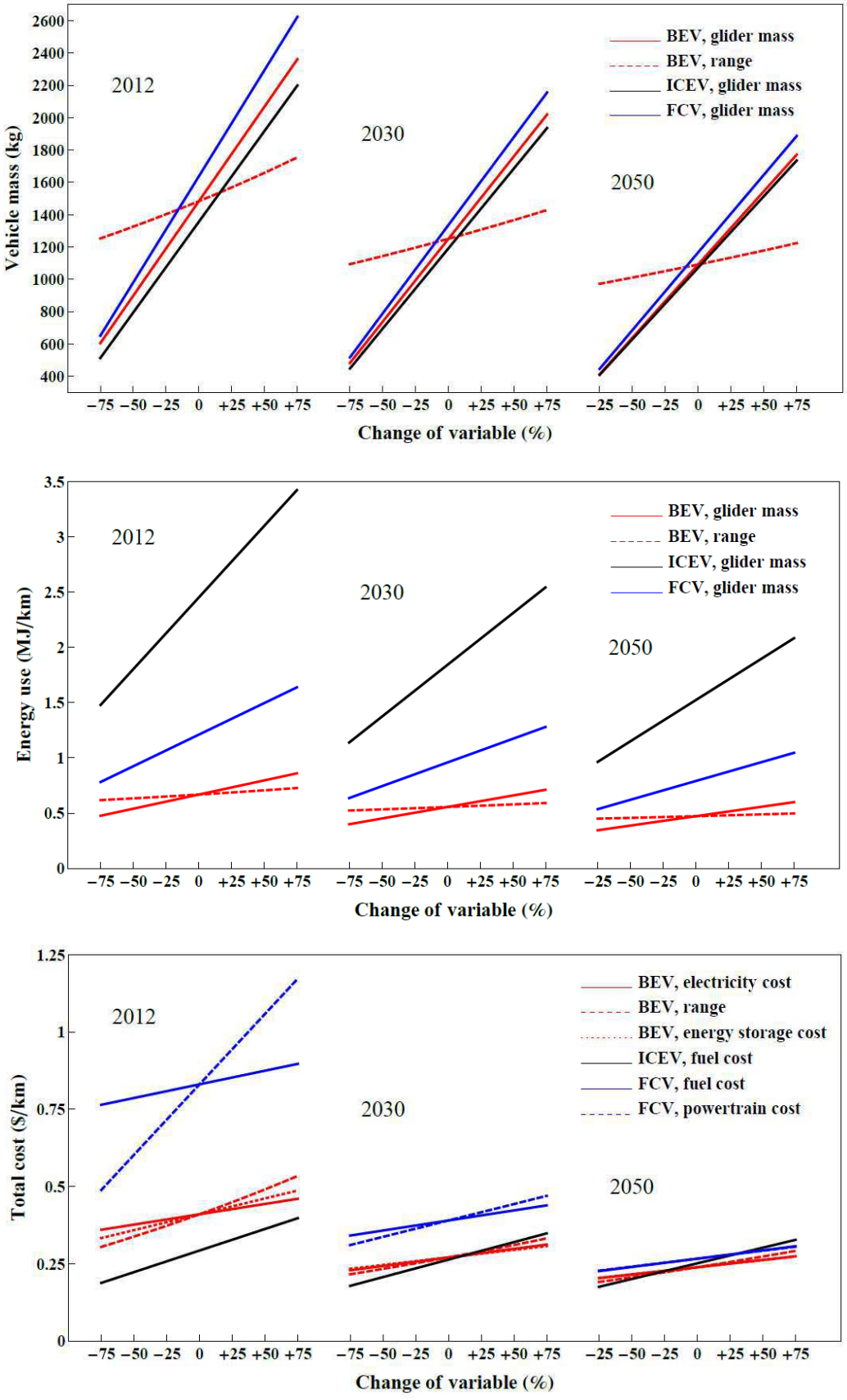

Figure 5.7: Sensitivity of vehicle mass, energy use, and total cost relative to variations of important parameters.

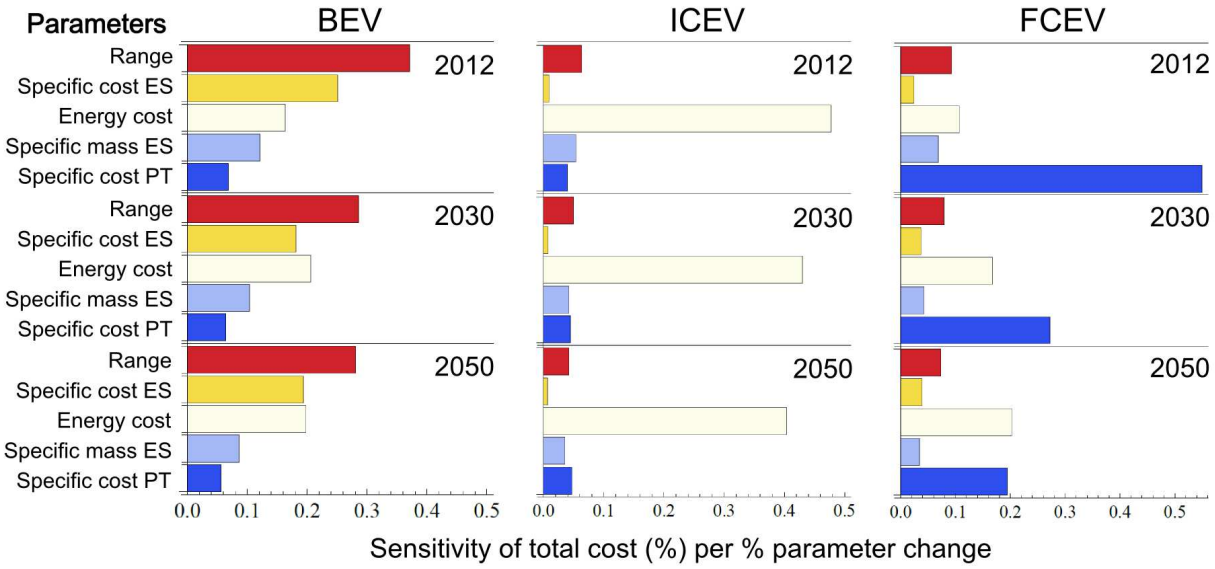

Figure 5.8: Comparison of the sensitivity of total cost to changes of important parameters by powertrain and year.

5.3.3 Probabilistic assessment

Though the sensitivity to parameter variations can be analyzed in a satisfactory way using the methods described in sections 5.3.1 and 5.3.2, sometimes it is useful to study the effect of probabilistic input assumptions on the resulting criteria. This can be achieved by using probabilistic random sampling of the input parameters and observing the distribution of calculated criteria. Such an approach is for example used in Monte Carlo simulations. With this method the influence of a certain probability distribution of one or several input parameters on the results can be investigated. The analytic method developed in section 5.1 allows fast calculation time and therefore a large number of input values approaching a continuous probability distribution.
As an example this method is applied to study the uncertainty of BEV criteria in 2030 using a probabilistic distribution with regard to battery specific energy and cost, and powertrain specific power and cost. In the example 10 million random input values with a normal distribution and a standard deviation of 10 % relative to the baseline are generated. Fig. 5.9 shows the probability density function (PDF) on the left for those inputs and the resulting PDF on the right for energy use, mass, manufacturing and total costs. The resulting uncertainty for manufacturing cost is highest because all four input distributions affect it, and lower for vehicle mass because it is only affected by two input distributions. The resulting uncertainty for energy use can be derived from vehicle mass and the uncertainty for total cost from manufacturing cost and energy use.

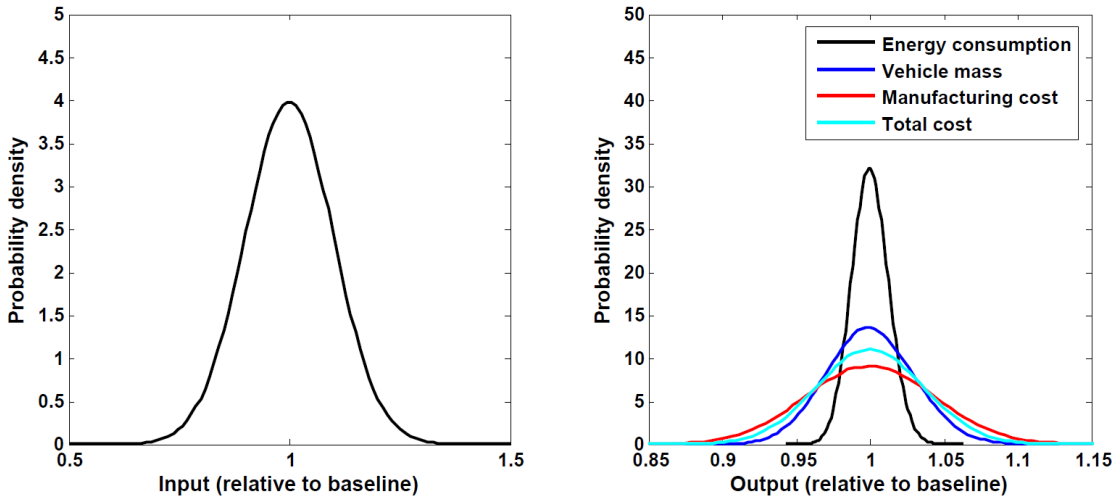

Figure 5.9: Probability density function of input parameters and resulting BEV criteria in 2030.

Chapter 6

Multi-criteria analysis

Sustainable development has many definitions. One of the most widely quoted has been specified by the Brundtland Commission in the book "Our Common Future" [Brundtland et al., 1987]: "Sustainable development is development that meets the needs of the present without compromising the ability of future generations to meet their own needs." Sustainable development goals are often defined to meet ecological, economic and social principles, the three pillars of sustainability. Over the past decades, sustainable development has been accepted as a guiding principle by governments and the society, however implementation has proven difficult and the progress towards sustainable development is slow [Drexhage & Murphy, 2010]. Of course, sustainable development is a visionary concept and the needed systemic changes to achieve this goal are enormous. In the context of transport, sustainability means a system which guarantees access to affordable, safe, and efficient mobility, while generating limited emissions, waste, land use and noise, as well as resource use at or below rates of formation.

Currently many advanced vehicle and fuel technologies are being developed with the aim of reducing the environmental impacts of road transport and its dependence on fossil oil. The THELMA project this thesis was embedded in, aimed at investigating the sustainability implications of widespread electric vehicle use in Switzerland. For this purpose a broad set of social, economic, and environmental sustainability indicators has been assessed and analyzed. In this chapter a smaller set of technical, economic, and environmental indicators for several current and future passenger vehicle options is compared. The analysis takes into account different drivetrain technologies, primary energy sources, vehicle size and utility classes. The simulation of indicators is based on the methodology as described in chapters 2 to 5. The high level of integration between technical assessment, powertrain simulation, and life cycle assessment enables a consistent comparison of the different vehicle technologies and the development of future scenarios. So far, many studies have analyzed the technical, economic, and environmental aspects of advanced passenger cars individually, however an integrated and transparent framework combining tech-

nology assessment, powertrain simulation, life cycle assessment, and scenario analysis is missing. The input assumptions to all calculations are transparently documented and can be easily modified. This multi-indicator comparison is presented in section 6.1, and is partly based on [Hofer et al., 2013a].
In addition, the multi-indicator simulation results are used for multi-criteria decision analysis (MCDA). MCDA methods help stakeholders to understand complex, multi-dimensional problems and to assist rational decision-making [Eisenführ et al., 2010]. MCDA is increasingly applied in the fields of energy and environmental sciences. The Laboratory for Energy Systems Analysis at PSI has been applying MCDA to a broad variety of sustainability assessments in the energy sector, including the China Energy Technology Program [Eliasson & Lee, 2003], the EU project NEEDS comparing the sustainability of current and future electricity supply options [Hirschberg et al., 2007; Schenler et al., 2009; Roth et al., 2009], the EU project SECURE exploring the impact of CO_2 policy options on energy security [Eckle et al., 2011], and a sustainability analysis of future vehicle technologies [Wilhelm, 2011a]. Several other studies have investigated the use of MCDA in transportation, e.g. to rank advanced passenger vehicle technologies and fuel options [Tzeng et al., 2005; Zhou et al., 2007; Safaei Mohamadabadi et al., 2009; Wilhelm, 2011b; Wilhelm & Wokaun, 2011; Wilhelm et al., 2011]. The work presented in section 6.2 combines novel approaches in vehicle modeling and LCA to generate a consistent set of vehicle alternatives and evaluation criteria. The vehicle options and indicator set are used for MCDA based on generic stakeholder weightings.
The method used in this chapter provides a range of advantages such as transparency in scenario assumptions and low computing time that is beneficial for interactive analysis. The implementation and functionality of the analysis tools developed for the applications in section 6.1 and 6.2 are described in section 6.3.

6.1 Multi-indicator assessment

6.1.1 Analysis framework

In this section a broad range of current and future passenger car options including conventional and electric powertrains, different size and range classes, and relevant primary energy sources are analyzed with regard to technical, economic, and environmental indicators. Vehicle criteria are split into exogenous and endogenous. Exogenous criteria are vehicle performance levels that are important to the individual consumer of the car (e.g. size, range, acceleration, etc.) and at the same time necessary input parameters to define a car, execute the vehicle simulation, and perform the life cycle assessment. Endogenous criteria are the simulation results, such as vehicle mass, energy consumption, cost, and environmental impacts.

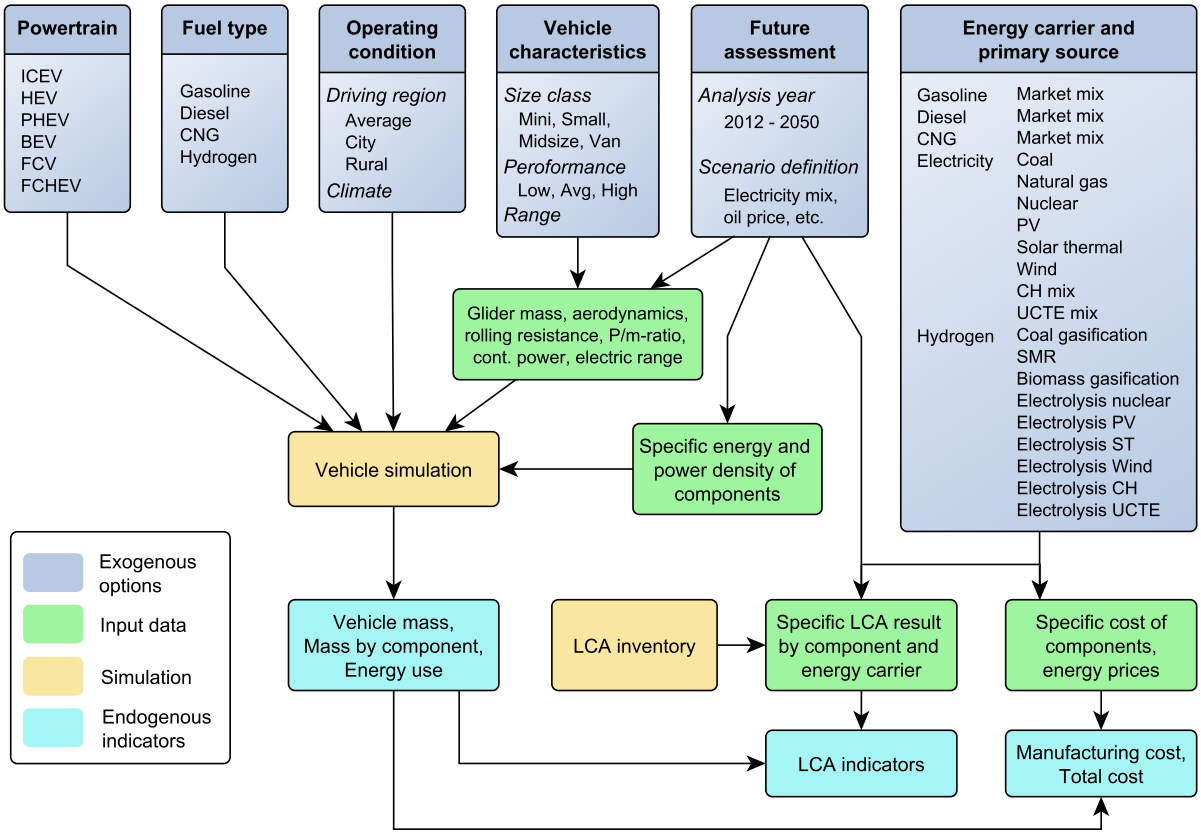

Figure 6.1: Analysis framework: Technical, cost, and environmental indicators for current and future passenger cars are calculated from a given set of exogenous options.

Fig. 6.1 illustrates the modeling framework used. The technology options are chosen to be independent, i.e. they can be combined in every possible way[1] to study the range of resulting criteria and to better understand the interdependencies between technology and fuel options, future developments, and the resulting economic and environmental criteria.

The technology options set is split into powertrain and fuel type, vehicle size, range and performance, primary energy source, and vehicle model year. The latter influences the inputs passed on to the powertrain, cost and LCA submodels in various ways as the following parameters are a function of time:

- Glider mass, aerodynamic drag, and tire rolling resistance coefficient are expected to decrease over time. Similarly powertrain component efficiencies are adjusted over time to

[1] Impossible combinations such as a BEV powered by hydrogen are of course not considered.

account for technical progress.

- Specific energy and power of technologies that are not yet fully developed (such as batteries) are expected to increase over time. This mass-related data is also used in the vehicle simulation to calculate vehicle weight and energy consumption.
- Specific component costs decrease over time as learning effects occur and/or production volume increases. Component costs and energy prices are used together with calculated component sizes and energy consumption to assess manufacturing and total costs.
- Cumulative LCA results by component and energy source change over time as technologies develop. This data is used together with component sizes and vehicle energy consumption to calculate aggregated LCA results.

All of these future developments are uncertain and depend on interlinked parameters such as technical developments, policy measures, consumer acceptance, production volumes, etc. The scenario assumptions used in this work are mainly based on data from the literature (according to chapter 4). The aim of this study is not to project vehicle costs and environmental impacts, but rather to provide a clear framework for the consideration of possible future developments within vehicle analysis and to apply it using transparent input data. The approach shown is also implemented in an interactive tool in which the user can modify scenario assumptions and see the immediate effect on the results. This is further explained in section 6.3.

6.1.2 Scenario assumptions

In this section the baseline scenario assumptions for the following analysis are summarized. Three passenger car classes are analyzed based on aggregate fleet data (compare section 3.2.1 and Table B.1): small, midsize, and large. The assumed values of glider mass, frontal area, aerodynamic drag coefficient, and glider cost are summarized in Table 2.4. These values are calculated as the sales-weighted mean for the mini/small, low-midsize/midsize, and up-midsize/MPV/SUV segment for the small, midsize, and large car class, respectively. Independent of the class a tire rolling resistance coefficient of 0.01 is assumed. Glider mass, aerodynamic drag, and tire rolling resistance are expected to be continuously reduced by manufacturers in order to reduce vehicle energy use and to fulfill new emission standards. In this scenario, glider mass, c_d, and c_r are reduced by 0.5 % per year, which equates to a total reduction of ca. 17 % by 2050. This rate of reduction seems realistic considering historic developments for these parameters and projections used in other studies [Kasseris & Heywood, 2007].

In order to take into account realistic driving conditions, the worldwide harmonized light vehicles test procedure (WLTP) as well as its low speed segment for urban driving are used. The variation

Table 6.1: Vehicle class characteristics for the year 2012 used in this chapter.

	Glider mass (kg)	Frontal area (m^2)	Aerodynamic drag (c_d)	Glider cost ($)
Small	687	2.0	0.33	7484
Midsize	1017	2.2	0.31	11264
Large	1298	2.7	0.33	15917

of energy demand parameterization coefficients can be assumed to be negligible over the range of vehicle characteristics analyzed, as pointed out in section 2.2.2. Vehicle traction and regeneration efficiencies for the different drivetrain technologies considered are calculated according to section 3.1.4. A regenerative braking fraction κ is assumed, that is 0.6 for the HEV and FCEV, and 0.8 for the BEV, FCHEV, and PHEV due to the larger battery capacity. Energy use and mass are calculated using Eq. 5.26 and 5.27, and auxiliary loads are assumed according to section 3.1.3. For the BEV and PHEV plug-to-wheel (PtW) energy consumption is calculated by taking into account losses that occur during charging. To convert from battery-to-wheel (BtW) to PtW energy consumption a charging efficiency of 92 % is assumed.

The set of evaluation criteria is split into direct vehicle indicators (i.e. vehicle mass, energy use, purchase price) and energy source dependent indicators (i.e. total costs and life cycle indicators). Energy source dependent indicators are indicated per vkm. For reference a total vehicle lifetime distance of 150,000 vkm and a discount rate of 5 % are assumed. Due to space constraints only a selected number of life cycle indicators for a selected number of energy source alternatives is presented in the following. The full set of results can be accessed in an online analysis tool as described in section 6.3. Three life cycle indicators are analyzed at their mid-point (i.e. GHG emissions, metal depletion, fossil depletion) and end-point levels (i.e. human health damage, ecosystem damage, resource depletion). With regard to electricity source options, results are shown for the current Swiss mix (CH mix), the current European mix (UCTE mix), current and future coal, natural gas, nuclear, wind, photovoltaic (PV) and hydro power generation. With regard to hydrogen production, results are shown for current and future steam methane reforming (SMR), coal gasification (CG), and electrolysis using the current Swiss and European electricity, as well as electrolysis using current and future nuclear, wind, PV, and hydro power. The corresponding energy prices and life cycle inventories are based on sections 4.2.2 and 4.3.

For all classes and years a power-to-mass ratio of 65 W/kg is assumed corresponding to an acceleration time of approximately 12 s from 0 to 100 km/h and a continuous top speed of 180 km/h. For the calculation of direct vehicle indicators in section 6.1.3, BEV electric ranges of 100 km, 200 km, and 300 km are assessed. For the calculation of energy source dependent indicators in section 6.1.4, the assumed electric and fuel based ranges are summarized in Table 6.2. Note that the increase of PHEV electric range results in an increase of the PHEV electric driving fraction over time as described in section 3.1.3.

Table 6.2: Assumed electric and fuel based ranges by drivetrain and year.

	Drivetrain	2012	2030	2050
Electric range (km)	BEV	150	300	500
	PHEV	50	100	150
Fuel range (km)	ICEV/HEV	700	700	700
	FCV/CNG	500	700	700
	PHEV	400	600	600

6.1.3 Direct vehicle indicators

Fig. 6.2 shows the breakdown of vehicle mass and purchase cost by component as well as energy use by source and energy carrier for all drivetrain types discussed in chapter 3 and 4. The results are for a midsize car, the WLTP driving cycle, and year 2012. The assumed electric range of the BEV and PHEV are indicated together with the drivetrain technology in the axis. ICEV/HEV-c and FCEV/FCHEV ranges are as given by Table 6.2.

Fig. 6.2 shows on top the breakdown of vehicle mass by drivetrain. The glider mass varies slightly among different drivetrain types due to structural support for powertrain and energy storage components which is accounted for within the glider. The breakdown by mass reveals a high sensitivity of BEV and PHEV mass to the electric range due to the relatively low energy density of current batteries. The additional mass for a PHEV relative to a conventional ICEV comes mainly from the engine, motor/generator, and the battery, and for a FCEV and FCHEV it comes from the hydrogen storage, fuel cell, and the battery.

As shown in Fig. 6.2 below, the purchase price of all electric vehicles is today significantly above their ICEV counterparts due to the additional cost of the battery, fuel cell, and electric motor. BEV and PHEV purchase price is very sensitive to the electric range. The figure also shows that the FCHEV can currently be produced more cheaply than the FCEV for the assumed battery and fuel cell cost.

Relative to the gasoline ICEV energy use is reduced by approximately 13 % with the diesel ICEV, 22 % with the gasoline HEV, 41 % with the FCEV, 45-49 % with the gasoline PHEV (depending on the electric range and as such the electric utility factor), and 65-70 % with the BEV (also depending on the electric range).

Fig. 6.2 shows on the bottom the corresponding breakdown of energy use by energy carrier. It is interesting to see the shift from fuel to electricity as the range of the PHEV increases due to the corresponding increase of the electric utility factor. Because of the higher efficiency in charge depleting vs. charge sustaining mode, PHEV energy use decreases at higher electric ranges. Note that this is only the case up to a certain electric range at which the increase of energy use due to higher vehicle mass outweighs the reduced energy use due to efficiency gains.

Fig. 6.3 shows the breakdown of vehicle mass, purchase price, and energy use by component for a selection of the drivetrain types discussed in Fig. 6.2 and three vehicle classes each (small, midsize, large) according to Table 6.1.
Fig. 6.3 shows on top that an increase in glider mass related to a change in class results in a higher mass and cost for other components (mainly the battery and fuel cell) as the same range and performance requirements must be achieved. The effect of a change of class on vehicle weight is most significant for the BEV and PHEV, particularly at high electric range.
Due to the high cost of the fuel cell and battery the effect of a change of class on purchase price is most significant for the FCEV, BEV, and PHEV.
The absolute change of energy use related to a change of class decreases with powertrain efficiency, i.e. it is highest for the ICEV-g and lowest for the BEV.

Fig. 6.4 depicts the breakdown of vehicle mass, purchase price, and energy use for a midsize car and the same selection of drivetrain types discussed in Fig. 6.3. Instead of different classes for each drivetrain, three manufacturing years (2012, 2030, 2050) are analyzed according to the scenario assumptions described in section 6.1.2.
As shown in Fig. 6.4 on top the mass of all vehicles is expected to decrease over time due to a lighter glider and increasing specific power and energy in the powertrain and energy storage. The increase of battery energy density also leads to a lower sensitivity of BEV and PHEV mass to range.
Today the purchase prices for the BEV, FCEV, and PHEV are still much higher than for the ICEV and HEV, but this is expected to strongly decrease in the future due to reductions in battery and fuel cell costs. The sensitivity of BEV and PHEV purchase price to range is lower in the future as the specific mass and cost of batteries decreases.
Energy use reduces for all powertrains over time as vehicle mass and other resistance parameters decrease and powertrain efficiency improves. The reductions are strongest for the ICEV and HEV.

Fig. 6.5 shows energy use by drivetrain in average and urban driving conditions. In urban driving the energy use of the ICEV is generally higher due to low engine efficiency at partial loads and because kinetic energy lost in braking accounts for a high fraction of the total energy demand. For electric drivetrains on the other hand, energy use for urban driving is usually lower (not considering contributions from auxiliary loads) because the powertrain efficiency remains high and part of the kinetic energy spent for acceleration can be regenerated. This makes electric vehicles particularly suited for urban driving conditions.

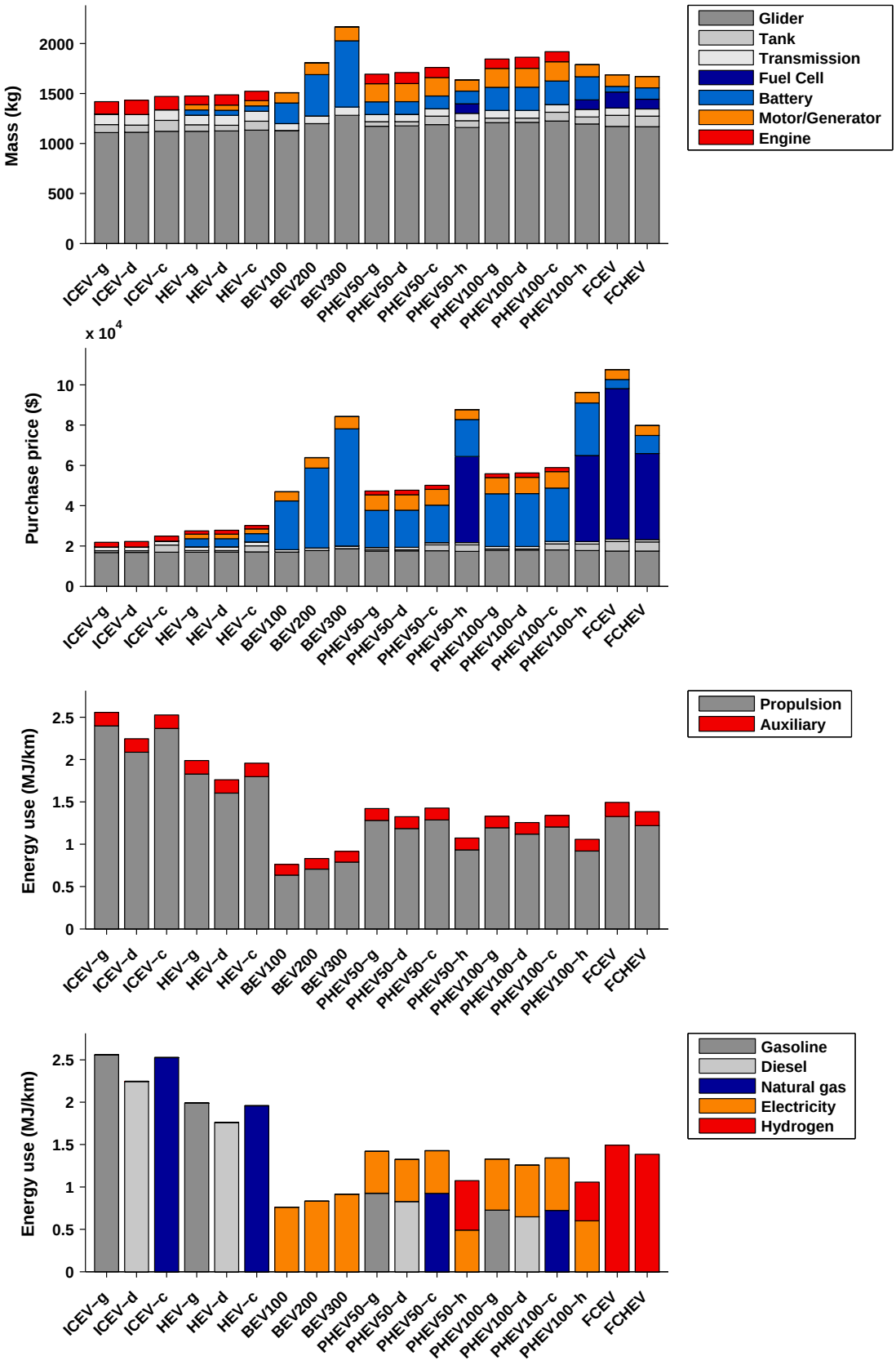

Figure 6.2: Breakdown of vehicle mass, purchase cost, and energy use by drivetrain for a midsize car in 2012.

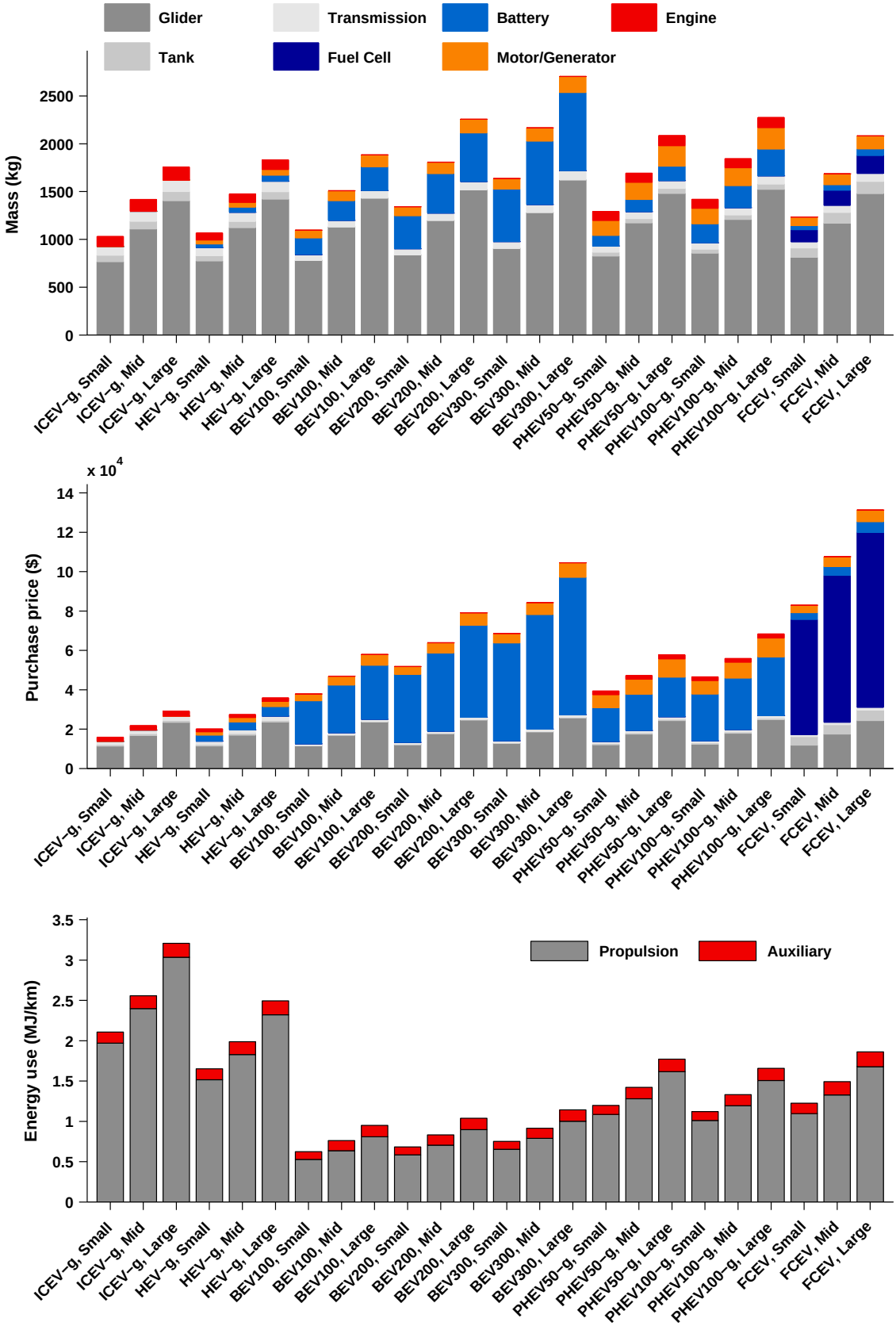

Figure 6.3: Breakdown of vehicle mass, purchase cost, and energy use by drivetrain and class for 2012.

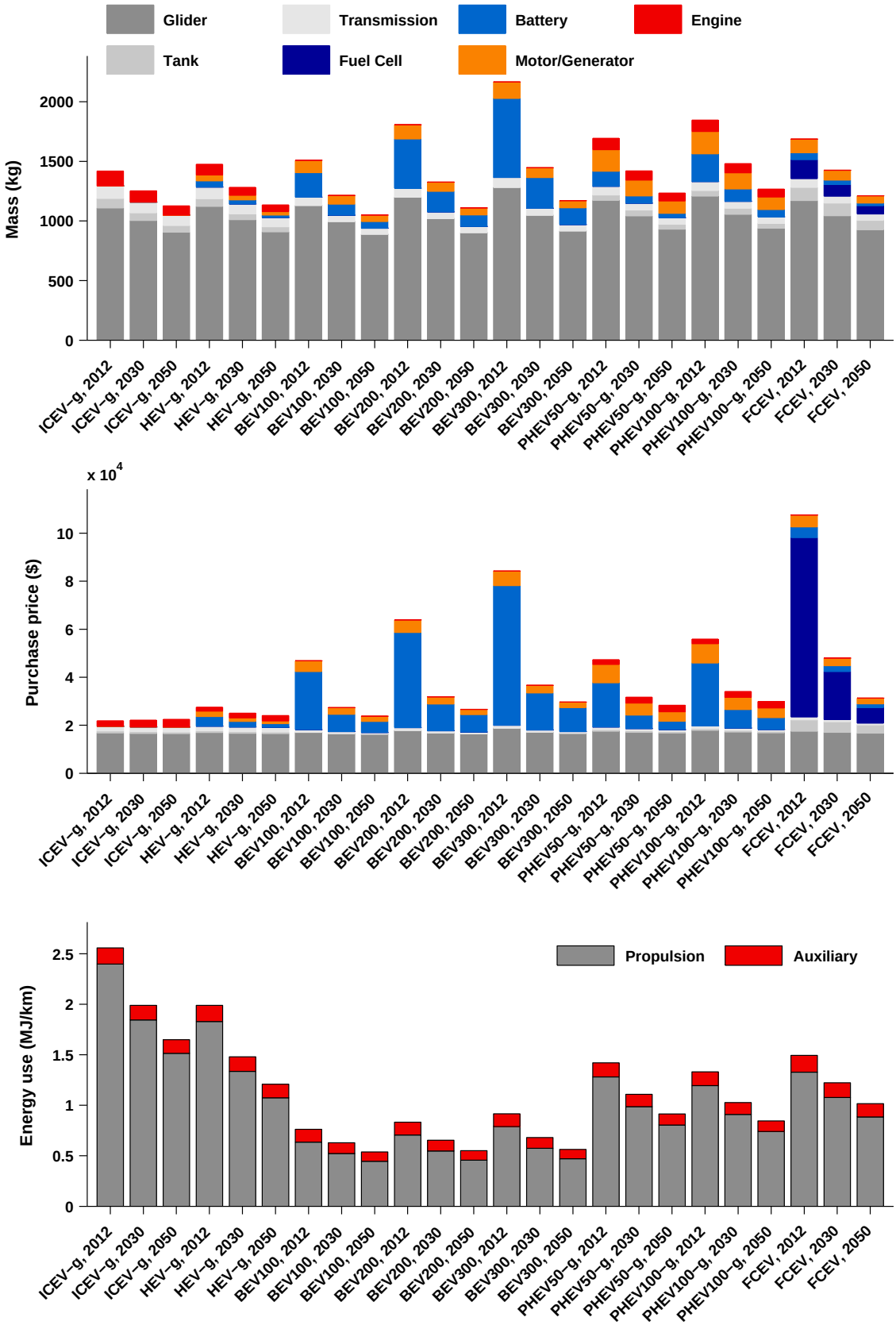

Figure 6.4: Breakdown of vehicle mass, purchase cost, and energy use by drivetrain for a midsize car from 2012 to 2050.

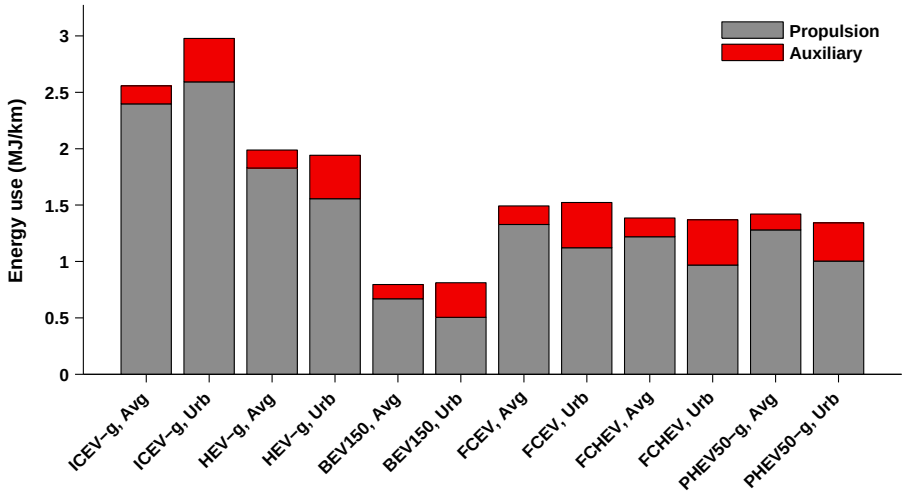

Figure 6.5: Energy use by drivetrain and driving cycle in 2012 for the average WLTP driving cycle and its low-speed urban part.

6.1.4 Energy source dependent indicators

Life cycle mid-point indicators

Fig. 6.6 compares life cycle GHG emissions, metal depletion, and fossil fuel depletion for a mid-size car in 2012 with regard to a selection of different drivetrains and primary energy sources. The figure shows the individual contributions of the road infrastructure, vehicle production by component, fuel and/or electricity supply, exhaust and non-exhaust emissions.

Overall GHG emissions from electric vehicles are very sensitive to the primary energy source of electricity or hydrogen production. Electric vehicles only provide a significant advantage relative to the ICEV and HEV if the electricity or hydrogen used is generated from a non-fossil primary source. If coal generation is used they perform even worse. This result is in agreement with other studies analyzing the life cycle GHG emissions of electric vehicles, e.g. [Hawkins et al., 2012b; Bauer & Simons, 2010; Althaus & Gauch, 2010]. Regarding the specific contributions to total GHG emissions, exhaust emissions dominate for the ICEV and HEV, while for electric vehicles it depends on the energy source which component dominates. Generally the impact from the production phase is higher for electric vehicles than for the ICEV.

Metal use is significantly higher for electric vehicles than for an ICEV due to the contributions from the battery, fuel cell, electric motor, and electricity or hydrogen production. Regarding the battery, fuel cell, and electric motor the main metals contributing to this indicator are manganese, nickel, and/or cobalt for the Li-ion battery (depending on the cathode chemistry), mainly plat-

inum (but also manganese, nickel, and tin) for the fuel cell, and rare earth metals for electric motor magnets. Copper is critical for all three components. Generally the contribution from the vehicle production phase is higher than the contribution from the driving phase. The contribution from electricity and hydrogen production is however significant, in particular if PV or wind electricity is used.
Fossil fuel depletion on the other hand is much lower for electric vehicles relative to an ICEV if a non-fossil primary energy source is used. In this case the contribution from vehicle production is higher than from its use phase. Note that for the employed ReCiPe LCIA method the characterization factors for different fossil energy sources are based on the energy equivalent relative to oil. In this sense this indicator expresses the cumulative fossil energy demand.

As shown in Fig. 6.7 the impact with regard to all three mid-point indicators decreases over time due to vehicle mass and energy use reductions, as well as due to efficiency improvements of electricity and hydrogen production.

Life cycle end-point indicators

Fig. 6.8 compares the contributions to three LCA end-point indicators – human health damage, ecosystem health damage, and resource depletion – for a midsize car in 2012 with regard to different drivetrains and primary energy sources (for the same technology options as shown in Fig. 6.6). The results are based on the ReCiPe LCIA method described in section 4.3 and the mid- to end-point characterization factors listed in Table 4.7.
The contributions to human health and ecosystem health damage are clearly dominated by the impacts of climate change. Therefore human and ecosystem health damage perform very similarly to GHG emissions as shown in Fig. 6.6, i.e. for electric vehicles they are very dependent on the primary energy source of electricity or hydrogen. In addition to climate change, there are also noticeable contributions to human health damage from particulate matter (PM) formation, human toxicity, and ionizing radiation.[2] Besides climate change there are smaller contributions to ecosystem health damage from urban and agricultural land use and natural land transformation. Land use is similar for all drivetrains and energy sources, but the contribution from land transformation is highest in the case of fossil oil based fuel supply.
Resource depletion is the sum of the increased cost to the society from the extraction of metals and fossil fuels.[3] As resource depletion is usually dominated by the contribution from fossil deple-

[2]Note that the LCIA method does not use regional characterization factors, i.e. there is no local differentiation of the attribution of emissions to human and ecosystem health damage. This means for example that PM emitted during electricity generation at remote locations has the same impact on human health as PM emission in densely populated areas, which is obviously not the case. The fact that the contribution from climate change is the dominating contribution to human and ecosystem health damage implies however that the general results would not be significantly different if regional characterization factors were used.

[3]For metals the additional cost is calculated based on the marginal cost increase for each mineral separately. For fossil fuels it is based on the additional cost for the exploitation of more costly unconventional oil. Within the ReCiPe

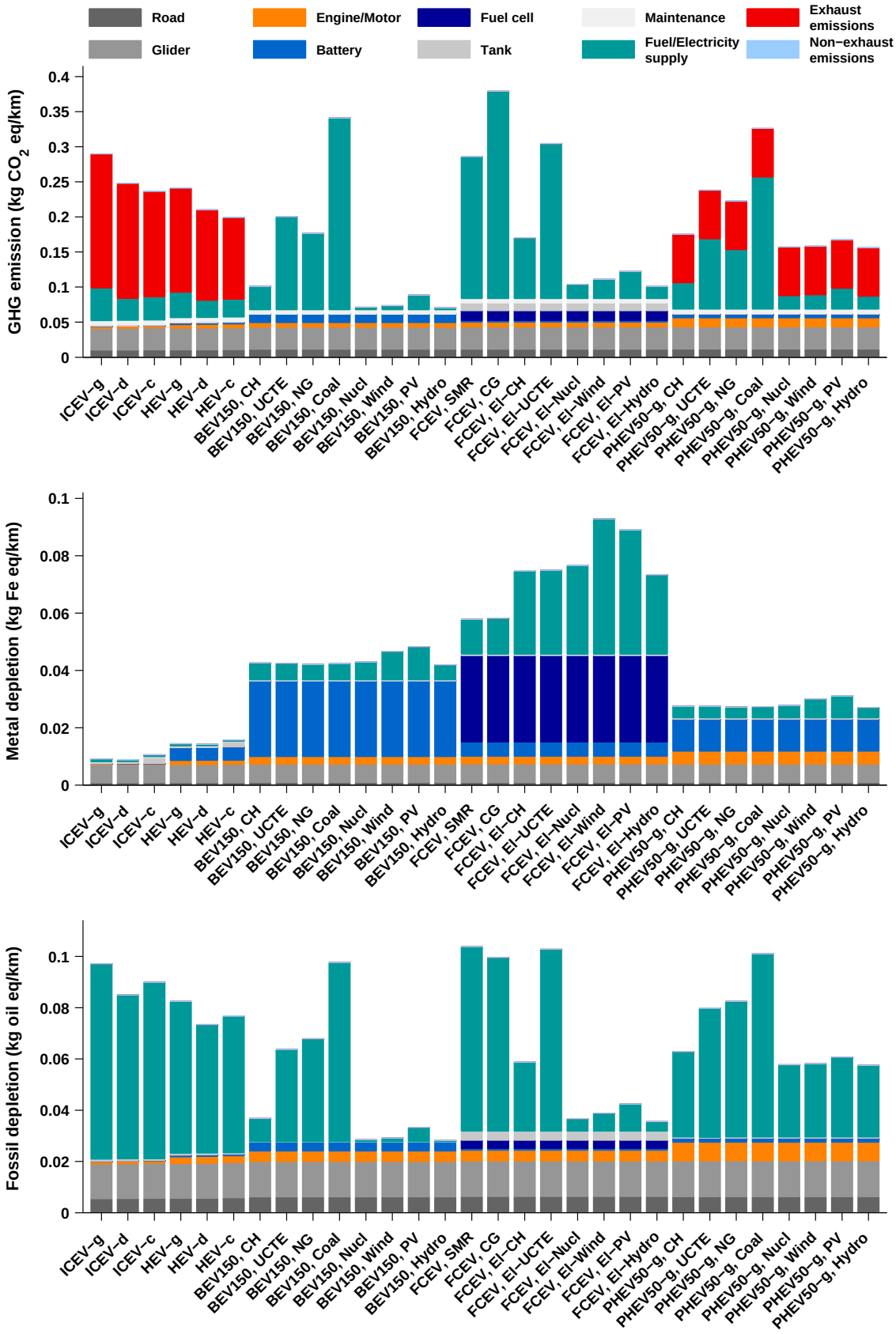

Figure 6.6: Mid-point indicators by drivetrain and energy source for a mid-size car in 2012.

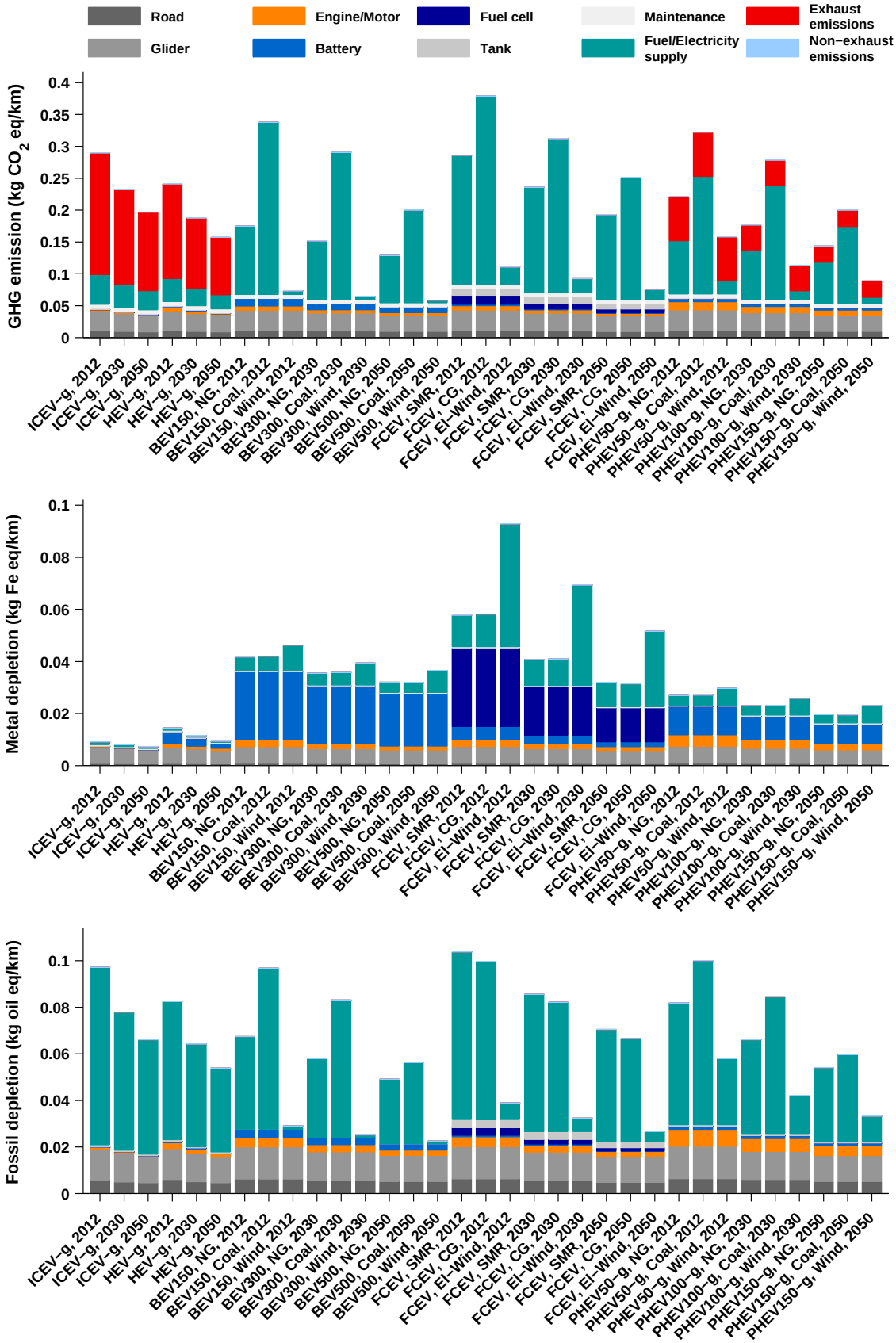

Figure 6.7: Mid-point indicators by drivetrain, energy source, and year for a midsize car.

tion it is highest if the vehicle uses a fossil primary energy source. Resource depletion is lowest if electricity or hydrogen from nuclear or renewable electricity is used. In this case metal and fossil depletion are approximately equal. The trade-off between metal and fossil depletion is also illustrated in Fig. 6.10.

Fig. 6.9 shows that the impact of all three end-point indicators decreases over time due to vehicle mass and energy use reductions, as well as due to efficiency improvements in electricity and hydrogen production.

method no differentiation is made for the scarcity of different fossil fuel types. The increased cost for natural gas and coal uses the same environmental mechanism as for oil [Goedkoop et al., 2009]. Therefore depletion of coal may be overestimated relative to the depletion of oil.

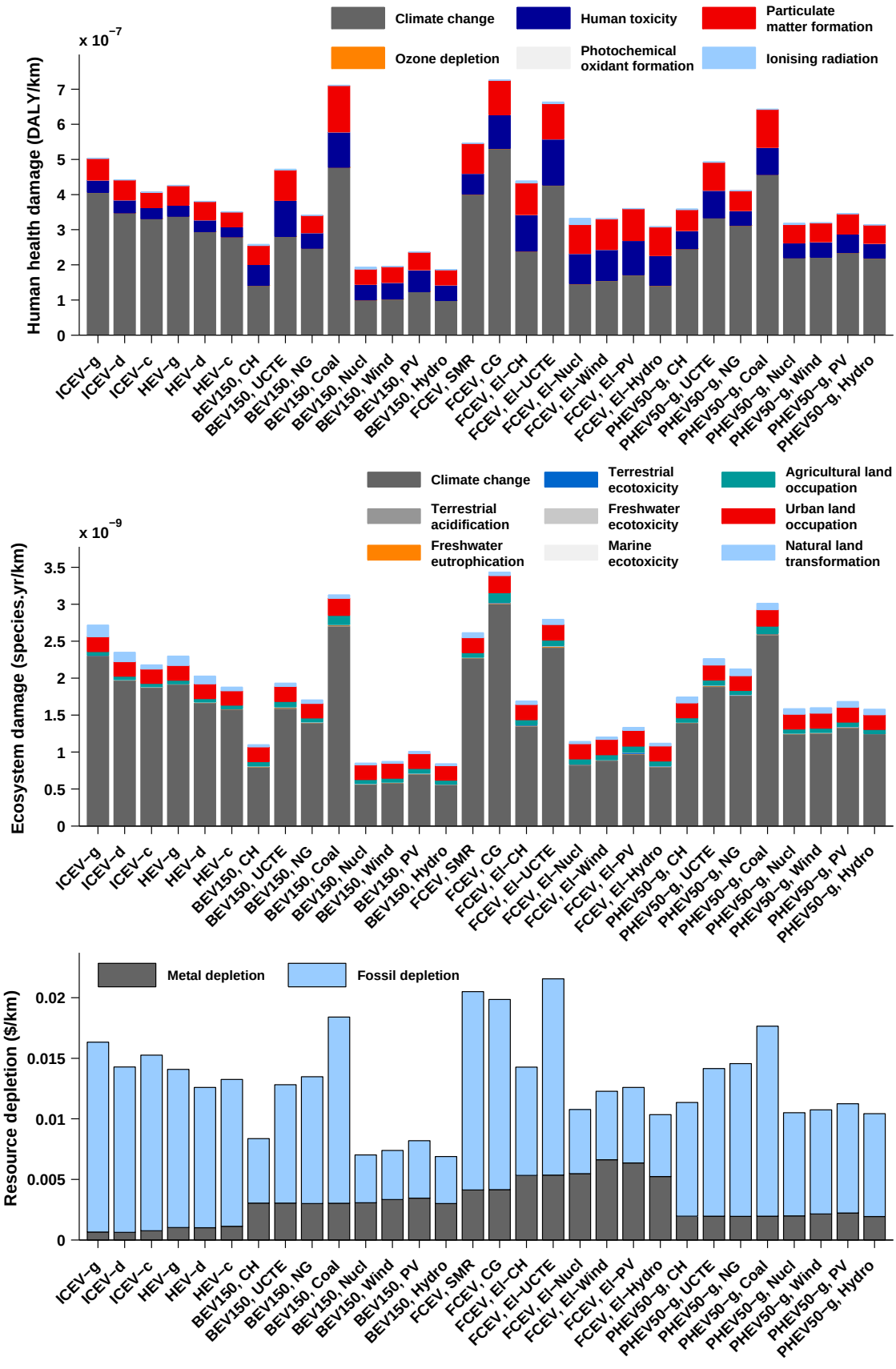

Figure 6.8: End-point indicators by drivetrain and energy source for a mid-size car in 2012.

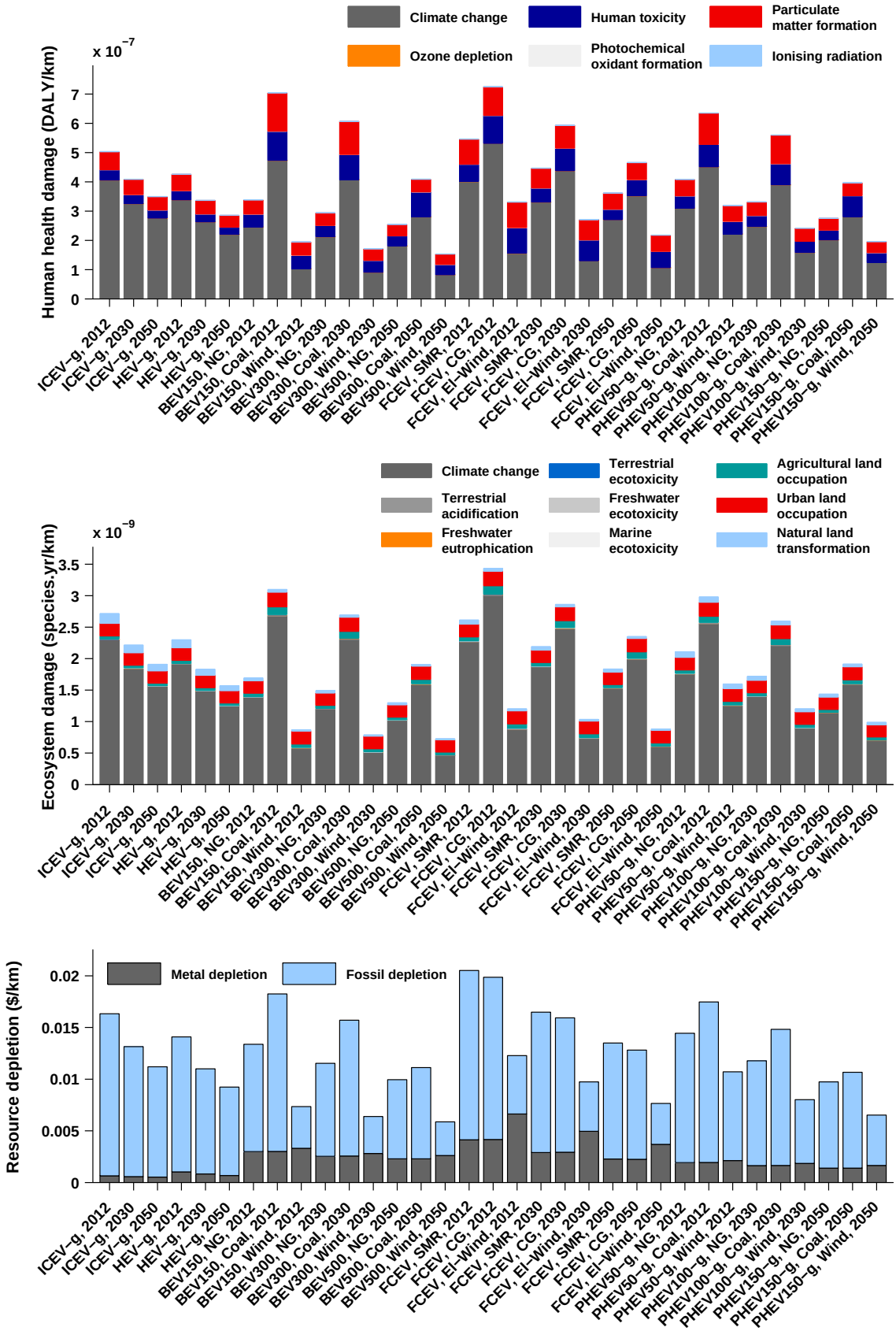

Figure 6.9: End-point indicators by drivetrain, energy source, and year for a midsize car.

Multi-dimensional analysis

The vehicle and fuel technologies analyzed in this thesis perform generally very different in terms of utility, cost, environmental indicators. Muli-dimensional representation can be used to visualize the tradeoffs between conflicting objectives. Fig. 6.10 shows this for total costs vs. GHG emissions and fossil vs. metal depletion. The figure compares how the different drivetrains and energy sources perform relative to each other and how this relation changes over time.

The top of Fig. 6.10 shows the relation of total costs to life cycle GHG emissions for a midsize car in three model years from 2012 to 2050. Five powertrains (ICEV-gasoline, HEV-gasoline, BEV-150/400, PHEV50-gasoline, FCEV) and three electricity and hydrogen sources (coal, natural gas, wind) are considered. Powertrains are distinguished by different colors and energy sources by different markers. Different points in time are connected by a line. The slope of the curve illustrates the direction of improvement over time. The main improvement for the BEV, PHEV, and FCHEV takes place in terms of total costs (vertical direction) due to reductions of battery and fuel cell costs. Total cost reductions from 2012 to 2030 are stronger than from 2030 to 2050. The ICEV and HEV mainly improve with respect to GHG emissions (horizontal direction) due to energy use reductions induced by lower vehicle resistance parameters and efficiency improvements. For the PHEV and BEV charged from coal electricity, significant reductions of GHG emissions are also seen due to a combination of reduced energy use and increased efficiency in electricity and hydrogen production. Note that the GHG emission reduction is stronger for the BEV-400 relative to the BEV-150 mainly because of additional battery weight reductions and associated reductions of energy use and LCA production phase impacts. In this comparison the best overall performance over the long term is achieved for the BEV, FCEV, and PHEV with electricity or hydrogen produced from wind power.

The bottom of Fig. 6.10 shows the tradeoff between metal and fossil depletion for the same vehicle and fuel options as discussed in the figure above. The analysis shows that reducing the dependence on fossil fuels with electric powertrains generally increases the use of metals. Again different points in time are connected by a line and the slope of the curve illustrates the direction of improvement over time. Vehicle options having high metal depletion (e.g. BEV and FCEV powered from wind electricity) mainly improve in terms of metal use (the vertical direction), while the ICEV, HEV, and BEV/FCEV powered from natural gas or coal primarily improve in terms of GHG emissions (the horizontal direction).

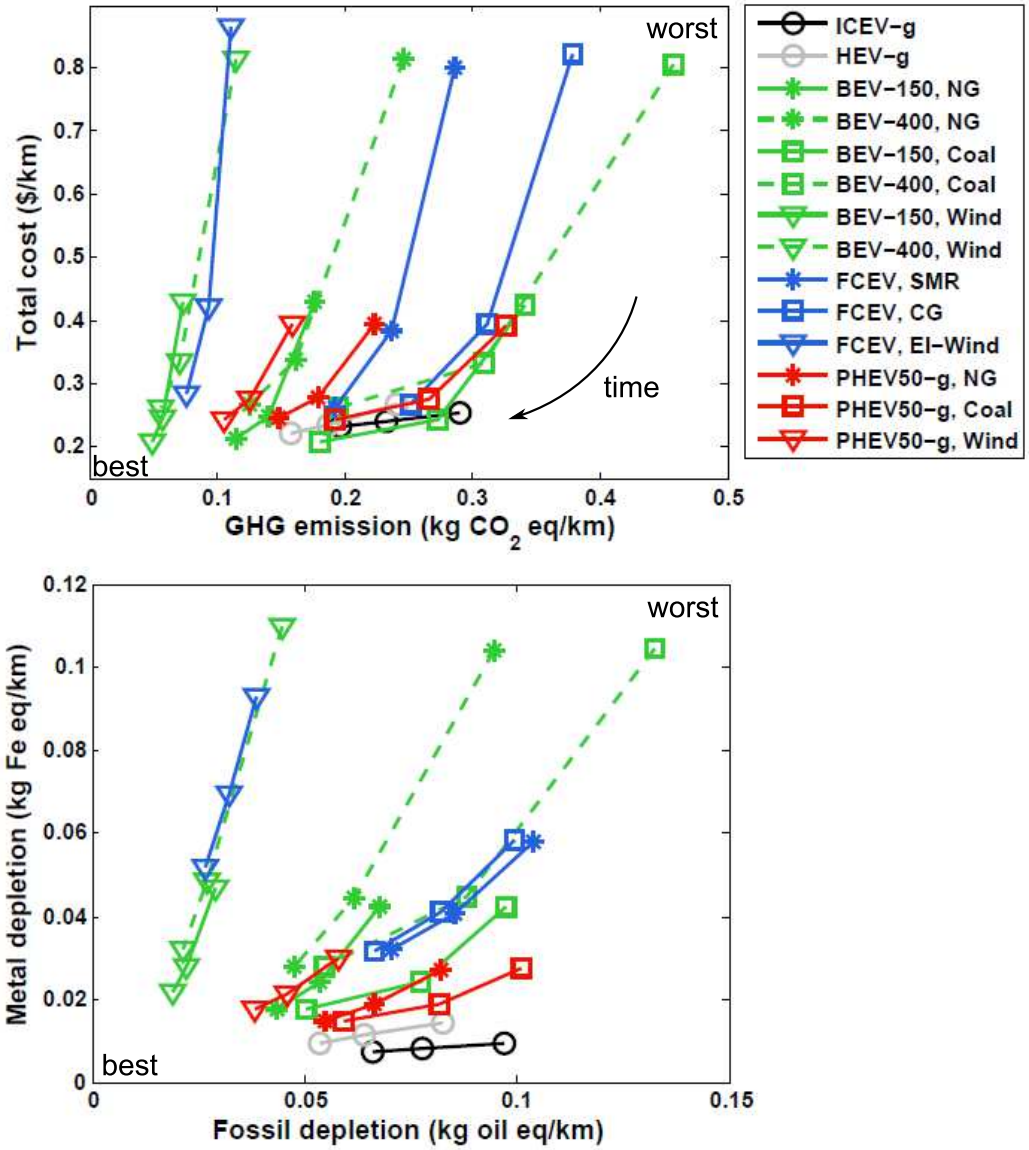

Figure 6.10: Development of total costs vs. life cycle GHG emissions and metal vs. fossil depletion for a midsize passenger car in three time steps from 2012 to 2050 (different points in time are connected by a line).

6.2 Multi-criteria decision analysis

As shown in the previous section, the various technology and fuel options analyzed perform very differently with regard to economic, utility, and environmental criteria. MCDA helps stakeholders understand and find solutions for such complex, multi-dimensional problems. It also actively involves participants in decision making, facilitates compromises, and helps to communicate the results [Pohekar & Ramachandran, 2004].

6.2.1 MCDA method

Table 6.3 shows the selection of criteria used in this MCDA example consisting of three categories including vehicle cost, utility, and environmental indicators. Note that the selection of indicators for this MCDA example is limited and does not reflect the broader scope of sustainability evaluation criteria assessed in the THELMA project (e.g. missing consideration of risk and security of supply). Powertrain options considered are ICEV-gasoline, HEV-gasoline, PHEV-gasoline, BEV, and FCEV. Energy source options include electricity and hydrogen production from natural gas, coal, wind, PV, and hydro power. The MCDA is performed separately for the years 2012 and 2050. The performance of the different technology options is evaluated for each specific indicator according to three different schemes. For charging/refueling time and all LCA indicators a linear scaling of the technology performance TP from zero (worst) to one (best) is used. In this case TP for indicator i and technology alternative t is calculated as

$$TP_{i,t} = \frac{\max(V_i) - V_{i,t}}{\max(V_i) - \min(V_i)} \tag{6.1}$$

where V_i is the array of values for indicator i. For vehicle range a linear scaling of TP is also used, however TP is non-zero for the lowest range vehicle. It is therefore calculated relative to the maximum range as

$$TP_{i,t} = \frac{V_{i,t}}{\max(V_i)} \tag{6.2}$$

For economic indicators a non-linear scaling of TP is used, inversely proportional to the indicator value

$$TP_{i,t} = \frac{\min(V_i)}{V_{i,t}} \tag{6.3}$$

This reflects the idea that a certain cost increase has a bigger influence at a low cost level than at high cost level.[4] The different scaling methods used and the possible values of TP are indicated together with the indicators in Table 6.3.

Table 6.3: MCDA indicators and technology performance scaling.

Category	Indicator	Unit	Direction of best perf.	Performance scaling
Economy	Purchase cost	$	min	non-linear, $0 < TP \leq 1$
	Operating cost	$/km	min	non-linear, $0 < TP \leq 1$
Utility	Range	km	max	linear, $0 < TP \leq 1$
	Charging/fueling time[5]	min	min	linear, $0 \leq TP \leq 1$
Environment	Human health damage	DALY/km	min	linear, $0 \leq TP \leq 1$
	Ecosystem damage	species.y/km	min	linear, $0 \leq TP \leq 1$
	Resource depletion	$/km	min	linear, $0 \leq TP \leq 1$

Many different algorithms exist to calculate the MCDA result for a specific criteria weighting. The most commonly used approach is the weighted-sum algorithm [Pohekar & Ramachandran, 2004; Wang et al., 2009]. Because it is the most easy to understand and accept by stakeholders it is used in this thesis.

Assuming N criteria the score S_t for a specific technology option t can be calculated as

$$S_t = \sum_{i=1}^{N} w_i \cdot TP_{i,t} \tag{6.4}$$

where w_i is the weight of importance for criteria i. The technology option which achieves the highest score according to Eq. 6.4 performs best.

Usually MCDA involves the participation of stakeholders whose weights for different criteria are assessed, for example in surveys. No such assessment has been performed within this thesis. The MCDA approach can however be used to study the MCDA result for generic weighting profiles to show the strength and weaknesses of the technology alternatives according to different characteristic preferences. The profiles analyzed in the following are: Equal weight on economic indicators, zero on others (A); equal weight on utility indicators, zero on others (B); equal weight on environmental indicators, zero on others (C); equal weight on economic and utility indicators, zero on others (D); equal weight on utility and environmental indicators, zero on others (E); equal weight on all indicators (F). The sum of all weights is normalized for each profile to one. Fig. 6.11

[4] In principal it would be better to base the exact form of the valuation curve on stakeholder opinions as explained for example in [Eisenführ et al., 2010]. However no such information was available.

[5] The following average fueling/charging rates for 2012-2050 are assumed: Gasoline/diesel (30 L/min), CNG (5-15 L gasoline eq/min), electricity (5-20 kW), hydrogen (0.8-2 kg/min). Note that using ultra fast chargers a charging power up to 100 kW can be achieved, however this is not considered in this example.

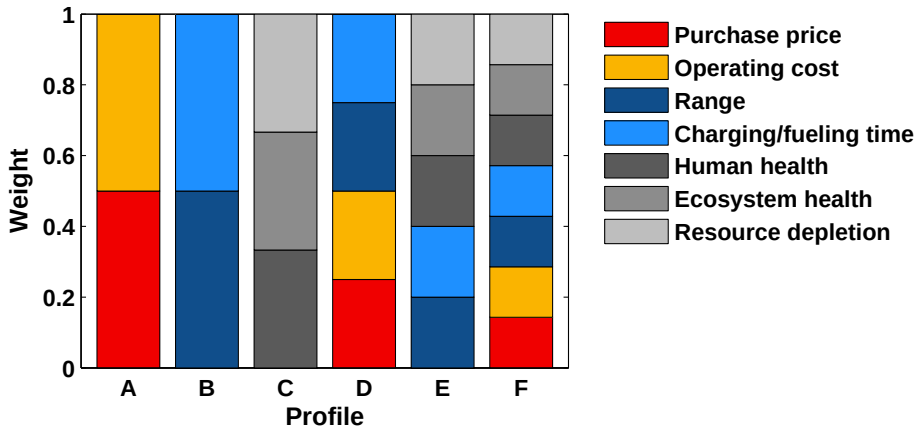

Figure 6.11: MCDA weighting profiles analyzed.

shows the weighting profiles used in the following analysis.

6.2.2 MCDA results

Fig. 6.12 shows the MCDA results for the weighting profiles A to C.
With equally weighted economic indicators (A), the ICEV is ranked highest in 2012 due to its low purchase price. It is followed by the HEV with relatively low purchase price and moderate operating costs. Third is the BEV powered from coal electricity which performs best with regard to operating costs. For this weighting profile which focuses on economic indicators the FCEV powered with PV electricity performs worst due to very high purchase and relatively high operating costs. In 2050 the HEV is ranked highest due to its good performance with regard to purchase and operating costs. It is closely followed by the BEV and PHEV. The FCEV performs worst, mainly due to high operating cost.[6]
For case B with full weight on utility indicators the ICEV and HEV perform best in 2012 and 2050 due to their high range and short refueling time. The ICEV and HEV are closely followed by the FCEV which performs well compared to other electric powertrain technologies. The performance of electric vehicles significantly improves over time, and in 2050 the FCEV reaches practically the same utility level as conventional vehicles. The BEV performs worst in both analysis years due to the limited range and relatively long charging time.
For equally weighted environmental indicators (C) the BEV charged with electricity from renewable sources performs best in 2012 and 2050 mainly due to low GHG emissions and fossil resource depletion. It is followed by the FCEV and the PHEV (fueled and charged from renewable sources) which also perform relatively well in terms of GHG emissions and fossil resource use. Among

[6]Note that the FCEV operating costs partly include infrastructure cost for hydrogen delivery and storage.

the renewable primary sources considered hydro power performs consistently best, followed by wind and PV electricity. Electric vehicles with coal as the primary energy source perform worst today and in the future. In between those extremes is the HEV, which performs similarly to the BEV and the PHEV charged with electricity generated from natural gas.

Fig. 6.12 shows the MCDA result for the weighting profiles D to F.
If economic and utility indicators are weighed equally (D) – which is probably the most relevant weighting for consumers not concerned about environmental impacts – the ICEV and HEV perform best in 2012 and 2050. Electric vehicles however improve significantly over time, and the FCEV with natural gas as the primary energy source nearly reaches the level of the ICEV and HEV by 2050. The PHEV and FCEV perform similarly in the sum of those indicators, whereas the FCEV has a higher score for utility indicators and the PHEV with regard to operating costs. The BEV is ranked last for this weighting due to its relatively bad performance with regard to range and charging time.
For equal weight on utility and environmental indicators (E) – a weighting which shows the strengths of a technology to reduce environmental impacts and to meet the utility expected by consumers, but which does not consider the costs and customer willingness to pay – the FCEV fueled with hydrogen produced from hydro power performs best in 2012 and 2050, closely followed by the PHEV charged with electricity from renewable sources. For this weighting profile the FCEV and PHEV with renewable primary energy clearly outperform the ICEV, HEV, and BEV.
If all the indicators considered are weighed equally (F), then the HEV performs best in 2012 followed by the PHEV charged from hydro power. In 2050 the PHEV charged with electricity from renewable sources performs best, closely followed by the FCEV fueled with hydrogen from renewable sources.

Overall the results show that purely fossil fuel based technologies (ICEV and HEV) perform best with regard to cost and utility indicators and that electric vehicles (BEV, PHEV, and FCEV) perform best with regard to environmental indicators if a renewable primary energy source is used. The results indicate that the main hurdle for the BEV relative to other powertrain technologies are low range and long charging time, and for the FCEV high costs. The PHEV charged from renewable primary energy is the the highest ranked powertrain option with regard to the full set of indicators considered. The BEV charged from renewable primary energy performs best if range and charging time are not important. The FCEV fueled from renewable primary energy performs very well overall if fuel cell costs and the costs of hydrogen production, storage, and delivery can be significantly reduced.

The MCDA presented in this section was based on generic weighting profiles to analyze the strengths and weaknesses of the different vehicle and fuel technologies relative to each other. In order to give stakeholders the opportunity to assess the performance of different technologies according to their own preferences interactive webtools have been developed. These applications

are presented in the next section.

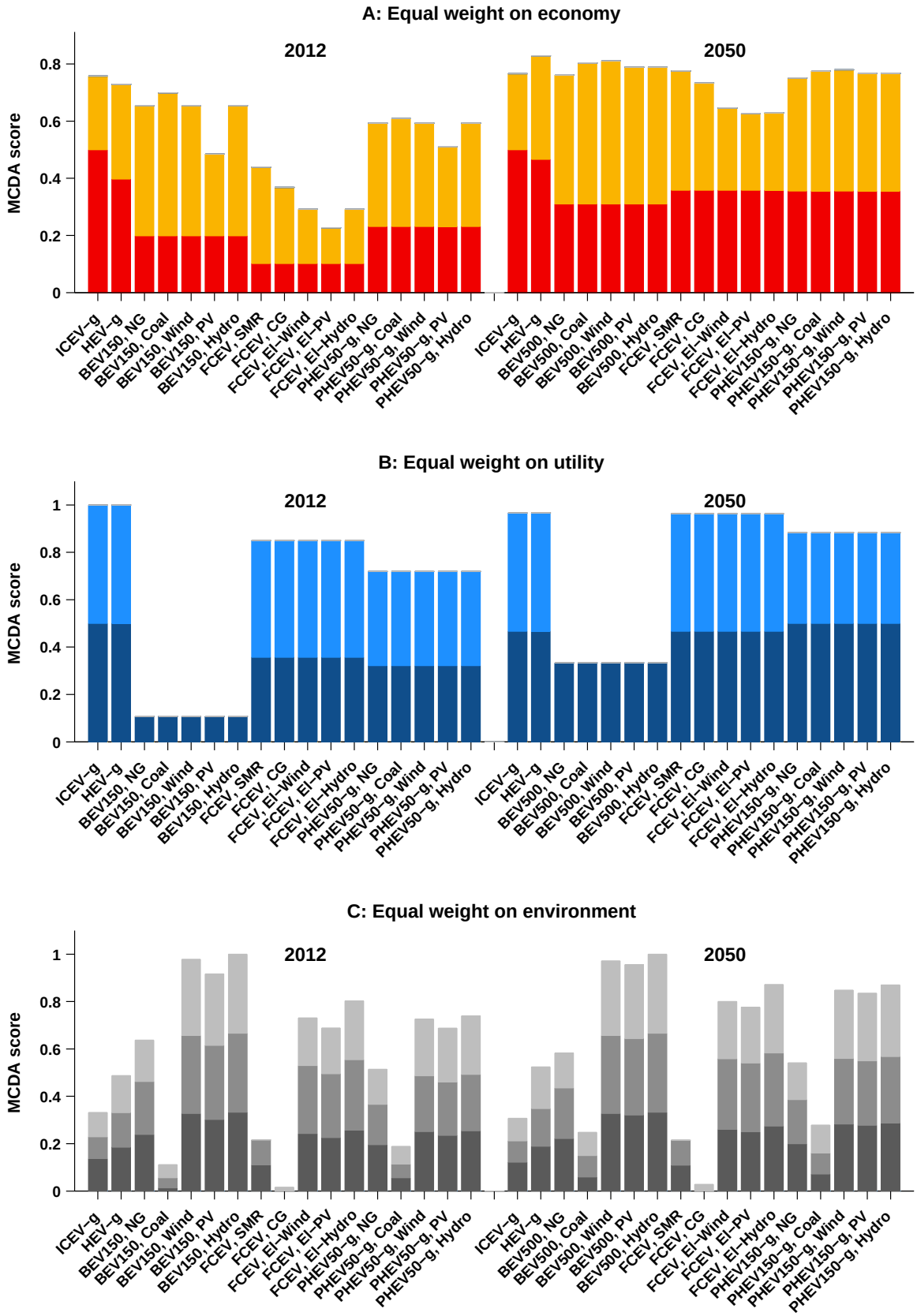

Figure 6.12: MCDA result for weighting profiles A to C.

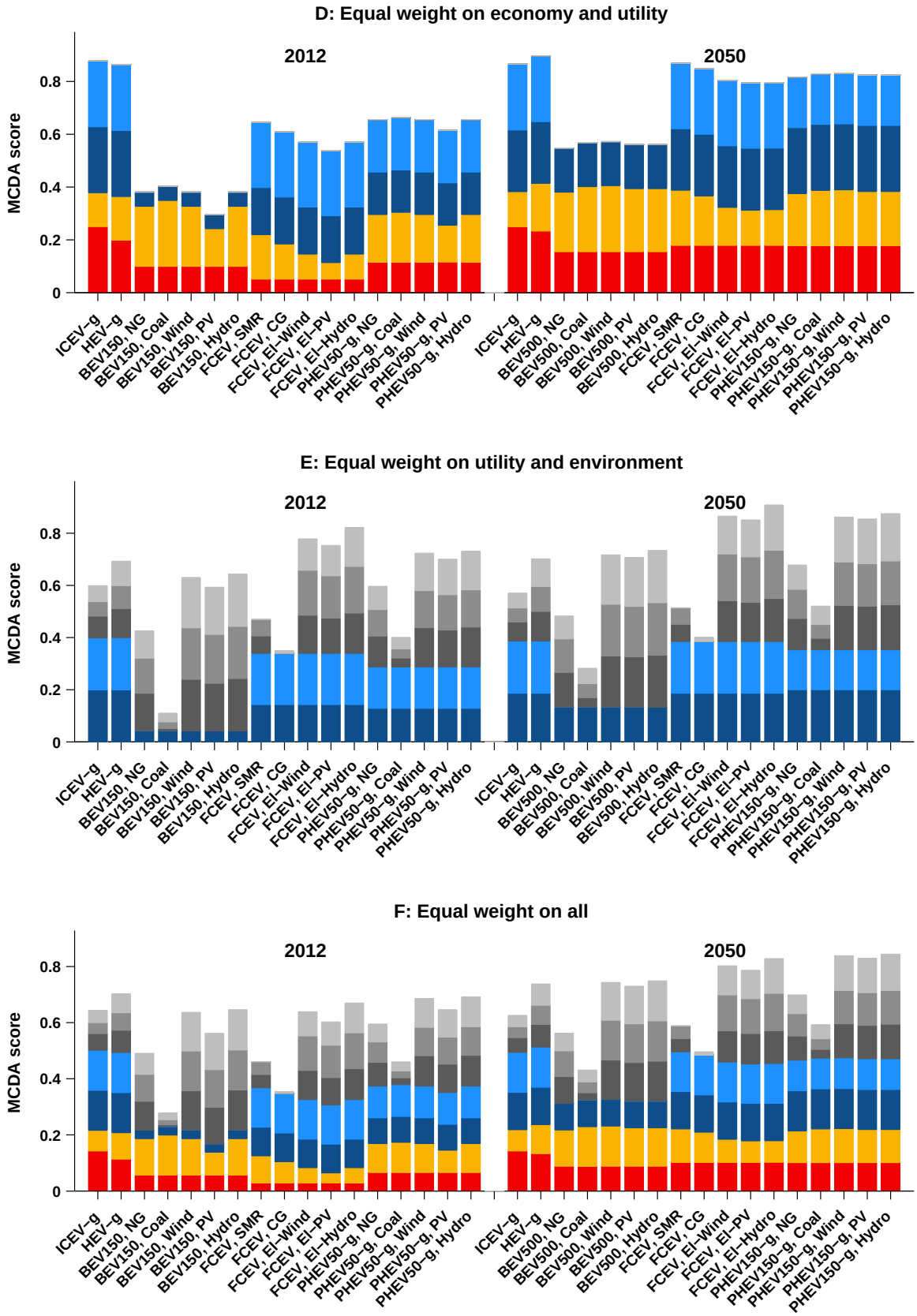

Figure 6.13: MCDA result for weighting profiles D to F.

6.3 Interactive analysis tools

The analytic modeling method used in this work allows fast calculation of vehicle indicators, which is very well suited for interactive analysis. This kind of analysis gives the user the opportunity to interactively select and compare different vehicle technologies and to modify scenario assumptions. This section describes the implementation of analysis tools corresponding to the applications presented in section 6.1 and 6.2.

6.3.1 Matlab GUI implementation

The criteria, vehicle options, and preference weights analyzed in section 6.1 and 6.2 represent only a very small subset of possible combinations. A graphical user interface (GUI) has been implemented in Matlab in which all indicators for the whole set of vehicle and energy options can be explored in more detail. The user can select and compare the technology options and criteria of interest. In addition, the baseline vehicle configuration parameters and scenario assumptions can be modified. Since all calculations are performed each time a user interaction occurs, the resulting effects can be immediately observed. The layout of the Matlab GUI is shown in Fig. 6.14. A similar analysis tool has been developed for the MCDA presented in section 6.2 that allows stakeholders to select vehicle alternatives, modify scenario assumptions, weigh the different criteria, and see the corresponding MCDA result.

6.3.2 Webtool implementation

The analysis tool implementation described in section 6.3.1 requires Matlab to be installed on the computer on which the application is used. In order to make the results available for a broader public several online analysis tools have been developed. The general procedure used to implement the Matlab based calculations in an online GUI is the following. The main functions in Matlab are converted to Java using the Matlab Java compiler. The resulting Java archive file can be executed on a web server that has the Java and Matlab runtime environments installed. The compiled Java files can then be accessed via a user interface from any web browser. Once a user interaction occurs all relevant information is passed to the server and the calculations are performed. The results are returned to the web browser and illustrated with Google Charts. The response time, i.e. the time it takes from a user selection to the resulting figure representation is below 0.5 seconds with good Internet connectivity. Using the current model implementation the capacity of the server with 4 GB RAM is limited to approximately 2000-4000 calls per minute, which means that about 20 users can work with the webtools in parallel with a response time of less than 0.5 seconds. Streamlining the calculations this capacity can be raised significantly. Fig. 6.15 shows screenshots of the webtools developed for multi-indicator analysis and MCDA. Both

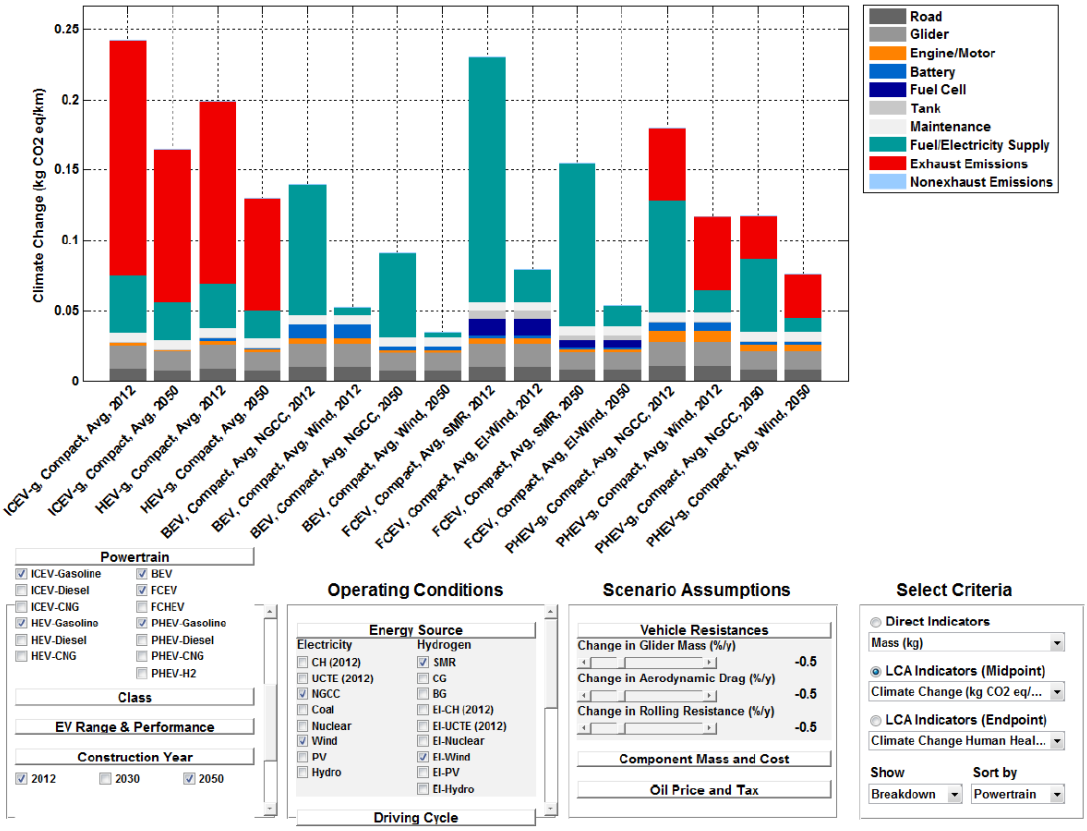

Figure 6.14: Matlab user interface for vehicle indicator analysis.

applications can be accessed at:

http://www.multi-criteria-analysis.com/

Figure 6.15: Screenshots of the multi-indicator analysis (a) and MCDA (b) webtools.

Chapter 7

Optimal use of advanced technologies

Many technology options exist to reduce vehicle energy use, GHG emissions, and fuel costs. Among these are engine efficiency improvements, hybridization, vehicle lightweighting, and other options like reduction of aerodynamic drag, rolling resistance and drivetrain losses. All these technologies have different costs and influence energy use in different ways. An integrated framework on how to best implement those technologies is missing.

Optimization is an often applied method in automotive research. Most previous studies however have focused on optimal power management and powertrain component sizing to achieve minimal vehicle energy use [Kim & Peng, 2007] or to reach minimal life cycle costs and GHG emissions [Shiau et al., 2010]. In [Wilhelm et al., 2012] we analyzed how lightweighting and powertrain efficiency technology can be optimally implemented to minimize vehicle lifetime costs. Depending on the complexity of the technology marginal cost functions, analytic solutions for the optimal degree of implementation are given. The study clearly shows the trade-off between investments in lightweighting versus powertrain efficiency technology, however the methodology has some limitations that prevent it from being used for specific drivetrain technologies: First, the analytic calculation of energy demand does not consider traction and regeneration separately and only a single vehicle efficiency is used which is not clearly assigned to traction or regeneration mode. This approach is valid for conventional vehicles without regeneration capability, but not generally for electric vehicles. Second, vehicle configuration parameters (such as range and performance) were not considered in the optimization problem. Therefore secondary mass and cost effects due to compounding of component sizes are not considered. The methodology developed in chapter 2 to 5 now considers both effects, i.e. regeneration capability and sizing of components. It also allows one to study the sensitivity of the optimal solutions to component specific parameters such as battery energy density or battery specific cost.

Vehicle cost and life cycle optimization have been investigated in several studies. An analytic method to find the optimal degree of lightweighting minimizing manufacturing and total costs

of a BEV has been developed in [Hofer et al., 2012c]. The method has been coupled with LCA to minimize life cycle GHG emission of conventional and electric passenger vehicles. The optimization of life cycle GHG emissions using lightweighting technology has been also studied in [Siegerist, 2013]. In the following chapter the optimal amount of lightweighting to minimize total costs is compared for conventional and electric vehicles as a function of relevant parameters.

7.1 Lightweighting technology and optimization

Reduction of vehicle mass can be achieved by shifting sales from larger and heavier vehicles to smaller and lighter vehicle categories, vehicle redesign, or material substitution [Cheah et al., 2009; Hofer et al., 2012c]. Lightweighting usually refers to the latter, i.e. the replacement of conventional materials such as steel with materials of higher strength and/or stiffness per weight such as high-strength steel (HSS), aluminum, magnesium, or carbon fiber composite in order to reduce vehicle mass while keeping other consumer criteria constant. In recent years many low carbon steel parts have been replaced by HSS and aluminum. In fact, the use of HSS doubled in the last two decades to make up approximately 13 % of the average new vehicle weight in 2007 and the use of aluminum increased from approximately 5% in 1980 to 9% in 2010 [Lutsey, 2010]. In addition, there is also an increasing trend towards the use of magnesium, plastics and polymer composites [Lutsey, 2010]. Several research projects have examined the mass-reduction potential for future lightweight vehicles [Lotus, 2010; FSV, 2011; IBIS, 2008; Goede et al., 2009; Lovins & Cramer, 2004; ThyssenKrupp, 2003]. Relative to today vehicle mass reductions of approximately 20 % seem to be possible with extensive use of HSS, about 40 % with use of aluminum, magnesium, plastics and polymer composites, and up to 60 % with use of carbon fiber composites. Lightweighting is now intensively used by the automotive industry to reduce vehicle energy use and to meet regulatory emissions standards. Recent examples include the Volkswagen Up, Tesla Model S, and BMW i3 having vehicle bodies made of high-strength steel, aluminum, and carbon fiber, respectively.

There are several interesting trade-offs related to the use of lightweighting. Lightweight parts are in general more expensive to manufacture per unit of weight. However, a lighter vehicle uses less energy and requires a smaller powertrain and energy storage at constant range and performance, which in turn reduces vehicle costs. In the following the estimated cost of lightweighting is compared against the reduced costs for the powertrain, energy storage, and vehicle operation. Analytic solutions for the optimal degree of lightweighting to minimize total costs of an ICEV and BEV are investigated as a function of relevant parameters. Previous studies have analyzed the impact of lightweighting on vehicle energy consumption, cost, and life-cycle energy use [Kim et al., 2011; Redelbach et al., 2012; Brooker et al., 2013; Wilhelm et al., 2012; Kim & Wallington, 2013]. This work extends these by combining vehicle simulation and cost assessment in an an-

alytic method to compare the benefits of lightweight material use in conventional and electric powertrains. The modeling method allows analyzing the sensitivity of the optimal solutions in an unprecedented way. In section 7.2 the effects of lightweighting on conventional and electric vehicle mass and energy use are analyzed. In section 7.3 analytic solutions for the optimal degree of lightweighting minimizing total costs are analyzed as a function of relevant parameters. The work presented in this chapter is partly based on [Hofer et al., 2012c; 2013b].

7.2 Effects of weight reduction on vehicle mass and energy use

Due to the different principles of energy conversion and storage the effects of lightweighting on vehicle configuration and energy use are very different in conventional and electric drivetrains. In the following the effects of weight reduction on vehicle mass and energy use of a BEV and ICEV are compared.

The baseline vehicle configuration analyzed in this chapter corresponds to a midsize passenger car with the characteristics listed in Table 7.1. In agreement with Eq. 4.1 vehicle mass is calculated as the sum of powertrain mass, energy storage mass, glider mass, and additional material necessary for structural support of the powertrain and energy storage beyond the glider baseline.[1] The reference glider is based on an inventory of the 2008 Mercedes-Benz A-Class [Hawkins et al., 2012b; Daimler, 2008]. 72 % of its mass is made of steel and 28 % of other materials. It is assumed that lightweighting is applied to the part consisting of steel (primarily used in the body, doors, and chassis). The part made of materials other than steel (mainly found in the vehicle interior, tires, powertrain fluids, etc.) is kept constant. The base glider mass is slightly higher for the ICEV than for the BEV due to additional mass for the transmission and exhaust system. Powertrain and energy storage mass and cost are calculated as the sum of a fixed amount and a fraction that scales linearly with power and energy storage capacity as described in section 4.1. Specific mass and cost assumptions for the BEV and ICEV components are according to Table 4.2 and 4.3 for the year 2012.[2] Evaluation of lightweighting effects for future scenarios is performed in [Hofer et al., 2012c].

Similar to section 5.1.2 the relation between vehicle mass, energy use, glider mass reduction, range, and other parameters can be calculated analytically. BEV and ICEV mass is calculated according to Eq. 5.11. Since the use of lightweight materials reduces vehicle mass but leaves size characteristics constant, no coupling of vehicle mass and size is considered (corresponding to Case A in section 5.1.2). To include the effect of glider mass reduction in Eq. 5.16 and 5.17, glider mass is expressed as the sum of a fixed mass and a variable part to which lightweighting is

[1] Note that the transmission is in this chapter accounted for within the glider instead of the powertrain as in section 4.1.

[2] In the following battery baseline fixed and variable costs of 4000 $ and 500 $/kWh are assumed instead of the values indicated in Table 4.3. Otherwise all values are identical to the values of Table 4.2 and Table 4.3.

Table 7.1: Reference vehicle configuration.

	ICEV	**BEV**
Frontal area (m^2)	2.2	
Aerodynamic drag (c_d)	0.28	
Rolling resistance (c_r)	0.01	
Glider mass (kg)	1070	1005
P/m-ratio (W/kg)	70	65
Range (km)	800	200/400

applied

$$m_{gl} = m_{gl,\,fix} + (1-\delta)\cdot m_{gl,\,var} \tag{7.1}$$

where $\delta \in [0,1]$ is the amount of variable glider mass reduction in percent.[3] Substituting Eq. 7.1 in Eq. 5.16 and 5.17 gives vehicle energy use and mass as a function of variable glider mass reduction

$$EC = \frac{EC_0 + \frac{\partial EC}{\partial m}\cdot(m_{gl,\,fix} + (1-\delta)\cdot m_{gl,\,var} + \gamma\cdot CM) - \gamma\cdot EC_0\cdot\frac{P}{m}\cdot SM_{pt,\,pm}}{1-\gamma\cdot\left(\frac{\partial EC}{\partial m}\cdot R\cdot SM_{es} - \frac{P}{m}\cdot SM_{pt,\,pm}\right)} \tag{7.2}$$

$$m = \frac{m_{gl,\,fix} + (1-\delta)\cdot m_{gl,\,var} + \gamma\cdot(CM + EC_0\cdot R\cdot SM_{es})}{1-\gamma\cdot\left(\frac{\partial EC}{\partial m}\cdot R\cdot SM_{es} - \frac{P}{m}\cdot SM_{pt,pm}\right)} \tag{7.3}$$

Fig. 7.1a and 7.1b show ICEV and BEV mass as a function of variable glider mass reduction for the baseline case analyzed. Even though the base glider mass is slightly higher for the ICEV than the BEV, total vehicle mass is higher for the BEV due to the additional mass of the battery. As the weight of the glider is reduced, the sizes of the powertrain and energy storage also decrease because acceleration performance and range are constant. This effect is referred to as secondary weight reduction in the following.[4] Fig. 7.1c shows vehicle energy use for the NEDC driving cycle as a function of variable glider mass reduction. Due to the lower powertrain efficiency and the lack of regeneration capability, the sensitivity of energy consumption to mass reduction is higher for the ICEV than the BEV. Note also that the sensitivity of energy consumption to mass reduction is generally higher in urban driving conditions, which makes lightweighting particularly useful in this case.

[3] As mentioned earlier, it is assumed that lightweighting is applied to the part of the glider consisting of steel, which corresponds to the variable glider mass.

[4] And sometimes as decompounding in the literature.

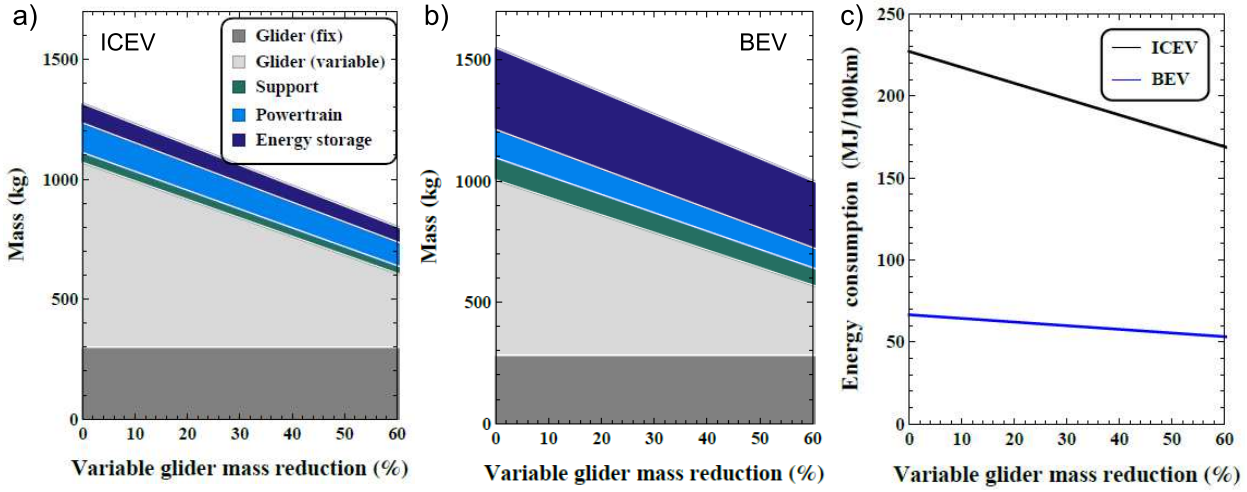

Figure 7.1: Vehicle mass (a,b) and energy consumption (c) for the ICEV and BEV-200 as a function of variable glider mass reduction.

The secondary weight reduction effect is particularly relevant for the BEV due to the high mass and cost of the battery. It is reflected in the total-to-primary weight reduction, i.e. the ratio of total vehicle mass reduction (including secondary effects) to primary glider mass reduction, which equates in the baseline case to 126 % for the BEV (at 200 km range) and 111 % for the ICEV. Secondary weight reduction effects in a BEV are particularly dependent on the battery size and as such on vehicle range and battery specific energy. Fig. 7.2 shows the total-to-primary vehicle weight reduction as a function of electric range and battery specific energy. It can be seen that secondary weight reduction is significant for current battery technology (ca. 100 Wh of usable energy per kg battery pack) at ranges above ca. 200 km. For future batteries reaching 300 Wh/kg the secondary weight effects become significant only above ca. 600 km range.

Note that the assessment as formulated here only takes into account secondary weight reduction effects within the powertrain, energy storage, and support structure but not within the glider itself, as for example investigated in [Alonso et al., 2012]. In principal Eq. 7.1 can be easily modified to include this effect. If secondary weight reduction within the glider were included, total secondary effects would be higher and the results shown in the following slightly more positive towards the use of lightweighting. However, the general conclusions regarding the relative benefits of lightweighting in conventional and electric vehicles remain unchanged.

7.3 Lightweighting costs

Lightweight parts are generally more expensive to manufacture per unit of weight. The actual increase in manufacturing costs is very much dependent on the particular materials used and

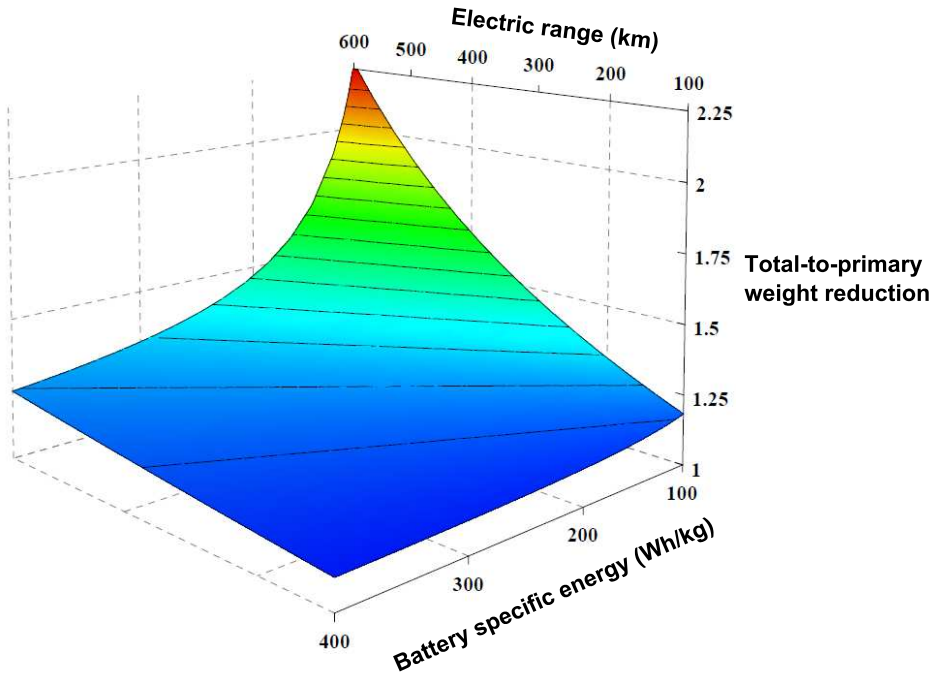

Figure 7.2: Total-to-primary BEV weight reduction as a function of vehicle electric range and battery specific energy.

the associated changes in tooling and assembly costs. As described in section 4.2 manufacturing costs are calculated as the sum of powertrain, energy storage and glider cost. Here glider cost MC_{gl} is calculated as the sum of a fixed cost for the part that is not lightweighted (corresponding to $m_{gl,\,fix}$) and a variable cost that is dependent on the amount of weight reduction implemented (corresponding to $m_{gl,\,var}$).

$$MC_{gl} \quad = \quad SC_{gl,\,fix} \cdot m_{gl,\,fix} + SC_{gl,\,var}(\delta) \cdot m_{gl,\,var} \tag{7.4}$$

Glider specific fixed cost is $SC_{gl,\,fix}$ = 14.3 \$/kg and variable baseline cost (without use of lightweight materials) is $SC_{gl,\,var}(0)$ = 5.7 \$/kg. Both specific cost values are based on the mass and manufacturing cost breakdown for a midsize passenger car given in [NRC, 2011]. Specific cost scaling is based on a literature review of the manufacturing cost increase of lightweight materials relative to steel. In order to analytically minimize vehicle cost a continuous lightweight cost function is used. This concept is rather artificial as in practice discrete material options lead to discrete weight reduction potentials and costs. However for the purpose of this analysis, i.e. the comparison of the cost reduction effects of lightweighting for different powertrain types, it is useful. Fig. 7.3 shows the literature data [FSV, 2011; Goede et al., 2009; ThyssenKrupp, 2003;

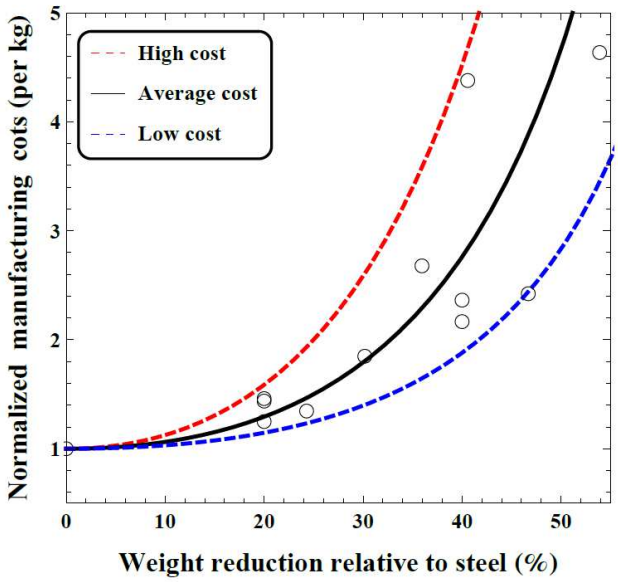

Figure 7.3: Lightweighting manufacturing cost increase relative to steel. Shown are literature data (circles) and a low, average, and high lightweighting cost function.

Smokers, 2011; Heuss, 2012] together with a fit for a quadratic polynomial with an asymptote at the assumed maximum amount of lightweighting δ_{max}

$$SC_{gl,var}(\delta) = SC_{gl,var}(0) \cdot \left(1 + \frac{e \cdot \delta^2}{1 - \delta/\delta_{max}}\right) \tag{7.5}$$

The average cost function in Fig. 7.3 corresponds to a least squares fit which yields $e = 5.5$ for $\delta_{max} = 80$ %. It will be referred to as the baseline lightweighting cost function in the following analysis. The data and fit show the general trend that the more mass the lightweight material can substitute relative to steel, the more expensive it is to manufacture (per unit of weight). Reductions of up to 20-30 % can be achieved at relatively low cost by substituting steel with high-strength steel. Higher reductions require materials with a higher amount of labor and energy input per kg of material, e.g. carbon fiber. Due to the spread and limited availability of data, two additional cost functions for a lower ($a = 2.75$) and a higher ($a = 11$) bound are defined.

To convert manufacturing costs to retail price, a markup factor of 1.4 is used [NRC, 2011]. Total costs are calculated as the sum of vehicle purchase and lifetime energy costs. Maintenance and repair costs are assumed to be independent of lightweighting and not considered. For simplicity no discounting, i.e. devaluation of future energy costs, is used. In the base case a lifetime of ten years, an annual driving distance of 15,000 km, a gasoline price of 2 \$/L and a total charging cost

of 0.35 $/kWh are assumed. Charging cost is based on an electricity price of 0.2 $/kWh, an energy based tax of 25 $/GJ, and 0.06 $/kWh charging station cost. For the BEV the total driving distance of 150,000 vehicle-kilometer is limited by the lifetime of the battery. For the ICEV a second base case with 300,000 vkm is analyzed.

7.4 Cost optimization

The cost minimum is found by setting the partial derivative of manufacturing and total costs to zero and solving for the optimal degree of lightweighting as a function of the parameters of interest. The explicit equations for the optimal degree of lightweighting are not given as they are generally rather long, instead the results are shown graphically. In the following the reference results and sensitivity analysis are discussed separately for the ICEV and BEV.

7.4.1 Cost effects for ICEV

Fig. 7.4 shows the breakdown of ICEV total cost as a function of variable glider mass reduction for the baseline lightweight cost function. Minimum manufacturing cost is reached at ca. 10 % variable glider mass reduction. It is apparent that the share of fuel costs to total costs is relatively high and dominates if no lightweight material is used. Due to the high share of fuel to total costs and the high sensitivity of fuel consumption to weight reduction, the difference between the optimal solutions minimizing manufacturing versus total costs is relatively large and increases further at higher driving distance. For 150,000 vkm (Fig. 7.4a) minimum total cost is reached at 22 % and for 300,000 vkm (Fig. 7.4b) at 31 % variable glider mass reduction.

Fig. 7.5a shows the sensitivity of the optimal weight reduction minimizing ICEV total cost relative to lifetime driving distance. As can be seen from the figure, the optimal degree of lightweighting is very sensitive to both parameters. Fig. 7.5b shows the corresponding total cost reduction. For the baseline lightweight cost function it is 1780 $ and 4130 $ for 150,000 and 300,000 vkm, respectively.

As shown in Fig. 7.5 the optimal use of lightweighting for an ICEV is very sensitive to factors affecting fuel costs. Fig. 7.6a shows the sensitivity of the optimal amount of lightweighting minimizing ICEV total cost as a function of vehicle driving distance and fuel price. In this case the baseline lightweight cost function is assumed. Fig. 7.6b shows the corresponding total cost reduction.

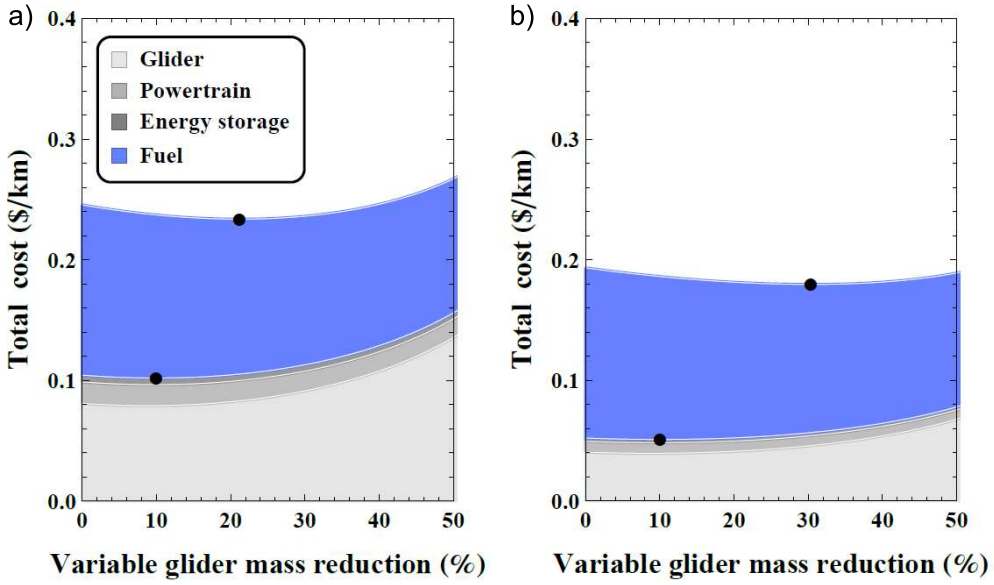

Figure 7.4: Effect of lightweighting on ICEV total cost for a) 150,000 and b) 300,000 vkm. Black points indicate optimal levels of lightweighting minimizing manufacturing and total costs.

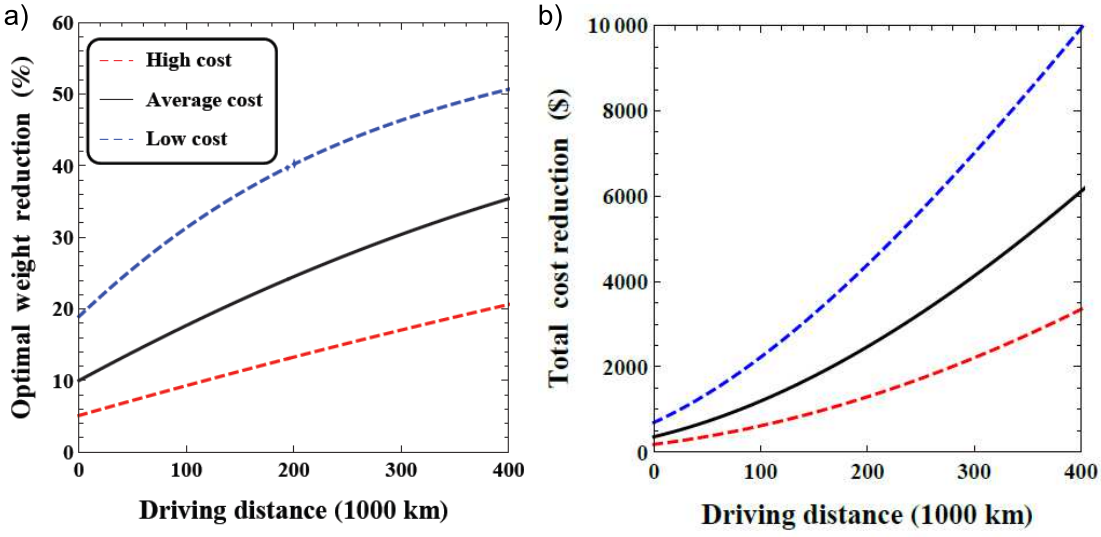

Figure 7.5: Optimal weight reduction minimizing ICEV total cost as a function of lifetime driving distance for different lightweight cost functions. b) Corresponding total cost reduction.

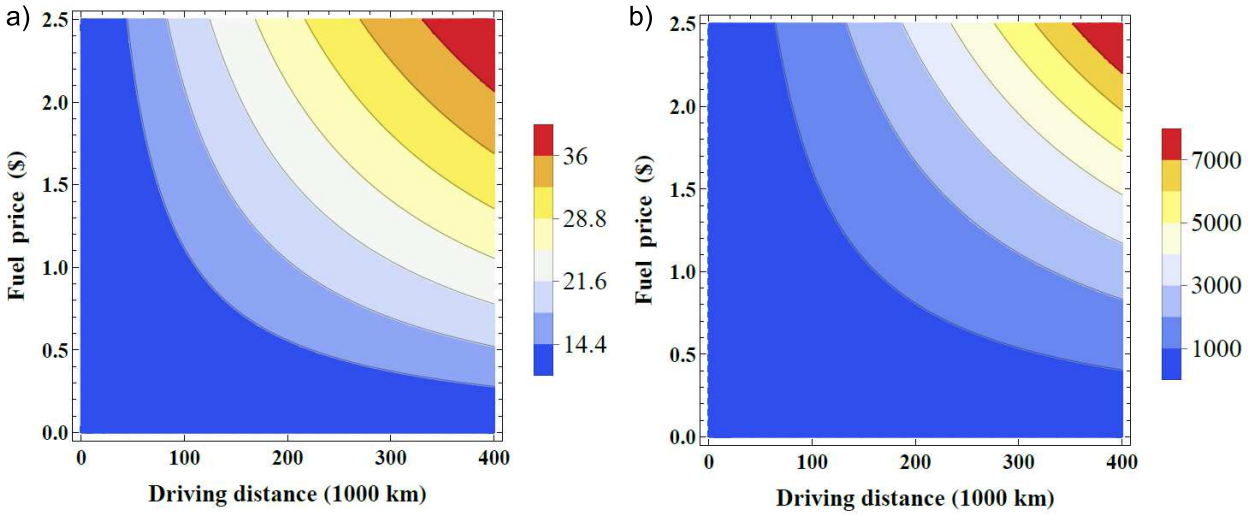

Figure 7.6: a) Optimal weight reduction (indicated in % in the legend) to minimize total cost of an ICEV as a function of fuel price and driving distance. b) Corresponding total cost reduction (in $).

7.4.2 Cost effects for BEV

Fig. 7.7a and 7.7b show BEV total cost as a function of weight reduction for a BEV with a range of 200 km and 400 km, respectively. In this case the baseline lightweight cost function and a driving distance of 150,000 vkm are assumed. Minimum manufacturing cost is reached at 24 % and 36 % variable glider mass reduction for ranges of 200 km and 400 km, respectively. The higher optimal use of lightweighting in the manufacturing phase relative to the ICEV (24 % and 36 % vs. 10 %) is due to the high cost of the battery. By reducing vehicle weight the battery can be downsized while maintaining the same driving range. This reduces manufacturing costs and results in the higher optimal degree of lightweighting relative to the ICEV. Minimal total cost is reached at 28 % and 39 % variable glider mass reduction for a BEV range of 200 km and 400 km, respectively. The small difference between the solutions minimizing manufacturing and total costs is due to the low share of electricity to total costs and the relatively low sensitivity of BEV energy consumption to weight reduction.

The high sensitivity of the optimal degree of lighweighting to BEV range is analyzed in Fig. 7.8. Fig. 7.8a shows the sensitivity of the optimal weight reduction minimizing BEV total cost for the three lightweight cost functions considered as a function of BEV range. Fig. 7.8b shows the corresponding total cost reduction. For the baseline lightweight cost function it is 3070 $ and 7620 $ for a range of 200 and 400 km, respectively. Note that the relation between total cost reduction and range at a given amount of lightweighting is nonlinear (as shown in Fig. 7.8b) due to secondary scaling effects that occur for an increase of range.

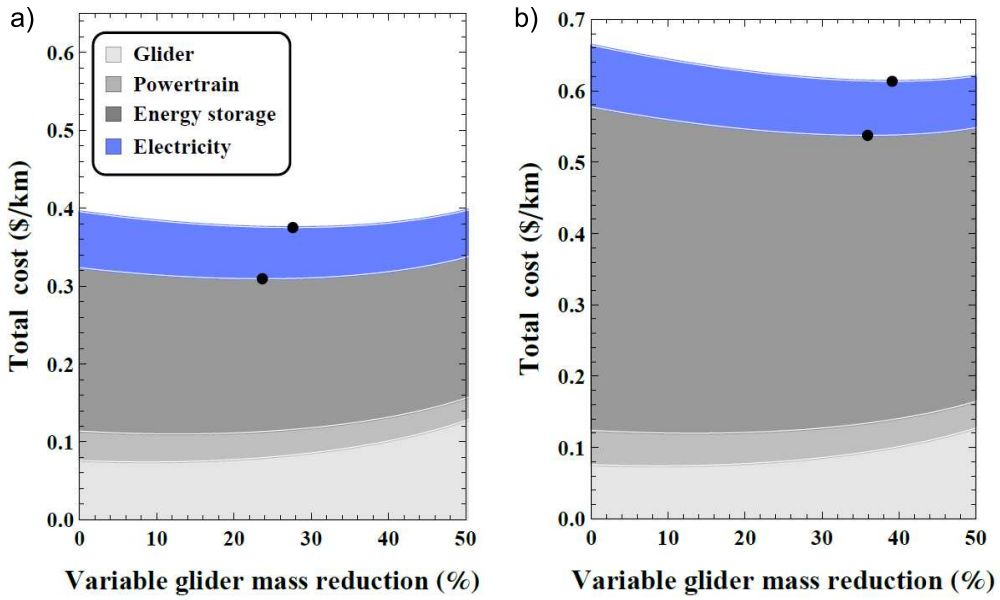

Figure 7.7: BEV total cost as a function of variable glider mass reduction for a) 200 km and b) 400 km range. Black points indicate optimal levels of lightweighting minimizing manufacturing and total costs.

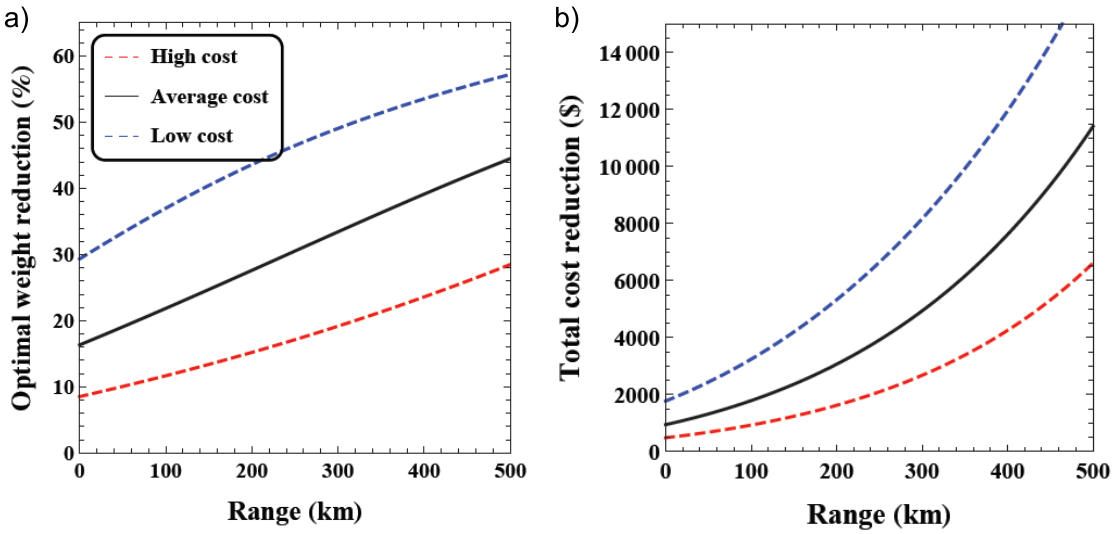

Figure 7.8: a) Optimal weight reduction minimizing BEV total cost as a function of vehicle range. b) Corresponding total cost reduction.

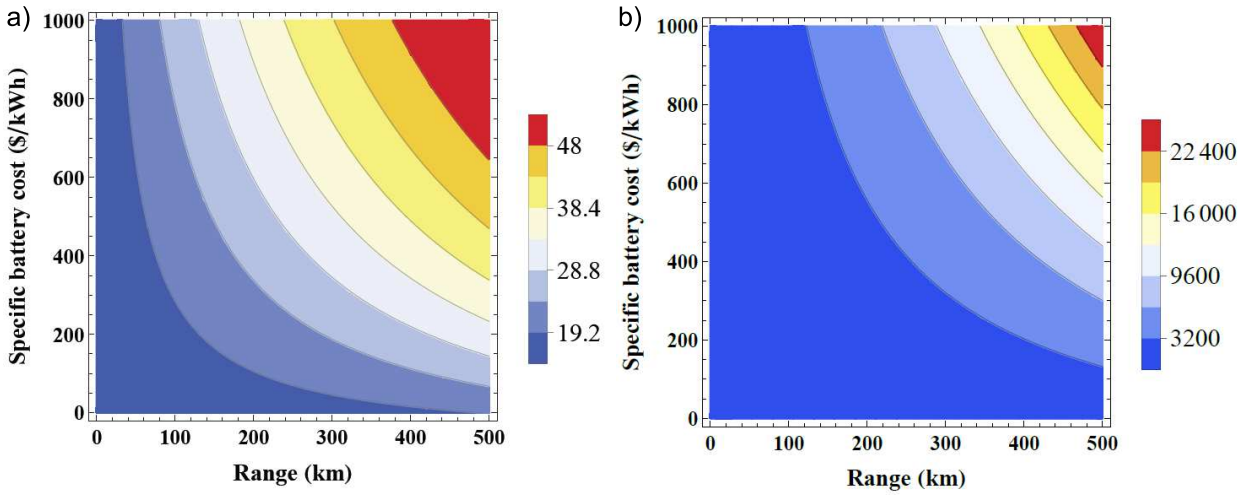

Figure 7.9: a) Optimal weight reduction (in %) minimizing BEV total cost as a function of specific battery cost and vehicle range. b) Corresponding total cost reduction (in $).

Fig. 7.9a shows the sensitivity of the optimal amount of lightweighting to minimize total costs as a function of vehicle range and battery cost for the baseline lightweighting cost function. Fig. 7.9b shows the corresponding reduction in total cost. It is obvious that as battery specific mass and cost decrease, the incentive for lightweighting decreases due to lower associated battery cost and mass reduction potentials.

7.5 Discussion

In this chapter an analytic optimization approach was applied to compare the effects of lightweighting on the mass, energy use, manufacturing and total costs of a midsize gasoline ICEV and BEV. The method was further used to study the sensitivity of the optimal solutions minimizing total costs as a function of important input parameters.

The results show a strong secondary weight and cost saving potential for the BEV due to the high mass and cost of the battery, but a higher sensitivity of vehicle energy consumption to mass reduction for the ICEV due to the relatively low powertrain efficiency and lack of regeneration capability. For current technology costs the optimal amount of lightweighting minimizing manufacturing costs is found to be higher for the BEV (24 % and 36 % at 200 and 400 km range, respectively) than for the ICEV (10 %) due to the high battery cost which can be reduced with the use of lightweight materials. The optimal amount of lightweighting to minimize total cost is similar for the BEV (28 % at 200 km range) and the ICEV (31 % at 300,000 vkm). The difference between the optimal solutions minimizing manufacturing versus total costs is higher for the ICEV than the

BEV due to the relatively low energy consumption and low share of electricity to total costs for the BEV. Furthermore the sensitivity to several input parameters was investigated. The optimal amount of lightweighting for the ICEV is very sensitive to parameters affecting lifetime fuel cost (most importantly fuel price and total driving distance) because it represents a high share of total costs. For the BEV the optimal amount of lightweighting and its cost benefits are more sensitive to parameters affecting battery cost, most importantly battery specific cost and vehicle range. The lightweighting cost function is very important for both drivetrains. The sensitivity of the results to those parameters was studied.

The research presented in this work can be used to evaluate and compare the implications of lightweighting on conventional and electric vehicles' mass, energy use and costs. Overall the results show that lightweighting is a promising technology option for the reduction of vehicle energy use and costs. In order to decide on the best lightweighting strategy it is important to also consider other aspects such as safety and life-cycle environmental impacts.[5]

[5]The optimization of life cycle GHG emissions has been studied in detail in [Siegerist, 2013]. Similar to the cost optimization, the sensitivity analysis shows that the optimal degree of lightweighting minimizing life cycle GHG emissions is strongly dependent on the driving cycle and total driving distance for the ICEV, the carbon intensity of electricity, vehicle range, and battery lifetime for the BEV, and the primary energy sources used in the vehicle production phase for both drivetrains.

Chapter 8

Swiss passenger car fleet analysis

While in all previous chapters the analysis has been focused on individual vehicle technologies, now the potential impacts of electric powertrains on the Swiss passenger car fleet will be evaluated. The chapter starts in section 8.1 with an overview of the general developments of the new passenger car market in Switzerland and Europe. In section 8.2 a decomposition method of specific CO_2 emissions with regard to changes in vehicle efficiency, mass, and fuel technology is introduced. It is applied to analyze emission reductions from 2000 to 2012 and to develop scenarios until 2020. In section 8.3 the implications of various scenarios on the Swiss passenger fleet from 2012 to 2050 are evaluated in terms vehicle stock, energy use, and GHG emissions.

8.1 New passenger cars in Switzerland and Europe

Due to the close relationship between Switzerland and the rest of Europe the development of average vehicle characteristics follows a similar pattern in both regions as shown in Fig. 8.1 [Auto-Schweiz, 2014; ICCT, 2012; ACEA, 2012]. However, Swiss cars are on average larger, heavier, and more powerful, which may in part be caused by the higher average GDP per capita in Switzerland compared to Europe. Over the last decade fuel consumption of new passenger cars continuously decreased in Europe and Switzerland as measured on the New European Driving Cycle. This trend was opposed by an increase in the average weight and power of new cars, reflecting consumer demand for increasing vehicle size, comfort, safety, and performance. From 2007 to 2009 a reversal of the trend to heavier and more powerful vehicles occurred, probably induced by the global financial crisis. The reduction of fuel consumption was mainly achieved by a shift of sales from gasoline to diesel and hybrid vehicles, as well as continuous incremental powertrain efficiency improvements and reductions of vehicle losses (such as aerodynamic drag or tire rolling resistance). Fig. 8.1 also shows the decoupling of engine power and displacement over time. The strong increase of engine specific power, i.e. the power-to-displacement ratio, re-

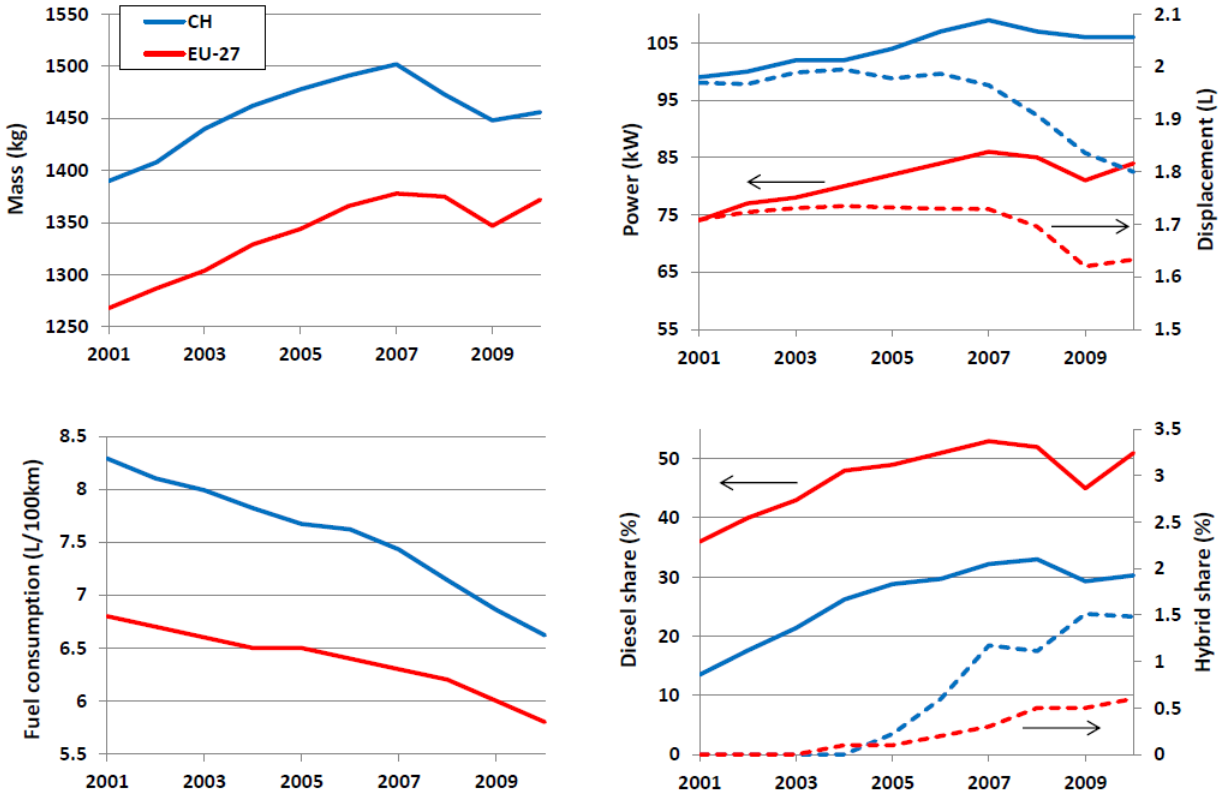

Figure 8.1: Comparison of the development of average new passenger car characteristics in Switzerland and Europe from 2001 to 2010.

flects powertrain efficiency improvements and engine downsizing. Engine downsizing usually refers to engine improvements enabling a reduction of engine displacement while maintaining performance (most often realized by turbocharging). This is accompanied by an increase of the power-to-displacement ratio and a reduction of fuel consumption due to reduction of engine part load operation [Leduc et al., 2003]. Note however, that the increase of specific power can be equally used to raise vehicle performance. This is also referred to as market upsizing, i.e. shifting sales toward vehicles of higher performance [Sprei & Karlsson, 2008]. Fig. 8.1 also shows the trend from gasoline to diesel cars which reached a market share of 37 % of Swiss [Auto-Schweiz, 2013] and 55 % of European new vehicle sales in 2012 [ICCT, 2013a]. The share of hybrid vehicles has significantly increased since 2005 and is slightly higher in Switzerland than in Europe.

Fig. 8.2 shows the development of new passenger vehicle sales in Switzerland by class separately for gasoline and diesel cars. For gasoline car sales the share of medium sized cars decreased while the share of small cars increased. For diesel vehicles the share of SUVs strongly increased.

CO_2 emissions from passenger cars contribute about 12 % of total CO_2 emissions in Europe and one third in Switzerland. As part of the European Commission (EC) strategy to reduce GHG

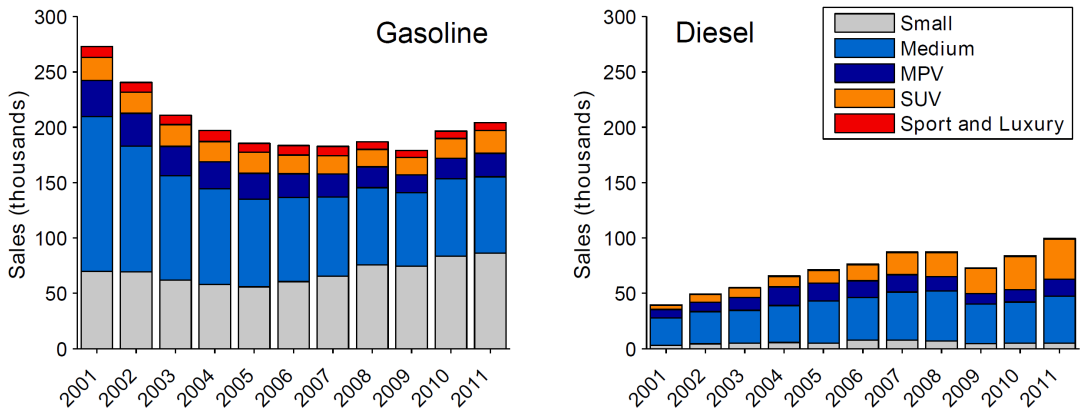

Figure 8.2: Development of new passenger vehicle sales in Switzerland by class for gasoline and diesel cars.

emissions, legislation has been ratified limiting the CO_2 emissions from new passenger cars to an average of 130 g/km by 2015 [EC, 2009]. Furthermore a proposal of 95 g/km by 2020 [EC, 2012a] is currently under discussion. The EU regulation limiting CO_2 emissions from new passenger cars to an average of 130 g/km by 2015 was also introduced in Switzerland [BFE, 2012]. The regulation specifies penalties for vehicle importers and manufacturers for exceeding the target: the first g/km overshoot is charged EUR 5 (CHF 7.50) per vehicle; with EUR 15 for the second, and EUR 25 for the third g/km. Above a 3 g/km overshoot the full penalty of EUR 95 (CHF 142.50) per gram applies. Note that vehicle importers or manufacturers can group together to meet the target. In Switzerland revenues from the penalty go to the infrastructure fund.
The emission limit is set according to vehicle mass using a so-called limit value curve (LVC), which allows higher emissions for heavier and lower emissions for lighter cars. It is set in such a way that the fleet average meets the CO_2 emission target. Permitted specific CO_2 emissions SE_{LVC} according to the LVC are calculated as

$$SE_{LVC} = SE_{avg} + s \cdot (M - M_{avg}) \tag{8.1}$$

where SE_{avg} is the fleet specific CO_2 emission target, M vehicle mass, M_{avg} the average fleet mass[1], and s the slope of the LVC. Note that the LVC does not regulate the emissions of each individual vehicle but of the fleet average. For the calculation of penalties the LVC is applied per manufacturer or importer group, i.e. in practice M refers to the average mass of all vehicles sold by this group.

[1] In the EU regulation M_{avg} refers to the average mass of the fleet for the previous three years.

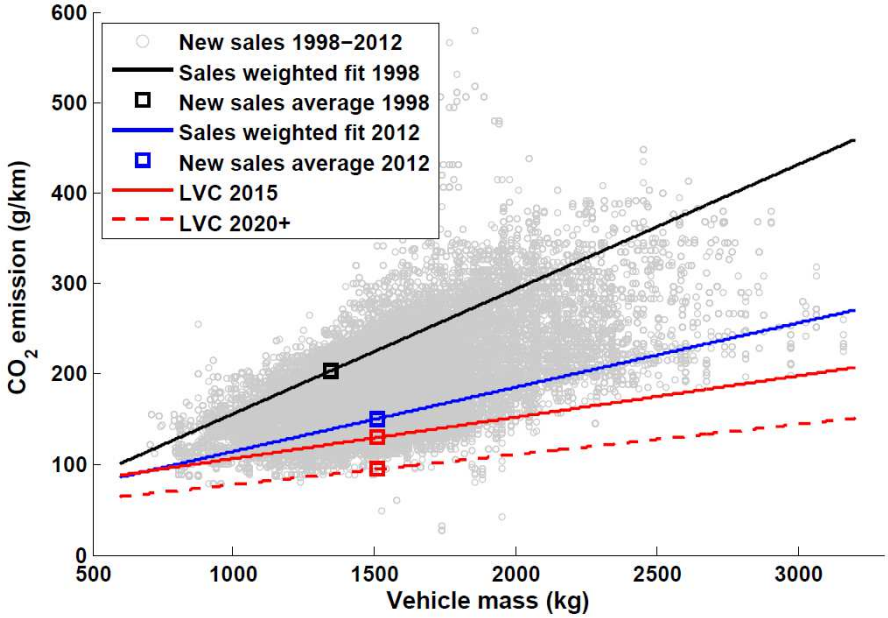

Figure 8.3: Specific CO_2 emissions from new Swiss passenger cars as a function of vehicle mass. The sales weighted fits for 1998 and 2012 are compared to the LVC for 2015 and 2020.

Fig. 8.3 shows the specific CO_2 emissions from new Swiss passenger cars for the years 1998 to 2012 as a function of vehicle mass. In addition to the data points, linear sales weighted fits for the years 1998 and 2012 are shown together with the LVC for 2015 and the LVC for 2020 as currently discussed [EC, 2012a].

The slope of the LVC is important as it defines how the regulation affects manufacturers of light vs. heavy vehicles. In addition, it influences the future distribution of vehicle mass in the fleet: if set artificially high it favors heavy over light cars and pushes the market towards higher mass vehicles, and vice versa. As outlined in [EC, 2012b; TNO, 2011] the procedure to define the slope of the LVC for a certain year is based on the slope of a sales weighted fit of CO_2 emission versus mass for the same year. To estimate the slope of the LVC for a future year, the sales weighted fit for a reference year is rotated through the origin until the desired emission target for a future year is reached.[2] The slopes as defined in [EC, 2009; 2012b] for the emission target of 130 g/km (in 2015) and 95 g/km (for 2020+) are 0.0457 and 0.0333 $gCO_2/(km\ kg)$, respectively.
Currently the timing of the legislation and the form of the LVC are heavily discussed. For example in [Frondel et al., 2011] the authors argue that the LVC does not accurately describe the market and recommend a nonlinear LVC, including linear and quadratic terms of emission vs. mass. In

[2]The origin is set at zero mass and CO_2 emission. To calculate the LVC for a future year, the sales weighted fit of a reference year is multiplied by an emissions reduction factor until the emission target is reached.

fact a nonlinear fit describes the relation of vehicle emissions and mass better as pointed out in section 3.2.1. The reason for this is that an increase in mass on average also leads to an increase of the power-to-mass ratio which negatively affects fuel economy. A multiple-linear regression of fuel consumption (and hence emissions) as a function of mass and the power-to-mass ratio leads to a much more even distribution of residuals than a linear regression of fuel consumption as a function of mass alone. This was investigated in detail in [Hofer et al., 2012a]. The author of this thesis advises against a nonlinear LVC as this does not correspond to the physical relation of energy demand and mass (compare e.g. chapter 2) and provides incentives for increasing vehicle mass. [Cuenot, 2009] even argues that an emissions limit completely independent of vehicle mass would have been more effective.

Due to the importance of the LVC it is worth while analyzing the development of the slope of a sales weighted fit for the Swiss and EU passenger car market and comparing it to the slope of the LVC for the 130 g/km target in 2015 as well as proposed for the 95 g/km target. Fig. 8.4 shows the slope of a sales weighted fit on the left according to Eq. 8.1 for Switzerland from 1998 to 2012 and the EU-27 in 2012.[3] A linear extrapolation is also shown based on the past Swiss trend and the slopes of the LVC for the target of 130 and 95 g/km. The development of the slope of a sales weighted fit is shown as a function of the average CO_2 emission on the right of Fig. 8.4. As average CO_2 emissions decrease over time the slope flattens (data points evolve from the top right downwards to the left) because powertrain efficiency improves, which reduces the sensitivity of energy use to mass. A fit for the Swiss and EU data points[4] is also shown and compared to the slopes of the LVC for the target of 130 and 95 g/km. It can be seen that the slope for the LVC corresponding to the target of 130 g/km is relatively low: for the EU market the target was nearly reached in 2012 (132.2 g/km). At the same time the slope of a sales weighted fit is 0.061 gCO_2/(km kg), which is considerably higher than the value of 0.0457 gCO_2/(km kg) used in the legislation. However, this way a further increase of fleet mass is not supported and it might well be that the slope of the market in 2015 will reach the value used in the legislation (as shown on the left side of Fig. 8.4), but probably at a lower average CO_2 emission than 130 g/km.

8.2 Specific CO_2 emissions from Swiss new passenger cars

This section examines the influence of changes in vehicle efficiency, mass, and fuel technology on the specific CO_2 emissions from new Swiss passenger cars, analyzing data from 2000 to 2012 and developing future scenarios to 2020.

From 2000 to 2012 average specific emissions decreased by 23 % from 197 g/km to 151 g/km as

[3] The analysis is based on complete datasets of Swiss and European passenger car sales from 1998-2012 and 2012, respectively [Auto-Schweiz, 2014; EEA, 2014].

[4] For a power function with the origin at zero the resulting fit is $s = 4.1^{-6} \cdot SE_{avg}^{1.96}$. Note that in the current EU regulation zero emissions are indeed possible as electric cars are counted as zero emission vehicles. Otherwise the origin should be set to the minimum achievable CO_2 emissions.

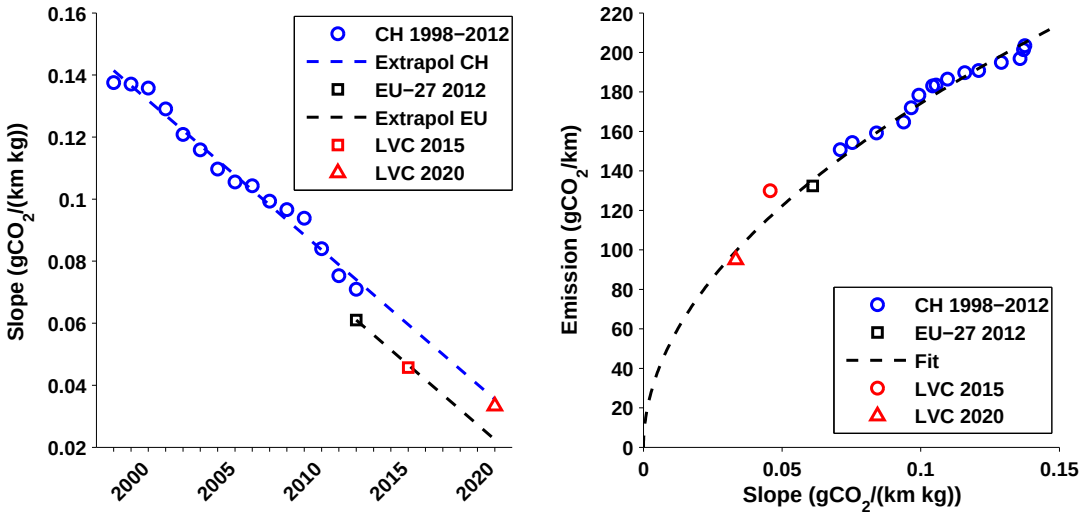

Figure 8.4: Development of the slope of a sales weighted fit for the Swiss and EU passenger car market relative to slope of the LVC.

shown in Fig. 8.5. At the same time average mass increased by 11 % from 1363 kg to 1510 kg due to a slight mass increase of gasoline cars from 1341 kg to 1374 kg, a strong increase of diesel car mass from 1567 kg to 1732 kg, and a shift from gasoline to diesel cars (which are on average heavier). Fig. 8.6 shows the shift from gasoline to diesel and hybrid vehicle sales, which make up approximately 37 % and 2 % of new vehicle sales in 2012, respectively. While the power-to-mass ratio (a measure for acceleration performance) of diesel cars strongly increased to nearly reach the level of gasoline vehicles in 2012, the fleet average power-to-mass ratio increased only slightly. A measure for powertrain efficiency independent of mass is the specific emissions-to-mass ratio, which continuously improved for the fleet average from 0.145 g/(km kg) in 2000 to 0.100 g/(km kg) in 2000. The decrease of the emission-to-mass ratio was higher for gasoline than for diesel cars, which might in part be caused by the significant performance upscaling of diesel vehicles. In 2012 the emission-to-mass ratio was about 19.5 % lower for diesel than for gasoline cars at nearly equal performance. This reflects the higher powertrain efficiency of diesel relative to gasoline vehicles.

Section 8.2.2 analyzes how much of the CO_2 emissions reduction that took place from 2000 to 2012 was achieved by improvements in powertrain efficiency and how much this was offset by the increase of vehicle mass. The individual contributions are identified using two different decomposition methods presented in section 8.2.1. The analysis presented is based on datasets of more than 60,000 unique vehicle models representing aggregated Swiss passenger car sales from 1998 to 2010, courtesy of Auto-Schweiz [Auto-Schweiz, 2014]. In addition to the number of vehicles sold, it gives a technical characterization of each model, including curb weight, power, and

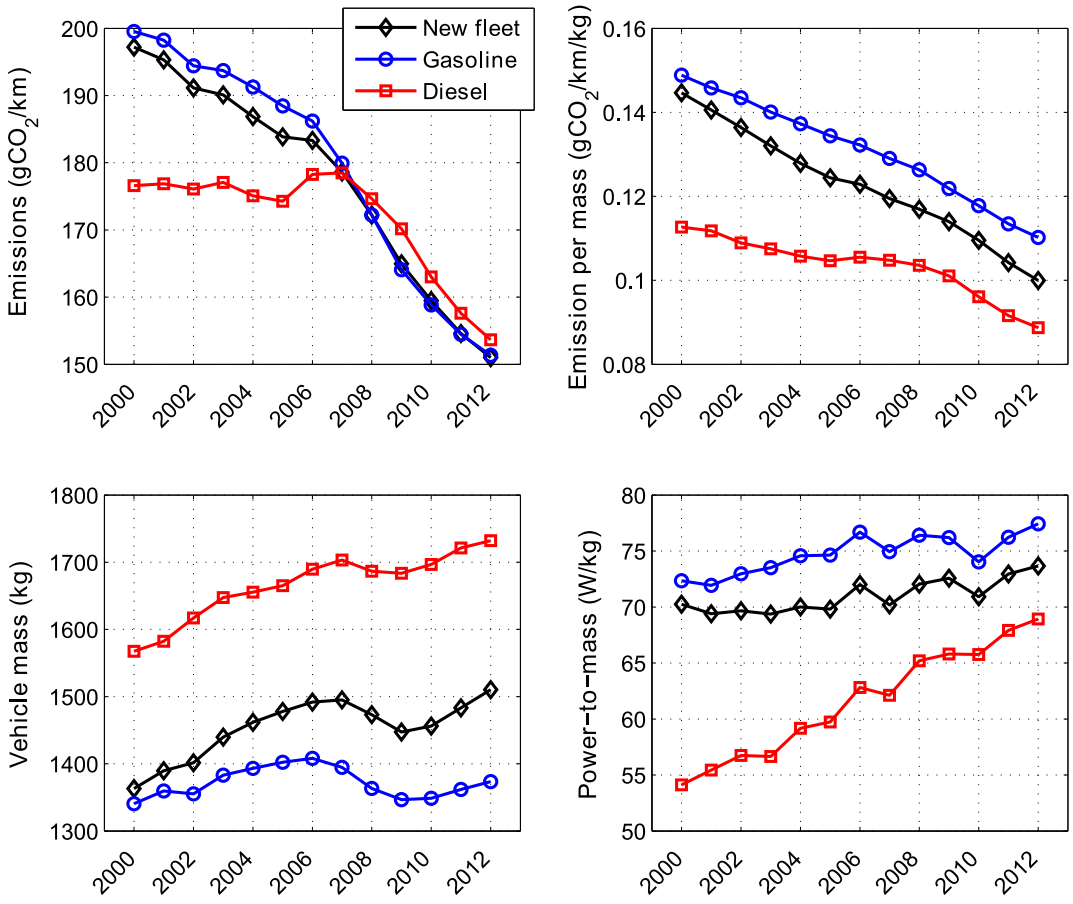

Figure 8.5: Gasoline, diesel, and new fleet average characteristics in Switzerland from 2000 to 2012.

fuel type, as well as fuel consumption and CO_2 emissions as reported by the vehicle manufacturer and measured in a dynamometer test for the NEDC driving cycle.[5] In section 8.2.3 the method developed in 8.2.1 is applied to analyze different scenarios of specific CO_2 emissions from new vehicles in Switzerland until 2020. The results are compared to the emission targets for 2015 and 2020.

8.2.1 Analytic methodology

Index decomposition analysis is a standard method used to quantify the relative contributions of different effects to temporal changes in energy use and emissions. Often the effects are dis-

[5]Note that the discrepancies between type-approval CO_2 emissions as measured for the NEDC and real-world emissions increased in recent years due to several reasons explained in [Mock et al., 2012]. These effects are not accounted for in the analysis, which may lead to overestimation of real-world efficiency gains.

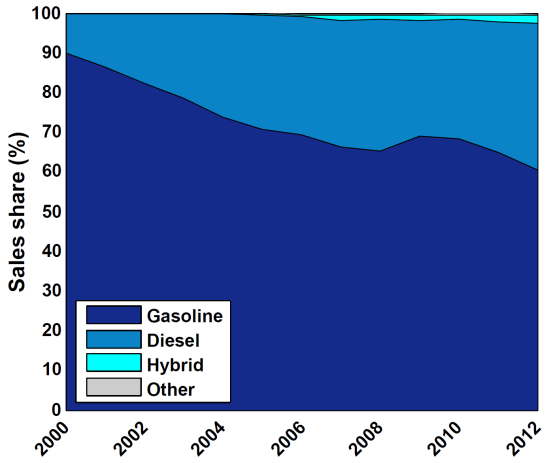

Figure 8.6: Sales share by fuel technology in Switzerland from 2000 to 2012.

aggregated into activity, structural, and intensity factors. In the case of passenger car transport this could for example correspond to the decomposition of the change of fleet fuel use into the effect of varying total mileage, fleet composition, and fuel economy, respectively. The most often used index decomposition methods are the Laspeyres and Divisia [Sun, 1998; Ang & Zhang, 2000]. Laspeyres index decomposition has been applied in several studies analyzing passenger vehicle energy use and emissions. For example, in [Papagiannaki & Diakoulaki, 2009] it is used to investigate the important factors contributing to total fleet CO_2 emissions reduction in Greece and Denmark from 1990 to 2005. In [Sheinbaum-Pardo & Chávez-Baeza, 2011] the Laspeyres method is applied to analyze the effects of changes in the sales structure and vehicle efficiency on the fuel economy of new vehicles in Mexico from 1988 to 2008, and in [Schipper & Fulton, 2013] it is used to identify the effects of CO_2 emission reduction in Europe from 1995 to 2009, in particular with regard to the shift from gasoline to diesel vehicle sales.

In this work two different methods are used to decompose the development of specific CO_2 emissions of Swiss new vehicles from 2000 to 2012 into the effects of changes in vehicle efficiency, mass, and fuel technology. For the first method new vehicle sales are grouped into different mass categories and the CO_2 emissions per mass category and fuel type are evaluated. The decomposition analysis is based on the additive Laspeyres index method. For many purposes such detailed technical and sales related data are not available. In the second approach the division into different mass categories is left out. Instead the aggregate mass and emissions-to-mass ratio by fuel type are used to calculate the contributions to emissions reduction.[6]

[6]Note that in [Hofer et al., 2012a] another method based on regression analysis is introduced to determine the contributions to the development of specific CO_2 emissions over time.

Laspeyres index decomposition

In the two factor Laspeyres decomposition model[7] vehicle sales are binned into equidistant mass categories. The sales shares as well as the specific emissions by mass category are evaluated based on the vehicle sales data. As an example of this approach Fig. 8.7 shows the distribution of sales share and average emission by mass category for all new vehicles sold in 2000 and 2012. For the two factor model, specific CO_2 emissions SE_t in year t are calculated as

$$SE_t = \sum_{m=1}^{M} S_{m,t} \cdot SE_{m,t} \tag{8.2}$$

where $S_{m,t}$ and $SE_{m,t}$ are the sales share and specific emissions by mass category m and year t, respectively. For the two factor model the total change in emission ΔE_{tot} is decomposed into the effects of a change in efficiency ΔSE_{eff} and mass ΔE_{mass}

$$\Delta SE_{tot} = \Delta SE_{eff} + \Delta SE_{mass} \tag{8.3}$$

where ΔSE_{eff} and ΔSE_{mass} are calculated as

$$\Delta SE_{eff} = \sum_{t=1}^{T} \sum_{m=1}^{M} \left(S_{m,t-1} \cdot (SE_{m,t} - SE_{m,t-1}) + \frac{1}{2} (S_{m,t} - S_{m,t-1}) \cdot (SE_{m,t} - SE_{m,t-1}) \right) \tag{8.4}$$

$$\Delta SE_{mass} = \sum_{t=1}^{T} \sum_{m=1}^{M} \left((S_{m,t} - S_{m,t-1}) \cdot SE_{m,t-1} + \frac{1}{2} (S_{m,t} - S_{m,t-1}) \cdot (SE_{m,t} - SE_{m,t-1}) \right) \tag{8.5}$$

Here the so-called refined Laspeyres decomposition method [Sun, 1998] is used, in which the interaction term $(S_{m,t} - S_{m,t-1}) \cdot (SE_{m,t} - SE_{m,t-1})$ is attributed to both effects equally, resulting in perfect decomposition of ΔSE_{tot}. Note that for the calculation of ΔSE_{eff} and ΔSE_{mass} a rolling base year is used, i.e. the effects of changes of $S_{m,t}$ and $SE_{m,t}$ are evaluated for each year individually. This approach is more precise than using a fixed base year [Heinen, 2013].

For the three factor decomposition analysis vehicle sales are grouped into sales by mass category and fuel technology. In this case the specific CO_2 emissions in year t are calculated as

[7] Two factor means that specific emissions are calculated as the product of one structural (i.e. sales share) and one intensity (i.e. specific emission) term. Three factor refers to the product of two structural terms and one intensity term. As fuel type is not considered in the two factor model, the decomposition is performed separately for gasoline, diesel, and all new vehicle sales.

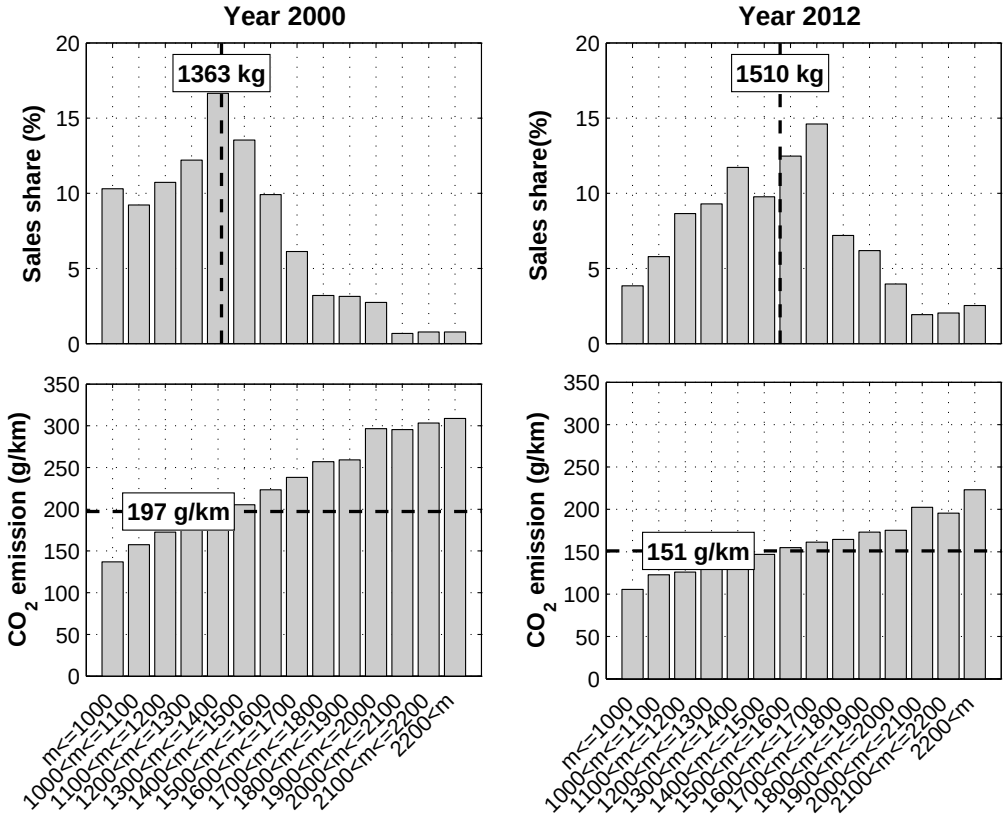

Figure 8.7: Distribution of sales and average specific emission by mass category for all new vehicles sold in 2000 and 2012.

$$SE_t = \sum_{f=1}^{F} \sum_{m=1}^{M} S_{f,t} \cdot S_{f,m,t} \cdot SE_{f,m,t} \tag{8.6}$$

where $S_{f,t}$ is the sales share by fuel technology f and year t. $S_{f,m,t}$ and $SE_{f,m,t}$ are the sales share and specific emissions by fuel technology f, mass category m, and year t, respectively. The total change in emission is now decomposed into the effects of a change in efficiency ΔSE_{eff}, mass ΔSE_{mass}, and fuel ΔSE_{fuel}, such that

$$\Delta SE_{tot} = \Delta SE_{eff} + \Delta SE_{mass} + \Delta SE_{fuel} \tag{8.7}$$

where ΔSE_{eff}, ΔSE_{mass}, and ΔSE_{fuel} are calculated as

$$\begin{aligned}\Delta SE_{eff} = \sum_{t=1}^{T}\sum_{f=1}^{F}\sum_{m=1}^{M}\Big(&S_{f,t-1}\cdot S_{f,m,t-1}\cdot\left(SE_{f,m,t}-SE_{f,m,t-1}\right)\\ &+\frac{1}{2}\cdot\left(SE_{f,m,t}-SE_{f,m,t-1}\right)\cdot\left(S_{f,t-1}\cdot\left(S_{f,m,t}-S_{f,m,t-1}\right)+\left(S_{f,t}-S_{f,t-1}\right)\cdot S_{f,m,t-1}\right)\\ &+\frac{1}{3}\cdot\left(S_{f,t}-S_{f,t-1}\right)\cdot\left(S_{f,m,t}-S_{f,m,t-1}\right)\cdot\left(SE_{f,m,t}-SE_{f,m,t-1}\right)\Big)\end{aligned} \tag{8.8}$$

$$\begin{aligned}\Delta SE_{mass} = \sum_{t=1}^{T}\sum_{f=1}^{F}\sum_{m=1}^{M}\Big(&S_{f,t-1}\cdot\left(S_{f,m,t}-S_{f,m,t-1}\right)\cdot SE_{f,m,t-1}\\ &+\frac{1}{2}\cdot\left(S_{f,m,t}-S_{f,m,t-1}\right)\cdot\left(S_{f,t-1}\cdot\left(SE_{f,m,t}-SE_{f,m,t-1}\right)+\left(S_{f,t}-S_{f,t-1}\right)\cdot SE_{f,m,t-1}\right)\\ &+\frac{1}{3}\cdot\left(S_{f,t}-S_{f,t-1}\right)\cdot\left(S_{f,m,t}-S_{f,m,t-1}\right)\cdot\left(SE_{f,m,t}-SE_{f,m,t-1}\right)\Big)\end{aligned} \tag{8.9}$$

$$\begin{aligned}\Delta SE_{fuel} = \sum_{t=1}^{T}\sum_{f=1}^{F}\sum_{m=1}^{M}\Big(&\left(S_{f,t}-S_{f,t-1}\right)\cdot S_{f,m,t-1}\cdot SE_{f,m,t-1}\\ &+\frac{1}{2}\cdot\left(S_{f,t}-S_{f,t-1}\right)\cdot\left(\left(S_{f,m,t}-S_{f,m,t-1}\right)\cdot SE_{f,m,t-1}+S_{f,m,t-1}\cdot\left(SE_{f,m,t}-SE_{f,m,t-1}\right)\right)\\ &+\frac{1}{3}\cdot\left(S_{f,t}-S_{f,t-1}\right)\cdot\left(S_{f,m,t}-S_{f,m,t-1}\right)\cdot\left(SE_{f,m,t}-SE_{f,m,t-1}\right)\Big)\end{aligned} \tag{8.10}$$

Tables D.1 and D.2 list the sales and specific emission data by mass and fuel type as used in the analysis.

Aggregate fleet data model

In the second approach no division into mass categories and no Laspeyres index decomposition are performed. Instead a simplified model has been developed based on the aggregate mass and emission-to-mass ratio by fuel type. In the two factor model formulation, specific emission in year t is calculated as the product of the aggregate mass m_t and the emission-to-mass ratio $\left(\frac{E}{m}\right)_t$, i.e.

$$SE_t = \left(\frac{SE}{m}\right)_t \cdot m_t \tag{8.11}$$

The contributions to the total change of emissions are calculated as

$$\Delta SE_{eff} = \sum_{t=1}^{T} \left(\left(\frac{SE}{m} \right)_t - \left(\frac{SE}{m} \right)_{t-1} \right) \cdot m_{t-1} \tag{8.12}$$

$$\Delta SE_{mass} = \sum_{t=1}^{T} \left(\frac{SE}{m} \right)_{t-1} \cdot (m_t - m_{t-1}) \tag{8.13}$$

For the three factor model, specific emissions in year t are calculated as the product of the sales share, emissions-to-mass ratio, and mass by fuel type f

$$SE_t = \sum_{f=1}^{F} S_{f,t} \cdot \left(\frac{SE}{m} \right)_{f,t} \cdot m_{f,t} \tag{8.14}$$

$$\tag{8.15}$$

The contributions to the total change of emissions are calculated as

$$\Delta SE_{eff} = \sum_{t=1}^{T} \sum_{f=1}^{F} S_{f,t-1} \cdot \left(\left(\frac{E}{m} \right)_{f,t} - \left(\frac{SE}{m} \right)_{f,t-1} \right) \cdot m_{f,t} \tag{8.16}$$

$$\Delta SE_{mass} = \sum_{t=1}^{T} \sum_{f=1}^{F} S_{f,t-1} \cdot \left(\frac{SE}{m} \right)_{f,t-1} \cdot \left(m_{f,t} - m_{f,t-1} \right) \tag{8.17}$$

$$\Delta SE_{fuel} = \sum_{t=1}^{T} \sum_{f=1}^{F} \left(S_{f,t} - S_{f,t-1} \right) \cdot \left(\frac{SE}{m} \right)_{f,t-1} \cdot m_{f,t-1} \tag{8.18}$$

8.2.2 Decomposition of emissions reduction from 2000 to 2012

In the following, the Laspeyres index decomposition and the aggregate fleet data method are applied to analyze the contributions to historic CO_2 emissions reduction from new vehicles in Switzerland. To simplify, the analysis shown in this section only takes into account gasoline and diesel cars which make up 100 % of the fleet in 2000 and 98 % in 2012. Therefore the new vehicle fleet refers to the sum of new gasoline and diesel cars. Fleet mass and emissions are calculated accordingly.

Two-factor models

Fig. 8.8 shows the separate decomposition of CO_2 emissions reduction due to a change of efficiency and mass, for both the gasoline and diesel vehicles. The blue line represents the potential

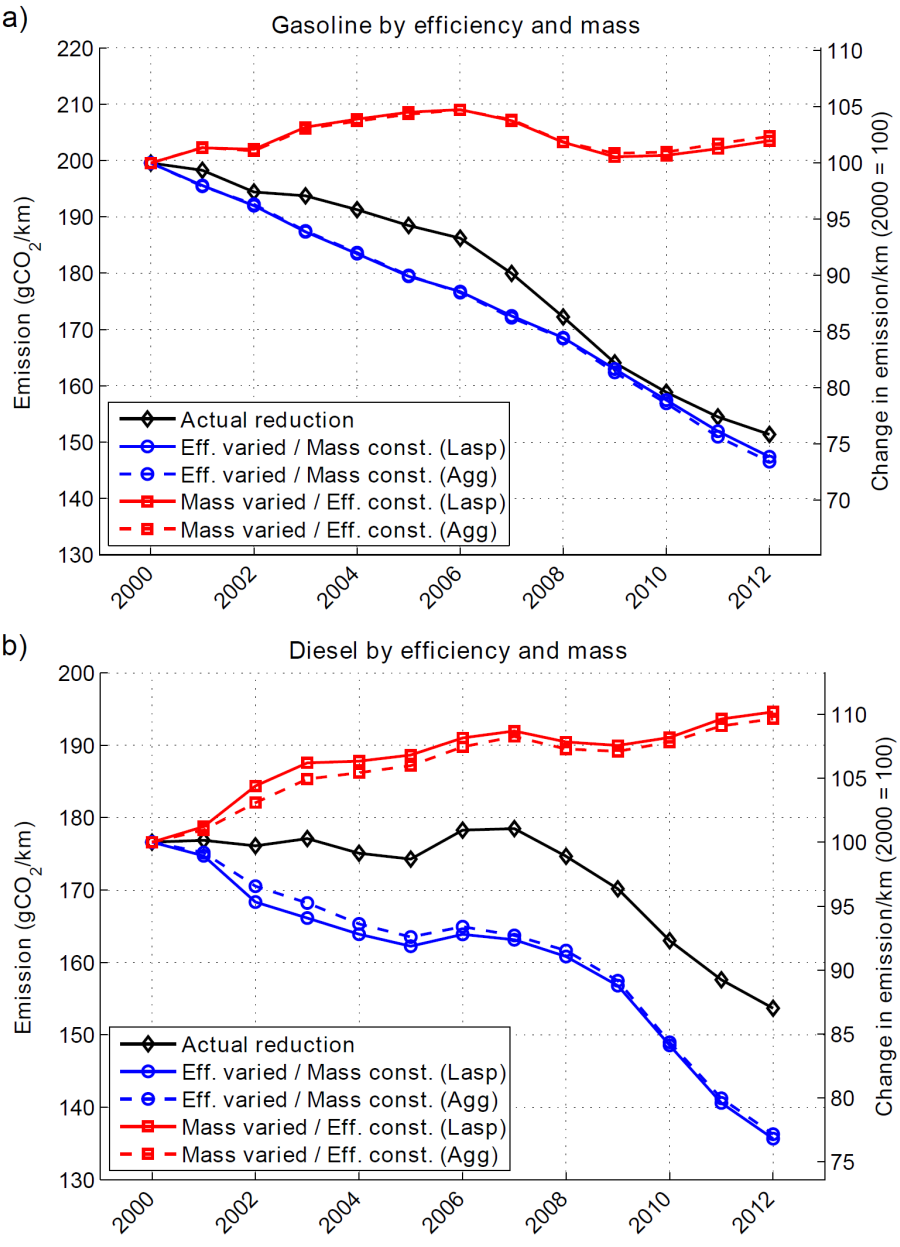

Figure 8.8: Effect of a change of efficiency and mass to total CO_2 emission reduction for (a) gasoline and (b) diesel vehicles. Abbreviations: Lasp=Laspeyres decomposition, Agg=Aggregated data model.

emissions reduction at constant mass, which is ca. 2 % and 10 % higher than the actual reduction for gasoline and diesel cars, respectively. The figure also shows that both models lead to similar results.

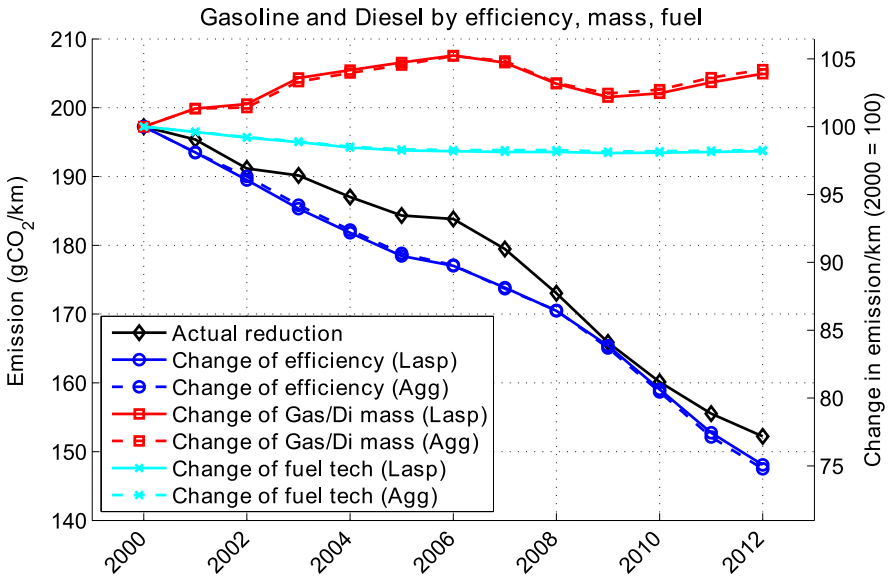

Figure 8.9: Decomposition of CO_2 emission from gasoline and diesel vehicles by the contributions from a change of efficiency, mass, and fuel.

Three-factor models

Fig. 8.9 shows the decomposition of CO_2 emissions from both gasoline and diesel vehicles due to the effects of changes in efficiency, mass, and fuel. The increase of gasoline and diesel mass (red line) oppose the effects of changes in efficiency (blue line) and fuel shift (turquoise line). Taking together the effects of efficiency and fuel change the potential emissions reduction at constant gasoline and diesel vehicle mass would have been approximately 6 % higher. Note that in this case only the individual mass of gasoline and diesel cars would be constant. Due to the shift from gasoline to diesel car sales fleet mass would still have increased as diesel cars are on average heavier than gasoline cars. Therefore the contribution of the change from gasoline to diesel as shown in Fig. 8.9 had only a small effect on emission reduction.

The effect of a shift from gasoline to diesel car sales on fleet emissions is further analyzed in Fig. 8.10a which shows the decomposition of the shift from gasoline to diesel into the contributions from efficiency improvement and mass increase. The blue line represents the potential fleet emissions reduction that would have occurred if people shifting from gasoline to diesel would have bought cars of equal weight.[8] The fleet emissions reduction due to the higher efficiency of diesel

[8]Comparing about 3000 current gasoline and diesel models with sizes of 10-14 m^3 and performance of 50-90 W/kg, representing more than 50 % of sales in 2010, it is shown in [Hofer et al., 2012b] that the average weight per volume and power is not more than 5 % higher for diesel than for gasoline cars. This means that for a car of given size and performance, the average weight increase when purchasing a diesel instead of a gasoline car should not be more than 5 %.

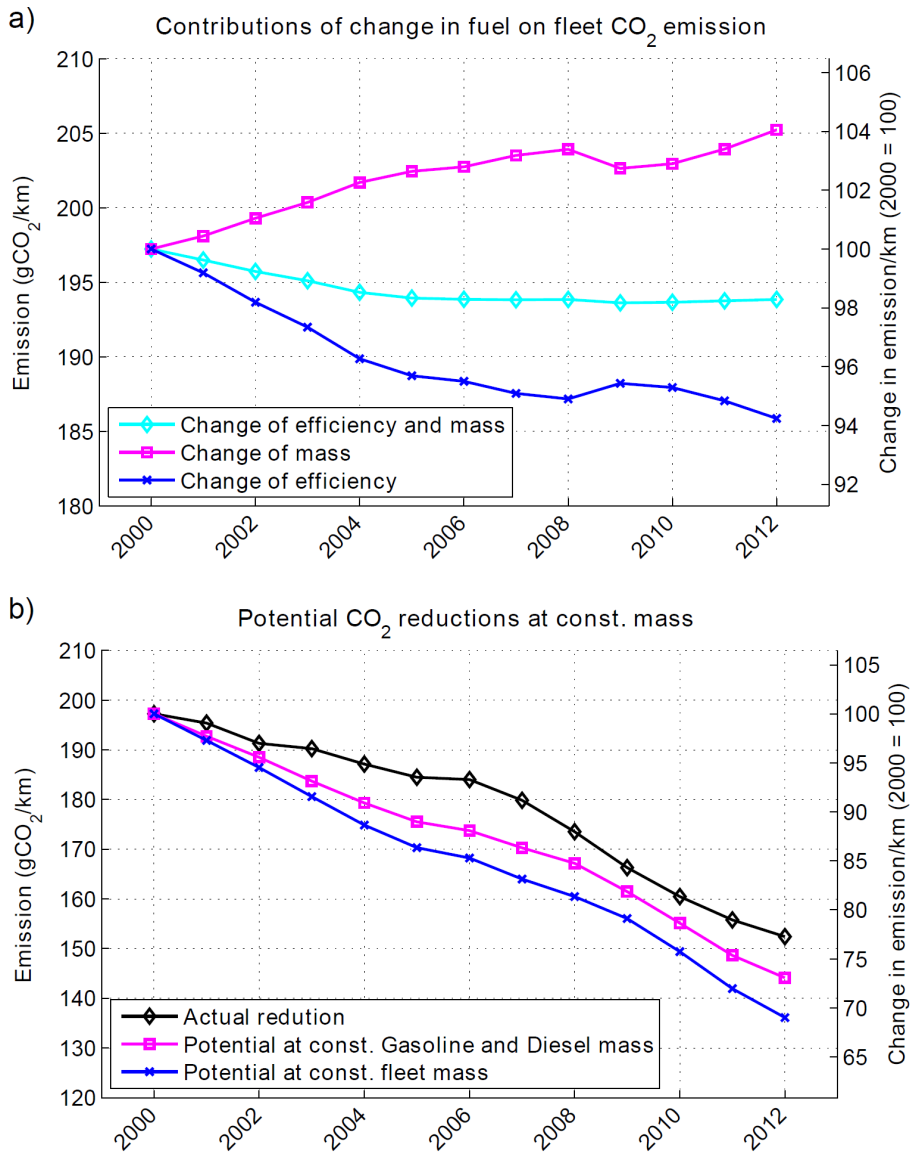

Figure 8.10: a) Decomposition of the shift from gasoline to diesel into the effects of efficiency improvement and mass. b) Potential fleet emission reduction at constant mass.

to gasoline cars amounts to ca. 6 % in 2012. This trend was opposed by the increase of average vehicle mass. In sum, the shift from gasoline to diesel vehicle sales had only a relatively small effect on fleet emissions reduction (ca. 2 %).

Summing up the effects of efficiency improvement of gasoline and diesel vehicles and the shift from gasoline to diesel car sales, Fig. 8.10b shows the potential fleet CO_2 emissions reduction for a) constant gasoline and diesel mass and b) constant fleet mass. Potential reductions at constant gasoline and diesel mass would have been ca. 4 % and potential reductions at constant fleet mass ca. 9 % higher than the actual emissions reduction.

8.2.3 Scenario analysis

Average CO_2 emissions from new cars sold in Switzerland are considerably higher than the EU average (151 g/km vs. 132 g/km in 2012). Thus, with Switzerland adopting the EU regulations for new passenger cars, the question becomes whether and how this target can be met. The aggregate fleet data model described in section 8.2.1 can be used to develop short-term specific CO_2 emission scenarios. Combining Eq. 8.14 with scenarios of future sales share, efficiency improvement, and mass changes by powertrain, future CO_2 emissions are calculated and compared to the emissions target. The scenario parameter assumptions are summarized in Table 8.1.

Three scenarios for future vehicle sales are analyzed. In the first (Diesel A) a continuation of the historic trend from gasoline to diesel vehicles is assumed. The diesel sales share increases linearly from about 37 % in 2012 to 52 % in 2020. In a second scenario (Diesel B) the same future development of sales share by fuel type is assumed. The difference between the two scenarios is that in Diesel A consumers shifting from gasoline to diesel cars buy diesel cars of the same mass as current average diesel cars, while in Diesel B consumers shifting buy diesel cars of the same mass as current average gasoline cars. Finally in the third scenario (Diesel B + EV) the same assumptions as in Diesel B apply, but in addition a high annual growth rate of 30 % for HEVs, and 50 % for BEVs/PHEVs at the expense of gasoline vehicles is assumed.[9] The sales share by fuel type for the different scenarios is depicted in Fig. 8.11. Note that these scenarios are not aimed to represent a very likely future development but rather to demonstrate the effect of different possible scenario options on future specific CO_2 emissions.

Efficiency improvements are implemented in the model by reducing the emission-to-mass ratio by powertrain. Historically the emissions-to-mass ratio decreased for gasoline vehicles on average by 2.5 % and 3.4 % per year in the period from 2000-2012 and 2008-2012, respectively. As shown in Fig. 8.5 the improvement was lower for diesel cars, caused in part by the strong performance increase. For the scenario analysis two cases of future efficiency improvement are considered (moderate and high). Additionally, efficiency improvements up to 2015 are assumed to be higher than in the period from 2015 to 2020. It is assumed that in the course of the introduction of the new emission regulation in Switzerland, the most efficient vehicles will first gain market share. Over the longer term efficiency improvement is limited by incremental technical progress. In the moderate efficiency improvement scenario, emissions per mass are annually reduced by 2.5 % until 2015, and by 1.5 % from 2015 to 2020, equally for gasoline, diesel, and HEVs. In the high efficiency improvement scenario, emissions per mass are annually reduced by 4 % until 2015, and by 2.5 % from 2015 to 2020.

From 2000 to 2012 average gasoline car mass increased by 2.5 %, diesel car mass by 10.5 %, and average fleet mass by 10.8 %. Regarding future vehicle mass two scenarios are distinguished: 1

[9] As pointed out by [Kromer et al., 2010] such high growth rates are possible for technologies that have not yet gained significant market share but are difficult to maintain once a higher level of market penetration is reached.

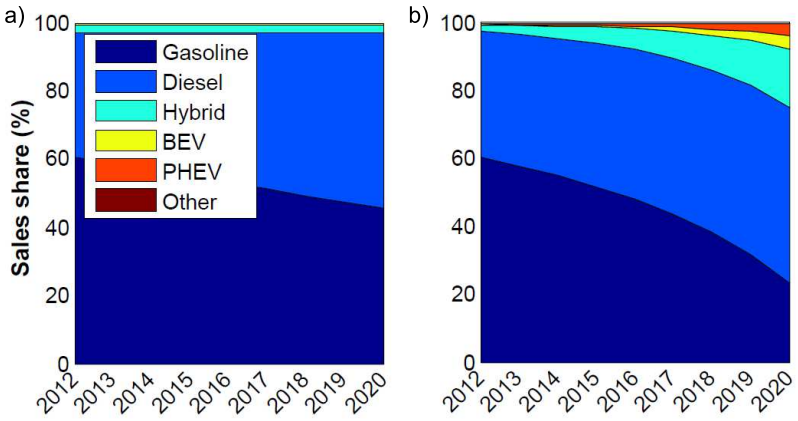

Figure 8.11: Future sales share by powertrain for (a) Diesel and (b) Diesel + EV scenario.

% annual reduction and 1 % annual increase by drivetrain. Again these two scenario options are expected to be limiting cases.

Table 8.1: Summary of scenario parameter settings.

Scenario parameter	**Scenario abbreviation**	**Description**
Future sales	Diesel A	Shift from gasoline to diesel (+15 % from 2012 to 2020). Consumers shifting buy average diesel mass.
	Diesel B	Shift from gasoline to diesel (+15 % from 2012 to 2020). Consumers shifting buy average gasoline mass.
	EV+Diesel B	Same as Diesel B and 30/50/50 % annual growth of HEV/BEV/PHEV at expense of gasoline.
Efficiency improvement	Moderate	2.5 % (2012-2015) and 1.5 % (2015-2020) annual reduction of CO_2 emission per mass by drivetrain.
	High	4 % (2012-2015) and 2.5 % (2015-2020) annual reduction of CO_2 emission per mass by drivetrain.
Vehicle mass	Mass +1 %/y	1 % annual increase of average new vehicle mass by drivetrain.
	Mass -1 %/y	1 % annual reduction of average new vehicle mass by drivetrain.

Fig. 8.12 shows the scenario results together with the CO_2 emission targets of 130 g/km by 2015 and 95 g/km by 2020. As can be seen from the figure, reaching short-term CO_2 reductions is particularly sensitive to the efficiency improvement of conventional diesel and gasoline vehicles brought on the market and to changes of their mass and performance. If the trend to heavier and higher performance vehicles continues these reduction targets will not be met, even if very efficient new powertrain technologies such as hybrid electric or battery electric vehicles penetrate the market at very optimistic rates. The analysis shows that the 2015 target of 130 g CO_2/km

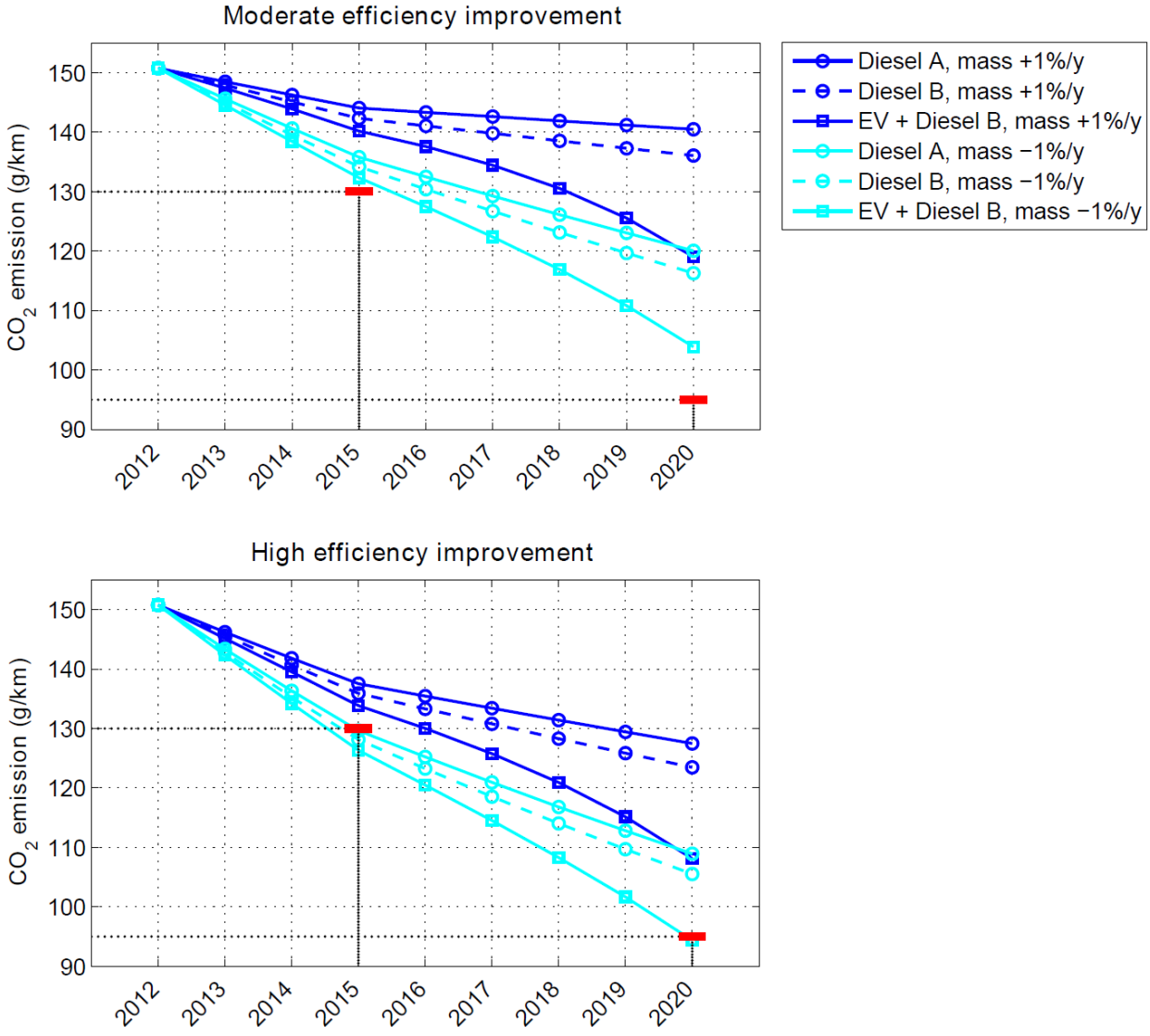

Figure 8.12: Specific CO_2 emissions from Swiss new vehicles for different scenarios from 2012 to 2020. Red markers indicate the definitive target for 2015 and as it is proposed for 2020.

can be reached if the high level efficiency improvement that has been observed for conventional gasoline vehicles over the last four years can be continued and annual reductions of ca. 1 % in vehicle weight occur. Due to the current dominance of conventional vehicle technologies, electric vehicles cannot play a significant role in meeting short-term CO_2 reduction targets. On the longer-term however, they offer significant reduction potential and may be important to meet reduction targets beyond 2015.[10]

8.3 Swiss passenger car fleet impacts

The previous section analyzed past and future specific CO_2 emissions from new passenger vehicles. In this section the Swiss passenger vehicle stock from 2012 to 2050 is calculated and the implications for tank-to-wheel (TtW) energy use and well-to-wheel (WtW) GHG emissions are evaluated.[11] Selected scenarios are analyzed based on limiting cases of future drivetrain sales shares of alternative powertrains, vehicle resistance improvements, and primary energy sources. The fleet model is designed in a very flexible way that allows easy modification of scenario parameters and recalculation of results.

8.3.1 Methodology and scenario assumptions

As Fig. 8.13 shows on the left, the Swiss passenger car stock has continuously grown since 1990 from about 3 million vehicles in 1990 to 4.3 million in 2013. It is largely dominated by gasoline and diesel powered vehicles. In 2013, the stock consisted of about 3.2 million gasoline (incl. HEV-gasoline), 1 million diesel (incl. HEV-diesel), 2700 electric (BEV or PHEV), and 48000 other (mainly CNG) vehicles [BFS, 2014]. Fig. 8.13 shows the age structure over time on the right. In 2013 the average age of passenger cars in the fleet is 8.2 years and 18 % of vehicles were first registered before 2000.

Vehicle stock is simulated by drivetrain type, fuel, and vehicle class according to chapter 3 and section 3.2.1. Fig. 8.14 shows an overview of the passenger car fleet model and the data flow between the main components.

Stock turnover is calculated for each year by combining historic and new vehicle sales, and by subtracting vehicles that leave the fleet. For this calculation historic and future sales are disaggre-

[10] In [Hofer et al., 2012b] the conditions for compliance with the CO_2 emissions target are analyzed in more detail. The paper also presents a model to estimate what average vehicle characteristics and fleet composition may be expected if consumers keep their current preferences for size and performance, but are faced with an increased purchase price based on the regulatory penalty to be imposed on vehicles exceeding the limit value of allowed CO_2 emissions.

[11] TtW energy use refers to the direct energy use of the vehicles and does not include energy use from the fuel or electricity supply. WtW GHG emission includes direct exhaust emissions and emissions from fuel and electricty supply. Note that WtW does not include the vehicle production and disposal phase and as such is different from the LCA performed in chapter 6.

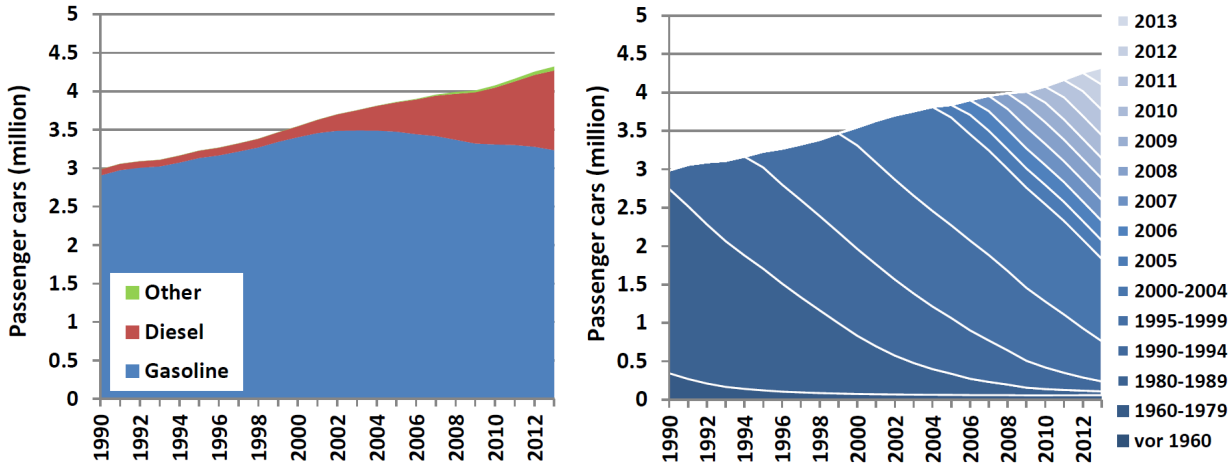

Figure 8.13: Swiss vehicle stock from 1990 to 2013 by fuel type (left) and year of first registration (right).

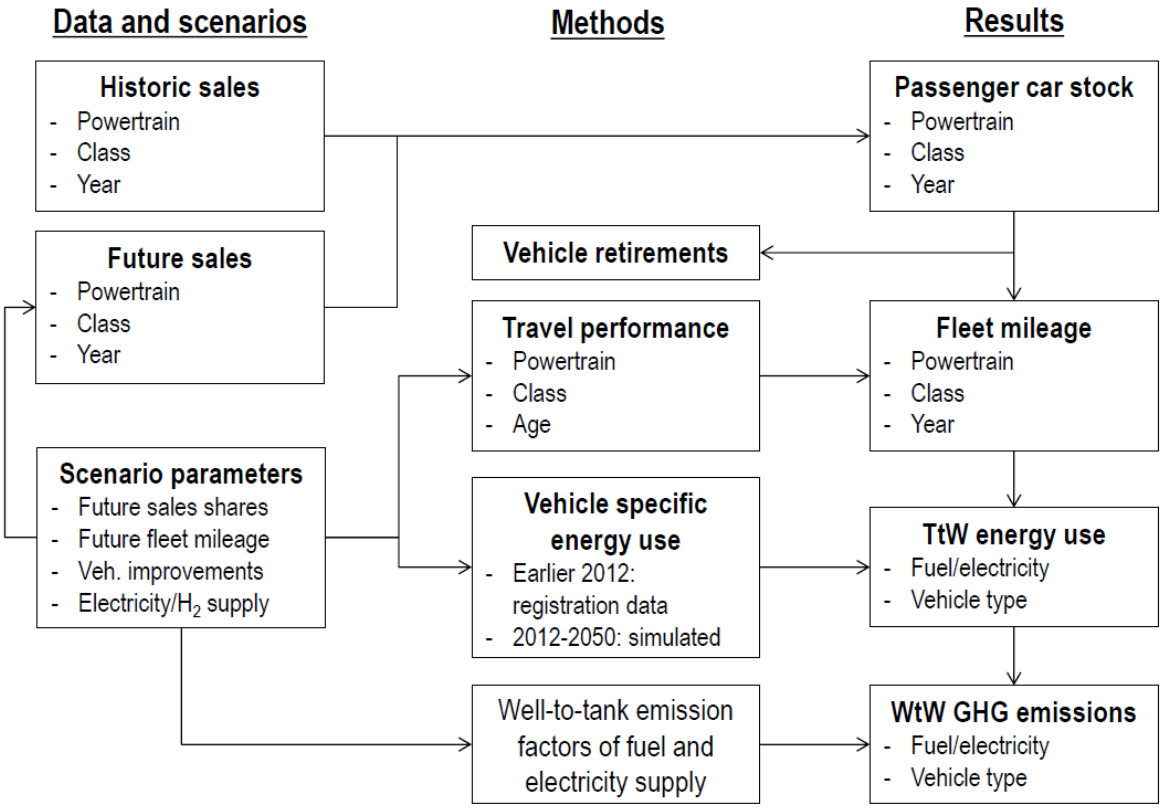

Figure 8.14: Overview of passenger car fleet model.

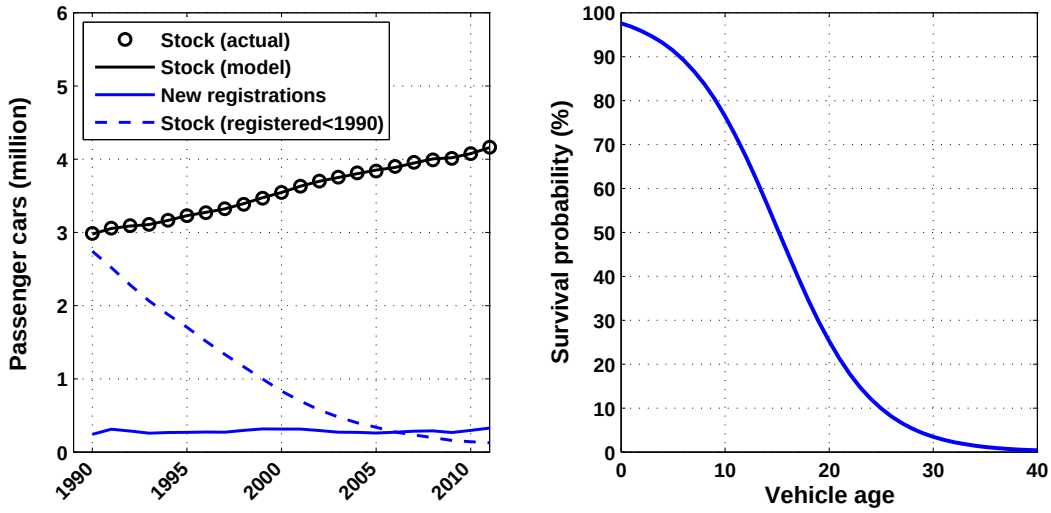

Figure 8.15: Swiss vehicle stock over time (left) and inferred survival probability (right).

gated by drivetrain and class. This includes 23 conventional and electric drivetrains (including three electric range categories for BEV and PHEV) per class. In total there are 299 vehicle options for each year. In order to calculate the removal of vehicles from the fleet, a survival probability SP depending on vehicle age t is used

$$SP(t) = \frac{1}{a + e^{b\,(t-T)}} \tag{8.19}$$

where the factors a, b, and T are determined based on historic fleet data in Switzerland. T corresponds to the average lifetime after which a vehicle leaves the fleet. Knowing the amount of vehicles in the stock that were registered before a certain point in time (in this case 1990), new registrations over time, and the actual amount of vehicles in the stock for each year, the coefficients a, b, and T in Eq. 8.19 are determined using a least squares fit. Fig. 8.15 shows the data used and the resulting survival probability. Taking into account all passenger cars in the fleet from 1990 to 2011, the following coefficients were found: T = 14.1 y, a = 0.99, and b = 0.224 y^{-1}. Note that the survival probability usually differs by powertrain type, driving performance, size class, and other factors. For simplicity this was not taken into account and it is assumed that all vehicles retire equally. Due to the continuous growth of the stock, the average age of vehicles in the fleet is lower than the average time vehicles stay in the fleet (8.2 years vs. 14.1 years). Once the number of vehicles in the stock stabilizes, the average age of vehicles in the fleet should approach T.

In order to perform the fleet simulation four limiting cases of future sales share by drivetrain are

analyzed:

- **Ref**: HEV sales share increases to 40 % and ICEV share decreases to 60 % by 2050. For both ICEV and HEV the share by fuel is 60 % gasoline and 40 % diesel. No natural gas and electric vehicles (BEVs, PHEVs, FCVs) are considered.
- **NG**: Same split by drivetrain as in Ref (60 % ICEVs and 40 % HEVs by 2050), but with a strong shift from gasoline and diesel to natural gas (75 % in 2050).
- **Mod-EV**: 50 % electric vehicle sales by 2050 (25 % BEVs, 15 % PHEVs, 10 % FCVs), 35 % ICEVs, and 15 % HEVs.
- **High-EV**: 85 % electric vehicle sales (30 % BEVs, 30 % PHEVs, 25 % FCVs), 15 % HEVs, and a phase out of conventional ICEVs by 2050.

Fig. 8.16 shows the scenarios of sales share by drivetrain, fuel type, and electric range. In the Mid-EV and High-EV scenarios, the sales distribution shifts over time from low to higher electric range categories for BEVs and PHEVs. For simplicity, the distribution of sales share by class is constant at the 2011 level in all scenarios and equal among all powertrains. This could be modified as it is probable that e.g. BEVs are primarily used as small city or sports cars for which electrification is most beneficial and limited range less problematic than for e.g. family vans [Lieven et al., 2011].

The absolute level of future sales (and as such the total amount of vehicles in the fleet) is based on the average travel performance per car and the assumed future development of total passenger car travel demand. The scenarios used in the Energy Perspectives for Switzerland [Prognos, 2012] are adopted. In the reference case this predicts a growth from 54 billion vkm/year in 2010 to 68 billion vkm/year in 2050. In the new energy policy scenario total fleet mileage stabilizes at about 56 billion vkm/year after 2020. The travel distance distribution is differentiated by powertrain, range, and class. This means for example that BEVs and small cars are assumed to drive less than conventional ICEVs and large vans.

As shown in Fig. 8.14, once vehicle stock and travel distance distribution are defined, the simulation proceeds by calculating fleet energy use based on vehicle specific energy use. For years earlier than 2012 this is based on Swiss new vehicle registrations per drivetrain and class. For example, Fig. 8.17 shows average specific CO_2 emissions by class for new gasoline vehicles registered in Switzerland from 2001 to 2011.[12] For future years, energy use per drivetrain and class is simulated using the same assumptions and models as described in section 6.1.2, except that now the full set of classes described in section 3.2.1 is simulated. To be compatible with past emissions data, the NEDC driving cycle is used for simulation of future vehicle energy use. Regarding

[12]To reveal information on the average emission by class, sales data that was originally issued from the Swiss Federal Roads Office (ASTRA) was complemented by IHS Global Insight with vehicle class related information.

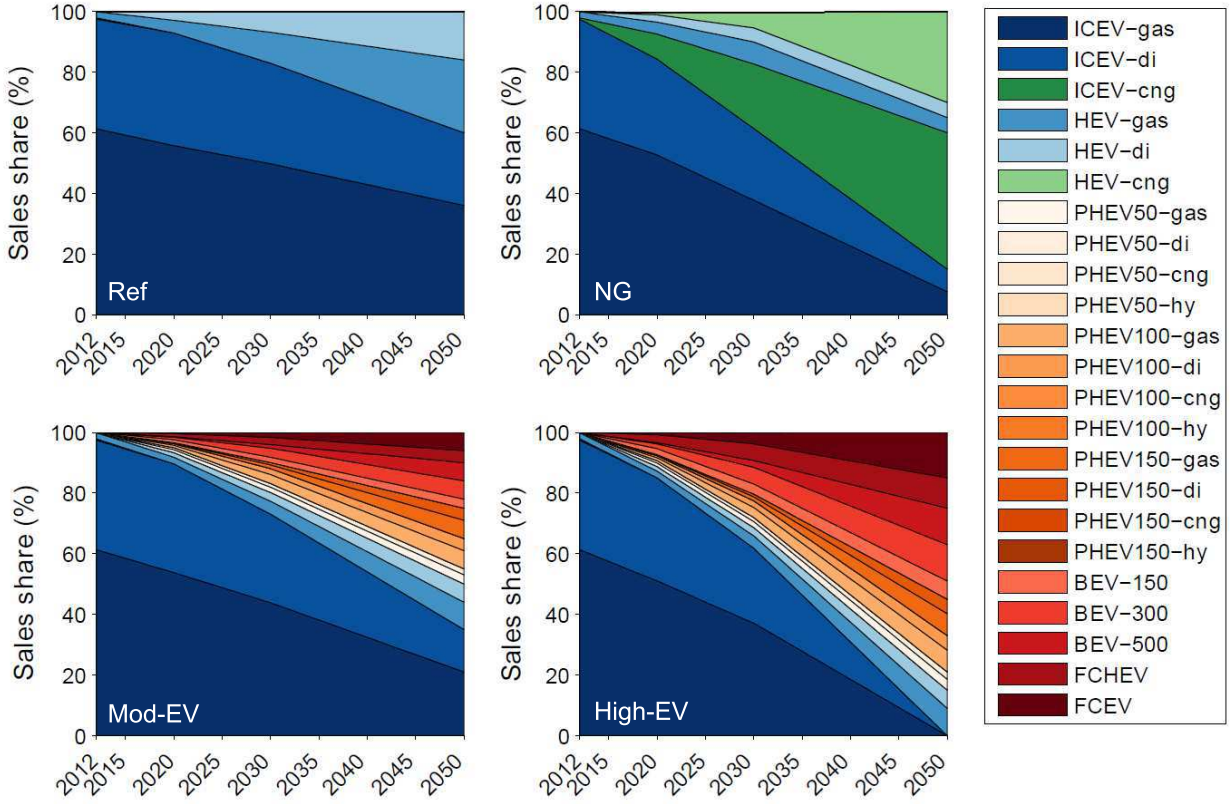

Figure 8.16: Future sales shares by powertrain for the different scenarios analyzed.

the reduction of vehicle resistance parameters (i.e. glider mass, aerodynamic drag, and rolling resistance coefficient) two scenarios are analyzed:

- **A**: Glider mass, c_d, and c_r constant at 2011 values.
- **B**: Glider mass, c_d, and c_r reduced annually by 0.5 %.

In order to calculate WtW GHG emissions the results of fleet energy use are coupled with WtW emission factors. For gasoline, diesel, and natural gas supply, unfortunately only a single dataset was available in ecoinvent based on the current market situation. The impacts due to the expected increase of unconventional oil and natural gas supply (by exploiting e.g. oil sands, shale gas, or deep water reservoirs) could thus not be considered. For electricity and hydrogen supply four different primary energy source options are considered:

- **Coal**: Electricity from coal, hydrogen from coal gasification
- **NG**: Electricity from natural gas, hydrogen from steam methane reforming

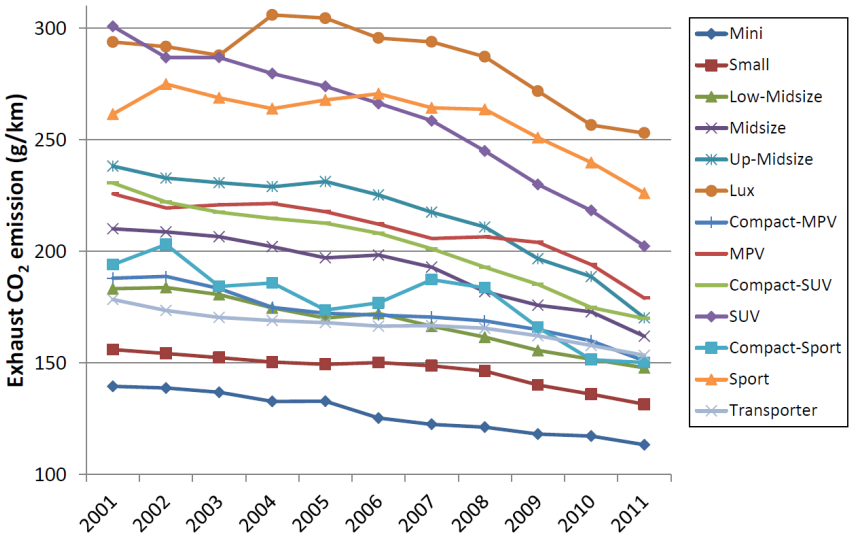

Figure 8.17: Average specific CO_2 emission by class for Swiss new gasoline vehicles from 2001 to 2011.

- **RE**: Mix of renewable primary sources for electricity and hydrogen production[13]
- **CH**: Potential future electricity mix and hydrogen production[14]

The WtW emission factors used are listed in Table 8.2.

Table 8.2: WtW GHG emission for fuel, electricity, and hydrogen supply and combustion (kg CO_2 eq/GJ).

		2012	2030	2050
Fuel	Gasoline	92.8	92.8	92.8
	Diesel	87.1	87.1	87.1
	CNG	72.1	72.1	72.1
Electricity	Coal	339.7	246.4	231.7
	NG	135.0	125.7	124.4
	CH mix	41.2	38.1	35.0
	RE mix	12.0	7.3	6.7
Hydrogen	Coal (CG)	197.9	193.6	189.2
	NG (SMR)	135.6	133.7	131.7
	CH mix	72.6	68.5	66.0
	RE mix	31.6	28.3	25.1

[13]The RE scenario assumes equal shares of wind, PV, and hydro for electricity production, and equal shares of wind, PV, hydro, and biomass gasification for hydrogen production.

[14]For 2050, the CH scenario assumes electricity production based on 45 % hydro, 30 % natural gas, 20 % PV, 5 % wind, and hydrogen production based on 40 % electrolysis using the Swiss electricity mix, 25 % SMR, 20 % electrolysis using PV, and 15 % biomass gasification.

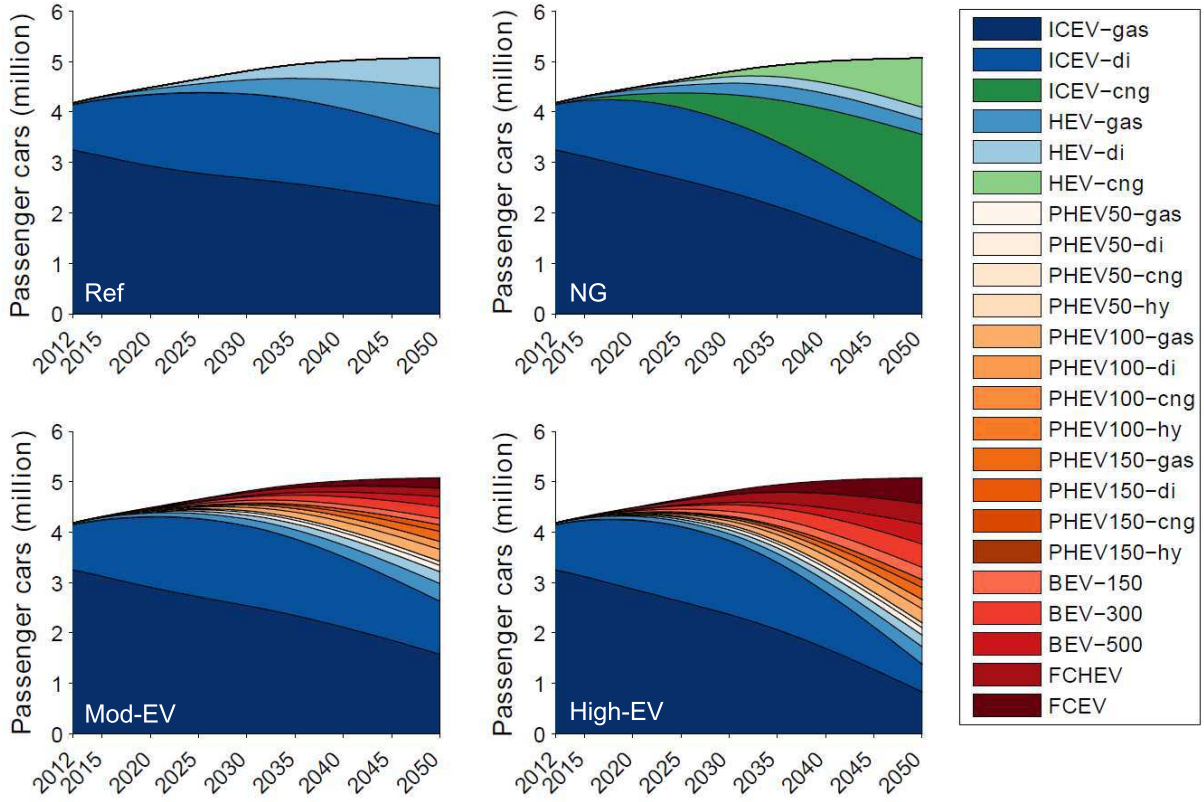

Figure 8.18: Passenger car stock by drivetrain in the four sales scenarios considered.

8.3.2 Scenario results

The scenarios for future sales, vehicle energy loss reductions, and primary energy sources as described in the last section are now combined and evaluated with regard to passenger car stock, fleet energy use, and WtW GHG emission.[15]

Fig. 8.18 shows the development of the passenger car stock by drivetrain for the four sales scenarios considered from 2012 to 2050. The temporal lag between vehicle sales and stock is interesting. For example for the High-EV scenario, which assumes zero ICEV sales by 2050, 26 % of vehicles in the stock in 2050 are still ICEV. Fig. 8.19 shows the corresponding distribution of vkm traveled by drivetrain, and Fig. 8.20 shows fleet energy use by drivetrain in the case of constant vehicle resistance characteristics (scenario A).

Fig. 8.21 compares the results of the different scenarios for fleet energy use by energy carrier in 2012, 2030, and 2050. Fleet energy use is reduced relative to 2012 in all future scenarios. The

[15]Only results with regard to the reference mileage scenario are shown. If a different development is assumed the results can be scaled accordingly.

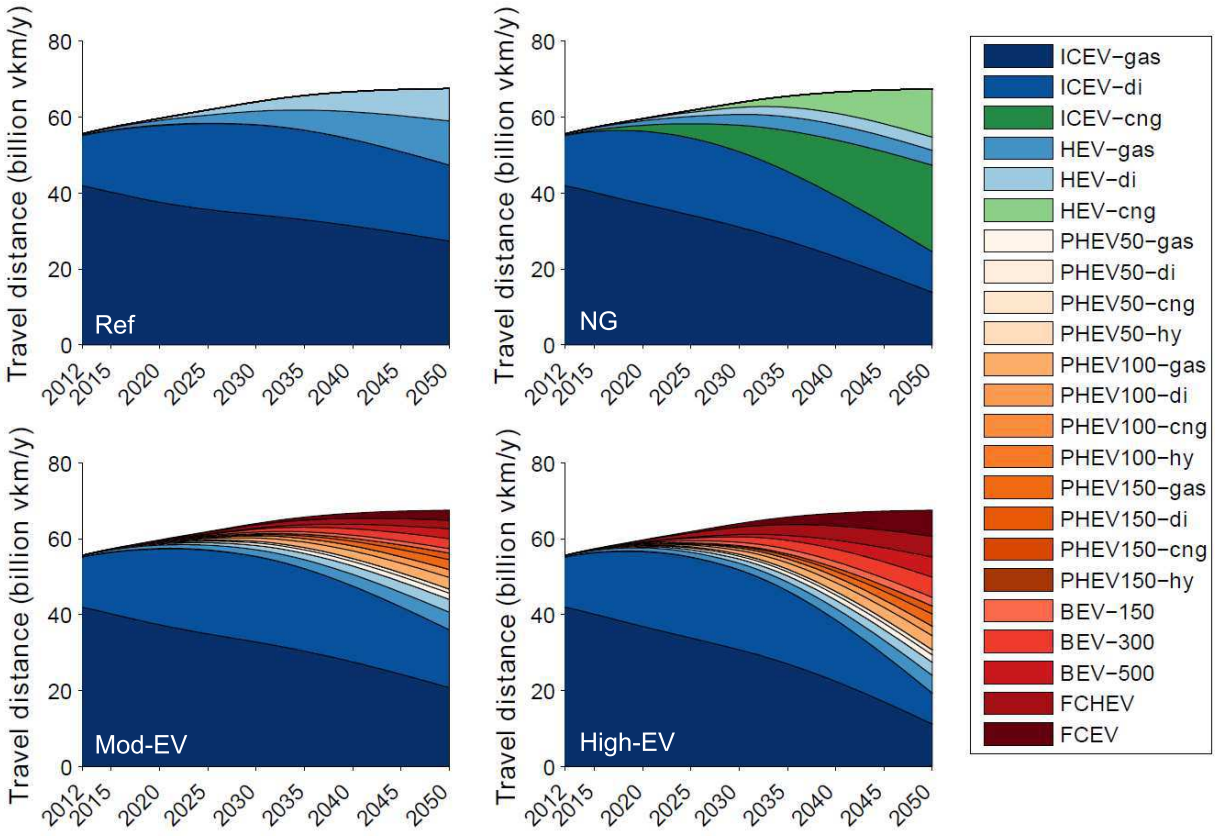

Figure 8.19: Distribution of total travel performance by drivetrain in the four sales scenarios considered.

reductions are largest for of a high share of electric cars. Interestingly, an ICE-based fleet combined with continuous reduction of vehicle resistances (Ref/B and NG/B) achieves nearly the same energy use reduction as moderate fleet electrification without reduction of vehicle resistances (Mod-EV/A). The same applies for Mod-EV/B compared to High-EV/A.

Fig. 8.22 compares fleet WtW GHG emissions by energy carrier for the different scenarios in 2050. Relative to 2012, WtW GHG emissions are reduced in all scenarios. However it strongly depends on the primary energy source whether a fleet of electric vehicles provides an emissions advantage relative to a fleet based on ICE powered vehicles. The degree of this sensitivity depends on the level of electric vehicles in the fleet. Relative to the Ref scenario, the EV scenarios perform worse if electricity and hydrogen production is based on coal, but significantly better if renewable energy sources are used. The ICE-based scenario with a shift to natural gas performs similarly to the EV scenarios where electricity and hydrogen are produced from natural gas.

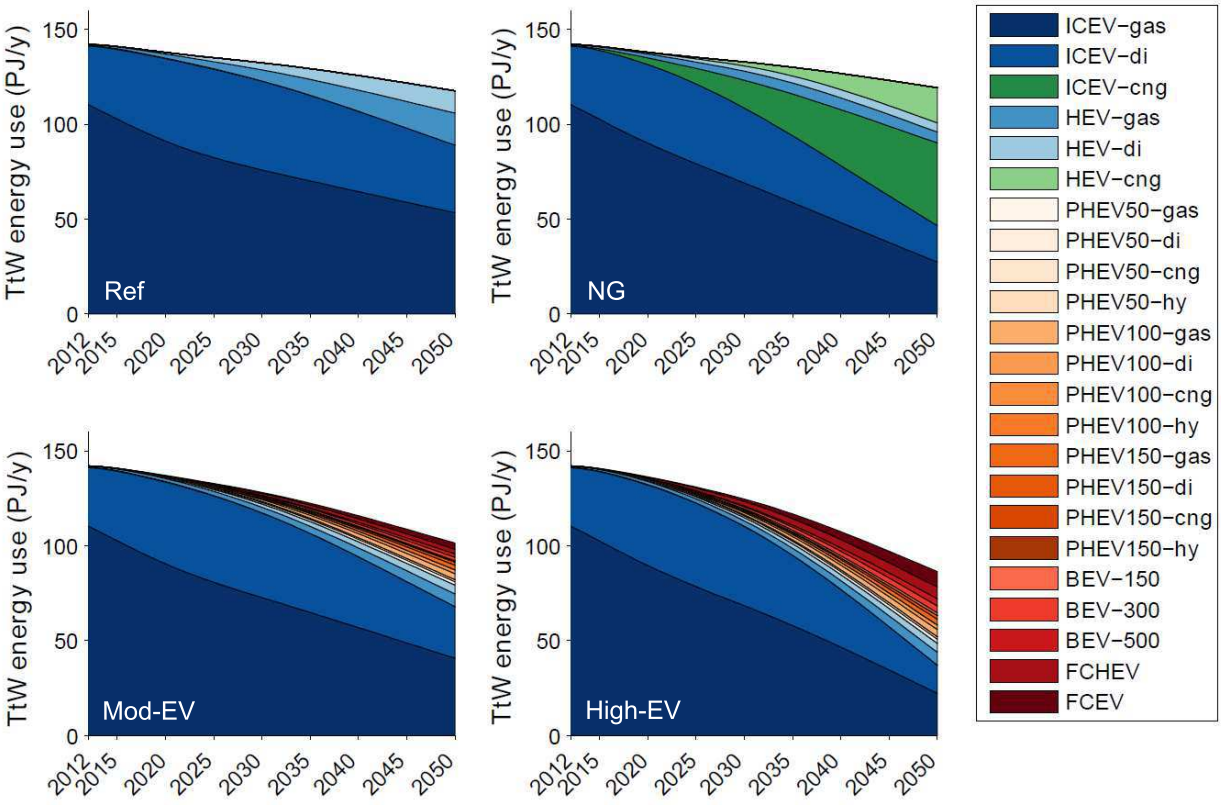

Figure 8.20: Fleet energy use by drivetrain in the case of constant vehicle resistance characteristics (scenario A).

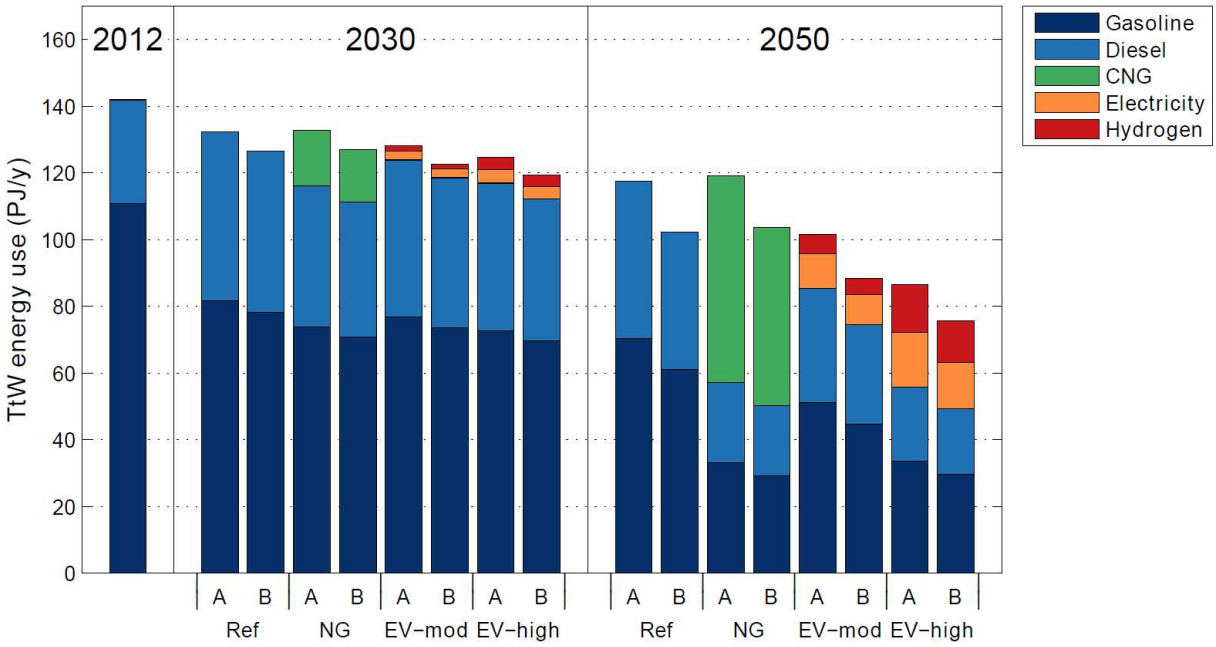

Figure 8.21: Fleet energy use by energy carrier in 2012, 2030, and 2050.

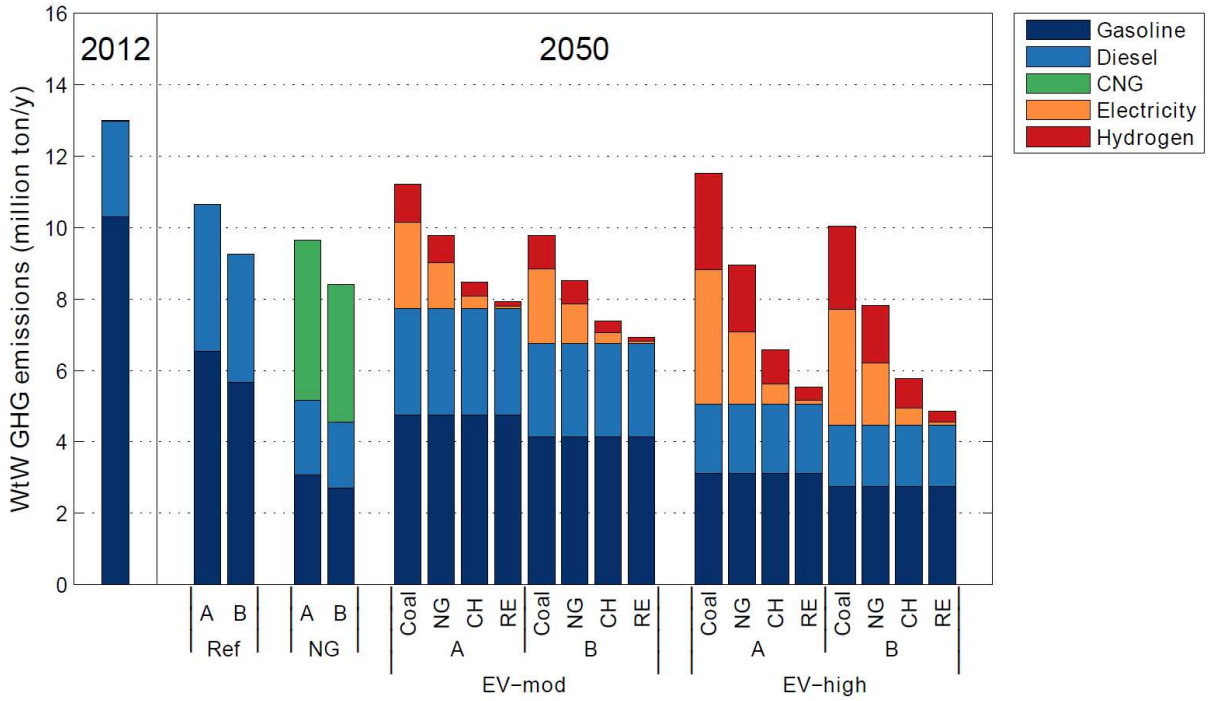

Figure 8.22: Fleet WtW GHG emissions by energy carrier in 2012 and 2050

.

Chapter 9

Conclusions and Outlook

9.1 Summary and conclusions

This chapter summarizes the main achievements, conclusions, and recommendations of this thesis.

Chapter 1 concluded that there is a need for sustainable vehicle technologies and outlined the scope and contents of the thesis.

Chapter 2 divided vehicle mechanical energy demand into the contributions of regenerative and dissipative energy demand. A comparison of the regenerative to tractive energy demand for different driving cycles revealed, that the regeneration potential is highest for urban driving cycles and increases with vehicle mass. Heavy vehicles in urban traffic conditions are therefore the best candidates for energy recuperation. The individual contributions to mechanical energy demand have been parameterized as a function of vehicle characteristics and driving cycle coefficients, and the variability of the parameterization coefficients to changes of vehicle characteristics has been analyzed.
The novelty of this parameterization method is that it splits up total mechanical energy demand into the contributions from aerodynamic drag, rolling resistance, and kinetic energy, separately for tractive and regenerative energy demand. This parameterization was performed for a variety of urban, highway, and average driving cycles. The parameterization approach is very useful to analytically study the sensitivity of mechanical energy demand to changes in vehicle characteristics. The analysis showed that reduction of vehicle mass should preferentially be applied to vehicles having high rolling friction, reduction of the rolling resistance coefficient is best applied to vehicles of high mass, and reduction of the aerodynamic drag coefficient is best applied to vehicles having a large frontal area. Comparing the sensitivity of mechanical energy demand for different driving cycles showed that reductions of vehicle weight and tire rolling resistance coefficient reduce energy demand most effectively in urban driving conditions. Reduction of the

aerodynamic drag coefficient is most effective in highway driving conditions.

Chapter 3 developed an original method for calculating the energy use of a broad range of powertrain technologies based on average operating point efficiencies. The details of the vehicle simulation, characteristics of the analyzed car classes, and performance related configuration parameters were presented.

Chapter 4 explained the methods for the calculation of vehicle mass and cost indicators and summarized the corresponding data inputs. It also showed how the simulation of vehicle component masses and energy use is coupled with life cycle assessment results to calculate life cycle related indicators.

Chapter 5 developed a new and integrated analytic method for the scaling of vehicle indicators (such as energy use) as a function of vehicle configuration (such as range) and component parameters (such as battery energy density). The method intrinsically considers the inter-dependencies of technical developments and configuration parameters and due to its analytic formulation allows studying the sensitivity to parameter variations in an unprecedented way. It has been applied to analyze ICEV, BEV, and FCEV mass, cost, and energy use as a function of range and glider mass. It has been further used for scenario analysis and to study the total cost difference between different drivetrain technologies as a function of relevant parameters.
The results showed that the desired range is a critical parameter affecting the weight and cost of drivetrains having low energy density and high specific cost (in particular the BEV), but that this sensitivity is expected to decrease over time. The influence of a change of glider mass on energy use is highest for low efficiency powertrains. Regarding the sensitivity of total costs, the BEV is most sensitive to range, the ICEV least sensitive to range and most sensitive to energy costs, the BEV and FCEV approximately equally sensitive to energy costs, and the FCEV most sensitive to powertrain costs.
In conclusion, the parametric-analytic method is a novel approach in vehicle simulation that can be used for an integrated assessment of vehicle criteria, combining vehicle configuration data and component technical developments in a single equation. The method also offers new opportunities for sensitivity analysis, including single or multiple parameter variations, analytic and probabilistic assessments.

Chapter 6 presented an integrated framework for the evaluation of a broad range of current and future passenger car options based on different drivetrain technologies, primary energy sources, vehicle size and utility classes. Direct vehicle indicators such as energy use and purchase price were simulated and integrated with life cycle assessment to evaluate the damage to human and ecosystem health, and resource depletion. Generally, the environmental impacts of electric vehicles are very dependent on the primary energy source. Life cycle GHG emissions and the related impacts on human and ecosystem health, as well as resource depletion can be greatly reduced if

non-fossil primary energy (such as hydro, wind, or PV power) is used for vehicle propulsion. For most indicators the impact from the production phase is higher for electric than for conventional vehicle technologies. In particular, metal depletion is significantly higher for electric vehicles due to the contributions from the energy storage, the electric powertrain, and energy production. The further development of alternative drivetrain technologies should aim at reducing the use of high value metals (e.g. by using induction instead of permanent-magnet motors) and recycling them more efficiently.

The high relevance of hydrogen and electricity production regarding the environmental impacts of electric vehicles, as well as the potential tradeoff between reduced use phase but increased production phase impacts should be considered when discussing the potential benefits of electric vehicles. It should be also considered in policy regulations that only target vehicle exhaust emissions (e.g. the EU regulation limiting exhaust CO_2 emissions from new passenger cars [EC, 2009]), as without such measures the relative impact of vehicle, electricity, and fuel production may increase.

The analysis presented in this chapter has also shown that electrification and weight reduction are most effective at reducing energy use in urban driving conditions. This makes light electric cars particularly suited for urban regions. Reduced local air pollution, noise, limited range and space are additional reasons.

MCDA has shown that conventional fossil fuel based technologies perform best for economic and utility indicators, and that electric vehicles perform better for environmental indicators if their primary energy comes from non-fossil sources. The BEV suffers from low range and high charging time, but performs best with regard to environmental indicators when charged from non-fossil primary electricity. The PHEV and FCEV offer utility comparable to conventional vehicles and potentially lower environmental impacts, depending on the primary energy source. The PHEV charged from renewable primary energy is the the highest ranked powertrain option with regard to the full set of indicators considered. The FCEV has great potential as an alternative to the ICEV and HEV if the costs of vehicle production and operation can be significantly reduced.

In general, there is no single technology which performs best in terms of all criteria at the same time, but different technologies tailored for specific usage patterns can provide advantages relative to each other, e.g. an EV performs better than an ICEV in urban driving conditions, a short-range BEV is better than a long-range BEV in terms of costs and environmental impacts, and a FCEV is better than a BEV in terms of range and fueling time. Overall, the PHEV is a robust technology option considering a broad set of utility, environmental, and economic criteria.

Due to its fast calculation time, the method developed in this thesis is very well suited for interactive analysis. The multi-indicator assessment and passenger vehicle MCDA have been implemented in online analysis tools that can be accessed at this website:
http://www.multi-criteria-analysis.com/

Chapter 7 showed how the analytic vehicle simulation method can be applied to optimize the use of advanced technologies. In particular it is used to find the optimal amount of lightweighting, minimizing the total costs of conventional and electric vehicles. The method allows analyzing the sensitivity of the optimal solutions to important input parameters in an unprecedented way.
The results showed a strong secondary weight and cost saving potential for the BEV, but a higher sensitivity of vehicle energy use to mass reduction for the ICEV, because of the relatively low powertrain efficiency and lack of regeneration capability. Generally, lightweighting has the potential to lower vehicle costs, however, the results are very sensitive to parameters affecting lifetime fuel costs for conventional and battery costs for electric vehicles. Based on current technology cost estimates it has been shown that the optimal amount of primary mass reduction minimizing total costs is similar for conventional and electric vehicles and ranges from 22 % to 39 %. Due to the relatively high battery and fuel cost for the BEV and ICEV, respectively, the benefits of lightweighting emerge for the BEV mainly in the vehicle production phase and for the ICEV in the vehicle use phase. The analytic method has been used to study the sensitivity of the optimal solutions to several important input parameters.
In general, the approach is not limited to the cost optimization of lightweighting, but can also be applied to other technology options (e.g. improvement of powertrain efficiency) or to solve other optimization objectives (e.g. LCIA indicators).

Chapter 8 developed a novel decomposition method to separate the contributions of the changes of mass, fuel technology, and efficiency to fleet average specific CO_2 emissions over time. It has been applied to analyze emission reductions of new vehicles in Switzerland from 2000 to 2012 and to develop emission scenarios until 2020.
The analysis showed that in the past powertrain efficiency improvements have to a large extent been offset by the increased mass and performance of new vehicles. In the period from 2000 to 2012, potential CO_2 reductions at constant fleet mass would have been ca. 9 % higher than the actual CO_2 emission reduction, i.e. much closer to the target of 130 g/km by 2015. Meeting the 2015 reduction target has been shown to be particularly dependent to the further development of the average weight and efficiency improvement of conventional gasoline and diesel passenger cars. If the trend to heavier and higher performance vehicles continues, the emission targets for 2015 and 2020 will be difficult to reach, even if very efficient new powertrain technologies enter the market at optimistic rates.
In conclusion, there needs to be a reversal of the overall historic trend to larger and more powerful vehicles if regulatory CO_2 emission targets are to be met, instead shifting sales to lighter and more efficient gasoline and diesel cars. Electric vehicles are important for meeting longer-term emission targets, but as mentioned earlier, the current EU regulation should be extended to consider the environmental impacts of vehicle, fuel, and electricity production.
Regarding the Swiss passenger car fleet, major drivetrain changes (BEV, FCV, PHEV) are not yet

ready for large scale adoption, and will take a long time to penetrate the fleet against the current dominance of gasoline and diesel powertrains (99 % of stock in 2013). Therefore alternative powertrain technologies cannot play a significant role for short-term fuel use and GHG emission reductions. On a long-term perspective (beyond 2030), electric vehicles offer the potential for large reductions of fleet fuel use and GHG emissions if electricity and hydrogen are produced from non-fossil primary sources. The fleet scenarios also show that a shift to lighter cars and reduction of vehicle resistances (such as aerodynamic drag and tire rolling resistance) are important to further reduce fleet fuel use and GHG emissions.

9.2 Limitations and outlook

This section discusses some limitations of the thesis and ideas for potential improvements.

The **analytic coupling** of vehicle parameters and energy use developed in section 5.1 focused on coupling vehicle mass and energy use. In addition, an extension of the method to include a feedback from a change of mass to the size (or frontal area) of the vehicle has been proposed and the effects were discussed in section 5.2.3. In general, it would be interesting to consider vehicle mass and size as two independent variables. This can be achieved by establishing a relation between vehicle frontal area and volume and assessing also component specific volumes, in addition to component specific masses. The inclusion of size as an independent variable can be important in the case of a) unproportional scaling of vehicle size relative to mass or b) scaling of vehicle components that have a particularly high or low volumetric mass density, such as compressed natural gas or hydrogen storage tanks.

Regarding **LCA**, the work exhibits several limitations and possibilities for improvements. As mentioned earlier, LCA data for fossil fuels was only available corresponding to the current market situation. The environmental impacts due to the expected increase of unconventional oil and gas (by exploiting e.g. oil sands and shale gas) could thus not be considered. The same applies to the future production of vehicle components where partial future LCA datasets were available, but contain large uncertainties.

The second major limitation related to LCIA is the absence of regionally differentiated impact assessment. While this is valid for global environmental mechanisms such as climate change, it fails to account for emissions having a direct and locally differentiated impact, such as human health damage due to exhaust particulate emissions in densely populated areas vs. particulate emissions from remote power plants. This is obviously important in the context of electric mobility and should be considered in future work. It can be included in the analysis by e.g. using site-dependent impact assessment factors [Mutel & Hellweg, 2009].

Even though the work presented in this thesis has aimed to represent realistic fuel consumption by considering advanced driving cycles in addition to the NEDC, emission of pollutants (such as

PM and NOx) in the LCA were based on limits prescribed by EU norms. Several studies showed that some types of real-driving emissions are much higher than those limits, due to the discrepancy between engine operation during real-driving and the homologation test procedure. For example [Chen & Borken-Kleefeld, 2014] have shown that NOx emissions from diesel cars have actually increased in real-driving conditions over time, although emission limits have progressively tightened. Future work should take these discrepancies into account.
In the current analysis, recycling of metals is usually implemented by considering a mix of primary and secondary resources, i.e. resources from mining and resources from recycled materials. This mix is based on the generic market mix contained in ecoinvent, which is in some cases based on rather old data sources and which may not correspond to the actual material mix used in the product of interest. Due to the high importance of metal resources for the assessment of electric vehicles, an updated and product specific assessment of metal use and recycling should be performed. This could be combined with a more profound analysis of metal depletion assuming a large-scale introduction of electric vehicles on a global scale.

The analysis presented in chapter 5 showed that future scenarios of vehicle development contain large **uncertainties** due to naturally uncertain developments of future energy prices, component efficiency improvements, mass and cost reductions, etc. Section 5.3 introduced several methods to evaluate such sensitivities related to a variation of configuration parameters and uncertain input data. In future work it would be interesting to assess these uncertainties in a more structured way. This could be achieved by e.g. defining a likely distribution (or a lower and upper limit) for each input parameter and assessing the corresponding uncertainties on vehicle indicators. In online applications, the definition of uncertainty bounds for some input parameters could be user defined.

In **MCDA**, stakeholders usually weigh different and possibly conflicting criteria according to their individual preferences. For the analysis presented in section 6.2, generic weighting profiles have been used to evaluate the strengths and weaknesses of different technologies relative to each other. A possible future extension would be to analyze the MCDA results based on a large number of real stakeholder interactions and weighting profiles. This could be based on an interactive online MCDA tool, as presented in section 6.3.
The MCDA approach could be also used for multi-objective (or Pareto) optimization, i.e. for a certain stakeholder preference (or group of preferences) the best technology configuration can be determined from a large set of vehicle alternatives. This can e.g. be used to evaluate the optimal electric range of a PHEV, considering the multi-objective preferences of vehicle buyers.

The **decomposition analysis** of new vehicle CO_2 emissions presented in section 8.2 is useful to analyze the contributions to emission reduction over time and to develop future emission scenarios. The methodology based on aggregated fleet data provides accurate results and does not rely on detailed data inputs. It can be applied to data from individual countries or manufacturers

to monitor efficiency improvements over time and to analyze possible measures for compliance with future emission targets.
Besides specific CO_2 emissions, the method can be applied to decompose other trends in vehicle characteristics, e.g. the development of vehicle mass into the contributions from a change of class vs. a change of fuel technology vs. a change of individual mass by segment and fuel type.

Regarding the modeling of the future **passenger car fleet**, several advancements are possible. The distribution of future sales by class was assumed to be constant and equal among all drivetrain types. As mentioned earlier, this could be modified so that advanced powertrains enter the market preferentially in the segments they are most suited for, e.g. BEVs could at the beginning mainly be used as small urban, second, or sports cars.
The analysis presented in section 8.3 considered the impacts of TtW energy use and WtW GHG emissions. This should be extended to include the vehicle production phase and other potentially relevant LCIA criteria. The analysis focused on the potential impacts from fleet electrification, which was an objective of the THELMA project of which his work was a part. As pointed out in [Prognos, 2012], biofuels (including e.g. biodiesel, bioethanol, biogas, and biomass gasification) could play an important role in fueling parts of the Swiss passenger car fleet of the future. In addition, it would be interesting to consider other alternatives for reducing petroleum use and GHG emissions in the transport sector e.g. including other modes of transport. These improvements and extensions will in part be implemented in the context of the currently starting Swiss Competence Center for Energy Research (SCCER) related to mobility research.

As pointed out in several contexts throughout this thesis, vehicle mass reduction is an important measure to decrease the environmental impacts of road transport. The results from section 8.2 and 8.3 for example show that mass reduction is critical in decreasing fleet fuel use and emissions. In addition, weight reduction can help to reduce the size and cost of other vehicle components as pointed out in section 7.2. However the question remains: Are weight reduction and **safety** conflicting objectives, as for example advocated by [Lave, 1981]?
Indeed for car-car frontal collisions the deceleration of a light and heavy car are inversely proportional to their mass ratios and there is evidence for the risk R of injury according to: $R_{light}/R_{heavy} = (m_{heavy}/m_{light})^n$ with $1 < n < 4$ [Ross & Wenzel, 2001]. However, this argument does not hold for collisions between cars of equal masses and single-car crashes, as pointed out by [Hutchinson & Anderson, 2010]. Besides safety to the individual driver, the safety in the vehicle fleet as a whole strongly depends on the distribution of mass in the fleet [Buzeman et al., 1998] and the appearance of specific high-risk vehicle models (such as SUVs), as investigated by [Wenzel & Ross, 2005].
Several more recent studies have also analyzed the reasons for the increase of fleet weight in recent years and whether there is a link between increased mass and safety improvements. In [Zachariadis, 2008] for example, a statistical analysis of vehicle mass versus EuroNCap stars has

been performed to find a possible connection between weight increase and passive safety improvements. The conclusion was that there is no statistical evidence that weight and safety are correlated.

In conclusion, a certain amount of weight is certainly required for passive safety. However the increase of vehicle mass in recent years might not be driven by improvements of safety but rather by other reasons such as increased size, comfort, and performance. A more detailed analysis of the relation of vehicle mass reduction and safety, in particular also with regard to lightweight materials, should be performed.

Appendix A

Vehicle efficiencies

Table A.1: Traction and regeneration efficiencies for average, urban, and highway driving by powertrain, power-to-mass ratio, PHEV operating mode, and year of assessment.

Powertrain	P/m (kW/kg)	Year	Period	PHEV mode	Average	Urban	Highway
ICEV-gas	50	2012	Traction	-	0.205	0.155	0.244
ICEV-gas	50	2012	Regen	-	-1.000	-1.000	-1.000
ICEV-gas	50	2030	Traction	-	0.232	0.176	0.277
ICEV-gas	50	2030	Regen	-	-1.000	-1.000	-1.000
ICEV-gas	50	2050	Traction	-	0.249	0.188	0.297
ICEV-gas	50	2050	Regen	-	-1.000	-1.000	-1.000
ICEV-gas	100	2012	Traction	-	0.184	0.139	0.226
ICEV-gas	100	2012	Regen	-	-1.000	-1.000	-1.000
ICEV-gas	100	2030	Traction	-	0.209	0.158	0.257
ICEV-gas	100	2030	Regen	-	-1.000	-1.000	-1.000
ICEV-gas	100	2050	Traction	-	0.224	0.169	0.275
ICEV-gas	100	2050	Regen	-	-1.000	-1.000	-1.000
ICEV-gas	150	2012	Traction	-	0.164	0.124	0.208
ICEV-gas	150	2012	Regen	-	-1.000	-1.000	-1.000
ICEV-gas	150	2030	Traction	-	0.186	0.140	0.236
ICEV-gas	150	2030	Regen	-	-1.000	-1.000	-1.000
ICEV-gas	150	2050	Traction	-	0.199	0.151	0.253
ICEV-gas	150	2050	Regen	-	-1.000	-1.000	-1.000
ICEV-diesel	50	2012	Traction	-	0.232	0.176	0.277
ICEV-diesel	50	2012	Regen	-	-1.000	-1.000	-1.000
ICEV-diesel	50	2030	Traction	-	0.257	0.194	0.307
ICEV-diesel	50	2030	Regen	-	-1.000	-1.000	-1.000
ICEV-diesel	50	2050	Traction	-	0.271	0.205	0.324
ICEV-diesel	50	2050	Regen	-	-1.000	-1.000	-1.000
ICEV-diesel	100	2012	Traction	-	0.221	0.167	0.270
ICEV-diesel	100	2012	Regen	-	-1.000	-1.000	-1.000
ICEV-diesel	100	2030	Traction	-	0.244	0.185	0.299

Powertrain	P/m (kW/kg)	Year	Period	PHEV mode	Average	Urban	Highway
ICEV-diesel	100	2030	Regen	-	-1.000	-1.000	-1.000
ICEV-diesel	100	2050	Traction	-	0.257	0.195	0.316
ICEV-diesel	100	2050	Regen	-	-1.000	-1.000	-1.000
ICEV-diesel	150	2012	Traction	-	0.209	0.158	0.264
ICEV-diesel	150	2012	Regen	-	-1.000	-1.000	-1.000
ICEV-diesel	150	2030	Traction	-	0.231	0.175	0.292
ICEV-diesel	150	2030	Regen	-	-1.000	-1.000	-1.000
ICEV-diesel	150	2050	Traction	-	0.244	0.184	0.307
ICEV-diesel	150	2050	Regen	-	-1.000	-1.000	-1.000
ICEV-cng	50	2012	Traction	-	0.210	0.159	0.251
ICEV-cng	50	2012	Regen	-	-1.000	-1.000	-1.000
ICEV-cng	50	2030	Traction	-	0.239	0.180	0.285
ICEV-cng	50	2030	Regen	-	-1.000	-1.000	-1.000
ICEV-cng	50	2050	Traction	-	0.256	0.193	0.305
ICEV-cng	50	2050	Regen	-	-1.000	-1.000	-1.000
ICEV-cng	100	2012	Traction	-	0.194	0.147	0.242
ICEV-cng	100	2012	Regen	-	-1.000	-1.000	-1.000
ICEV-cng	100	2030	Traction	-	0.221	0.167	0.274
ICEV-cng	100	2030	Regen	-	-1.000	-1.000	-1.000
ICEV-cng	100	2050	Traction	-	0.236	0.179	0.294
ICEV-cng	100	2050	Regen	-	-1.000	-1.000	-1.000
ICEV-cng	150	2012	Traction	-	0.179	0.135	0.232
ICEV-cng	150	2012	Regen	-	-1.000	-1.000	-1.000
ICEV-cng	150	2030	Traction	-	0.203	0.153	0.264
ICEV-cng	150	2030	Regen	-	-1.000	-1.000	-1.000
ICEV-cng	150	2050	Traction	-	0.217	0.164	0.282
ICEV-cng	150	2050	Regen	-	-1.000	-1.000	-1.000
HEV-gas	50	2012	Traction	-	0.246	0.223	0.274
HEV-gas	50	2012	Regen	-	0.487	0.476	0.487
HEV-gas	50	2030	Traction	-	0.294	0.274	0.313
HEV-gas	50	2030	Regen	-	0.497	0.486	0.497
HEV-gas	50	2050	Traction	-	0.318	0.297	0.338
HEV-gas	50	2050	Regen	-	0.508	0.496	0.508
HEV-gas	100	2012	Traction	-	0.240	0.212	0.263
HEV-gas	100	2012	Regen	-	0.463	0.452	0.463
HEV-gas	100	2030	Traction	-	0.281	0.260	0.301
HEV-gas	100	2030	Regen	-	0.473	0.462	0.473
HEV-gas	100	2050	Traction	-	0.303	0.282	0.324
HEV-gas	100	2050	Regen	-	0.483	0.472	0.483
HEV-gas	150	2012	Traction	-	0.228	0.200	0.252
HEV-gas	150	2012	Regen	-	0.439	0.430	0.439
HEV-gas	150	2030	Traction	-	0.267	0.247	0.288
HEV-gas	150	2030	Regen	-	0.449	0.439	0.449
HEV-gas	150	2050	Traction	-	0.289	0.267	0.311

Powertrain	P/m (kW/kg)	Year	Period	PHEV mode	Average	Urban	Highway
HEV-gas	150	2050	Regen	-	0.458	0.448	0.458
HEV-diesel	50	2012	Traction	-	0.285	0.253	0.311
HEV-diesel	50	2012	Regen	-	0.487	0.476	0.487
HEV-diesel	50	2030	Traction	-	0.318	0.283	0.347
HEV-diesel	50	2030	Regen	-	0.497	0.486	0.497
HEV-diesel	50	2050	Traction	-	0.338	0.302	0.368
HEV-diesel	50	2050	Regen	-	0.508	0.496	0.508
HEV-diesel	100	2012	Traction	-	0.272	0.240	0.299
HEV-diesel	100	2012	Regen	-	0.463	0.452	0.463
HEV-diesel	100	2030	Traction	-	0.304	0.269	0.333
HEV-diesel	100	2030	Regen	-	0.473	0.462	0.473
HEV-diesel	100	2050	Traction	-	0.323	0.287	0.353
HEV-diesel	100	2050	Regen	-	0.483	0.472	0.483
HEV-diesel	150	2012	Traction	-	0.259	0.228	0.287
HEV-diesel	150	2012	Regen	-	0.439	0.430	0.439
HEV-diesel	150	2030	Traction	-	0.289	0.255	0.319
HEV-diesel	150	2030	Regen	-	0.449	0.439	0.449
HEV-diesel	150	2050	Traction	-	0.308	0.272	0.339
HEV-diesel	150	2050	Regen	-	0.458	0.448	0.458
HEV-cng	50	2012	Traction	-	0.258	0.229	0.282
HEV-cng	50	2012	Regen	-	0.487	0.476	0.487
HEV-cng	50	2030	Traction	-	0.295	0.263	0.322
HEV-cng	50	2030	Regen	-	0.497	0.486	0.497
HEV-cng	50	2050	Traction	-	0.319	0.285	0.347
HEV-cng	50	2050	Regen	-	0.508	0.496	0.508
HEV-cng	100	2012	Traction	-	0.246	0.217	0.270
HEV-cng	100	2012	Regen	-	0.463	0.452	0.463
HEV-cng	100	2030	Traction	-	0.282	0.250	0.309
HEV-cng	100	2030	Regen	-	0.473	0.462	0.473
HEV-cng	100	2050	Traction	-	0.305	0.270	0.333
HEV-cng	100	2050	Regen	-	0.483	0.472	0.483
HEV-cng	150	2012	Traction	-	0.234	0.206	0.259
HEV-cng	150	2012	Regen	-	0.439	0.430	0.439
HEV-cng	150	2030	Traction	-	0.268	0.236	0.296
HEV-cng	150	2030	Regen	-	0.449	0.439	0.449
HEV-cng	150	2050	Traction	-	0.290	0.256	0.320
HEV-cng	150	2050	Regen	-	0.458	0.448	0.458
BEV	50	2012	Traction	-	0.731	0.739	0.708
BEV	50	2012	Regen	-	0.508	0.519	0.476
BEV	50	2030	Traction	-	0.731	0.747	0.708
BEV	50	2030	Regen	-	0.508	0.530	0.476
BEV	50	2050	Traction	-	0.739	0.754	0.715
BEV	50	2050	Regen	-	0.519	0.541	0.486
BEV	100	2012	Traction	-	0.705	0.720	0.683

Powertrain	P/m (kW/kg)	Year	Period	PHEV mode	Average	Urban	Highway
BEV	100	2012	Regen	-	0.473	0.493	0.443
BEV	100	2030	Traction	-	0.713	0.728	0.690
BEV	100	2030	Regen	-	0.483	0.504	0.453
BEV	100	2050	Traction	-	0.720	0.736	0.697
BEV	100	2050	Regen	-	0.493	0.514	0.462
BEV	150	2012	Traction	-	0.687	0.702	0.665
BEV	150	2012	Regen	-	0.449	0.468	0.421
BEV	150	2030	Traction	-	0.694	0.709	0.672
BEV	150	2030	Regen	-	0.458	0.478	0.430
BEV	150	2050	Traction	-	0.702	0.717	0.679
BEV	150	2050	Regen	-	0.468	0.488	0.439
FCEV	50	2012	Traction	-	0.369	0.346	0.385
FCEV	50	2012	Regen	-	0.458	0.468	0.449
FCEV	50	2030	Traction	-	0.386	0.362	0.402
FCEV	50	2030	Regen	-	0.468	0.478	0.458
FCEV	50	2050	Traction	-	0.400	0.375	0.417
FCEV	50	2050	Regen	-	0.478	0.488	0.468
FCEV	100	2012	Traction	-	0.360	0.338	0.375
FCEV	100	2012	Regen	-	0.436	0.445	0.427
FCEV	100	2030	Traction	-	0.377	0.353	0.392
FCEV	100	2030	Regen	-	0.445	0.455	0.436
FCEV	100	2050	Traction	-	0.390	0.366	0.406
FCEV	100	2050	Regen	-	0.455	0.464	0.445
FCEV	150	2012	Traction	-	0.351	0.329	0.366
FCEV	150	2012	Regen	-	0.414	0.423	0.405
FCEV	150	2030	Traction	-	0.367	0.344	0.382
FCEV	150	2030	Regen	-	0.423	0.432	0.414
FCEV	150	2050	Traction	-	0.380	0.356	0.396
FCEV	150	2050	Regen	-	0.432	0.441	0.423
FCHEV	50	2012	Traction	-	0.388	0.374	0.399
FCHEV	50	2012	Regen	-	0.458	0.468	0.449
FCHEV	50	2030	Traction	-	0.406	0.391	0.417
FCHEV	50	2030	Regen	-	0.468	0.478	0.458
FCHEV	50	2050	Traction	-	0.421	0.405	0.432
FCHEV	50	2050	Regen	-	0.478	0.488	0.468
FCHEV	100	2012	Traction	-	0.379	0.364	0.389
FCHEV	100	2012	Regen	-	0.436	0.445	0.427
FCHEV	100	2030	Traction	-	0.396	0.381	0.407
FCHEV	100	2030	Regen	-	0.445	0.455	0.436
FCHEV	100	2050	Traction	-	0.410	0.395	0.421
FCHEV	100	2050	Regen	-	0.455	0.464	0.445
FCHEV	150	2012	Traction	-	0.369	0.355	0.379
FCHEV	150	2012	Regen	-	0.414	0.423	0.405
FCHEV	150	2030	Traction	-	0.386	0.371	0.396

Powertrain	P/m (kW/kg)	Year	Period	PHEV mode	Average	Urban	Highway
FCHEV	150	2030	Regen	-	0.423	0.432	0.414
FCHEV	150	2050	Traction	-	0.399	0.384	0.411
FCHEV	150	2050	Regen	-	0.432	0.441	0.423
PHEV-gas	50	2012	Traction	CS	0.229	0.221	0.232
PHEV-gas	50	2012	Regen	CS	0.458	0.468	0.449
PHEV-gas	50	2030	Traction	CS	0.262	0.254	0.266
PHEV-gas	50	2030	Regen	CS	0.468	0.478	0.458
PHEV-gas	50	2050	Traction	CS	0.284	0.275	0.288
PHEV-gas	50	2050	Regen	CS	0.478	0.488	0.468
PHEV-gas	100	2012	Traction	CS	0.223	0.216	0.226
PHEV-gas	100	2012	Regen	CS	0.436	0.445	0.427
PHEV-gas	100	2030	Traction	CS	0.256	0.247	0.259
PHEV-gas	100	2030	Regen	CS	0.445	0.455	0.436
PHEV-gas	100	2050	Traction	CS	0.277	0.268	0.281
PHEV-gas	100	2050	Regen	CS	0.455	0.464	0.445
PHEV-gas	150	2012	Traction	CS	0.217	0.210	0.220
PHEV-gas	150	2012	Regen	CS	0.414	0.423	0.405
PHEV-gas	150	2030	Traction	CS	0.249	0.241	0.253
PHEV-gas	150	2030	Regen	CS	0.423	0.432	0.414
PHEV-gas	150	2050	Traction	CS	0.270	0.261	0.273
PHEV-gas	150	2050	Regen	CS	0.432	0.441	0.423
PHEV-diesel	50	2012	Traction	CS	0.259	0.251	0.263
PHEV-diesel	50	2012	Regen	CS	0.458	0.468	0.449
PHEV-diesel	50	2030	Traction	CS	0.290	0.281	0.294
PHEV-diesel	50	2030	Regen	CS	0.468	0.478	0.458
PHEV-diesel	50	2050	Traction	CS	0.309	0.299	0.313
PHEV-diesel	50	2050	Regen	CS	0.478	0.488	0.468
PHEV-diesel	100	2012	Traction	CS	0.253	0.245	0.257
PHEV-diesel	100	2012	Regen	CS	0.436	0.445	0.427
PHEV-diesel	100	2030	Traction	CS	0.283	0.274	0.287
PHEV-diesel	100	2030	Regen	CS	0.445	0.455	0.436
PHEV-diesel	100	2050	Traction	CS	0.301	0.292	0.306
PHEV-diesel	100	2050	Regen	CS	0.455	0.464	0.445
PHEV-diesel	150	2012	Traction	CS	0.246	0.238	0.250
PHEV-diesel	150	2012	Regen	CS	0.414	0.423	0.405
PHEV-diesel	150	2030	Traction	CS	0.276	0.267	0.280
PHEV-diesel	150	2030	Regen	CS	0.423	0.432	0.414
PHEV-diesel	150	2050	Traction	CS	0.294	0.284	0.298
PHEV-diesel	150	2050	Regen	CS	0.432	0.441	0.423
PHEV-cng	50	2012	Traction	CS	0.235	0.227	0.238
PHEV-cng	50	2012	Regen	CS	0.458	0.468	0.449
PHEV-cng	50	2030	Traction	CS	0.269	0.261	0.273
PHEV-cng	50	2030	Regen	CS	0.468	0.478	0.458
PHEV-cng	50	2050	Traction	CS	0.292	0.282	0.296

Powertrain	P/m (kW/kg)	Year	Period	PHEV mode	Average	Urban	Highway
PHEV-cng	50	2050	Regen	CS	0.478	0.488	0.468
PHEV-cng	100	2012	Traction	CS	0.229	0.221	0.232
PHEV-cng	100	2012	Regen	CS	0.436	0.445	0.427
PHEV-cng	100	2030	Traction	CS	0.263	0.254	0.266
PHEV-cng	100	2030	Regen	CS	0.445	0.455	0.436
PHEV-cng	100	2050	Traction	CS	0.284	0.275	0.288
PHEV-cng	100	2050	Regen	CS	0.455	0.464	0.445
PHEV-cng	150	2012	Traction	CS	0.223	0.216	0.226
PHEV-cng	150	2012	Regen	CS	0.414	0.423	0.405
PHEV-cng	150	2030	Traction	CS	0.256	0.248	0.259
PHEV-cng	150	2030	Regen	CS	0.423	0.432	0.414
PHEV-cng	150	2050	Traction	CS	0.277	0.268	0.281
PHEV-cng	150	2050	Regen	CS	0.432	0.441	0.423
PHEV-h2	50	2012	Traction	CS	0.376	0.365	0.382
PHEV-h2	50	2012	Regen	CS	0.458	0.468	0.449
PHEV-h2	50	2030	Traction	CS	0.393	0.381	0.400
PHEV-h2	50	2030	Regen	CS	0.468	0.478	0.458
PHEV-h2	50	2050	Traction	CS	0.407	0.395	0.414
PHEV-h2	50	2050	Regen	CS	0.478	0.488	0.468
PHEV-h2	100	2012	Traction	CS	0.367	0.356	0.373
PHEV-h2	100	2012	Regen	CS	0.436	0.445	0.427
PHEV-h2	100	2030	Traction	CS	0.383	0.372	0.390
PHEV-h2	100	2030	Regen	CS	0.445	0.455	0.436
PHEV-h2	100	2050	Traction	CS	0.397	0.385	0.404
PHEV-h2	100	2050	Regen	CS	0.455	0.464	0.445
PHEV-h2	150	2012	Traction	CS	0.357	0.347	0.363
PHEV-h2	150	2012	Regen	CS	0.414	0.423	0.405
PHEV-h2	150	2030	Traction	CS	0.373	0.362	0.380
PHEV-h2	150	2030	Regen	CS	0.423	0.432	0.414
PHEV-h2	150	2050	Traction	CS	0.387	0.375	0.393
PHEV-h2	150	2050	Regen	CS	0.432	0.441	0.423
PHEV-gas	50	2012	Traction	CD	0.731	0.739	0.708
PHEV-gas	50	2012	Regen	CD	0.508	0.519	0.476
PHEV-gas	50	2030	Traction	CD	0.731	0.747	0.708
PHEV-gas	50	2030	Regen	CD	0.508	0.530	0.476
PHEV-gas	50	2050	Traction	CD	0.739	0.754	0.715
PHEV-gas	50	2050	Regen	CD	0.519	0.541	0.486
PHEV-gas	100	2012	Traction	CD	0.705	0.720	0.683
PHEV-gas	100	2012	Regen	CD	0.473	0.493	0.443
PHEV-gas	100	2030	Traction	CD	0.713	0.728	0.690
PHEV-gas	100	2030	Regen	CD	0.483	0.504	0.453
PHEV-gas	100	2050	Traction	CD	0.720	0.736	0.697
PHEV-gas	100	2050	Regen	CD	0.493	0.514	0.462
PHEV-gas	150	2012	Traction	CD	0.687	0.702	0.665

Powertrain	P/m (kW/kg)	Year	Period	PHEV mode	Average	Urban	Highway
PHEV-gas	150	2012	Regen	CD	0.449	0.468	0.421
PHEV-gas	150	2030	Traction	CD	0.694	0.709	0.672
PHEV-gas	150	2030	Regen	CD	0.458	0.478	0.430
PHEV-gas	150	2050	Traction	CD	0.702	0.717	0.679
PHEV-gas	150	2050	Regen	CD	0.468	0.488	0.439
PHEV-diesel	50	2012	Traction	CD	0.731	0.739	0.708
PHEV-diesel	50	2012	Regen	CD	0.508	0.519	0.476
PHEV-diesel	50	2030	Traction	CD	0.731	0.747	0.708
PHEV-diesel	50	2030	Regen	CD	0.508	0.530	0.476
PHEV-diesel	50	2050	Traction	CD	0.739	0.754	0.715
PHEV-diesel	50	2050	Regen	CD	0.519	0.541	0.486
PHEV-diesel	100	2012	Traction	CD	0.705	0.720	0.683
PHEV-diesel	100	2012	Regen	CD	0.473	0.493	0.443
PHEV-diesel	100	2030	Traction	CD	0.713	0.728	0.690
PHEV-diesel	100	2030	Regen	CD	0.483	0.504	0.453
PHEV-diesel	100	2050	Traction	CD	0.720	0.736	0.697
PHEV-diesel	100	2050	Regen	CD	0.493	0.514	0.462
PHEV-diesel	150	2012	Traction	CD	0.687	0.702	0.665
PHEV-diesel	150	2012	Regen	CD	0.449	0.468	0.421
PHEV-diesel	150	2030	Traction	CD	0.694	0.709	0.672
PHEV-diesel	150	2030	Regen	CD	0.458	0.478	0.430
PHEV-diesel	150	2050	Traction	CD	0.702	0.717	0.679
PHEV-diesel	150	2050	Regen	CD	0.468	0.488	0.439
PHEV-cng	50	2012	Traction	CD	0.731	0.739	0.708
PHEV-cng	50	2012	Regen	CD	0.508	0.519	0.476
PHEV-cng	50	2030	Traction	CD	0.731	0.747	0.708
PHEV-cng	50	2030	Regen	CD	0.508	0.530	0.476
PHEV-cng	50	2050	Traction	CD	0.739	0.754	0.715
PHEV-cng	50	2050	Regen	CD	0.519	0.541	0.486
PHEV-cng	100	2012	Traction	CD	0.705	0.720	0.683
PHEV-cng	100	2012	Regen	CD	0.473	0.493	0.443
PHEV-cng	100	2030	Traction	CD	0.713	0.728	0.690
PHEV-cng	100	2030	Regen	CD	0.483	0.504	0.453
PHEV-cng	100	2050	Traction	CD	0.720	0.736	0.697
PHEV-cng	100	2050	Regen	CD	0.493	0.514	0.462
PHEV-cng	150	2012	Traction	CD	0.687	0.702	0.665
PHEV-cng	150	2012	Regen	CD	0.449	0.468	0.421
PHEV-cng	150	2030	Traction	CD	0.694	0.709	0.672
PHEV-cng	150	2030	Regen	CD	0.458	0.478	0.430
PHEV-cng	150	2050	Traction	CD	0.702	0.717	0.679
PHEV-cng	150	2050	Regen	CD	0.468	0.488	0.439
PHEV-h2	50	2012	Traction	CD	0.731	0.739	0.708
PHEV-h2	50	2012	Regen	CD	0.508	0.519	0.476
PHEV-h2	50	2030	Traction	CD	0.731	0.747	0.708

Powertrain	P/m (kW/kg)	Year	Period	PHEV mode	Average	Urban	Highway
PHEV-h2	50	2030	Regen	CD	0.508	0.530	0.476
PHEV-h2	50	2050	Traction	CD	0.739	0.754	0.715
PHEV-h2	50	2050	Regen	CD	0.519	0.541	0.486
PHEV-h2	100	2012	Traction	CD	0.705	0.720	0.683
PHEV-h2	100	2012	Regen	CD	0.473	0.493	0.443
PHEV-h2	100	2030	Traction	CD	0.713	0.728	0.690
PHEV-h2	100	2030	Regen	CD	0.483	0.504	0.453
PHEV-h2	100	2050	Traction	CD	0.720	0.736	0.697
PHEV-h2	100	2050	Regen	CD	0.493	0.514	0.462
PHEV-h2	150	2012	Traction	CD	0.687	0.702	0.665
PHEV-h2	150	2012	Regen	CD	0.449	0.468	0.421
PHEV-h2	150	2030	Traction	CD	0.694	0.709	0.672
PHEV-h2	150	2030	Regen	CD	0.458	0.478	0.430
PHEV-h2	150	2050	Traction	CD	0.702	0.717	0.679
PHEV-h2	150	2050	Regen	CD	0.468	0.488	0.439

Table A.2: Parameterization coefficients to calculate traction and regeneration efficiencies by powertrain, driving region, power-to-mass ratio, and year of assessment.

Powertrain	Period	Driving region	PHEV mode	c_1	c_2	c_3	c_4
ICEV-gas	Traction	Avg	-	2.57	0.0152	4.16	0.9932
		Urb	-	3.22	0.0267	5.51	0.9573
		Hwy	-	2.28	0.0096	3.40	0.9896
	Regen	Avg	-	-	-	-	-
		Urb	-	-	-	-	-
		Hwy	-	-	-	-	-
ICEV-diesel	Traction	Avg	-	2.84	0.0105	2.51	0.7972
		Urb	-	4.19	0.0204	3.88	0.8089
		Hwy	-	2.49	0.0062	2.01	0.7853
	Regen	Avg	-	-	-	-	-
		Urb	-	-	-	-	-
		Hwy	-	-	-	-	-
ICEV-cng	Traction	Avg	-	2.45	0.0147	3.78	0.9071
		Urb	-	2.88	0.0248	6.05	1.1583
		Hwy	-	2.19	0.0092	3.25	0.9873
	Regen	Avg	-	-	-	-	-
		Urb	-	-	-	-	-
		Hwy	-	-	-	-	-
HEV-gas	Traction	Avg	-	2.31	0.0051	2.22	0.4209
		Urb	-	2.44	0.0068	3.16	0.6291
		Hwy	-	2.17	0.0047	2.32	0.5631
	Regen	Avg	-	1.57	0.0019	0.24	-0.0263
		Urb	-	1.75	0.0022	0.27	0.0010

Powertrain	Period	Driving region	PHEV mode	c_1	c_2	c_3	c_4
		Hwy	-	1.48	0.0018	0.21	-0.0631
HEV-diesel	Traction	Avg	-	2.24	0.0048	1.61	0.4225
		Urb	-	2.47	0.0062	1.99	0.4648
		Hwy	-	2.19	0.0043	1.34	0.3136
	Regen	Avg	-	1.57	0.0019	0.24	-0.0263
		Urb	-	1.75	0.0022	0.27	0.0010
		Hwy	-	1.48	0.0018	0.21	-0.0631
HEV-cng	Traction	Avg	-	2.22	0.0051	2.29	0.4966
		Urb	-	2.46	0.0066	2.67	0.4835
		Hwy	-	2.12	0.0046	2.23	0.5435
	Regen	Avg	-	1.57	0.0019	0.24	-0.0263
		Urb	-	1.75	0.0022	0.27	0.0010
		Hwy	-	1.48	0.0018	0.21	-0.0631
BEV	Traction	Avg	-	-0.08	0.0014	119.56	90.0178
		Urb	-	0.06	0.0015	99.27	79.6222
		Hwy	-	0.92	0.0014	5.14	17.1310
	Regen	Avg	-	-0.52	0.0041	107.44	49.3183
		Urb	-	-3.77	0.0046	676.53	120.4838
		Hwy	-	-2.44	0.0039	408.28	102.1332
FCEV	Traction	Avg	-	1.29	0.0096	5.20	4.8997
		Urb	-	1.53	0.0122	7.99	5.5480
		Hwy	-	1.20	0.0089	4.66	4.7681
	Regen	Avg	-	-6.26	0.0046	1439.05	177.7361
		Urb	-	-6.17	0.0051	1306.52	159.0280
		Hwy	-	-2.39	0.0043	387.51	94.0440
FCHEV	Traction	Avg	-	1.27	0.0041	9.14	7.4215
		Urb	-	1.72	0.0048	6.23	5.2675
		Hwy	-	1.34	0.0039	6.06	5.9395
	Regen	Avg	-	-6.26	0.0046	1439.05	177.7361
		Urb	-	-6.17	0.0051	1306.52	159.0280
		Hwy	-	-2.39	0.0043	387.51	94.0440
PHEV-gas	Traction	Avg	CS	2.16	0.0064	4.26	1.2355
		Urb	CS	2.43	0.0069	4.34	1.1269
		Hwy	CS	2.07	0.0061	4.02	1.2008
	Regen	Avg	CS	-6.26	0.0046	1439.05	177.7361
		Urb	CS	-6.17	0.0051	1306.52	159.0280
		Hwy	CS	-2.39	0.0043	387.51	94.0440
	Traction	Avg	CD	-0.08	0.0014	119.56	90.0178
		Urb	CD	0.06	0.0015	99.27	79.6222
		Hwy	CD	0.92	0.0014	5.14	17.1310
	Regen	Avg	CD	-0.52	0.0041	107.44	49.3183
		Urb	CD	-3.77	0.0046	676.53	120.4838
		Hwy	CD	-2.44	0.0039	408.28	102.1332
PHEV-diesel	Traction	Avg	CS	-0.52	0.0041	107.44	49.3183

Powertrain	Period	Driving region	PHEV mode	c_1	c_2	c_3	c_4
		Urb	CS	-3.77	0.0046	676.53	120.4838
		Hwy	CS	-2.44	0.0039	408.28	102.1332
	Regen	Avg	CS	-6.26	0.0046	1439.05	177.7361
		Urb	CS	-6.17	0.0051	1306.52	159.0280
		Hwy	CS	-2.39	0.0043	387.51	94.0440
	Traction	Avg	CD	-0.08	0.0014	119.56	90.0178
		Urb	CD	0.06	0.0015	99.27	79.6222
		Hwy	CD	0.92	0.0014	5.14	17.1310
	Regen	Avg	CD	-0.52	0.0041	107.44	49.3183
		Urb	CD	-3.77	0.0046	676.53	120.4838
		Hwy	CD	-2.44	0.0039	408.28	102.1332
PHEV-cng	Traction	Avg	CS	2.08	0.0062	4.32	1.2922
		Urb	CS	2.36	0.0067	4.18	1.0976
		Hwy	CS	2.10	0.0059	3.44	1.0239
	Regen	Avg	CS	-6.26	0.0046	1439.05	177.7361
		Urb	CS	-6.17	0.0051	1306.52	159.0280
		Hwy	CS	-2.39	0.0043	387.51	94.0440
	Traction	Avg	CD	-0.08	0.0014	119.56	90.0178
		Urb	CD	0.06	0.0015	99.27	79.6222
		Hwy	CD	0.92	0.0014	5.14	17.1310
	Regen	Avg	CD	-0.52	0.0041	107.44	49.3183
		Urb	CD	-3.77	0.0046	676.53	120.4838
		Hwy	CD	-2.44	0.0039	408.28	102.1332
PHEV-h2	Traction	Avg	CS	1.58	0.0041	4.10	4.3346
		Urb	CS	1.41	0.0045	9.10	6.9892
		Hwy	CS	1.41	0.0039	5.32	5.3701
	Regen	Avg	CS	-6.26	0.0046	1439.05	177.7361
		Urb	CS	-6.17	0.0051	1306.52	159.0280
		Hwy	CS	-2.39	0.0043	387.51	94.0440
	Traction	Avg	CD	-0.08	0.0014	119.56	90.0178
		Urb	CD	0.06	0.0015	99.27	79.6222
		Hwy	CD	0.92	0.0014	5.14	17.1310
	Regen	Avg	CD	-0.52	0.0041	107.44	49.3183
		Urb	CD	-3.77	0.0046	676.53	120.4838
		Hwy	CD	-2.44	0.0039	408.28	102.1332

Appendix B

Vehicle class characteristics

Table B.1: Sales average characteristics by class for the German passenger car market in 2011. Values for frontal area, aerodynamic drag coefficient, and glider mass are estimated.

	Power (kW)	Mass (kg)	CO_2 emission (g/km)	Retail price (Euro)	P/m ratio (W/kg)	Frontal area (m^2)	Aerodynamic drag (c_d)	Glider mass (kg)
Mini	53	936	113	10935	56	1.9	0.34	612
Small	66	1113	127	14067	59	2	0.31	762
Low-Midsize	89	1358	132	22014	66	2.1	0.31	944
Midsize	120	1582	143	33148	76	2.2	0.31	1091
Up-Midsize	162	1753	162	47333	92	2.3	0.3	1186
Luxury	233	1998	213	88352	117	2.4	0.3	1328
Compact-MPV	88	1444	143	21577	61	2.6	0.32	1032
MPV	114	1758	158	31356	65	2.8	0.34	1266
Compact-SUV	108	1549	161	27430	70	2.6	0.33	1085
SUV	172	2039	197	51312	84	2.9	0.35	1442
Compact-Sport	112	1291	151	24577	86	2.1	0.33	858
Sport	212	1501	200	68363	141	2	0.35	917
Transporter	74	1447	149	18327	51	3.1	0.34	1046

Appendix C

Life cycle impact assessment data

Table C.1: LCIA data of vehicle components.

		Vehicle production with EOL						
		Glider	ICEV drivetrain	Electric motor and controller	Battery, lithium-ion	PEM fuel cell system	Hydrogen tank, 700 bar	CNG tank, 250 bar
Impact category	**Unit**	kg^{-1}	kg^{-1}	kg^{-1}	kg^{-1}	kg^{-1}	kg^{-1}	kg^{-1}
Midpoint								
CC	kg CO2 eq	3.82E+00	3.24E+00	9.00E+00	5.84E+00	1.32E+01	1.94E+01	2.75E+00
OD	kg CFC-11 eq	2.26E-07	5.14E-07	9.20E-07	4.70E-07	8.85E-05	1.59E-06	1.44E-07
TA	kg SO2 eq	1.41E-02	1.31E-02	3.54E-02	3.08E-02	2.84E-01	7.12E-02	1.08E-02
FE	kg P eq	2.10E-03	1.99E-03	5.74E-03	3.61E-03	1.08E-02	9.99E-03	1.89E-03
ME	kg N eq	9.53E-04	7.13E-04	2.12E-03	1.49E-03	3.48E-03	1.05E-02	6.04E-04
HT	kg 1,4-DB eq	2.97E+00	2.58E+00	5.80E+00	4.79E+00	1.54E+01	7.21E+00	2.08E+00
POF	kg NMVOC	1.50E-02	1.43E-02	2.67E-02	2.09E-02	4.92E-02	3.73E-02	8.68E-03
PMF	kg PM10 eq	6.16E-03	4.62E-03	1.41E-02	1.17E-02	7.43E-02	2.21E-02	7.65E-03
TET	kg 1,4-DB eq	6.88E-04	5.04E-04	4.50E-03	1.10E-03	1.20E-03	1.83E-03	3.17E-04
FET	kg 1,4-DB eq	6.02E-02	5.10E-02	1.75E-01	8.07E-02	4.08E-01	1.50E-01	6.21E-02
MET	kg 1,4-DB eq	6.12E-02	4.56E-02	1.87E-01	8.61E-02	4.00E-01	1.57E-01	6.35E-02
IR	kg U235 eq	1.40E+00	1.33E+00	3.75E+00	1.62E+00	3.21E+00	7.76E+00	9.08E-01
ALO	m2a	3.99E-01	7.89E-02	4.66E-01	1.49E-01	2.44E-01	2.10E-01	5.90E-02
ULO	m2a	3.92E-02	3.36E-02	8.83E-02	7.26E-02	1.20E-01	5.01E-02	2.13E-02
NLT	m2	5.57E-04	8.52E-04	1.05E-03	9.74E-04	1.76E-03	3.34E-03	3.67E-04
WD	m3	3.76E-02	2.66E-02	1.03E-01	5.87E-02	1.01E-01	9.30E-02	2.72E-02
MD	kg Fe eq	7.75E-01	3.47E-01	3.54E+00	1.29E+01	2.83E+01	4.99E-01	2.92E+00
FD	kg oil eq	1.68E+00	1.12E+00	2.16E+00	1.73E+00	3.03E+00	6.12E+00	8.26E-01
Endpoint								
HH	DALY	9.06E-06	7.56E-06	2.04E-05	1.48E-05	4.88E-05	3.82E-05	7.31E-06
ED	species.yr	3.71E-08	3.33E-08	7.97E-08	5.10E-07	5.54E-07	1.58E-07	3.16E-08
RA	$	3.41E-01	2.16E-01	6.22E-01	1.22E+00	2.56E+00	1.08E+00	3.51E-01

Table C.2: LCIA data of road, vehicle maintenance, and exhaust emissions.

	Road		Maintenance		Exhaust emissions					
	Provision, Switzerland	Operation and maintenance	ICEV	EV	Petrol	Petrol, regulated, Euro 5	Petrol, regulated, Euro 6	Diesel	Diesel, regulated, Euro 5	Diesel, regulated, Euro 6
Impact category	$(kgv \cdot km)^{-1}$	km^{-1}	unit	unit	kg^{-1}	km^{-1}	km^{-1}	kg^{-1}	km^{-1}	km^{-1}
Midpoint										
CC	4.65E-06	3.60E-03	9.53E+02	9.34E+02	3.22E+00	3.97E-04	3.47E-04	3.15E+00	4.67E-05	4.11E-05
OD	1.67E-12	4.52E-10	7.94E-05	7.81E-05	0.00E+00	0.00E+00	0.00E+00	0.00E+00	0.00E+00	0.00E+00
TA	2.53E-08	1.49E-05	3.00E+00	2.59E+00	9.35E-05	1.74E-05	1.73E-05	5.92E-05	5.27E-05	5.24E-05
FE	7.65E-10	3.03E-06	4.21E-01	4.07E-01	0.00E+00	0.00E+00	0.00E+00	0.00E+00	0.00E+00	0.00E+00
ME	1.44E-09	1.31E-06	1.50E-01	1.44E-01	2.76E-06	1.21E-06	1.21E-06	1.47E-06	3.67E-06	3.65E-06
HT	8.41E-07	2.69E-03	3.97E+02	3.64E+02	1.07E-03	3.62E-04	3.18E-04	1.03E-03	5.84E-03	5.20E-03
POF	6.44E-08	1.45E-05	2.19E+00	2.09E+00	1.62E-06	6.74E-05	6.49E-05	1.62E-06	1.21E-04	1.19E-04
PMF	2.49E-08	5.45E-06	9.95E-01	8.99E-01	1.36E-05	7.87E-06	7.82E-06	9.12E-06	2.47E-05	2.14E-05
TET	5.27E-10	5.57E-07	6.78E-02	6.57E-02	6.02E-05	6.94E-08	6.09E-08	6.02E-05	1.14E-06	1.01E-06
FET	1.90E-08	4.93E-05	8.35E+00	7.97E+00	8.06E-06	2.86E-08	2.51E-08	8.07E-06	4.80E-07	4.28E-07
MET	1.80E-08	5.08E-05	8.02E+00	7.64E+00	4.89E-04	1.41E-07	1.24E-07	4.89E-04	2.68E-06	2.39E-06
IR	2.16E-06	1.55E-02	3.01E+02	2.94E+02	0.00E+00	0.00E+00	0.00E+00	0.00E+00	0.00E+00	0.00E+00
ALO	2.80E-08	1.02E-04	1.96E+01	1.91E+01	0.00E+00	0.00E+00	0.00E+00	0.00E+00	0.00E+00	0.00E+00
ULO	4.73E-08	8.83E-03	2.73E+00	2.52E+00	0.00E+00	0.00E+00	0.00E+00	0.00E+00	0.00E+00	0.00E+00
NLT	2.65E-09	6.18E-07	1.03E-01	9.95E-02	0.00E+00	0.00E+00	0.00E+00	0.00E+00	0.00E+00	0.00E+00
WD	1.14E-07	1.24E-04	4.42E+00	4.20E+00	0.00E+00	0.00E+00	0.00E+00	0.00E+00	0.00E+00	0.00E+00
MD	3.49E-07	3.22E-04	4.09E+01	3.72E+01	0.00E+00	0.00E+00	0.00E+00	0.00E+00	0.00E+00	0.00E+00
FD	3.15E-06	1.00E-03	1.23E+00	1.73E+00	0.00E+00	0.00E+00	0.00E+00	0.00E+00	0.00E+00	0.00E+00
Endpoint										
HH	1.38E-11	8.60E-09	1.88E-03	1.80E-03	4.51E-06	2.86E-09	2.74E-09	4.42E-06	1.06E-08	9.27E-09
ED	4.15E-14	3.81E-11	7.61E-06	7.46E-06	2.56E-08	3.26E-12	2.86E-12	2.50E-08	8.49E-13	7.84E-13
RA	5.60E-07	1.94E-04	3.15E+00	2.97E+00	0.00E+00	0.00E+00	0.00E+00	0.00E+00	0.00E+00	0.00E+00

Table C.3: LCIA data of exhaust emissions, non-exhaust emissions, and fuel supply.

	Exhaust emissions			Non-exhaust emissions				Fuel supply (at service station)		
	Natural gas	Natural gas, regulated, Euro 5	Natural gas, regulated, Euro 6	Tyre wear	Break wear	Road wear	Petrol, evaporation	Petrol, 2012	Diesel, 2012	CNG, 2012
Impact category	kg^{-1}	km^{-1}	km^{-1}	km^{-1}	km^{-1}	km^{-1}	km^{-1}	kg^{-1}	kg^{-1}	kg^{-1}
Midpoint										
CC	2.66E+00	1.09E-03	9.70E-04	0.00E+00	0.00E+00	0.00E+00	0.00E+00	7.88E-01	6.00E-01	5.92E-01
OD	0.00E+00	0.00E+00	0.00E+00	0.00E+00	0.00E+00	0.00E+00	0.00E+00	5.50E-07	5.71E-07	5.35E-07
TA	4.65E-04	4.62E-06	8.00E-06	0.00E+00	0.00E+00	0.00E+00	0.00E+00	6.16E-03	4.32E-03	2.10E-03
FE	0.00E+00	0.00E+00	0.00E+00	0.00E+00	0.00E+00	0.00E+00	0.00E+00	1.12E-04	8.54E-05	4.17E-05
ME	1.65E-05	3.21E-07	5.57E-07	1.68E-11	2.77E-13	0.00E+00	0.00E+00	1.37E-04	1.15E-04	5.70E-05
HT	6.81E-03	7.50E-06	6.73E-06	1.42E-07	5.17E-06	0.00E+00	2.40E-06	1.38E-01	1.07E-01	4.28E-02
POF	2.17E-06	6.77E-05	7.09E-05	0.00E+00	0.00E+00	0.00E+00	4.45E-05	5.12E-03	4.72E-03	2.47E-03
PMF	6.26E-05	2.22E-06	3.53E-06	4.07E-09	4.36E-09	4.14E-09	0.00E+00	1.79E-03	1.33E-03	6.26E-04
TET	1.34E-06	2.67E-10	2.39E-10	2.54E-09	1.24E-08	0.00E+00	2.32E-10	2.50E-04	2.18E-04	5.33E-05
FET	4.33E-08	1.32E-10	1.18E-10	3.65E-09	2.45E-09	0.00E+00	1.42E-10	3.51E-03	2.96E-03	7.86E-04
MET	7.80E-06	2.16E-09	1.94E-09	5.38E-09	9.41E-08	0.00E+00	2.50E-09	3.60E-03	2.84E-03	1.65E-03
IR	0.00E+00	0.00E+00	0.00E+00	0.00E+00	0.00E+00	0.00E+00	0.00E+00	8.98E-02	7.03E-02	1.69E-01
ALO	0.00E+00	0.00E+00	0.00E+00	0.00E+00	0.00E+00	0.00E+00	0.00E+00	2.91E-03	2.13E-03	1.64E-03
ULO	0.00E+00	0.00E+00	0.00E+00	0.00E+00	0.00E+00	0.00E+00	0.00E+00	6.96E-03	5.91E-03	1.95E-03
NLT	0.00E+00	0.00E+00	0.00E+00	0.00E+00	0.00E+00	0.00E+00	0.00E+00	1.54E-03	1.35E-03	7.66E-04
WD	0.00E+00	0.00E+00	0.00E+00	0.00E+00	0.00E+00	0.00E+00	0.00E+00	4.84E-03	4.48E-03	1.62E-03
MD	0.00E+00	0.00E+00	0.00E+00	0.00E+00	0.00E+00	0.00E+00	0.00E+00	1.82E-02	1.37E-02	1.17E-02
FD	0.00E+00	0.00E+00	0.00E+00	0.00E+00	0.00E+00	0.00E+00	0.00E+00	1.29E+00	1.23E+00	1.23E+00
Endpoint										
HH	3.75E-06	2.12E-09	2.28E-09	1.16E-12	4.75E-12	1.08E-12	3.42E-12	1.67E-06	1.26E-06	1.02E-06
ED	2.11E-08	8.71E-12	7.74E-12	3.87E-16	1.89E-15	0.00E+00	3.56E-17	6.33E-09	4.82E-09	4.72E-09
RA	0.00E+00	0.00E+00	0.00E+00	0.00E+00	0.00E+00	0.00E+00	0.00E+00	2.20E-01	2.10E-01	2.10E-01

Table C.4: LCIA data of electricity supply.

	Electricity supply (at low voltage grid)									
	Swiss consumption mix, 2012	Average European mix, 2012	NGCC, 2012	NGCC, 2020	NGCC, >2030	Coal (European average), 2012	Coal, 2020	Coal, >2030	Swiss nuclear, 2012	Swiss wind, 2012
Impact category	kWh^{-1}	kWh^{-1}	kWh^{-1}	kWh^{-1}	kWh^{-1}	kWh^{-1}	kWh^{-1}	kWh^{-1}	kWh^{-1}	kWh^{-1}
Midpoint										
CC	1.48E-01	5.94E-01	4.86E-01	4.53E-01	4.48E-01	1.22E+00	8.87E-01	8.34E-01	1.59E-02	2.55E-02
OD	1.98E-08	2.92E-08	6.92E-08	7.28E-08	6.77E-08	6.54E-09	3.72E-09	3.51E-09	3.52E-08	1.39E-09
TA	6.71E-04	2.54E-03	4.47E-04	4.67E-04	3.98E-04	5.24E-03	8.24E-04	7.80E-04	1.45E-04	1.66E-04
FE	1.56E-04	6.14E-04	3.53E-05	3.76E-05	3.84E-05	5.87E-04	7.57E-04	7.13E-04	3.51E-05	4.65E-05
ME	4.15E-05	1.69E-04	1.71E-05	1.73E-05	1.81E-05	2.26E-04	1.90E-04	1.79E-04	7.70E-06	1.03E-05
HT	1.70E-01	4.46E-01	7.46E-02	7.63E-02	7.71E-02	4.34E-01	5.11E-01	4.85E-01	7.58E-02	9.06E-02
POF	3.49E-04	1.26E-03	5.53E-04	5.60E-04	5.23E-04	2.95E-03	7.53E-04	7.09E-04	7.75E-05	9.02E-05
PMF	2.48E-04	8.07E-04	1.59E-04	1.62E-04	1.75E-04	1.59E-03	2.81E-04	2.66E-04	5.86E-05	8.88E-05
TET	3.59E-05	6.01E-05	2.64E-05	2.54E-05	2.72E-05	3.24E-05	2.61E-05	2.56E-05	1.94E-05	2.07E-05
FET	2.59E-03	8.86E-03	7.74E-04	8.06E-04	8.24E-04	8.85E-03	1.07E-02	1.01E-02	8.26E-04	1.31E-03
MET	2.75E-03	8.87E-03	1.01E-03	1.04E-03	1.02E-03	8.85E-03	1.05E-02	9.93E-03	9.49E-04	1.46E-03
IR	7.76E-01	4.66E-01	1.65E-03	2.09E-03	6.34E-03	2.04E-02	7.36E-03	6.96E-03	1.46E+00	4.09E-03
ALO	3.38E-03	8.55E-03	1.25E-03	1.22E-03	1.69E-03	2.71E-02	1.45E-02	1.37E-02	1.59E-03	1.48E-03
ULO	6.96E-04	1.99E-03	3.99E-04	3.58E-04	5.70E-04	7.94E-03	5.21E-03	4.91E-03	4.20E-04	1.61E-03
NLT	2.12E-05	6.39E-05	1.08E-04	1.05E-04	9.55E-05	5.85E-05	3.53E-05	3.33E-05	3.79E-06	3.50E-06
WD	5.29E-03	4.84E-03	3.77E-03	3.51E-03	3.46E-03	3.08E-03	2.23E-03	2.10E-03	9.81E-03	2.39E-04
MD	2.64E-02	2.62E-02	2.42E-02	2.40E-02	2.44E-02	2.56E-02	2.37E-02	2.36E-02	2.82E-02	4.47E-02
FD	4.08E-02	1.61E-01	1.80E-01	1.69E-01	1.72E-01	3.13E-01	2.12E-01	2.00E-01	3.72E-03	6.54E-03
Endpoint										
HH	4.04E-07	1.36E-06	7.74E-07	7.29E-07	7.28E-07	2.43E-06	1.67E-06	1.58E-06	1.15E-07	1.22E-07
ED	1.20E-09	4.77E-09	3.86E-09	3.60E-09	6.11E-09	1.20E-08	1.29E-07	7.44E-09	9.89E-10	2.96E-10
RA	8.83E-03	2.93E-02	3.24E-02	3.04E-02	3.09E-02	5.51E-02	3.78E-02	3.56E-02	2.66E-03	4.33E-03

Table C.5: LCIA data of electricity and hydrogen supply.

	Electricity supply (at low voltage grid)				Hydrogen supply (700 bar, at service station)					
	Swiss PV, 2012	Swiss PV, 2020	Swiss PV, >2030	Swiss hydro, 2012	Steam methane reforming, 2012	Steam methane reforming, >2030	Coal gasification, 2012	Coal gasification, >2030	Biomass gasification, 2012	Biomass gasification, >2030
Impact category	kWh^{-1}	kWh^{-1}	kWh^{-1}	kWh^{-1}	kg^{-1}	kg^{-1}	kg^{-1}	kg^{-1}	kg^{-1}	kg^{-1}
Midpoint										
CC	6.15E-02	4.17E-02	3.50E-02	1.16E-02	1.63E+01	1.58E+01	2.38E+01	2.27E+01	8.50E+00	6.34E+00
OD	1.14E-08	9.49E-09	2.25E-09	5.11E-10	4.78E-06	4.81E-06	2.87E-06	2.91E-06	3.15E-06	3.27E-06
TA	3.06E-04	2.51E-04	2.28E-04	1.02E-04	2.42E-02	2.36E-02	4.61E-02	3.73E-02	3.79E-02	1.92E-02
FE	7.09E-05	3.63E-05	3.57E-05	3.50E-05	1.99E-03	8.15E-04	8.09E-03	5.64E-03	6.17E-03	1.10E-03
ME	2.40E-05	1.67E-05	7.46E-06	4.11E-06	8.00E-04	5.30E-04	2.82E-03	2.19E-03	2.07E-03	6.92E-04
HT	1.24E-01	9.84E-02	8.79E-02	7.28E-02	2.00E+00	1.37E+00	6.19E+00	4.64E+00	5.14E+00	3.86E+00
POF	2.28E-04	1.87E-04	1.21E-04	5.01E-05	1.68E-02	1.60E-02	1.62E-02	1.28E-02	1.95E-02	1.26E-02
PMF	1.19E-04	1.02E-04	9.76E-05	5.47E-05	8.17E-03	8.13E-03	1.21E-02	9.51E-03	1.26E-02	7.28E-03
TET	1.24E-04	1.43E-04	2.51E-05	1.87E-05	5.03E-04	6.57E-04	4.33E-04	3.50E-04	5.48E-03	3.93E-02
FET	1.48E-03	9.50E-04	9.47E-04	7.51E-04	5.02E-02	3.67E-02	1.53E-01	1.19E-01	1.12E-01	3.85E-02
MET	1.80E-03	1.40E-03	1.18E-03	8.72E-04	5.53E-02	4.39E-02	1.52E-01	1.19E-01	1.13E-01	4.29E-02
IR	1.76E-02	7.79E-03	8.19E-03	1.57E-03	1.16E+00	8.97E-01	2.38E+00	1.78E+00	4.62E+00	3.32E+00
ALO	2.99E-03	3.18E-03	2.32E-03	1.18E-03	6.88E-02	1.18E-01	5.33E-01	6.31E-01	2.28E+00	2.19E+00
ULO	5.37E-04	9.40E-04	8.84E-04	2.97E-04	2.21E-02	2.31E-02	1.27E-01	1.26E-01	5.57E-02	5.15E-02
NLT	1.18E-05	1.13E-05	9.08E-06	8.08E-06	3.38E-03	3.57E-03	1.06E-03	1.03E-03	1.29E-03	1.28E-03
WD	6.24E-04	3.71E-04	2.88E-04	1.17E-04	3.43E-02	3.36E-02	5.64E-02	5.25E-02	6.57E-02	5.74E-02
MD	3.47E-02	4.57E-02	5.00E-02	2.36E-02	9.74E-01	1.10E+00	1.01E+00	1.04E+00	9.57E-01	1.14E+00
FD	1.68E-02	1.17E-02	9.34E-03	2.11E-03	5.79E+00	5.71E+00	5.46E+00	5.25E+00	2.19E+00	1.81E+00
Endpoint										
HH	2.05E-07	1.54E-07	1.36E-07	8.15E-08	2.63E-05	2.52E-05	4.08E-05	3.76E-05	1.88E-05	1.35E-05
ED	6.45E-10	9.48E-10	3.19E-10	1.56E-10	1.30E-07	1.26E-07	1.89E-07	1.81E-07	6.89E-08	5.67E-08
RA	5.36E-03	5.29E-03	5.19E-03	2.06E-03	1.06E+00	1.05E+00	1.00E+00	9.67E-01	4.41E-01	3.89E-01

Table C.6: LCIA data of hydrogen supply.

	Hydrogen supply (700 bar, at service station)									
	Electrolysis (Swiss mix), 2012	Electrolysis (European mix), 2012	Electrolysis (Swiss nuclear), 2012	Electrolysis (Swiss nuclear), >2030	Electrolysis (Swiss wind), 2012	Electrolysis (Swiss wind), >2030	Electrolysis (Swiss PV), 2012	Electrolysis (Swiss PV), >2030	Electrolysis (Swiss hydro), 2012	Electrolysis (Swiss hydro), >2030
Impact category	kg^{-1}	kg^{-1}	kg^{-1}	kg^{-1}	kg^{-1}	kg^{-1}	kg^{-1}	kg^{-1}	kg^{-1}	kg^{-1}
Midpoint										
CC	6.97E+00	1.78E+01	1.63E+00	1.50E+00	2.19E+00	1.99E+00	3.10E+00	2.45E+00	1.38E+00	1.28E+00
OD	3.87E-06	4.51E-06	4.78E-06	4.53E-06	2.86E-06	2.85E-06	3.31E-06	2.88E-06	2.80E-06	2.79E-06
TA	2.33E-02	3.51E-02	1.89E-02	1.77E-02	1.94E-02	1.81E-02	2.50E-02	2.18E-02	1.64E-02	1.55E-02
FE	5.01E-03	1.03E-02	2.55E-03	2.25E-03	2.60E-03	2.30E-03	2.62E-03	2.28E-03	2.55E-03	2.25E-03
ME	1.22E-03	2.76E-03	6.20E-04	5.52E-04	7.17E-04	6.36E-04	1.13E-03	5.40E-04	4.15E-04	3.73E-04
HT	7.17E+00	1.03E+01	5.14E+00	4.56E+00	5.29E+00	4.70E+00	6.43E+00	5.17E+00	4.97E+00	4.42E+00
POF	1.23E-02	2.36E-02	7.37E-03	6.72E-03	8.23E-03	7.48E-03	1.37E-02	8.88E-03	5.80E-03	5.35E-03
PMF	9.58E-03	1.29E-02	7.19E-03	6.71E-03	8.77E-03	8.10E-03	9.70E-03	8.66E-03	6.96E-03	6.52E-03
TET	1.44E-03	1.65E-03	1.27E-03	1.13E-03	1.33E-03	1.18E-03	8.31E-03	1.41E-03	1.23E-03	1.09E-03
FET	1.11E-01	1.82E-01	7.66E-02	7.01E-02	8.68E-02	7.89E-02	8.37E-02	7.61E-02	7.24E-02	6.63E-02
MET	1.22E-01	1.91E-01	8.53E-02	7.79E-02	9.69E-02	8.80E-02	1.11E-01	8.95E-02	8.09E-02	7.40E-02
IR	2.57E+01	1.91E+01	8.35E+01	7.30E+01	3.21E-01	2.91E-01	5.95E-01	5.50E-01	2.39E-01	2.19E-01
ALO	1.12E-01	1.61E-01	1.06E-01	9.71E-02	1.04E-01	9.51E-02	1.97E-01	1.34E-01	8.28E-02	7.64E-02
ULO	3.33E-02	5.28E-02	3.20E-02	2.90E-02	4.50E-02	4.03E-02	6.18E-02	5.22E-02	2.50E-02	2.29E-02
NLT	1.30E-03	2.99E-03	3.05E-04	2.78E-04	4.05E-04	3.66E-04	7.33E-04	5.43E-04	5.51E-04	4.93E-04
WD	2.25E-01	2.39E-01	5.79E-01	5.07E-01	3.28E-02	2.95E-02	3.93E-02	3.10E-02	2.47E-02	2.25E-02
MD	2.33E+00	2.35E+00	2.49E+00	2.29E+00	3.79E+00	3.43E+00	3.49E+00	3.38E+00	2.22E+00	2.06E+00
FD	2.17E+00	5.71E+00	3.98E-01	3.69E-01	5.73E-01	5.21E-01	8.57E-01	6.50E-01	3.06E-01	2.89E-01
Endpoint										
HH	1.77E-05	3.57E-05	9.11E-06	8.24E-06	9.05E-06	8.18E-06	1.14E-05	9.31E-06	7.23E-06	6.59E-06
ED	5.60E-08	1.42E-07	1.34E-08	1.24E-08	1.80E-08	1.64E-08	2.65E-08	2.00E-08	1.15E-08	1.07E-08
RA	5.37E-01	1.14E+00	2.47E-01	2.27E-01	3.70E-01	3.35E-01	3.97E-01	3.54E-01	2.12E-01	1.97E-01

Appendix D

Swiss new vehicle sales and CO_2 emission by mass category

Table D.1: Distribution of average CO_2 emission (g/km) by mass category.

	Year	<1000 kg	1000-1100	1100-1200	1200-1300	1300-1400	1400-1500	1500-1600	1600-1700	1700-1800	1800-1900	1900-2000	2000-2100	2100-2200	>2200 kg
Gasoline	2000	141	160	178	188	200	218	236	248	269	277	313	313	324	375
	2001	138	158	173	182	197	214	229	245	268	278	316	307	315	309
	2002	135	153	165	179	191	212	230	247	259	271	296	332	306	346
	2003	134	148	162	176	188	205	222	238	253	274	281	312	315	344
	2004	130	144	159	175	184	204	214	233	243	269	284	299	304	340
	2005	126	144	155	168	180	201	208	229	236	267	274	305	280	348
	2006	121	146	152	166	177	202	203	223	238	264	263	298	252	339
	2007	117	145	152	163	171	192	198	214	240	251	263	295	283	325
	2008	115	141	149	160	166	182	193	213	232	245	273	287	281	333
	2009	112	137	141	153	163	180	190	206	228	236	266	284	278	249
	2010	112	133	137	148	158	176	184	195	210	227	239	270	272	245
	2011	109	128	131	147	152	170	178	184	199	212	233	255	252	292
	2012	107	125	129	142	146	163	171	180	197	200	229	250	239	291
Diesel	2000	81	139	132	140	142	157	168	190	213	223	243	285	261	255
	2001	81	153	130	138	144	155	166	182	206	219	231	285	248	288
	2002	83	111	124	133	143	152	167	176	199	210	210	234	241	264
	2003	85	116	119	133	143	151	162	179	184	202	214	224	244	265
	2004	85	115	119	133	139	147	163	174	185	204	215	225	235	259
	2005	90	114	134	131	138	148	161	168	180	199	214	222	235	256
	2006	106	116	133	133	139	148	161	171	183	202	213	221	240	259
	2007	97	113	130	131	140	149	159	171	182	198	211	221	239	259
	2008	93	111	129	137	134	147	155	169	184	195	208	220	232	254
	2009	94	110	125	136	127	144	153	167	179	191	199	214	228	245
	2010	90	108	111	117	122	141	146	158	174	181	191	197	212	236
	2011	87	106	105	111	119	132	145	150	162	171	176	192	202	225
	2012	87	95	103	106	114	129	140	147	158	166	167	187	191	218

Table D.2: Distribution of sales by mass category.

	Year	<1000 kg	1000-1100	1100-1200	1200-1300	1300-1400	1400-1500	1500-1600	1600-1700	1700-1800	1800-1900	1900-2000	2000-2100	2100-2200	>2200 kg
Gasoline	2000	31709	29016	32054	36165	47627	36042	26699	17324	8654	7250	7130	1013	1767	1153
	2001	25680	29059	26730	36623	38443	37794	33136	19347	8776	8070	4291	1300	2057	1812
	2002	15450	25911	27150	27598	28107	35819	24296	13706	7041	6844	3233	1412	381	1672
	2003	11645	23102	28694	21058	27347	32804	24864	16822	7128	4754	4121	2294	1246	2629
	2004	6982	26513	24552	17623	26248	29504	26677	15712	7210	6425	3664	1904	1062	2271
	2005	6337	21436	24856	16318	24781	23950	25468	15303	9679	4945	3959	1757	1514	1882
	2006	10321	15537	26072	19319	24227	19813	25676	18107	9656	4582	5016	1827	1952	2141
	2007	10785	14733	24834	20057	23822	18520	23304	18228	6968	4729	3159	1778	1316	2070
	2008	12710	18811	27324	23155	26245	19063	24534	17726	7211	4724	2217	1695	726	1012
	2009	13394	21855	22062	24287	26509	17396	23607	13964	5180	4762	1482	986	484	1175
	2010	11823	23793	27441	26122	28577	18820	21833	18410	5038	3788	2005	1107	661	1755
	2011	9589	20856	28042	24362	32575	17636	19395	22778	6651	4485	1727	940	443	1050
	2012	11282	16929	24076	22579	27675	17878	20361	21354	5292	5995	1999	1481	602	1003
Diesel	2000	758	77	1772	2340	4726	6664	4578	2001	1443	2665	1497	1125	656	1278
	2001	997	201	2175	1919	4709	8225	8349	3615	2472	4283	2292	1032	1265	1040
	2002	554	369	1794	2092	5099	5323	10009	7742	2485	4124	2093	961	2017	2347
	2003	230	363	2702	2361	4723	6581	12160	8688	3869	4576	1875	2108	3551	2992
	2004	146	712	2758	2499	5082	10468	14458	10683	5320	3496	4262	1618	4006	4291
	2005	75	323	3448	2292	5444	11933	9735	14980	7177	4680	3433	2453	3394	4874
	2006	143	170	2301	4936	5566	10503	8453	14958	8329	8138	3192	2485	3652	6026
	2007	154	419	2002	4636	6498	9982	8545	17348	9568	7579	3037	2677	3293	7664
	2008	158	707	2128	3793	7097	10285	13351	20473	9506	10242	3703	2450	4938	5704
	2009	99	330	1971	2355	7035	7352	10807	14643	8043	10113	3716	1843	2726	4202
	2010	85	202	1678	3513	5620	8700	12155	18510	10069	8826	4460	3173	3331	4564
	2011	50	82	1256	2504	6139	8511	13546	20018	14898	11351	5654	3560	4506	4991
	2012	16	84	1307	2602	6395	9563	15836	21004	15372	11465	9177	4164	5387	5985

Bibliography

ABB (2014). Ladeinfrastruktur für Elektrofahrzeuge. Data sheet: http://www.abb.ch/evcharging.

ACEA (2012). European Automobile Manufacturers Association. http://www.acea.be/.

Ahn, J. H., Kang, H., Lee, H. S., Jung, H. W., Baek, C., & Kim, Y. (2014). Heating performance characteristics of a dual source heat pump using air and waste heat in electric vehicles. *Applied Energy*, 119, 1–9.

Alonso, E., Lee, T. M., Bjelkengren, C., Roth, R., & Kirchain, R. E. (2012). Evaluating the Potential for Secondary Mass Savings in Vehicle Lightweighting. *Environmental Science & Technology*, 46(5), 2893–2901.

Althaus, H. & Gauch, M. (2010). Vergleichende Ökobilanz individueller Mobilität: Elektromobilität versus konventionelle Mobilität mit Bio- und fossilen Treibstoffen. Report, EMPA, Dübendorf.

André, M. (2004). The ARTEMIS European driving cycles for measuring car pollutant emissions. *Science of the total Environment*, 334, 73–84.

Ang, B. W. & Zhang, F. (2000). A survey of index decomposition analysis in energy and environmental studies. *Energy*, 25(12), 1149–1176.

ARE (2006). Perspektiven des schweizerischen Personenverkehrs bis 2030. Bundesamt für Raumentwicklung.

Auto-Schweiz (2013). 17. Berichterstattung im Rahmen der Energieverordnung über die Absenkung des spezifischen Treibstoff-Normverbrauchs von Personenwagen 2012.

Auto-Schweiz (2014). Website: Vereinigung schweizer Automobil-Importeure. Website: http://www.auto-schweiz.ch/.

BAFU (2010). Pollutant Emissions from Road Transport, 1990 to 2035. Bundesamt für Umwelt.

BAFU (2012). Bundesamt für Umwelt, Website: http://www.bafu.admin.ch/luft/11640/11646.

BAFU (2014). Emissionen nach CO2 Gesetz und Kyoto Protokoll. Bundesamt für Umwelt.

Bandivadekar, A., Bodek, K., Cheah, K., Evans, C., Groode, C., Heywood, J., Kasseris, E., Kromer, M., & Weiss, M. (2008). On the Road in 2035. Reducing Transportations Petroleum Consumption and GHG Emissions. Report, MIT Laboratory for Energy and the Environment, Cambridge, Massachusetts.

Bauer, C. & Simons, A. (2010). Oekobilanz der Elektromobilitaet. Report. Paul Scherrer Institut.

BFE (2012). CO2-Emissionsvorschriften für neue Personenwagen. Bundesamt für Energie. http://www.bfe.admin.ch/themen/00507/05318/index.html?lang=de.

BFS (2012). Mobilität in der Schweiz. Ergebnisse des Mikrozensus Mobilität und Verkehr 2010. Bundesamt für Statistik.

BFS (2014). Bundesamt für Statistik. Website: http://www.bfs.admin.ch/.

BP (2013). Statistical Review of World Energy 2013.

Bradley, T. & Qinn, C. (2010). Analysis of plug-in hybrid electric vehicle utility factors. *Journal of Power Sources*, 195, 5399–5408.

Brooker, A., Ward, J., & Wang, L. (2013). Lightweighting Impacts on Fuel Economy, Cost, and Component Losses. *SAE International*.

Brundtland, G. H., on Environment, W. C., & Development (1987). *Our common future*, volume 383. Oxford University Press.

Brusa (2014). Batterien 400 V. Data sheet: http://www.brusa.biz/index.php?id=189.

Buzeman, D. G., Viano, D. C., & Lövsund, P. (1998). Car occupant safety in frontal crashes: a parameter study of vehicle mass, impact speed, and inherent vehicle protection. *Accident Analysis & Prevention*, 30(6), 713–722.

Campanari, S., Manzolini, G., & Garcia de la Iglesia, F. (2009). Energy analysis of electric vehicles using batteries or fuel cells through well-to-wheel driving cycle simulations. *Journal of Power Sources*, 186(2), 464–477.

Chang, D. e. a. (2012). Financial Viability Of Non-Residential Electric Vehicle Charging Stations. Report. UCLA, Luskin School of Public Affairs.

Cheah, L., Evans, C., Bandivadekar, A., & Heywood, J. (2009). *Factor of two: halving the fuel consumption of new US automobiles by 2035*. Springer.

Chen, M. & Rincon-Mora, G. A. (2006). Accurate electrical battery model capable of predicting runtime and IV performance. *IEEE transactions on energy conversion*, 21(2), 504–511.

Chen, Y. & Borken-Kleefeld, J. (2014). Real-driving emissions from cars and light commercial vehicles–results from 13 years remote sensing at zurich/ch. *Atmospheric Environment*, 88, 157–164.

Cuenot, F. (2009). CO2 emissions from new cars and vehicle weight in Europe; How the EU regulation could have been avoided and how to reach it? *Energy Policy*, 37(10), 3832–3842.

Daimler (2008). Environmental certificate A-class. Report, Daimler AG, Mercedes-Benz, Stuttgart, Germany.

De Haan, P., Zah, R., & Althaus, H.-J. (2013). Chancen und Risiken der Elektromobilität in der Schweiz. VDF Hochschulverlag AG an der ETH Zürich.

DOE (2014). H2A Production Analysis. US Department of Energy. Excel models: http://www.hydrogen.energy.gov/.

Drexhage, J. & Murphy, D. (2010). Sustainable development: from Brundtland to Rio 2012. Background paper prepared for consideration by the High Level Panel on Global Sustainability at its first meeting 19 September 2010.

Duleep, G., van Essen, H., Kampman, B., & Gruenig, M. (2011). Assessment of electric vehicle and battery technology. CE Delft, report prepared for European Commission.

EC (2009). Regulation (EC) No 443/2009. Europe Commission.

EC (2012a). COM/2012/393 - Proposal for a Regulation to define the modalities for reaching the 2020 target for reducing CO2 emissions from new passenger cars.

EC (2012b). Impact assessment part II, accompanying the documents: Proposal for a regulation of the European Parliament and of the Council amending Regulation (EC) No 443/2009 to define the modalities for reaching the 2020 target to reduce CO2 emissions from new passenger cars.

Eckle, P., Burgherr, P., & Hirschberg, S. (2011). Final Report on Multi-Criteria Decision Analysis (MCDA). Deliverable no D6.2. Security of Energy Considering its Uncertainty, Risk and Economic implications (SECURE). Brussels, Belgium.

Ecoinvent (2014). Swiss Centre for Life Cycle Inventories. http://www.ecoinvent.org/.

Edwards, R., Larivé, J., & Beziat, J. (2011). Well-to-wheels Analysis of Future Automotive Fuels and Powertrains in the European Context. Report, European Commission Joint Research Center.

EEA (2014). European Environment Agency. http://www.eea.europa.eu.

Eisenführ, F., Weber, M., & Langer, T. (2010). *Rational Decision Making*. Springer.

Elcom (2014). Strompreis-Webseite der ElCom. http://www.strompreis.elcom.admin.ch.

Eliasson, B. & Lee, Y. Y. (2003). *Integrated Assessment of Sustainable Energy Systems in China, The China Energy Technology Program: The China Energy Technology Program: a Framework for Decision Support in the Electric Sector of Shandong Province*, volume 4. Springer.

Frondel, M., Schmidt, C. M., & Vance, C. (2011). A regression on climate policy: The European Commission's legislation to reduce CO2 emissions from automobiles. *Transportation Research Part A: Policy and Practice*, 45(10), 1043–1051.

FSV (2011). Future Steel Vehicle. Report, World Auto Steel.

Gantt, L. R. (2011). Energy Losses for Propelling and Braking Conditions of an Electric Vehicle. Master thesis, Virginia Polytechnic Institute and State University.

Gao, D. W., Mi, C., & Emadi, A. (2007). Modeling and simulation of electric and hybrid vehicles. *Proceedings of the IEEE*, 95(4), 729–745.

Gerssen-G., S. & Faaij, A. (2012). Performance of batteries for electric vehicles on short and longer term. *Journal of Power Sources*, 212, 111–129.

Goede, M., Stehlin, M., Rafflenbeul, L., Kopp, G., & Beeh, E. (2009). Super Light Car—lightweight construction thanks to a multi-material design and function integrlight. *European Transport Research Review*, 1(1), 5–10.

Goedkoop, M., Heijungs, R., Huijbregts, M., De Schryver, A., Struijs, J., & van Zelm, R. (2009). ReCiPe 2008 - A life cycle impact assessment method which comprises harmonised category indicators at the midpoint and the endpoint level. Report, PRe Consultants.

Goodall, H. W. & Thompson, G. D. (1977). Prediction of vehicle reference frontal area. Report, Environmental Protection Agency, USA.

Graham, R. (2001). Comparing the Benefits and Impacts of Hybrid Electric Vehicle Options. Report, Electric Power Research Institute.

Guzzella, L. & Sciarretta, A. (2013). Vehicle Propulsion Systems: Introduction to Modeling and Optimization. Springer Verlag, Berlin Heidelberg.

Habermacher, F. (2011). Modeling material inventories and environmental impacts of electric passenger cars. Master thesis, EMPA.

Hawkins, T., Gausen, O. M., & Strømman, A. H. (2012a). Environmental impacts of hybrid and electric vehicles—a review. *The International Journal of Life Cycle Assessment*, 17(8), 997–1014.

Hawkins, T., Singh, B., Majeau-Bettez, G., & Stromman, A. (2012b). Comparative Environmental Life Cycle Assessment of Conventional and Electric Vehicles. *Journal of Industrial Ecology*, 17, 53–64.

Heinen, S. (2013). Analyzing Energy Use with Decomposition Methods. Presentation, Energy Training Week, IEA, Paris.

Heisler, H. (2002). Advanced vehicle technology. Society of Automotive Engineers Inc.

Heuss, R. e. a. (2012). Lightweight, heavy impact. Report, McKinsey & Company.

Hirschberg, S., Bauer, C., Burgherr, P., Dones, R., Schenler, W., Bachmann, T., & Gallego, D. (2007). Environmental, economic and social criteria and indicators for sustainability assessment of energy technologies. Deliverable no D3.1 - Research Stream RS2b. New Energy Externalities Developments for Sustainability (NEEDS). Brussels, Belgium.

Hofer, J., Simons, A., & Schenler, W. (2013a). Multi-criteria analysis of passenger vehicles based on technical, economic, and environmental indicators. *Proceedings of the 27th International Electric Vehicle Symposium, Barcelona, Spain.*

Hofer, J., Wilhelm, E., & Schenler, W. (2012a). Fuel Economy Improvements of Swiss and European New Passenger Cars. Proceedings of the International Advanced Mobility Forum (IAMF), Geneva, Switzerland.

Hofer, J., Wilhelm, E., & Schenler, W. (2012b). Impacts of technology evolution and consumer choice on the direct CO2 emissions from new passenger cars in Switzerland. Proceedings of the Smart Energy Strategies Conference 2012, ETH Zurich.

Hofer, J., Wilhelm, E., & Schenler, W. (2012c). Optimal Lightweighting in Battery Electric Vehicles. *Proceedings of the 26th International Electric Vehicle Symposium*.

Hofer, J., Wilhelm, E., & Schenler, W. (2013b). Comparing the mass, energy, and cost effects of lightweighting in conventional and electric passenger vehicles. *Proceedings of the 8th Conference on Sustainable Development of Energy, Water, and Environment Systems, Dubrovnik, Croatia*.

Hua, T., Ahluwalia, R., Peng, J., Kromer, M., Lasher, S., McKenney, K., & Sinha, K. (2010). Technical Assessment of Compressed Hydrogen Storage Tank Systems for Automotive Applications. Report, Argonne National Laboratory.

Hutchinson, T. P. & Anderson, R. W. (2010). Vehicle mass as a determinant of fuel consumption and secondary safety performance: A comment. *Transportation research part D: transport and environment*, 15(2), 123–125.

IBIS (2008). Aluminum Vehicle Structure: Manufacturing and Lifecycle Cost Analysis Hybrid Drive and Diesel Vehicles. Report, IBIS Associates Inc.

ICCT (2012). The International Council on Clean Transportation. http://www.theicct.org/.

ICCT (2013a). European Vehicle Market Statistics, 2012. http://www.theicct.org/european-vehicle-market-statistics-2012.

ICCT (2013b). Worldwide harmonized light vehicles test procedure (WLTP), Policy Update. Report, International Council on Clean Transportation.

IEA (2007). Fuel Cells. OECD/IEA Energy Technology Perspectives ETE 06.

IEA (2009). Transport, Energy and CO2. Moving Toward Sustainability.

IEA (2012a). Energy Technology Perspectives 2012. Pathways to a Clean Energy System. OECD/IEA.

IEA (2012b). World Energy Outlook 2012. OECD/IEA.

IEA (2013a). CO2 Emissions from Fuel Combustion. OECD/IEA.

IEA (2013b). Success factors for hybrid and electric vehicle deployment. IEA Implementing Agreement for co-operation on Hybrid and Electric Vehicle Technologies and Programmes.

Infras (2007). Der Energieverbrauch des Verkehrs 1990-2035. Infras AG, commissioned by Bundesamt für Energie.

IPCC (2013). Summary for Policymakers. In: Climate Change 2013: The Physical Science Basis. Contribution of Working Group I to the Fifth Assessment Report of the Intergovernmental Panel on Climate Change.

ISO (2006a). ISO 14040. Environmental management – life cycle assessment – principles and framework. *International Organisation for Standardisation, Geneva.*

ISO (2006b). ISO 14044. Environmental management – life cycle assessment – requirements and guidelines. *International Organisation for Standardisation, Geneva.*

James, B. (2012). Hydrogen Storage Cost Analysis. Strategic Analysis Inc., report prepared for U.S. Department of Energy.

Kalhammer, F., Bruce, M., Swan D., Roan, V., & Walsh, M. (2007). Status and Prospects for Zero Emissions Vehicle Technology. Report prepared for State of California Air Resources Board.

Kasseris, E. P. & Heywood, J. B. (2007). Comparative Analysis of Automotive Powertrain Choices for the Next 25 Years. *SAE Technical Paper 2007-01-1605*.

Katrašnik, T. (2009). Analytical framework for analyzing the energy conversion efficiency of different hybrid electric vehicle topologies. *Energy Conversion and Management*, 50(8), 1924–1938.

Katrašnik, T. (2010). Analytical method to evaluate fuel consumption of hybrid electric vehicles at balanced energy content of the electric storage devices. *Applied Energy*, 87(11), 3330–3339.

Katrašnik, T. (2011). Energy conversion phenomena in plug-in hybrid-electric vehicles. *Energy Conversion and Management*, 52(7), 2637–2650.

Kim, H. C. & Wallington, T. J. (2013). Life-cycle energy and greenhouse gas emission benefits of lightweighting in automobiles: Review and harmonization. *Environmental Science & Technology*, 47(12), 6089–6097.

Kim, H.-J., Keoleian, G. A., & Skerlos, S. J. (2011). Economic assessment of greenhouse gas emissions reduction by vehicle lightweighting using aluminum and high-strength steel. *Journal of Industrial Ecology*, 15(1), 64–80.

Kim, M.-J. & Peng, H. (2007). Power management and design optimization of fuel cell/battery hybrid vehicles. *Journal of Power Sources*, 165(2), 819–832.

Kromer, M., Bandivadekar, A., & Evans, C. (2010). Long-term greenhouse gas emission and petroleum reduction goals: Evolutionary pathways for the light-duty vehicle sector. *Energy*, 35, 387–397.

Kromer, M. & Heywood, J. B. (2007). Electric Powertrains: Opportunities and Challenges in the U.S. Light-Duty Vehicle Fleet. Report, MIT Laboratory for Energy and the Environment, Cambridge, Massachusetts.

Lave, L. B. (1981). Conflicting objectives in regulating the automobile. *Science*, 212(4497), 893–899.

LEA (2010). Nachhaltige Elektrizität: Wunschdenken oder bald Realität? Energie-Spiegel Nr. 20. Laboratory for Energy Analysis, Paul Scherrer Institute.

Leduc, P., Dubar, B., Ranini, A., & Monnier, G. (2003). Downsizing of gasoline engine: an efficient way to reduce co2 emissions. *Oil & Gas Science and Technology*, 58(1), 115–127.

Lee, S., Cho, Y., Song, H.-K., Lee, K. T., & Cho, J. (2012). Carbon-Coated Single-Crystal LiMn2O4 Nanoparticle Clusters as Cathode Material for High-Energy and High-Power Lithium-Ion Batteries. *Angewandte Chemie International Edition*, 51(35), 8748–8752.

Lieven, T., Mühlmeier, S., Henkel, S., & Waller, J. F. (2011). Who will buy electric cars? An empirical study in Germany. *Transportation Research Part D: Transport and Environment*, 16(3), 236–243.

Lotus (2010). An Assessment of Mass Reduction Opportunities for a 2017-2020 Model Year Vehicle Program. Report, Lotus Engineering Inc.

Lovins, A. B. & Cramer, D. R. (2004). Hypercars, hydrogen, and the automotive transition. *International Journal of Vehicle Design*, 35(1), 50–85.

Lutsey, N. (2010). Review of technical literature and trends related to automobile mass-reduction technology. Report, Institute of Transportation Studies, UC Davis.

Markel, T., Brooker, A., Hendricks, T., Johnson, V., Kelly, K., Kramer, B., O'Keefe, M., Sprik, S., & Wipke, K. (2002). ADVISOR: a systems analysis tool for advanced vehicle modeling. *Journal of Power Sources*, 110(2), 255–266.

MathWorks (2014). http://www.mathworks.ch/ch/help/stats/boxplot.html.

Miotti, M. (2013). Life cycle and cost assessment of current and future fuel cell vehicles. Master thesis, Paul Scherrer Institute, ETH Zurich.

Mock, P., German, J., Bandivadekar, A., & Riemersma, I. (2012). Discrepancies between type-approval and real-world fuel consumption and CO2 values in 2001-2011 European passenger cars. Report, International Council on Clean Transportation.

Murray, J. & King, D. (2012). Climate policy: Oil's tipping point has passed. *Nature*, 481(7382), 433–435.

Mutel, C. L. & Hellweg, S. (2009). Regionalized life cycle assessment: computational methodology and application to inventory databases. *Environmental science & technology*, 43(15), 5797–5803.

Nelson, P., Bloom, K., & I Dees, D. (2011). Modeling the performance and cost of lithium-ion batteries for electric-drive vehicles. Report, Argonne National Laboratory.

Neubauer, J., Brooker, A., & Wood, E. (2012). Sensitivity of battery electric vehicle economics to drive patterns, vehicle range, and charge strategies. *Journal of Power Sources*, 209, 269–277.

Notter, D., Gauch, M., Widmer, R., Wäger, P., Stamp, A., Zah, R., & Althaus, H. (2010). Contribution of Li- Ion Batteries to the Environmental Impact of Electric Vehicles. *Environmental Science and Technology*, 44, 6550–6556.

NRC (2011). National Research Council. Assessment of Fuel Economy Technologies for Light-Duty Vehicles. National Academies Press.

Ott, T., Zurbriggen, F., Onder, C., & Guzzella, L. (2013). Cycle-averaged efficiency of hybrid electric vehicles. *Proceedings of the Institution of Mechanical Engineers, Part D: Journal of Automobile Engineering*, 227(1), 78–86.

Ottaviano, D. (2012). Technical Assessment and Modeling of Lithium-Ion Batteries for Electric Vehicles. Master thesis, Paul Scherrer Institute, ETH Zurich.

Papagiannaki, K. & Diakoulaki, D. (2009). Decomposition analysis of CO2 emissions from passenger cars: The cases of Greece and Denmark. *Energy Policy*, 37(8), 3259–3267.

Pohekar, S. & Ramachandran, M. (2004). Application of multi-criteria decision making to sustainable energy planning–a review. *Renewable and Sustainable Energy Reviews*, 8(4), 365–381.

Prognos (2012). Die Energieperspektiven für die Schweiz bis 2050. Energienachfrage und Elektrizitätsangebot in der Schweiz 2000 - 2050. Report, Prognos, commissioned by Federal Office for Energy.

Redelbach, M., Klötzke, M., & Friedrich, H. E. (2012). Impact of lightweight design on energy consumption and cost effectiveness of alternative powertrain concepts. European Electric Vehicle Conference, Brussels, Belgium.

Ross, M. & Wenzel, T. (2001). Losing weight to save lives: a review of the role of automobile weight and size in traffic fatalities.

Roth, S., Hirschberg, S., Bauer, C., Burgherr, P., Dones, R., Heck, T., & Schenler, W. (2009). Sustainability of electricity supply technology portfolio. *Annals of Nuclear Energy*, 36(3), 409–416.

Safaei Mohamadabadi, H., Tichkowsky, G., & Kumar, A. (2009). Development of a multi-criteria assessment model for ranking of renewable and non-renewable transportation fuel vehicles. *Energy*, 34(1), 112–125.

Schenler, W., Hirschberg, S., Burgherr, P., & Makowski, M. (2009). Final report on sustainability assessment of advanced electricity supply options". Deliverable no D10.2 - Research Stream RS2b. New Energy Externalities Developments for Sustainability (NEEDS). Brussels, Belgium.

Schipper, L. & Fulton, L. (2013). Dazzled by diesel? The impact on carbon dioxide emissions of the shift to diesels in Europe through 2009. *Energy Policy*, 54(C), 3–10.

Sheinbaum-Pardo, C. & Chávez-Baeza, C. (2011). Fuel economy of new passenger cars in mexico: Trends from 1988 to 2008 and prospects. *Energy Policy*, 39(12), 8153–8162.

Shiau, C.-S. N., Kaushal, N., Hendrickson, C. T., Peterson, S. B., Whitacre, J. F., & Michalek, J. J. (2010). Optimal plug-in hybrid electric vehicle design and allocation for minimum life cycle cost, petroleum consumption, and greenhouse gas emissions. *Journal of Mechanical Design*, 132, 091013.

Siegerist, T. (2013). Life cycle assessment of lightweighting in conventional and electric passenger vehicles. Master thesis. Paul Scherrer Institute, ETH Zurich.

Simbeck, D. & Chang, E. (2002). Hydrogen Supply: Cost Estimate for Hydrogen Pathways. Report, National Renewable Energy Laboratory.

Simons, A. (2013). Road transport: new life cycle inventories for fossil-fuelled passenger cars and non-exhaust emissions in ecoinvent v3. *The International Journal of Life Cycle Assessment*, (pp. 1–15).

Simons, A. & Bauer, C. (2010). Life Cycle Assessment of Battery Electric and Internal Combustion Engine Drivetrains for a Small Passenger Car. *Proceedings of the 18th international Symposium on Transport and Air pollution.*

Simons, A. & Bauer, C. (2011a). Life Cycle Assessment of Hydrogen Use in Passenger Vehicles. *Proceedings of the 2011 International Advanced Mobility Forum.*

Simons, A. & Bauer, C. (2011b). Transition to Hydrogen: Pathways Toward Clean Transportation. Chapter 2 - Life cycle assessment of hydrogen production. Cambridge University Press.

Simpson, A. (2006). Cost-Benefit Analysis of Plug-In Hybrid Electric VehicleInstitute. Report, National Renewable Energy Laboratory.

Simpson, A. G. (2005). Parametric modelling of energy consumption in road vehicles. PhD thesis, University of Queensland.

Smokers, R. e. a. (2011). Support for the revision of Regulation (EC) No 443/2009 on CO2 emissions from cars. Report on behalf of the European Commission.

Sovran, G. (2013). Revisiting the Formulas for Tractive and Braking Energy on the EPA Driving Schedules. *SAE International Journal of Passenger Cars-Mechanical Systems*, 6(1), 269–282.

Sovran, G. & Blaser, D. (2003). A contribution to understanding automotive fuel economy and its limits. *SAE transactions*, 112(3), 1715–1740.

Spendelow, J., Papageorgopoulos, D., & Garbak, J. (2011). Fuel Cell Stack Durability. US DOE Fuel Cell Technologies Program Record 11003.

Spielmann, M., Bauer, C., Dones, R., & Tuchschmid, M. (2007). Transport Services. ecoinvent report No. 14. Swiss Centre for Life Cycle Inventories, Dübendorf.

Sprei, F. & Karlsson, S. (2008). The role of market and technical downsizing in reducing carbon emissions from the swedish new car fleet. *Energy Efficiency*, 1(2), 107–120.

Sun, J. (1998). Changes in energy consumption and energy intensity: a complete decomposition model. *Energy economics*, 20(1), 85–100.

Takeshita, T. (2011). Global scenarios of air pollutant emissions from road transport through to 2050. *International journal of environmental research and public health*, 8(7), 3032–3062.

ThyssenKrupp (2003). New Steel Body. Report, ThyssenKrupp Stahl.

TNO (2011). Support for the revision of Regulation (EC) No 443/2009 on CO2 emissions from cars. Final report.

Tran, M., Banister, D., Bishop, J. D., & McCulloch, M. D. (2012). Realizing the electric-vehicle revolution. *Nature Climate Change*, 2(5), 328–333.

Troen, E. & Lundtang, P. (1989). European wind atlas. Risoe National Laboratory, Roskilde.

Tseng, H.-K., Wu, J. S., & Liu, X. (2013). Affordability of electric vehicles for a sustainable transport system: An economic and environmental analysis. *Energy Policy*, 61(0), 441 – 447.

Tzeng, G.-H., Lin, C.-W., & Opricovic, S. (2005). Multi-criteria analysis of alternative-fuel buses for public transportation. *Energy Policy*, 33(11), 1373–1383.

Wang, J.-J., Jing, Y.-Y., Zhang, C.-F., & Zhao, J.-H. (2009). Review on multi-criteria decision analysis aid in sustainable energy decision-making. *Renewable and Sustainable Energy Reviews*, 13(9), 2263–2278.

WBCSD (2004). Mobility 2030: Meeting the challenges to sustainability.The Sustainable Mobility Project. Full Report. World Business Council for Sustainable Development.

WEC (2011). Global transport scenarios 2050. World Energy Council.

WEF (2011). Repowering Transport. Project White Paper.World Economic Forum.

Wenzel, T. P. & Ross, M. (2005). The effects of vehicle model and driver behavior on risk. *Accident Analysis & Prevention*, 37(3), 479–494.

Werber, M., Fischer, M., & Schwartz, P. V. (2009). Batteries: Lower cost than gasoline? *Energy Policy*, 37(7), 2465–2468.

Wilhelm, E. (2011a). Multi-criteria analysis of heuristically designed vehicles. PhD thesis, Paul Scherrer Institute, ETH Zurich.

Wilhelm, E. (2011b). Transition to Hydrogen: Pathways Toward Clean Transportation. Chapter 3: Technical characterisation and multi-criteria analysis of light-duty vehicles. Cambridge University Press.

Wilhelm, E., Hofer, J., & Schenler, W. (2011). Multi-Criteria Analysis of Driver Preference for New Vehicle Technologies to Identify Robust Alternatives. *Proceedings of the 2011 International Advanced Mobility Forum*.

Wilhelm, E., Hofer, J., Schenler, W., & Guzzella, L. (2012). Optimal Implementation of Lightweighting and Powertrain Efficiency Technology in Passenger Vehicles. *Transport*, 27, 237–249.

Wilhelm, E. & Wokaun, A. (2011). Multi-Criteria Decision Analysis of Heuristically Designed Light-Duty Vehicles Today and in 2035. *Proceedings of the 2011 SAE World Congress, 2011-01-0727*.

Wipke, K., Sprik, S., Kurtz, J., Ramsden, T., Ainscough, C., & Saur, G. (2012). National Fuel Cell Electric Vehicle Learning Demonstration. Final Report. National Renewable Energy Laboratory.

Zachariadis, T. (2008). The effect of improved safety on fuel economy of european cars. *Transportation Research Part D: Transport and Environment*, 13(2), 133–139.

Zhou, Z., Jiang, H., & Qin, L. (2007). Life cycle sustainability assessment of fuels. *Fuel*, 86(1), 256–263.